

6th International Geosciences Student Conference
13 -16 July 2015 | Prague, Czech Republic
ABSTRACT BOOK

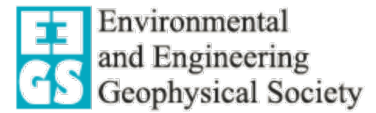


Crossing the Boundaries



www.igsc6.wz.cz





Platinum sponsor:



Gold sponsors:



Welcome to Prague, the heart of Europe,

welcome to the 6th International Geosciences Student Conference 2015, which takes place at Faculty of Science, Charles University in Prague. Our faculty is well-known because of our students; we have extraordinary research topics and very interesting student environment. Our geophysical department deals with various aspects of geoscience. We consider a multidisciplinary approach as crucial. Hence our idea was to bring together the best students of all geosciences (not only geophysicists), and to give them a chance to share their latest research or case studies in a friendly and dignified manner. All together, we attempted to cross the boundaries between all of the geoscience branches.

Based on the scope of the 6th IGSC conference 2015, the contributions were divided into three main thematic groups: Geology, Applied Geophysics and Oil&Gas & Seismicity. To maintain a thematic integrity of the contributions, they are arranged as they were presented within the technical programme of the conference.

On behalf of the 6th IGSC committee

Petr Taborik, Technical Programme Manager

TECHNICAL SESSIONS

SCHEDULE - oral presentations

GEOLOGY

MONDAY, 13 July

Charimen: Paulina Kotlarek, Ondřej Krýza

12 : 30	Determination of Carboniferous sediments of Lublin Basin, Poland	Filip Bolesta
12 : 45	Mineralogical composition of Productive Series and its source area, western South Caspian Basin	Jalilzadeh Aysura
13 : 00	Sequence Stratigraphy and Composition of Oligocene to Eocene Shelf-Edge Deltas: Implications from Facies-Cycle Wedges in the Eastern Niger Delta, Nigeria	David O. Anomneze, Anthony U. Okoro, Norbert E. Ajaegwu, Chibuzor V. Ahaneke, Nnaemeka I. Okoli
13 : 15	Lithological and geochemical differences between light and dark, well layered sediments of Badenian age from the "Bukova glava" quarry outcrop, Croatia	Anja Jarić, Antonio Drnasin
13 : 30	Crustal-scale buckling and associated crustal flow - lessons from analogue modeling	Ondrej Kryza, Ondrej Lexa, Karel Schulmann, Denis Gapais, Alexandra Guy, John Cosgrove
13 : 45	Geological compass vs. mobile applications	Paulina Kotlarek, Jacek Piotr Kubalski
14 : 00	Development of Favosites bohemicus (Tabulata) on soft and unstable sediments covering slopes of the Emsian Kess-Kess mounds of Hamar Laghdad (Morocco)	Jan J. Król
14 : 15	Late Quaternary sea level effects on coral reef evolution and growth in Southern Kimberley, North West Australia.	Giada Bufarale, Lindsay Collins, Michael O'Leary, Alexandra Stevens, Moataz Kordi, Tubagus Solihuddin
14 : 30	The relation of structural and petroleum geology - a case study from the Pannonian Basin, SW Hungary	Rebeka Oross



Determination of Carboniferous sediments of Lublin Basin, Poland

Filip Bolesta¹,

email: filipbolesta@gmail.com

¹ AGH University of Science and Technology, Krakow, Poland

Summary

Determination of electrofacies in silty-shaly carboniferous profile can be successfully obtained by using IPSOM module in Techlog system. In this paper six electrofacies were identified in Carboniferous profile in A-well, which is located in Lublin Basin, Poland. The learnt model was applied to B-well from the same geological area. In this paper, literature studies of neighboring wells, mud-logging geological profile and box plots were very useful in lithological interpretation of electrofacies. This approach allowed to assign electrofacies to a particular lithology.

Introduction

It is well known that facies, sequence and sedimentation environment can be described using traditional geological methods i.e. from field observations or from observation of cores. On the other hand, faces can be determined from well logging data. This method is known as *well logging approach*. Thus, the term “electrofacies” should be used. “*This term was introduced by Serra and Abbott (1980) and has been defined as the set of log responses which characterizes a bed and permits to be distinguished from others*” (Kumar et al., 2006).

In this paper determination of electrofacies was performed in Techlog System in IPSOM module. This module uses Kohonen neural network. What is more, IPSOM allows to learn neural network in one well and apply the learnt model to localize electrofacies in another wells. Well logging data comes from two wells (A-well and B-well) from the area of Lublin Basin, Poland, and they were drilled by Orlen Upstream Company in exploration of shale gas (in Silurian sediments).

In this paper only Carboniferous silty-shaly formations were investigated. Carboniferous was not perspective for the investor, so neither cores nor petrographical information were available. For this reason, analysis and interpretation of electrofacies in Carboniferous were based on used mud-logging data, geological literature about Carboniferous in Lublin Basin and petrographical documentations from the neighbouring wells.

Geology of the area

Both wells were drilled in the central part of Lublin Basin, which is localized in eastern Poland.

There are the same four formations in both wells (from the top):

Lublin Formation (Westfal A-B) – mainly composed of mudstones and claystones, less often sandstones. This is productive formation of coal. On the bottom clays have marine fauna.

Dęblin Formation (Namur A-Westfal A) – sandstones, mudstones and claystones with coal seams and a few inserts of marine limestone. Lower part of the formation is mainly silty-shaly and the upper part is more sandy.

Terebin Formation (Upper Wizen – Namur A) –silty-shaly cyclothems prevail in the lower part of the formation in which beds of limestones and sandstones occur. The upper part is similar, but without limestones.

Huczwa Formation (Upper Wizen) – In the lower part there are conglomerates with silty- shaly and lime-marly beds and mudstones with thin layers of coal . The upper part is represented mainly by limestones, marls and claystones.

Methodology

Seven logs were used for determination of electrofacies in IPSOM module: compressional slowness (DT), neutron porosity (NPHI), bulk density (RHOB), photoelectric factor (PEF), potassium (POTA), thorium (THOR) and uranium (URAN). Such diversity of logs allows more precise determination of electrofacies.

In the A-well the length of Carboniferous profile was about 907 meters and in the B-well this length was 717 meters. Thus, neural network was learning in unsupervised mode in the first well in all formations due to more representative Carboniferous profile. Fuzzy classification method was chosen in unsupervised mode, because it gave better results than using hierarchical clustering methods (results were clearer and easier for interpretation). In the learning process 6 electrofacies were identified: 1-coal, 2-carbonaceous claystone, 3-mudstone, 4-claystone, 5-sandstone, 6-limestone. After the learning process the model was automatically applied to the B-well.

Results

Three curves were obtained as a result: Classes (electrofacies) distribution, Class Probability and Cumulative Probability. Probability curve in B-well had usually smaller values than probability curve from A-well. Worse quality of logs and breakouts in the borehole could contribute for that. Six electrofacies were obtained for the whole Carboniferous profile and each of them was interpreted as a different lithology. Claystones, mudstones, and carbonaceous claystones were challenging to differentiate in terms of electrofacies. These rocks have very similar values on logs.

In order to compare modelled electrofacies in terms of values box plots for NPHI, DT, RHOB, POTA, URAN, THOR were constructed (fig.1). Except of literature studies (Waksumundzka, 2007) and mud-logging (which was not perfect), these plots also helped for better recognition of electrofacies. Carbonaceous claystones have bigger values of NPHI than others mudstone-claystone facies and also values of RHOB were more varied. Mudstones usually have smaller NPHI and DT values, so after visualisation (fig.1) it was possible to distinguish them from other facies. According to coal, sandstone and limestone it was much easier to classify them. Each of these three lithology has characteristic values of each log.

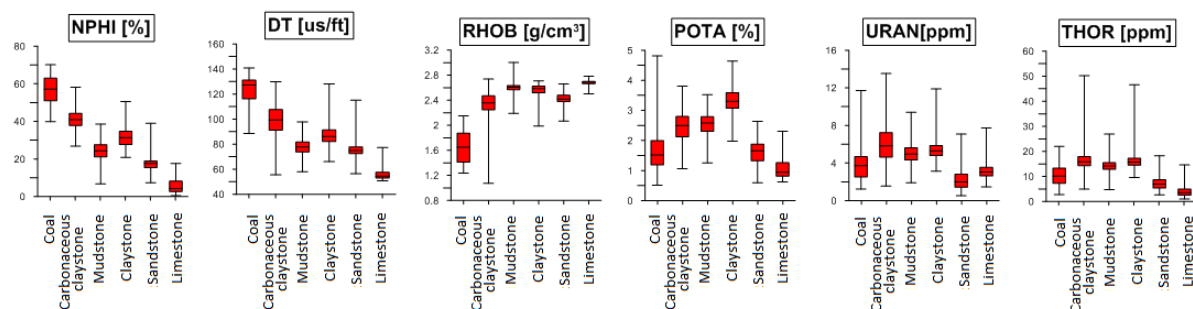


Figure 1 Box plots of electrofacies for NPHI, DT, RHOB, POTA, URAN, THOR.

Conclusions

In the absence of sufficient geological data, determination of electrofacies in IPSOM module in unsupervised mode can give good results and allow to assign electrofacies to a particular lithology even in silty-shaly formations. The model which was learnt by neural network in unsupervised mode was applied to another well from the area in Lublin Basin with a moderate satisfaction of author. It shows that good quality of data and experience is essential in electrofacies determination. If cores were available, application of the model in the B-well would be much better.



References

Kumar, B. and Kishore, M., [2006] Electrofacies Classification – A Critical Approach, 6th International Conference & Exposition on Petroleum Geophysics “Kolkata 2006”, 822-825.

Serra, O. and Abbott, H.T. [1980] The contribution of logging data to sedimentology and stratigraphic. SPE 9270, 55th Annual Fall Technical Conference and Exhibition. Dallas, 19p.

Waksmundzka, M. I. [2007] Karbon – Wyniki badań litologicznych, sedymentologicznych i stratygraficznych. Profile głębokich otworów wiertniczych – Lublin IG1, 114-134.



Mineralogical composition of Productive Series and its source area, western South Caspian Basin

Jalilzadeh Aysura

email: aysura.jalilzadeh@gmail.com

¹ Azerbaijan State Oil Academy

Summary

The main aim of the work is based on mineralogical composition to identify source area for the Upper Division of Productive Series (Pliocene) from western South Caspian Basin. Previous studies show two different facies for Productive Series from western South Caspian Basin: "Kura Facies" and "Absheron Facies". The Russian platform, the Greater Caucasus, the Lesser Caucasus were source areas for western South Caspian Basin. The analyses show that Greater Caucasus was source area during deposition of the Upper Division of Productive Series and changing content of carbonate may reflect the change of sea level.

Introduction

The Caspian Sea is the largest lake in the world with total area 375.000 km² (Buryakovskiy et al., 2001). The main goal of research is to study the mineralogical composition of Upper Productive Series and its potential source rocks from Absheron Peninsula, western South Caspian Basin. Productive Series is a part of Pliocene sequence and the main reservoir unit in the South Caspian Basin (Hinds et al., 2004). The Productive Series consist of sandstone, siltstone, and shale. In respect to microfauna composition the Upper Productive Series is divided into the Lower division (Kala suite, Pre Kirmaky Suite, Kirmaky Suite, Post Kirmaky Sand Suite, Post Kirmaky Clay Suite) and the Upper Division (Fasile Suite, Balakhany Suite, Sabunchi Suite, Surakhany Suite).

Western South Caspian Basin was supplied with sediments by the Volga River, Samur River and Kura River. The Russian Platform, the Greater Caucasus and the Lesser Caucasus were potential sources for western South Caspian Basin. According to mineralogical composition of the Productive Series two different facies was found, "Absheron facies" and "Kura facies". The "Absheron facies" is characterized by higher percentage of sand, which is represented by high amount of well sorted quartz. The "Kura facies" is characterized by high amount of feldspar and lithic fragments (Morton et al., 2003). The "Absheron facies" was drained from Russian Platform and the "Kura facies" was drained from the Lesser Caucasus.

Method and/or Theory

Sand, silt, clay fractions were separated by sieving methods. For reconstruction potential source of our research area 46 samples were investigated in order to identify quartz, feldspar, lithic fragments by polarization microscopy. In addition, the content of carbonate was identified to study sea level.

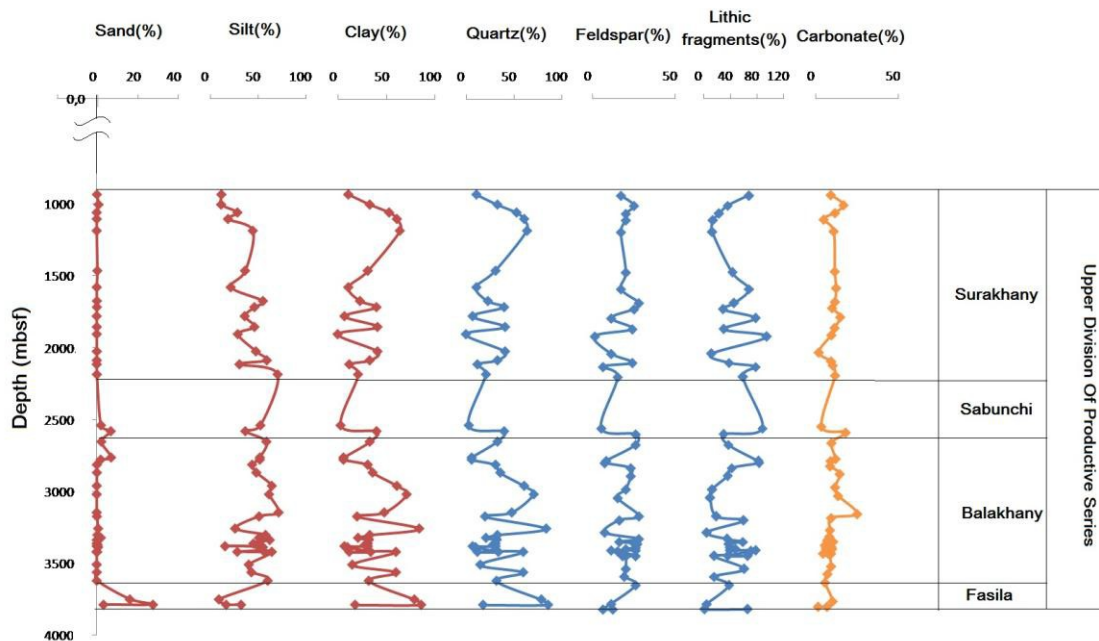


Figure 1 Sand content (<0,25 mm),silt content (0,1-0,01 mm),clay content (<0,01 mm) and abundance of quartz, lithic fragments, carbonate in the Upper Division of Productive Series from western South Caspian Basin.

Conclusions

The analyses show that the amount of quartz changes between: 19-87 % in Fasile suite, 7-85 % in Balakhany suite, 4-41 % in Sabunchi suite, 1-65 % in Surakhany suite; the amount of feldspar ranges from: 7-13 % in Fasile suite, 8-29 % in Balakhany suite, 6-27 % in Sabunchi suite , 2-29 % in Surakhany suite; the amount of lithic fragments varies between 4-68 % in Fasile suite, 7-85 % in Balakhany suite, 32-90 % in Sabunchi Suite, 14-97 % in Surakhany suite. The Upper Division of the Productive Series is characterized by low amount of sand fractions: 3.4 -28 % in Fasile suite, 0-7.2 % in Balakhany suite, 2.1-7 % in Sabunchi suite, 0-0.9 % in Surakhany suite. The high amount of carbonate is observed in the interval 2550-3100 m, 18.9–25.9 % in Balakhany-Sabunchi suites. We see the high amount of quartz and low amount of feldspar in Fasile suite. The rise in percentage of lithic fragments in Balakhany and Surakhany suites is noticeable. The Sabunchi suite is characterized by low amount of quarts and feldspar (Figure 1).

The granulometric fraction and also mineral composition indicate that the sediments from Upper Division of the Productive Series do not correspond with mineralogical content of the “Absheron facies” and “Kura facies”. The mineralogical composition may indicate that the Greater Caucasus was source area.



References

Some examples can be found here. . Buryakovsky , L., Chilingar , G. and Aminzadeh F. [2001] Petroleum Geology of the South Caspian Basin. Gulf Professional Publishing

Morton, A., Allen, M., Simmons, M., Spathopoulos, F., Still, J., Hinds, D., Ismail-Zadeh, A. and Kroonenberg, S.[2003] Provenance patterns in a neotectonic basin: Pliocene and Quaternary sediment supply to the South Caspian . Basin Research (2003) 15, 321–337.

Hinds, D., Aliyeva, E., Allen, M., Davies, C., Kroonenberg, S., Simmons, M. and Vincent, S. [2004] Sedimentation in a discharge dominated fluvial-lacustrine system: the Neogene Productive Series of the South Caspian Basin, Azerbaijan. *Marine and Petroleum Geology*, 21, 613-618.

Sequence Stratigraphy and Composition of Oligocene to Eocene Shelf-Edge Deltas: Implications from Facies-Cycle Wedges in the Eastern Niger Delta, Nigeria

David O. Anomneze¹, Anthony U. Okoro¹, Norbert E. Ajaegwu¹, Chibuzor V. Ahaneku¹, Nnaemeka I. Okoli¹

davanomneze@gmail.com
¹ Nnamdi Azikiwe University

Summary

This paper presents data from a regional 3D seismic within the Eastern Niger Delta with different 3D geometry. These data was used to first identify the shelf-edge position geometrically, in combination with paleobathymetry and well logs data and then to describe the exploration scale lowstand sandy facies relative to this position on a sequence stratigraphic framework. The shelf-edge position was identified around clinoform geometries within wedges bounded by regional growth faults and counter regional faults having a dominant paleobathymetry of Middle Neritic to Outer Neritic. The wedges which indicate sudden break in the sedimentation pattern internally represent a lateral change in sedimentation rate and a local facies change vertically.

Introduction

With the current global interest in rejuvenation of older fields and the search for deep-frontier plays such as the Shelf-edge deltas, thus, there is need for an in-depth understanding of the stratigraphy, sedimentology and geomorphology of Shelf-edge settings.

Methodology

This study was carried out using the concepts of sequence stratigraphy, sedimentology and geomorphology. The sequence stratigraphy was carried out using the third-order sequence stratigraphic interpretation approach (fig. 1) utilizing seismic, well logs and biostratigraphy data. The sedimentology was carried out using well log and core data analysis while the geomorphology was effectively carried out using the RMS attribute analysis (fig. 2).

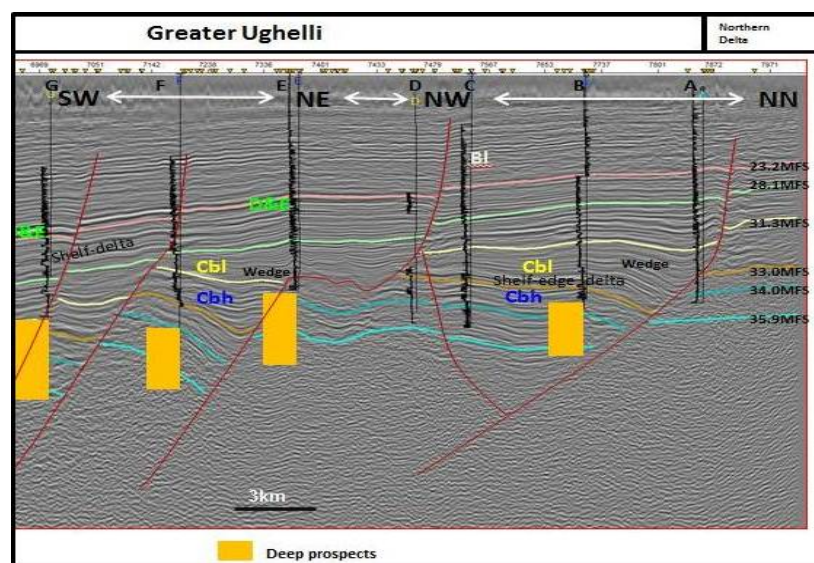


Figure 1: Structural and sequence-stratigraphic framework (with seismic facies insert).

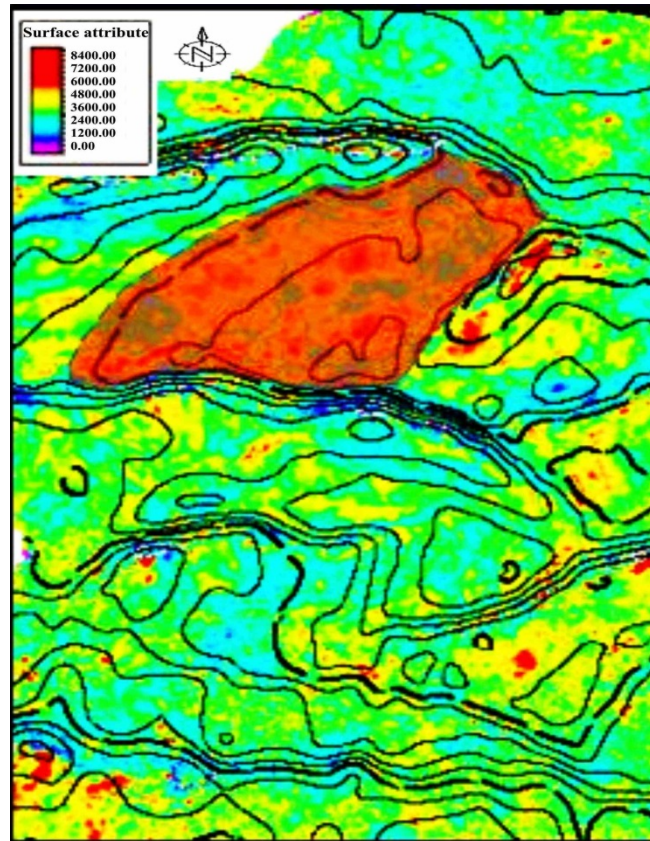


Figure 2: High RMS Attribute of 33.0 - 34.0ma MFS shows the geometry of the shelf edge delta.

Conclusion

The shelf-edge position was identified around clinoform geometries within wedges bounded by regional growth faults and counter regional faults having a dominant paleobathymetry of Middle Neritic to Outer Neritic. These wedges were found at greater depth of more than 7000ft. The wedges which indicate sudden break in the sedimentation pattern internally represent a lateral change in sedimentation rate and a local facies change vertically. However, two of these wedges were interpreted to represent two concurrent sequences existing in older proximal sequences and adjacent younger distal sequences. The lower wedge sequence was observed to be sandier having seismic geometries similar to a sedimentary drag while the upper wedge sequence was observed to be shalier at the top and sandier at the base. The lateral changes in sedimentation rate implied the change in lithology from sand to silt and to shale showing a decrease in sand percentage within the wedges in the basinward direction. This study has aided the comparison based on wedge positioning and the basic differences in lithology distribution within the wedges in a shelf-edge setting. Also a comparison in terms of sequence stratigraphy and reservoir geometry of other shelf edge deltas within the Niger Delta was done with this data. It was concluded that Shelf-edge deltas prograde more in the lowstand system tract which is in agreement with the findings of Adereti et al., 2012 and Fieldman et al., 2013. Also in map view they show aguate geometry - a proximal slim part growing into a much distal broader part which is similar to the findings of Van-Heijst et al., 2002. Assessment procedures for this play require a look-alike facies interpretation and positioning of the wedge in terms of paleobathymetry and age. This will serve in providing drilling targets to more independent operators with fields within the shelf-edge environment.



References

Adereti, O., Feldman, H., Unomah, G., Ahmed, B., Ajibola, O., Alalade, B., Farre, J., Tsakma, J., Garfield, T., Lopez, C., Reistroffer, J. and Sweet, M. (2012) Key elements of a world class petroleum system: Lowstand shelf edge reservoirs in the southeastern Niger Delta, Nigeria. NAPE Bulletin, v.24 (1), pp. 38-42.

Fieldman, H., Adereti, O., Ahmed, B., Ajibola, O., Alalade, B., Lopez, C., Sweet, M., Tsakma, J., Unomah, G. and Farre, J. (2013) Predicting large-scale reservoir architecture: Application of data from shelf edge reservoirs in the Eastern Niger Delta. NAPE Bulletin, v. 25 (1), pp. 52-60.

Van-Heijst, M.W.I.M., Postma, G., Van-Kesteren, W.P. and De-Jongh, R.G. (2002) Control of syndepositional faulting on systems tract evolution across growth-faulted shelf margins: An analog experimental model of the Miocene Imo River field, Nigeria. AAPG Bulletin, v.86 (8), pp. 1335-1366.



Lithological and geochemical differences between light and dark, well layered sediments of Badenian age from the “Bukova glava” quarry outcrop, Croatia

Anja Jarić, Antonio Drnasin
Email: ajaric90@gmail.com
University of Zagreb

Summary

In the “Bukova glava” quarry near the town of Našice (Croatia) rock samples from several layers were taken. From previous research it is known that organic matter is present in some of them. Chronostratigraphically, they are of Badenian and Sarmatian age. There are three types of sediment: the dark layered with organic matter, the light layered sediment and a greyish laminated sediment that is interbedded with light laminae. Lithological, micropaleontological, geochemical and granulometric research was made to determine why organic matter is present just in the dark layer.

Introduction

The locality of “Bukova glava” is in the north-western part of Croatia, near the town of Našice. That particular site is interesting because it is situated on the northern slopes of Mt Krndija which is on the south-western margin of the Pannonian basin.

There are three different types of bedding which are of interest in this location. Dark layers that contain organic matter, grey laminated layers, and light coloured laminated layers. These layers are of Badenian and Sarmatian age and are known for breccia, conglomerate, sandstone, marl, marly sandstone, limestone, andesite, basalt and tuff deposition (Krkalo, 1998).

There are a number of **dark** layers in the studied area with the thickness that varies from 130 to 220 mm. Those layers are interbedded with white (beige) laminae that are 5,6 to 12,5 mm thick. Zečević (2008) studied the presence of carbon in organic compounds on that location from five chosen samples. There was determined that two of the five samples had a low percentage of carbon in organic compounds (0,52% and 0,48%), but the other three had a significant amount that even reached 8,90% of carbon. The results of Rock – Eval pyrolysis were very high ($S_2 = 48,82$ mgHC/g rock) that suited the high content of organic matter. These results indicated great source rock potential.

Grey layers have a thickness in the range from 75 to 235 mm. They are interbedded with laminae that are 5,5 to 20 mm thick and thin layers (up to 27,5 mm). Colour of lamina and layers varies from white, beige to grey and dark grey.

Sediment has been deposited into a shallow marine environment, possibly in a sheltered lagoon. Some of the grey layers have a characteristic microfault domino – type system. Those type of extension fractures are associated with the expansion and sinking of the basin.

Light layers are up to 400 mm thick. These layers are interbedded with up to 8 mm thick laminae which occur cyclic after the deposition of approximately 50 mm of white sediment.

Method and/or Theory

First, field reconnaissance study has been made. After compiling enough data, geological columns were constructed. The samples with the purest colour distinction were carefully chosen from the Badenian and Sarmatian part of the quarry and taken for further analysing. Granulometric research was made to determine the size of particles and micropaleontological research was used to find out if

some important fossil content can be found (any fossils that could indicate a lagoon environment which is suitable for oil development) and also it has been used in distinction of geologic periods. In the end, Rock – Eval pyrolysis was used to determine source rock potential.



Figure 1 View of the analysed three layers. Under the dark layer with organic matter lies a light layered sediment. On top of the same dark layer lies a greyish laminated layer that is interbedded with light laminae.

Conclusions

The objects of the study are rocks of Badenian age which are oil-bearing rocks for most of the oil found in the Pannonian basin. They are the object of this study and of major importance as the outcrops at the locality of “Bukova glava” have been found on the surface.

Acknowledgements

We would like to express our deep regards to Professor Josipa Velić for her contribution and conceptual support as well as help and guidance given during this whole project.



References

Krkalo, E. (1998). Ležišta neogenskih kvarcnih pijesaka u rubnim područjima slavonskih planina (Hrvatska), Institut za geološka istraživanja.

Zečević, M. (2008). Naftnogeološko značenje, paleoekologija i biostratigrafija badenskih taložina sjevernih obronaka Krndije, Doktorska disertacija. Rudarsko-geološko-naftni fakultet.



Crustal-scale buckling and associated crustal flow – lessons from analogue modeling

Ondrej Kryza¹, Ondrej Lexa^{1,2}, Karel Schulmann^{2,3}, Denis Gapais⁴, Alexandra Guy⁴,
John Cosgrove⁵

email: kryza@natur.cuni.cz

¹Institute of Petrology and Structural Geology, Charles University in Prague, Albertov 6, 128 43, Czech Republic

²Czech Geological Survey, Centre for Lithosphere Research, Klarov 3, 118 21 Prague 1, Czech Republic

³Université de Strasbourg, IPG-EOST, UMR 7516, 1 Rue Blessig, Strasbourg 67084, France

⁴Géosciences Rennes, UMR 6118 CNRS, Université de Rennes 1, 35042 Rennes cedex, France

⁵Department of Earth Sciences and Engineering, Imperial College, London, Prince Consort Road, UK

Introduction

Recent structural and geophysical observations from central Asia show that the crustal-scale buckling of Mongol-Okhotsk subduction zone was accompanied with heterogeneous thickening of adjacent crust and deformation of lithospheric mantle. In order to simulate processes related to this oroclinal bending and deformation of surrounding lithosphere we present a complex analogue model of buckling of vertically layered domain which is surrounded by horizontally anisotropic material.

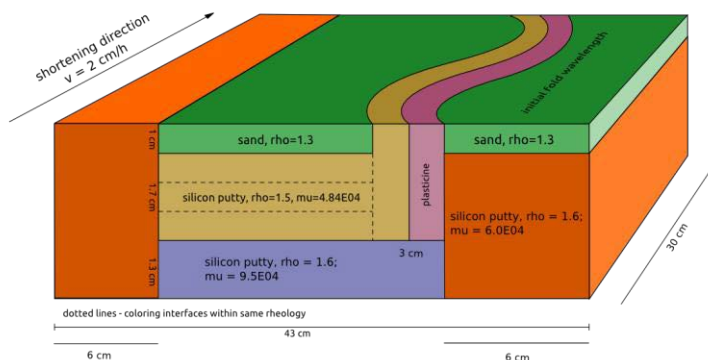
Model setup

In our experiments we used 43/26/4 cm (width/length/height) modeling domain and one sided piston mechanism. Modeled domain is formed by several layers oriented along two principal directions (see fig. 1A). Central part is formed by two vertical and gently arcuated ductile layers oriented parallel to the shortening direction. This subdomain is situated next to horizontal two-layer (brittle/ductile) segment which is located also in the central domain part. Both subdomains lies at the ductile mantle layer (supported by high viscosity material) and representing a space of future full length fold amplification. This structures are also embedded in ductile material of variable viscosity to suppress negative influence of lateral boundary conditions. For investigation of brittle deformation in both directions of fold propagation (in front of and behind the indenting fold hinges) we covered a surrounding material - between vertically oriented subdomain and the side wall of the modeling box – by sand layer of the same thickness as in central domain part.

Model materials

Materials and geometry of the model are scaled according to standard analogue modeling principles (Brun, 2002; Ramberg, 1981; Hubbert, 1937). Upper crustal layer is formed by Fontainebleau sand with specific and well-known material properties (Cagnard, 2006; Brun, 2002). Ductile lower crust and vertical „weak” layer are represented by silicone putty of same and relatively low viscosity, while upper mantle layer is represented by high viscosity silicone. For the most competent vertical layer (buckling controlling layer), we used high viscosity plastic layer which could be imagined like embedded boundary condition. Curvature of this driving layer also representing initial condition of experiment because deformation is significantly sensitive to shape of driving layer and initial strain-rate depend on this parameter. It should be noted that all used silicone putties are Newtonian materials deformed at constant temperature.

A)



B)

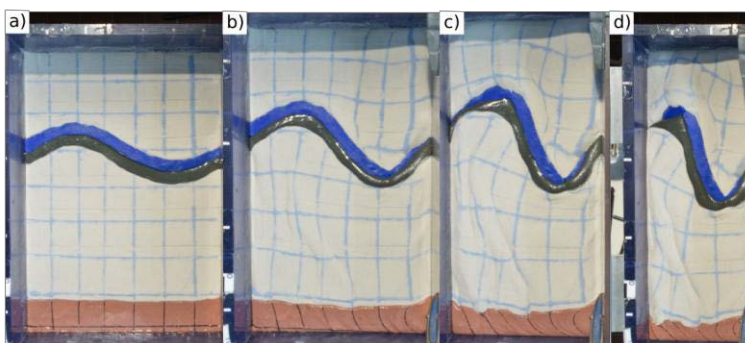


Figure 1 A) Setup of experiments and model domain geometrical propositions. B) Example of model domain evolution during different stages of shortening a) – d) 0%, 17%, 34% and 50%.

Results and discussion

Following evolutionary trends were commonly observed (see fig. 1B): 1) Amplification of main fold, indentation of its hinges into surrounding subdomains and propagation of brittle deformation behind the fold arcs which is associated with opening of a new space for deeper material redistribution. This brittle deformation is represented by forming of a thrust and strike-slip systems of perpendicular orientation respective to shortening direction of the entire domain. Because of pure-shear deformation geometry and vertical thickening of horizontal layers, the fold amplification is relatively smaller due to resistance of the central domain. 2) This implies slowing down of an amplification of main fold in latest evolution stages and rapid propagation and amplification of all vertically oriented perturbations in whole domain (pure shear dominant stage). 3) The indentation of central domain is compensated by lower crustal horizontal flow in opposite direction. 4) Exhumation of both fold hinges and torsion in inflection point because of a free-surface boundary condition. 5) The mantle material is filling the region beneath and after the propagating fold hinge. This implies rapid exhumation of mantle material in combination with vertical thickening.

Conclusions

We suggest that our model may simulate the folding of Mongol-Okhotsk subduction zone together with ribbon continent and deformation of adjacent oceanic crust during Asain Paleozoic orogeny. The model is set up to explain mechanical behavior of surrounding crust, its thickening, horizontal flow of deep crust and deformation of lithospheric mantle. The results are discussed in the frame of current tectonic models of Central Asian Orogenic Belt.



References

Brun J.-P. (2002) Deformation of the continental lithosphere: Insights from brittle-ductile models. *Geological Society, London, Special Publications*; v. **200**; p. 355-370.

Cagnard F., Brun J.-P., Gapais D. (2006) Modes of thickening of analogue weak lithospheres. *Tectonophysics*, **421**, 145–160.

Hubbert, K. (1937) Theory of scale models as applied to the study of geological structures. *Geological Society of America Bulletin*, **48**, 1459-1520.

Ramberg H. (1981) Gravity Deformation and the Earth Crust. *Academic Press*, London and New York.



Geological compass vs. mobile applications

Paulina Kotlarek, Jacek Piotr Kubalski
e-mail: pa.kotlarek@gmail.com,
Adam Mickiewicz University

Summary

"Geological compass vs. mobile applications" is a project that aimed to test the geological compass applications, available for smartphones and tablets, including the evaluation of their performance during use in mountainous terrain as well as in the laboratory. The intention of the test was to compare measurements made by Samsung GT-S6310 and HTC One S with traditional geological compasses by Freiberg and Krantz. Field studies were conducted in different weather conditions in The Tatra Mountains.

Introduction

Nowadays traditional mapping methods go to rest. Even one of the main geological instruments (among a hammer, maps, pencils and so on), which is geological compass can be replaced by a smartphone with the appropriate software.

At the moment, each smart phone user has easy access to free and paid applications that advertise themselves as an alternative to geological compass. In addition to the measurement of spatial orientation of rock layers and tectonic structures those applications allow to simultaneously record GPS coordinates, create maps and to generate stereographic projections. At issue is the reliability of these measurements.

Method

Traditional compasses are able to determine north and south due to the magnet's interaction with the Earth's magnetic field. Smartphones do have a small magnetometer, which can measure the Earth's magnetic field. The component that handset makers are exploiting to make these feats possible is the three-axis magnetometer. The sensor system's job is to home in on Earth's magnetic field and use that as a reference for determining the handset's orientation along the x-, y-, and z-axes. Three axes are important because that third sensor allows the handheld device to correct for the orientation of Earth's magnetic field at a given location, as well as the relative position of the device. GPS receivers can also be used as compass but due to harsh terrain, often covered with forest it is useless.

This information is combined with an accelerator inside the phone. The accelerator gets information regarding the phone's position in space. It is able to pinpoint the phone's position from solid-state sensors within the phone that can measure their tilt and movement. The information provided by these devices mean that the compass applications can display cardinal directions no matter which orientation the phone is in, according to the algorithmic software.

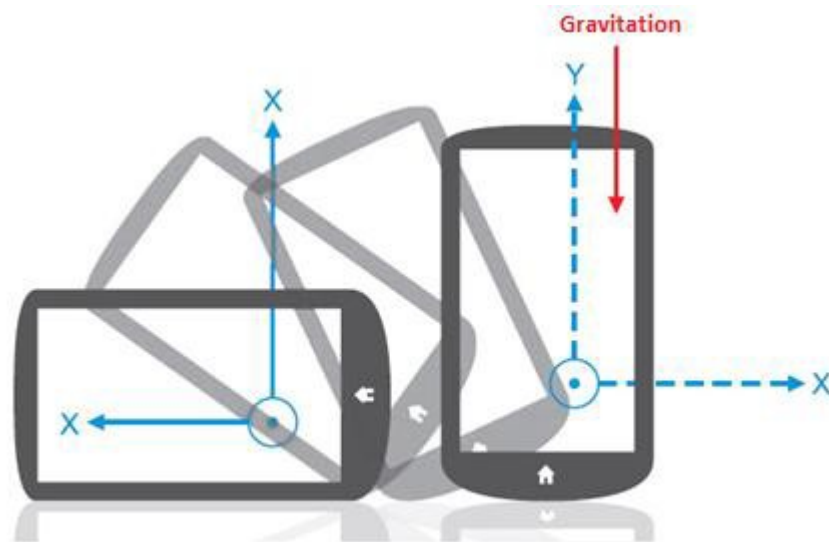


Figure 1 Example of how smartphone magnetometers work.

Based on this properties and high precision of smartphones measurements of spatial orientation of rock layers and tectonic structures applications was conducted. During the study, a series of measurements was made with traditional geological compasses (Freiberg and Krantz) and smartphones (Samsung GT-S6310 and HTC One S). Test took into account two applications: RockLogger and FieldMove Clino. It was assumed that the most proper measurements were made by Freiberg compass and constitutes basis for comparison.

Acknowledgements

Assistance provided by Aleksandra Redlińska - Marczyńska was greatly appreciated. Special thanks are extended to the staff of Tatra Mountains National Park.



Development of *Favosites bohemicus* (Tabulata) on soft and unstable sediments covering slopes of the Emsian Kess-Kess mounds of Hamar Laghdad (Morocco)

Jan J. Król¹

email: jan.jozef.krol@amu.edu.pl

¹ Adam Mickiewicz University in Poznań

Summary

Favosites bohemicus, tabulate coral colonies coming from the Hamar Laghdad area have been studied in respect to their growth patterns and colony development. They settled largely on the relatively steep slopes of the Emsian Kess-Kess mud mounds, which have been subsequently covered by soft, muddy sediment. It has been analyzed how the sediment creeping down the slope affected the coral colonies and how they responded to such conditions.

Introduction

Kess-Kess mud mounds are conical carbonate build-ups cropping out in the Hamar Laghdad mountain range of the eastern Anti-Atlas. They were formed around hydrothermal vents, where carbonate mud precipitated from the mixture of hydrothermal fluids and seawater (Bełka, 1998). The mounds developed in a relatively deep, low energy environment, below fair weather wave base. Corals settled numerously on their steep (commonly about 50°), muddy, unstable slopes (Brachert *et al.*, 1992; Berkowski, 2012). Favositids and other tabulate corals are known to had developed different strategies for settling and survival on a soft bottom (see: Seilacher & Thomas, 2012). However, it has not yet been studied, how they could survive on a steeply inclined surface, covered by soft, unstable substrate, where mass movements have to be taken into account.

Methods

Coralla of *F. bohemicus* were collected from the Emsian marls of the Hamar Laghdad area, covering the mud mounds and their vicinity. Specimens were cut longitudinally, polished and lacquered, to give a good picture of the growth patterns and development of each individual colony. Additionally, thin sections have been made from selected samples, to investigate the growth of specimens in greater detail.

Results

Studied coralla are massive, but display a strong variability in shape and size. Most of the specimens are of spherical and sub-spherical shape, but conical coralla are common as well. The most distinguishable feature of every collected corallum is that its growth is either tilted in one direction (Fig. 1A) or it displays signs of being continuously turned (Fig. 1C-D). The latter is the case for the smaller coralla (a couple centimetres in diameter). It is also noteworthy, that the studied corals commonly settled on the skeletons of other organisms, (i.e. other tabulate coralla, solitary rugose corals or crinoids (Fig. 1A-B). Some of the specimens display a flat base, an adaptation against sinking in the soft sediment. Other had their lower part submerged, acting as a sort of an anchor for the colony (Fig. 1B)(cf. Seilacher & Thomas, 2012).

Conclusions

The tilted direction of growth of the colonies was likely caused by the slow creeping of the sediment down the slope. The colonies were being slowly moved along with it (cf. Berkowski, 2012). Considering the sediment "pushing" the colony towards the base of a mound, it is likely that the corals did not grow towards the summit but rather in the opposite direction, where there was more space

available. That could cause shifting of the center of gravity of a colony, which would lead either to its toppling or turning. Larger colonies could use their mass to their advantage, stabilizing themselves with the lower part of the corallum sunk into the sediment. However, this was not possible on the steeper slopes. Colonies which settled on the steepest parts of the mound would be turned or toppled more easily. When a coral colony passed a certain critical point in mass and size, it would lose stability. For that reason the *F. bohemicus* colonies settled on the steeper slopes were generally smaller than the corals settled on a gentler one. A colony growing on a steep slope could roll downhill and survive, if it was stopped at a favourable spot (Fig. 1C). Although, it is important to mention, that such movement could not be abrupt, but rather slow and steady. However, more often than not, a tabulate colony, especially with its growth tilted towards the base of the mound, would be toppled and not survive. Therefore it is inferred that the slope inclination was the main factor controlling the growth of *F. bohemicus* colonies settled on soft substrate.

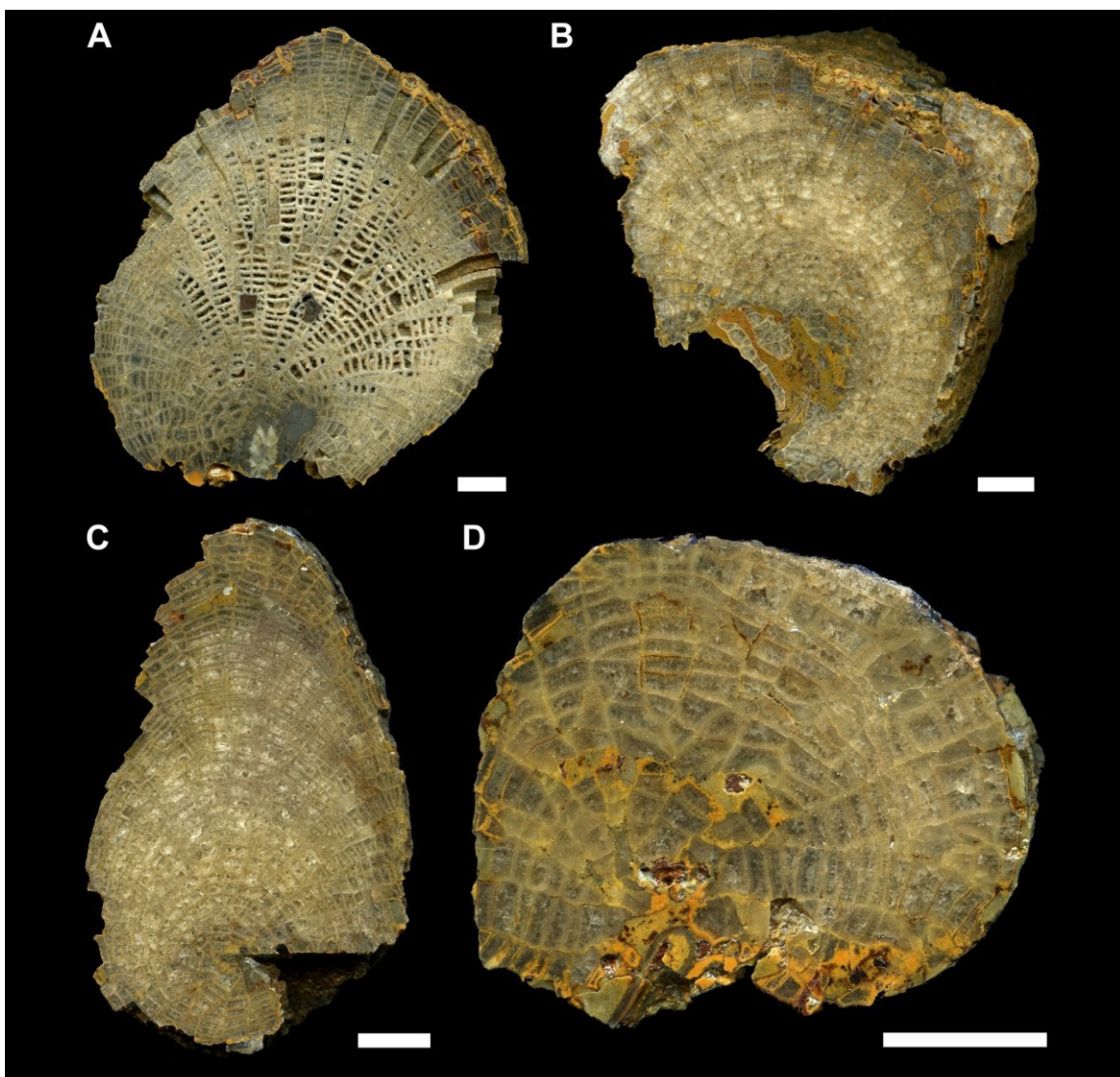


Figure 1 Lacquered slabs of *Favosites bohemicus* colonies. A-B: Colonies settled on skeletons of other corals. C-D: Colonies affected by turning. All scale bars are 1 cm.



References

Belka, Z. (1998). Early Devonian Kess-Kess carbonate mud mounds of the eastern Anti-Atlas (Morocco), and their relation to submarine hydrothermal venting. SEPM.

Berkowski, B. (2012). Life strategies and function of dissepiments in rugose coral *Catactotoechus instabilis* from the Lower Devonian of Morocco. Polish Academy of Sciences.

Brachert, T. C., Buggisch, W., Flügel, E., Hüssner, H. M., Joachimski, M. M., Tourneur, F., and Walliser, O. H. (1992). Controls of mud mound formation: the Early Devonian Kess-Kess carbonates of the Hamar Laghdad, AntiAtlas, Morocco. Springer.

Seilacher, A. and Thomas, R.D.K. (2012). Self-organization and emergent individuality of favositid corals adapted to live on soft substrates. Wiley-Blackwell.



Late Quaternary sea level effects on coral reef evolution and growth in Southern Kimberley, North West Australia.

Giada Bufarale¹, Lindsay Collins, Michael O'Leary, Alexandra Stevens, Moataz Kordi, Tubagus Solihuddin

email: giada.bufarale@postgrad.curtin.edu.au

¹ Curtin University

Summary

High resolution shallow seismic studies were conducted on various reefs in the southern Kimberley region to evaluate stratigraphic evolution, interaction with different substrates, morphological patterns and distribution. The new datasets demonstrated that large scale processes (pre-existing Proterozoic foundation, Quaternary sea level oscillations and subsidence) have interplayed with the modern ecological conditions (macrotidal systems, high turbidity and tropical monsoonal climate) and significantly influenced the onset and growth of a prolific coral reef system, both along the coast (inshore reefs) and over the mid-shelf and continental shelf edge (offshore reefs).

Introduction

The Kimberley coast is located along the continental margin of northwest Australia and is characterised by a unique and complex geology, geomorphology and marine environment, significantly influenced by macrotides (up to 11 m), which result in extensive intertidal zones, where atypical coral reefs proliferate (Figure 1). Due to the complexity, inaccessibility and size of the region, a combination of satellite and aerial remote sensing, high-resolution shallow seismic surveys, reef coring and radiocarbon dating represented the most effective method to determine the internal reef architecture and morphostratigraphic evolution of selected Kimberley reefs.

Methods and Theory

About 300 km of seismic profiles were collected using a boomer SBP system in order to assess the growth and the internal stratigraphy and architecture of a dozen high value reefs. Acoustic datasets were calibrated with the information provided by the Cockatoo Reef study (Solihuddin et al., 2015) and a petroleum exploration well drilled in 1982, on the northern tip of Adele Island (Ingram, 1982; Marshall, 1995) were used to produce a classification scheme developed for the specialised, macrotidal reefs in the southern Kimberley. Vertical and lateral differences were identified and categorised according to their shape and acoustic reflection characteristics along the hiatuses and internal reflectors.

The datasets assisted in providing a better understanding of Quaternary reef growth. The pre-existing substrate has influenced the successive morphology of fringing reefs, intertidal platforms and platform reefs. Global sea level change, controlled by ice age fluctuation events, provides a signal which is recorded in successive stages of reef growth separated by hiatuses. Two acoustic reflectors can be consistently distinguished across the inner shelf reefs (Sunday Group, Buccaneer Archipelago and Montgomery Reef), marking the boundaries between Holocene reef (Marine Isotope Stage 1, MIS1, last 12,000 years) commonly 10-15 m thick, and MIS 5 (last 125,000 years) and an ancient Neoproterozoic rock foundation over which Quaternary reef growth occurred. Three acoustic horizons characterise the offshore reefs (Adele complex, Figure 1), highlighting multiple reef building stages.

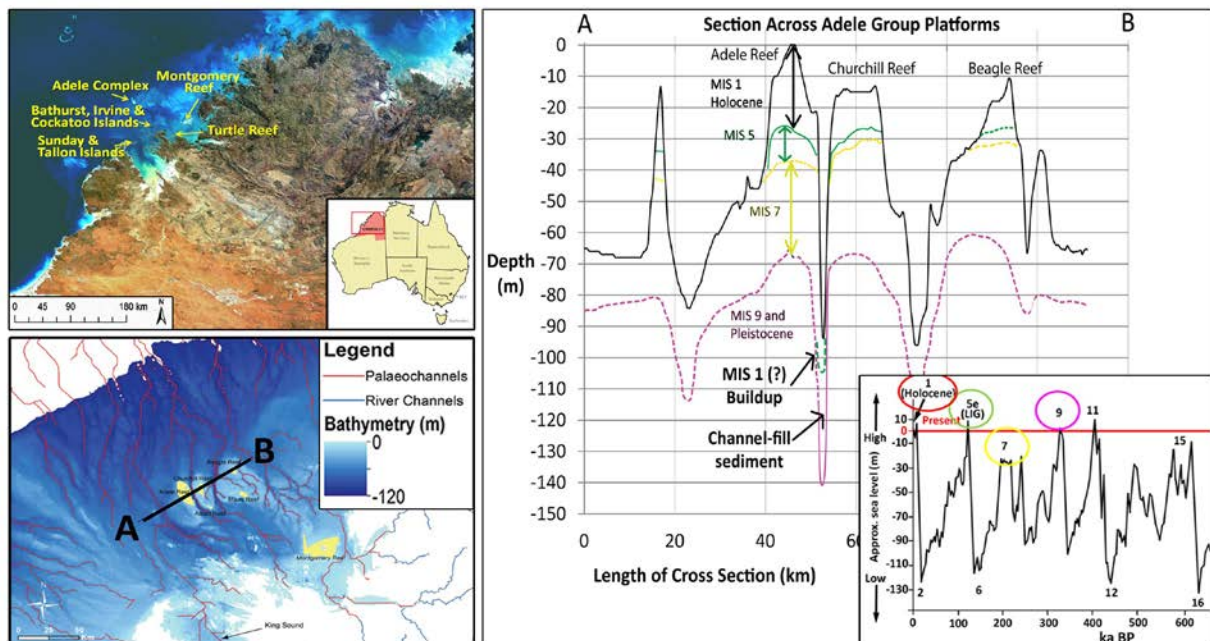


Figure 1 Top left corner: satellite view of the Kimberley (image from Geoscience Australia) showing the studied reefs. Right side: schematic representation of a cross section across Adele complex. Reef building events are vertically stacked within the reefs as repeated platform growth has occurred during sea level highstands (MIS 1, 5, 7, 9; see inset sea level curve, bottom right corner, modified after Berger, 2008), as interpolated from seismic data. Bottom left corner: palaeochannels incised by rivers during sea level lowstands, which separates the platforms (modified after Bufarale et al., in review).

Conclusions

The study represents the first analysis of Kimberley reef growth and demonstrates that Kimberley reefs are significant geological structures where the Holocene reef growth commenced over antecedent highs (Proterozoic rock foundation or older fossil reefs). The reef growth occurred during past interglacial periods (at least 3 stages of growth offshore, 2 onshore), defeating challenging environmental conditions and oscillating sea levels.

A fuller account will be published in Marine Geology.



References

Berger, W.H., 2008. Sea level in the late Quaternary: patterns of variation and implications, *International Journal of Earth Sciences* 97 (6), 1143-1150.

Bufarale, G., Collins, L.B., O'Leary, M.J., Stevens, A. M., Kordi, M., Solihuddin, T., in review. Geomorphology, internal architecture and growth patterns of macrotidal reefs of the Kimberley Biozone, Northwest Australia. *Marine Geology*.

Ingram, B.S. (1982). Palynological examination of samples from Adele Island No. 1 from Well Completion Report, Brunswick Oil N.L.

Marshall, N.G. (1995). Adele Island No. 1 Palynological Report. Woodside Offshore Petroleum.

Solihuddin, T., Collins, L.B., Blakeway, D., O'Leary, M.J. (2015). Holocene Reef Growth and Sea Level in a Macrotidal, High Turbidity Setting: Cockatoo Island, Kimberley Bioregion, Northwest Australia. *Marine Geology*. Volume 359, pp 50–60

The relation of structural and petroleum geology – a case study from the Pannonian Basin, SW Hungary

Rebeka Oross¹, János Csizmeg², Imre Szilágyi^{1,3}, Lilla Tőkés¹
 email: orossrebeka@gmail.com

¹Eötvös Loránd University, ²Hungarian Horizon Energy Ltd., ³MOL Hungarian Oil and Gas Plc.

Summary

The study area is an important hydrocarbon bearing territory where all of the identified petroleum fields are related to structural features. Beside the Alp-Carpathian evolution of the Pannonian Basin in the Cretaceous the area's deformation is a Neogene phenomenon with three different deformation phases. By the interpretation of seismic surveys reactivation of basement thrusts, normal faults and a dextral strike-slip fault with an advanced Riedel fault system can be recognised, which have important roles in the development of the area's petroleum system.

Introduction

The Drava Basin is situated in the southwest part of the Pannonian Basin, on the border of Croatia and Hungary (Figure 1). This is a deep half-graben structure filled with 5-7 km thick Neogene sediments. The basin has a productive hydrocarbon system with multi-level Miocene source rocks, the reservoirs are known within the Miocene basin filling sedimentary sequences and the pre-Neogene basement as well. The traps are mainly related to structural features (Safic et al., 2003).

The study area is covered with a 3D and several 2D seismic surveys and there are numerous boreholes, which were drilled in purpose to produce hydrocarbons. There is a big basement anticlinal structure (Görgeteg-Babócsa High) in the territory, which was one of the main target of the oil companies. Besides of this structure there are several smaller basement highs as well. My study deals with the structural development of these anticlines and the effect of other younger deformations to petroleum bearing sediments, migration and trap formation.

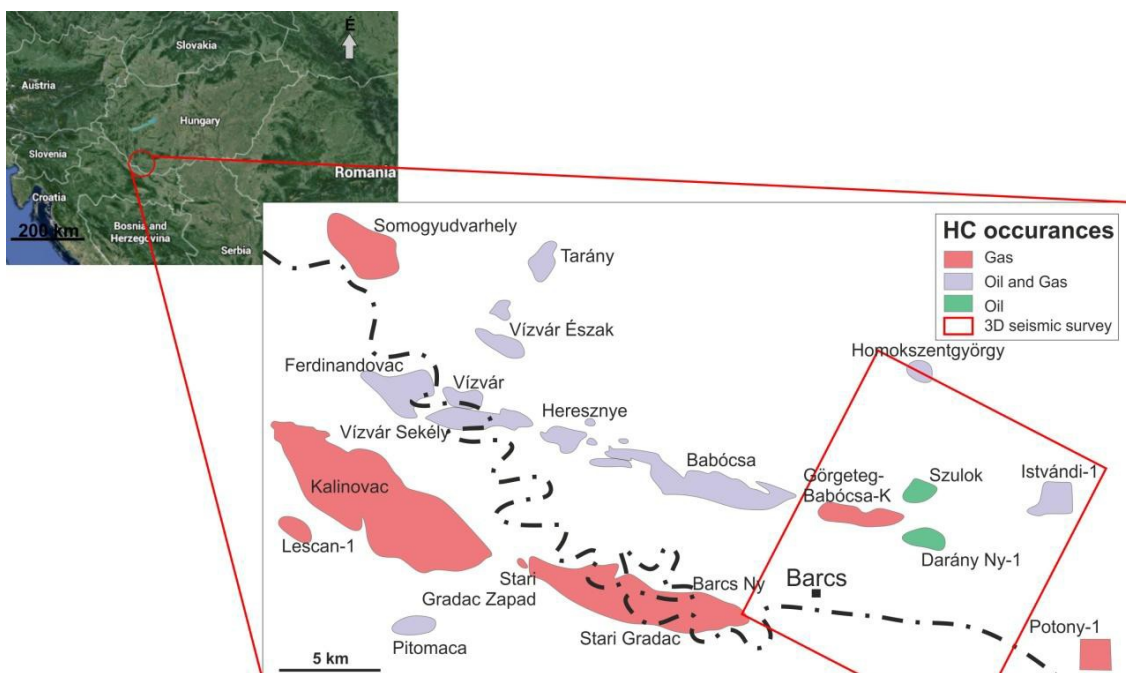


Figure 1 The geographical location of the study area and the related hydrocarbon fields



Method

The aim of the research is to gain accurate knowledge of the structural elements of the Drava Basin by interpreting a 3D and several 2D seismic surveys. To get more information I also used the data of wells drilled in the area and the geophysical logs measured in them. For better interpretation and illustration I also made some seismic attributes from the 3D survey (chaos, variance, antrack, coherence). To prepare these attributes I used Petrel software, and IHS Kingdom software for the seismic and well log interpretation.

Examples

The interpretation of the seismic surveys both in amplitude or antrack attribute maps and section give the same results. In nearly all time slices show normal faults with NNW-SSE strike. These faults are located mainly in the NE part of the study area and they follow each other in a definite way. The antrack attribute map shows that the previously mentioned normal faults with NNW-SSE strike may be related to a dextral strike-slip fault as Riedel fractures.

The stress field which could create the strike-slip fault and the related Riedel faults are ENE-WSW extension and perpendicular compression. A simplified fault pattern can be seen in figure 1. The data are from the seismic surveys this is the reason the dips of the presented faults in the stereogram are not presented. The time of this strike slip fault must be very young, neotectonic, as the faults cut through the whole sedimentary sequence of the basin.

Conclusion

The structural development of the Drava Basin is a little bit different from the other parts of the Pannonian Basin. The deformation of the study area can be divided into three main part. First the basement thrusts reactivated during the early Middle-Miocene, around 10 Ma. The second phase can be detected in normal faults which go up to the shelfslope sediments, so the timing should be around 6 million year (after Magyar et al., 2013). The dextral strike-slip fault and the Riedel faults are related to a neotectonic event which is still in progress in the area. The development of hydrocarbon traps is mainly related to the first tectonic phase, while the second phase faults could be rather the main migration pathways for the accumulation of the oil and gas fields.

Acknowledgement

I owe grate thank to Hungarian Horizon Energy Ltd and MOL Plc for the data. My supervisors, Imre Szilágyi and János Csizmeg helped me a lot during my work, I also gained huge support from László Fodor and Lilla Tőkés. I would like to say thanks for MOL Group and the Department of Physical and Applied Geology of the Eötvös Loránd University for supporting me financially to take part in the conference.



References

Magyar, I., Radivojevic, D., Sztanó O., Synak, R., Ujszászi, K., Pócsik, M. (2013). Progradation of the paleo-Danube shelf margin across the Pannonian Basin during the Late Miocene and Early Pliocene. *Global and Planetary Change*, vol. 103, p. 168-173.

Saftic, B., Velic, J., Sztanó, O., Juhász Gy. and Ivakovic Z. (2003). Tertiary Subsurface Facies, Source Rocks and Hydrocarbon Reservoir in the SW Pannonian Basin (Northern Croatia and South- Western Hungary). *Geologica Croatica, Zabreb*, vol. 56/1, p. 101-122.

TECHNICAL SESSIONS

SCHEDULE - poster presentations



GEOLOGY

MONDAY, 13 July, 16:30-17:30

Personal attendance required

The Distributions Of Plio-Quaternary Sediments In The Inner Cilicia Basin	Canan Cifti, Mahmut Okyar
GIS-based Morphometric Characterisation of Alluvial Fans in Northern Oman	Annette Leuschner, Frank Mattem, Stephan van Gasselt
Sandstone Provenance in Alci Basin SW of Ankara, Turkey	Barbaros Demircan
The Distribution of Terrigenous Organic Matter of Mungaroo Formation, in North Carnarvon Basin	Niu Xing
Petrographic investigations of materials used in Gothic church tabernacle from the St. Elisabeth's Church, Wrocław, Poland	Mateusz Szadkowski, Katarzyna Zbońska
Microfacies and sea level fluctuation analyses of the uppermost Jurassic and Lower Cretaceous deposits in the Carpathian basement in the Ropczyce area	Tomasz Krogulec
Physical and geochemical fluctuations of mineral springs in Slanic Moldova ,Romania	Diana Hughineata
Mineralogical, geochemical and textural characterisation of siliciclastic deposits of Ulmet Valey, Romania	Ungureanu Constantin
Mid-Late Holocene evolution of a carbonate-clastic barrier bank, during changing sea levels (Shark Bay, Western Australia)	Giada Bufarale, Lindsay Collins
Sedimentary Facies Analysis, Cyclicity and Reservoir Characterization of the Northeastern Offshore Nile Delta (Ha'py Field Case Study)	Nada Amer, Darwish M., El Barkooky A., Sharaf E.
Foraminiferal distribution in a tropical meso-tidal estuary on the south east coast of Nigeria	Victoria I. Antia, CHimezie N. Emeka, Etie B. Akpan, Edak E. Efiom
Growth and evolution of syn-sedimentary deltaic faults in Tomboy Field, Niger Delta	Omosanya K.O., Lawal, M.A, Kaigama, U.
Subsurface structure of the saline hot spring in Krabi, Southern Thailand, from an integrated geoscientific investigation	Wipada Ngansom, Helmut Dürrast
Chemical and textural variability within the Adamello tonalites: Implications for melt extraction from crystal mush	Alina Fiedrich, Olivier Bachmann, Chad Deering, Peter Ulmer
Primary results on geochemistry of copper slags from Kondratów and Leszczyna, SW Poland	Katarzyna Kądziołka, Jakub Kierczak
Design of inexpensive fluid flow cell for testing multiple rock parameters	Petr Lebedev, Bryce Teo



The Distributions Of Plio-Quaternary Sediments In The Inner Cilicia Basin

Canan CIFTCI¹ and Mahmut OKYAR¹
cananciftci@sdu.edu.tr

¹Suleyman Demirel University, Engineering Faculty, Department of Geophysics, West Campus 32260
Isparta/TURKEY

Summary

The Cilicia basin is a Neogene depocenter located between the Turkey and Cyprus in the eastern Mediterranean. Due to its natural structure, Cilicia Basin has been subject of several investigations from past to present. In this study, the distributions of sediments accumulated during the Plio-Quaternary in the basin were interpreted from the seismic reflection data that obtained with permission from the Turkish Petroleum Corporation. Thickness map was prepared with the average velocity of 1700 m/s based on previous studies. According to the interpretation results, the thickness of Plio-Quaternary sediments in the basin ranges from 235 m to 2170 m.

Introduction

The Cilicia basin is an arcuate and elongate Neogene depocenter located between the Turkey and Cyprus in the eastern Mediterranean. It has been formed since the mid to late Miocene by the effect of subduction of the African plate beneath the Anatolian plate along the Cyprus arc (Biju-Duval et al., 1978). The Cilicia basin can be divided into E-W trending deeper Outer Cilicia basin in the west and a NE-SW trending shallower Inner Cilicia basin in the northeast (Aksu et. al., 2005a). The study area lies between about 34°-35° E longitude and 36°-37° N latitude in Inner Cilicia basin (Fig.1).

Seyhan, Ceyhan, Tarsus and Göksu Rivers are the four rivers that provide most of siliciclastic material into the basin (Aksu et al., 2005a,b; Bridge et al., 2005; Burton-Ferguson et al., 2005; Hall et al., 2005) (Fig. 1). In the Cilicia Basin the continental shelf is ≤ 5 km wide, but widens considerably to > 45 km off the mouths of present day deltas (Aksu et al., 2005a).

In this study, we aimed to study the distributions of sediments, accumulated during the Plio- Quaternary in the basin. We used seismic data obtained from the Turkish Petroleum Corporation.

Method

Migrated air gun seismic reflection profiles were interpreted using the seismic stratigraphic methods explained by Vail et al. (1977). Thickness map was prepared by using the average velocity of 1700 m/s based on previous studies (Aksu et al., 2005a). The bathymetric data were provided by the Global Data Explorer USGS.

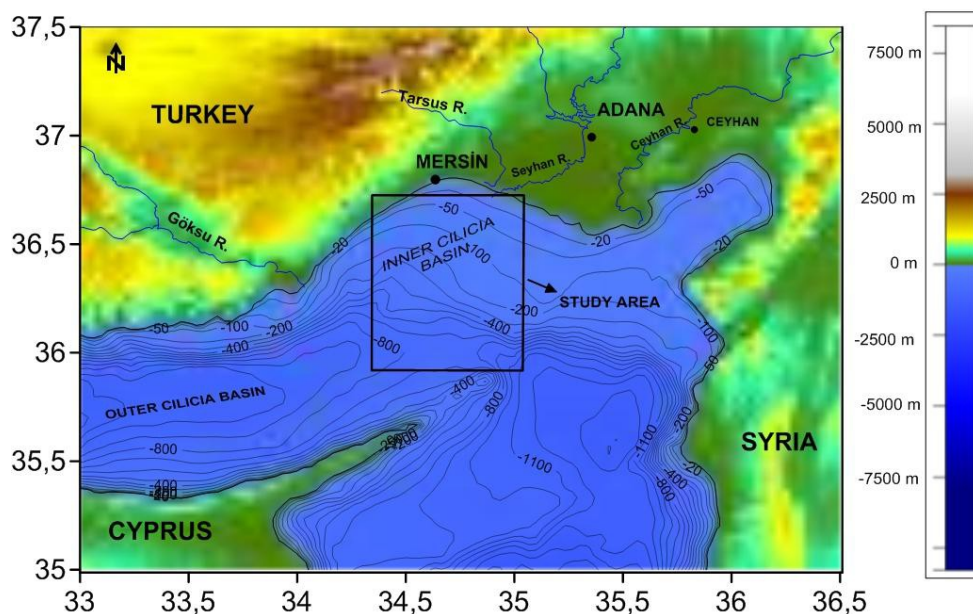


Figure 1 Bathymetric map of the study area and its surrounding.

Conclusions

Two different reflective characters were determined by the interpretation of seismic profiles in the Plio-Quaternary sedimentary unit. The first; regular, strong and continuous reflection package and the second; weak, discontinuous and parallel reflection package that lies at the base of the Plio- Quaternary successions in the basin. The thicknesses of sediment range from 235 m to 2170 m. Central part of the study area is marked by the thick sedimentary cover, this may reflect greater sediment input to the basin from the Tarsus, Seyhan, Ceyhan and Göksu Rivers (Fig. 2).

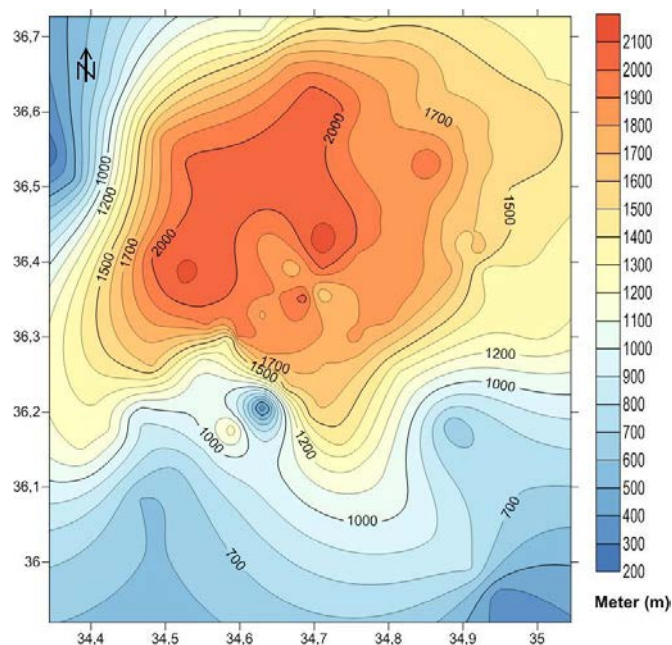


Figure 2 The distribution of Plio-Quaternary sediments as meters in the study area.



References

Aksu, A.E., Calon, T.J., Hall, J., Mansfield S., Yaşar D. (2005a). The Cilicia–Adana basin complex, Eastern Mediterranean: Neogene evolution of an active fore-arc basin in an obliquely convergent margin. *Mar. Geol.* 221, 121–159.

Aksu, A.E., Calon, T.J., Hall, J., Burton, R., (2005b). Origin and evolution of the Neogene Iskenderun Basin, Northeastern Mediterranean Sea. *Mar. Geol.* 221, 161–187.

Biju-Duval, B., Letouzey, J., Montadert, L. (1978). Structure and evolution of the Mediterranean Basins. In: (K Hsü, Montadert, L. et al., editors), *Initial Reports of the Deep-Sea Drilling Project*, Washington, D.C.: U.S. Govt. Printing Office, Bull., 42(1), 951-984.

Bridge, C., Calon, T.J., Hall, J., Aksu, A.E. (2005). Salt tectonics in two convergent margin basins of the Cyprus Arc, northeastern Mediterranean. *Mar. Geol.* 221, 223–259.

Burton-Ferguson, R., Aksu, A.E., Calon, T.J., Hall, J., 2005. Seismic stratigraphy and structural evolution of the Adana Basin, Eastern Mediterranean. *Mar. Geol.* 221, 189–222.

Hall, J., Aksu, A.E., Calon, T.J., Yaşar, D. (2005). Varying tectonic control on basin development at an active microplate margin: the Iskenderun - Latakia Basin complex, Eastern Mediterranean. *Mar. Geol.* 221, 15–60.

Vail, P.R., Mitchum, Jr. R.M. (1977). Seismic Stratigraphy And Global Changes of Sea Level Part 1. In: (C.E. Payton, Editor). *Seismic Stratigraphy Applications To Hydrocarbon Exploration*, Am. Assoc. Petrol. Geol. Mem., 26 Tulsa Oklahoma, 51-52.

<http://gdex.cr.usgs.gov/gdex/>



GIS-based Morphometric Characterisation of Alluvial Fans in Northern Oman

Annette Leuschner¹, Frank Mattern², Stephan van Gasselt¹
email: a.c.leuschner@fu-berlin.de

¹Freie Universitaet Berlin, Department of Earth Sciences, Institute of Geological Sciences, Germany,
²Sultan Qaboos University, Department of Earth Sciences, Oman

Summary

The morphology of alluvial fans is a product of fluvial deposition and environmental control which are both subject to various environmental factors (Harvey 2002). The aim of our study is to reconstruct the morphologic evolution of alluvial fans and relate morphology to past and present climate conditions. By using remotely-sensed satellite imagery and digital elevation models, quantitative morphologic parameters can be derived from spatial analysis by semi-automatized procedures. We compared our results to data from other locations in different climate zones which allows us to constrain environmental boundary conditions and their potential influence on morphology and shape.

Introduction

For a better understanding of the potential impact of climate variations on landforms and deposits, it is essential to understand the relationships between climate variability, water cycles and geomorphic processes. Numerous geological records at different locations document important changes in climatic conditions during the Quaternary and are important tracers for assessing past climate conditions (Blechsmidt et al. 2009). In this context, alluvial fans can be considered as prime targets as they are a product of fluvial erosion, transportation and deposition and are considered sensitive to changes in environmental conditions which directly affect their formation and morphology (Bull 1977; Harvey 1997). In this study we try to assess the morphological evolution and relate it to past and present climate conditions of a now arid environment. In order to achieve this, we first characterize alluvial fans based on their climatic settings and conditions and classify them accordingly using satellite image data and digital elevation models.

The Oman Mountains are famous for the world's largest intact and best exposed obducted ophiolite complex, the Semail Ophiolite (Robertson, et al 1990) and have been selected as a study area because of their extent, accessibility and distinct climate characteristics (Fig. 1). They are today subject to a desert climate (Bwh), influenced by the Indian Ocean but they have experienced extensive pluvial periods in the geologic past. Formation of alluvial fans was, therefore, likely triggered by the interplay of increased sediment production caused by high rainfalls with enhanced erosion of hillslopes and transport rates during extensive periods of precipitation (Blechsmidt et al. 2009).

Approaches

An analysis of hydrodynamic parameters considered important for alluvial fan genesis was conducted using remote-sensing datasets. For mapping of different alluvial fan bodies freely available digital datasets of the Landsat Enhanced Thematic Mapper (ETM+) (NASA Landsat Program, 2003) with a spatial resolution of 15–30 m/px were processed and used. For the detection of morphometric parameters as input data for subsequent hydrological studies digital terrain model data of the Shuttle Radar Topography Mission (SRTM) (Shuttle Radar Topography Mission, 2004) with a geometric resolution of 3 arcsec (corresponding to roughly 90 m/px), was employed. A pre-assessment was conducted using analog data records. All data were integrated, filtered and pre-processed and analysed within the commercial GIS package ArcGIS 10.2.

The main focus of these investigations was put on the identification of morphological characteristics, i.e. individual morphometries. These include *direct* measurements of fan sizes and their slope angles, but also *indirectly* measured parameters such as sizes of drainage basins, networks or transport areas as derived from spatial semi-automatic procedures. Flow directions and flow accumulation were calculated in order to delineate the drainage basins. Channels were derived from the flow accumulation data and visually matched with channels that can be identified in satellite imagery. A contributing drainage area threshold of 16.2 km² was considered appropriate.

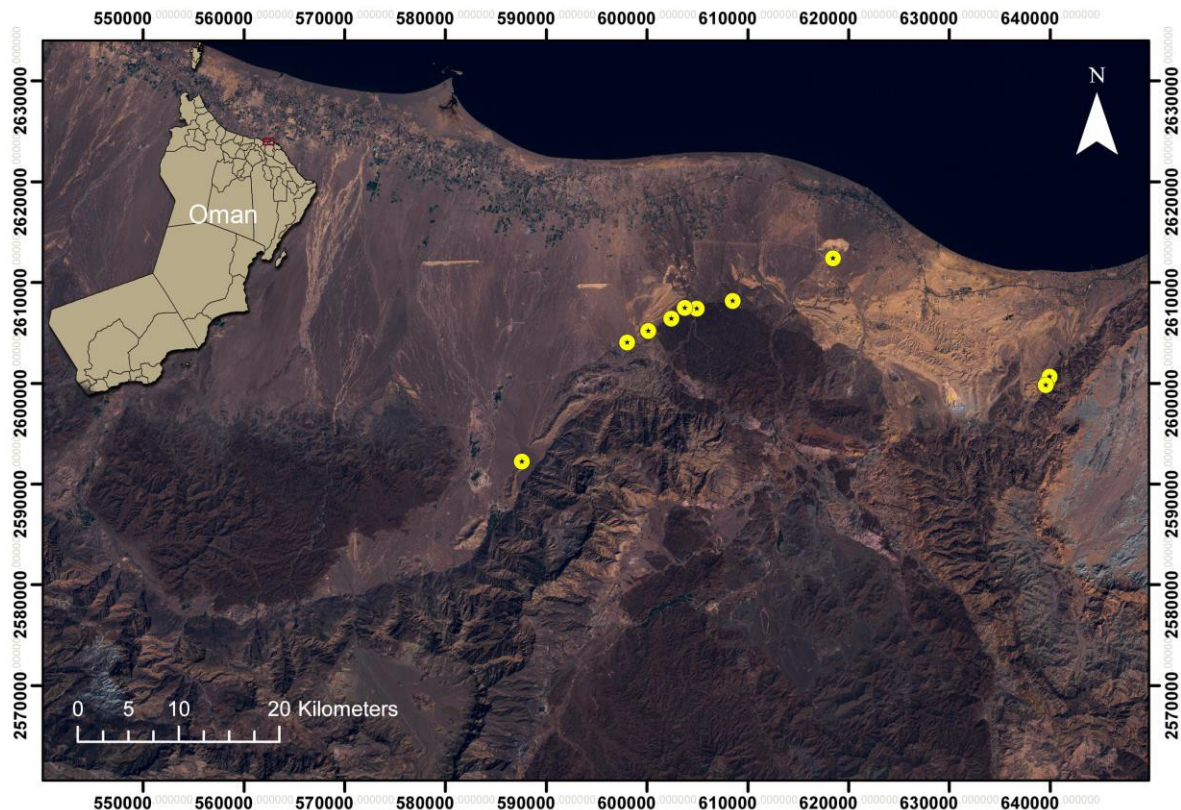


Figure 1 Landsat 7 ETM+ image composite showing the study area around Muscat, North-Eastern Oman. Band 3(red), Band 2 (green), Band 1 (blue) were used. The investigated alluvial fans are marked with yellow circles.

Conclusion

Our analyses generally verify that there is a high positive correlation between fan areas and sizes of catchment areas as well as between fan areas and lengths of valleys of associated rivers. Furthermore, our analyses show a negative correlation between average fan slopes and sizes of catchment areas. The observations are in good agreement with previous analyses from other areas (e.g. Bahrami, S., 2013; Harvey 2002 and Sánchez-Núñez et al. 2015) and to studies in the same location (e.g. Blechschmidt et al. 2009; Al-Farraj and Harvey 2000 and 2005). Thus far, the applied methodology has proven to be adequate to be combined with field investigations and to establish a data basis for alluvial fans in similar climate regimes. Flow events are dominant in fan evolution, but the way in which alluvial fan systems responded to fluvial environmental conditions differs among systems under different climate conditions. We started to compare our results to data from other places located in varying climate zones (Crosta and Frattini 2004; Mills 1983; Viseras, et al. 2003 and Wilford 2005) in order to identify characteristic correlations.



References

- Al-Farraj, A., Harvey, A., 2000. Desert pavement characteristics on wadi terrace and alluvial fan surfaces: Wadi Al-Bih, U.A.E. and Oman. *Geomorphology* 35, p279–297.
- Al-Farraj, A., Harvey, A. 2005. Morphometry and depositional style of Late Pleistocene alluvial fans; Wadi Al-Bih, northern UAE and Oman. In Harvey, A.M., Mather, A.E. & Stokes, M. (eds.) 2005. *Alluvial Fans: Geomorphology, Sedimentology, Dynamics*. Geological Society, London, Special Publications, 251, 85-94.
- Bahrami, S., 2013. Tectonic controls on the morphometry of alluvial fans around Danekhoshk anticline, Zagros, Iran. *Geomorphology* 180–181, p.217–230.
- Blechs Schmidt et al., 2009. Monsoon triggered formation of Quaternary alluvial megafans in the interior of Oman. *Geomorphology* 110, p128–139.
- Bull, W., 1977. The alluvial-fan environment. *Progress in Physical Geography*; 1; 222-270.
- Crosta, G., Frattini, P. 2004. Controls On Modern Alluvial Fan Processes in The Central Alps, Northern Italy. *Earth Surface Processes and Landforms* 29, 267–293.
- Harvey, A. 1997. The role of alluvial fans in arid zone fluvial systems. In: Thomas, D.S.G. (ed.) *Arid Zone Geomorphology: Process, Form and Change in Drylands*, 2nd edn. Wiley, Chichester, 231-259.
- Harvey, A. 2002. Factors influencing the geomorphology of dry-region alluvial fans: case study from southeast Spain and Nevada. *Geomorphology*, 45, 67-87.
- Mills, H. 1983. Piedmont evolution at Roan Mountain, North Carolina, USA. (S. 111-126). *Geografiska Annaler A*, 65. 111-126.
- NASA Landsat Programm 2003. USGS, Sioux Falls, 2000-2002.
- Robertson, A. H. F., Searle, M. P. & Ries, A., 1990. *The Geology and Tectonic of the Oman Region*. The Geological Society London, UK.
- Sánchez-Núñez, J., Macías, J., Saucedo, R., Zamoranod, J., Noveloe, D., Mendozaf, M., Torres-Hernández, J., 2015. Geomorphology, internal structure and evolution of alluvial fans at Motozintla, Chiapas, Mexico. *Geomorphology* 230 (2015) 1–12.
- Shuttle Radar Topography Mission 2004. USGS, Global Land Cover Facility, University of Maryland, College Park, Maryland, 2000.
- Viseras, C., Calvache, M., Soria, J., Fernández, J., 2003. Differential features of alluvial fans controlled by tectonic or eustatic accommodation space. Examples from the Betic Cordillera, Spain. *Geomorphology* 50, p181–202.
- Wilford, D., Sakals, M., Innes, J., Sidle, R., 2005. Fans with forests: contemporary hydrogeomorphic processes on fans with forests in west central British Columbia, Canada. In: Harvey, A., Mather, A., Stokes, M. (eds) *Alluvial Fans: Geomorphology, Sedimentology, Dynamics*. London, Geological Society. Special Publications 251, 24–40.



Sandstone Provenance in Alci Basin SW of Ankara, Turkey

Barbaros Demircan
email: bobdemircan7@gmail.com
Middle East Technical University, Ankara-Turkey

Summary

The present study aims to determine type(s) of the source area(s) of Alci Formation (Kocyigit and Lunel, 1987) and to reconstruct the paleogeography of the region by using light mineral content of the sandstone.

Introduction

Study area, which is SW of Ankara, is one of the key regions in Turkey for the recognition of evolutionary events of the Tethys (Rojay and Suzen, 1997). Several researches which are related to the stratigraphy, volcanism, and the tectonics of the SW of Ankara region were done (Rojay and Suzen, 1997). Yet there is no research concerning provenance of the sandstone (Alci Formation) (Kocyigit and Lunel, 1987) in the Alci Basin.

Alci Formation is Paleocene in age. General geology of the region including study area is shown in Fig 1. Alci Formation consists of pebbly sandstone and siltstones with rudist bearing limestone olistoliths (Rojay and Suzen, 1997). Sandstone in the Alci Formation is yellowish and in some parts grey in color, mostly calcareous. This sandstone is related with fan-delta system (Kocyigit and Lunel, 1987). Sandstone is immature and poorly sorted. 4 samples were collected parallel and perpendicular to the strike of the sandstone. According to the classification of Folk (1980) 2 samples are classified as subarkose and the other 2 of them are classified as litharenite. There is 1.8km lateral distance between these two different classified groups. By using feldspar, quartz, and rock fragment properties and Dickinson's (1983) Tectonic Setting Model, Recycled Orogenic and Undissected Arc were found. These results are relevant with the geological setting of the area.

In the provenance studies when a multi-technique approach is used, the result of the study is more close to the real case. Therefore heavy mineral based provenance study will also be applied for this research to compare the results from light mineral content.

Methods

- Fieldwork for sampling and general geology of the region
- Petrography
- Light mineral based provenance study

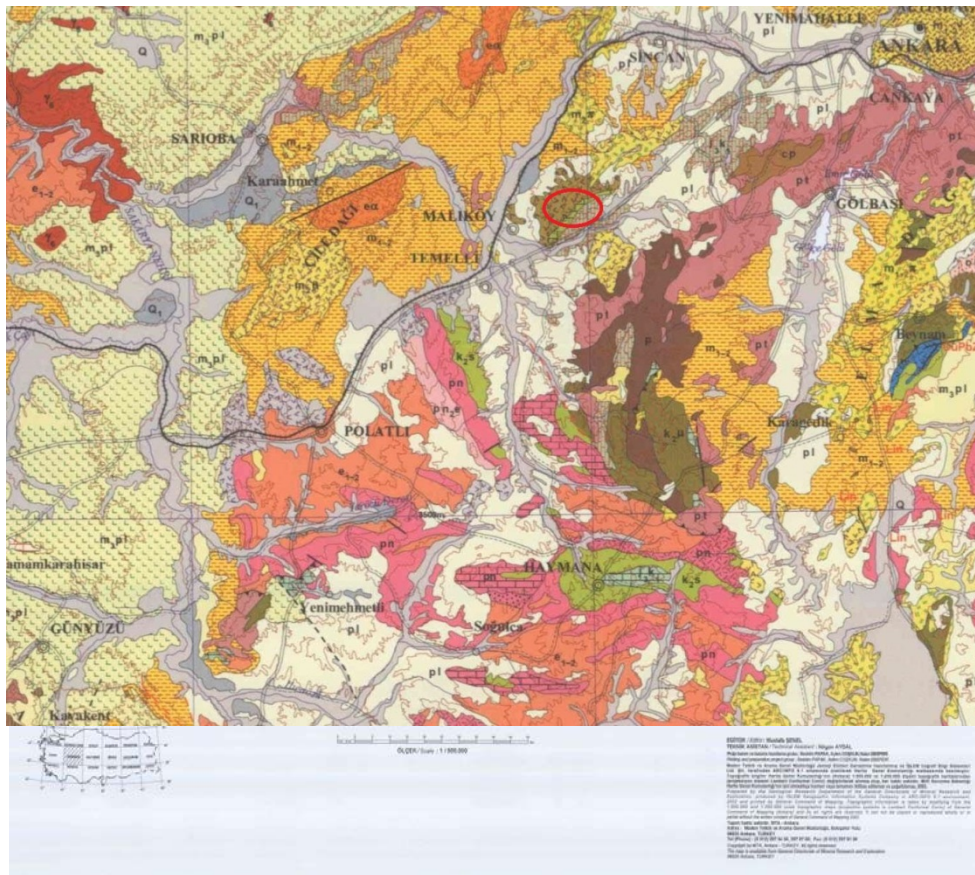


Figure 1 This figure shows the geological map of SW Ankara. Study area is indicated by red circle.

Conclusions

Sandstone provenance in the Alci Formation was studied by using light mineral content. As a result of this study sources were determined as Recycled Orogenic and Undissected Arc. This study helps to reconstruct the paleogeography of the region which is one of the key regions to observe the evaluation steps of Tethys. This study can be extended by analysing more samples from the sandstone.

Acknowledgements

I would like to thank Assoc. Prof. Dr. Ismail Omer Yilmaz for his constructive guidance and discussions.



References

Kocyigit, A. and Lunel, T. (1987). Ankara orogenic phase, its age and transition from thrusting-dominated paleotectonic period to the strike-slip neotectonic period, Ankara (Turkey). Turkish Journal of Earth Sciences.

Rojay, B. and Suzen, L. (1997). Tectonostratigraphic Evolution of the Cretaceous Dynamic Basins on Accretionary Ophiolitic Melange Prism. The of Turkish Association of Petroleum Geologists.



The Distribution of Terrigenous Organic Matter of Mungaroo Formation, in North Carnarvon Basin

Niu Xing¹

email: whdidazk@163.com

¹ China University of Geoscience, Wuhan, 430074-Wuhan, China

Summary

North Carnarvon basin is located south of northwest shelf of Australia, having an area of approximately 535 000 km². Multiple world-class gas fields have been found in this basin. Mungaroo Formation, the main hydrocarbon-bearing strata, consists of thick sediments of shallow-water delta controlled by Circum-Tethys mega-monsoon and it deposited in Carnarvon Basin in the middle-late Triassic. The distribution of Terrigenous Organic Matter (TOM) in this kind of delta differentiates from that of other deltas without relationship to mega-monsoon event. Mungaroo delta is a good example to study the characteristics of TOM in the delta controlled by mega-monsoon event.

Geological setting

North Carnarvon basin is a hydrocarbon-rich basin and occurs continuous subsidence during the late Paleozoic-Cenozoic. In Triassic, it belongs to pericratonic depression. And it was located northern margin of the east Gondwana land and southern margin of the Tethys ocean, where is the tropical-subtropical humid climate zone^[1-3]. In addition, it was affected by mega-monsoon^[3]. Meanwhile, Onslow Microflora occurred in North Carnarvon basin in late Triassic, which marked tropical rainforest climate^[4]. Onslow Microflora consists of a large number of hygrophytic molecule, dominated by Falcisporites, and a small amount of European molecules, which is xerophytic^[4].

Methods

According to the study of core, logging and seismic data, this paper divided Mungaroo Formation into four sedimentary subfacies: proximal delta plain, distal delta plain, delta front and prodelta. We calculate the content of TOC in source rocks and maceral in organic matter from different sedimentary subfacies; then use these data to do scatter diagram or pie chart; finally we analysis the distribution rule of TOC and maceral in different sedimentary subfacies.

Conclusions

Under the influence of mega-monsoon, Mungaroo Formation is notable for the followings: 1) well widespread delta plain and narrow delta front and prodelta belts; 2) thick channel sandstone frequently sandwich with mudstone which is rich of TOM; 3) hygrophytic molecule coexists with xerophytic molecule in sediments.

Based on the analysis of well-to-seismic tie, Mungaroo delta can be divided into four sedimentary sub-facies: proximal delta plain, distal delta plain, delta front and prodelta. In additional, organic matter distribution in four sedimentary sub-facies has distinct differences (figure 1) : 1) for the proximal delta plain, sandy conglomerate rocks developed with intercalations of thin layers of mudstone. The average organic-carbon content is 1.59% and the main maceral in the mudstone is inertinite as most of the vitrinite suffered oxidation; 2) for the distal delta plain, medium-thick bedded distributary channel sandstone interbedded with medium bedded mudstone and thin coal seams. peat swamp, characterized by multiple thin coal seams, is well developed in this subfacies. The mudstone is rich in TOM that average organic-carbon content can be up to 4.11%. The vitrinite in distal delta plain is higher than that in proximal delta plain and prodelta; 3) the content of TOM in mudstone is low within small-scale delta front and prodelta sub-facies belts. The average organic-carbon content is 1.05% and the content of exinite is higher than that of the two subfacies previously mentioned. In generally, the organic-carbon and vitrinite content gradually decreases from distal plain delta to proximal plain delta (landward) and delta front and prodelta (basinward).

Both Monsoon floods and storm currents have an important effect on the distribution of TOM. TOM in the proximal delta plain is easily destroyed and oxidized by strong floods, whereas TOM in

the delta front-prodelta is diluted and dispersed by waves and currents. However, the TOM in the distal delta plain could be saved with weaker influence of monsoon floods, waves, and currents. Proposed TOM dispersal patterns should serve as a useful reference for potential reservoir and source rocks in similar deltas around the world.

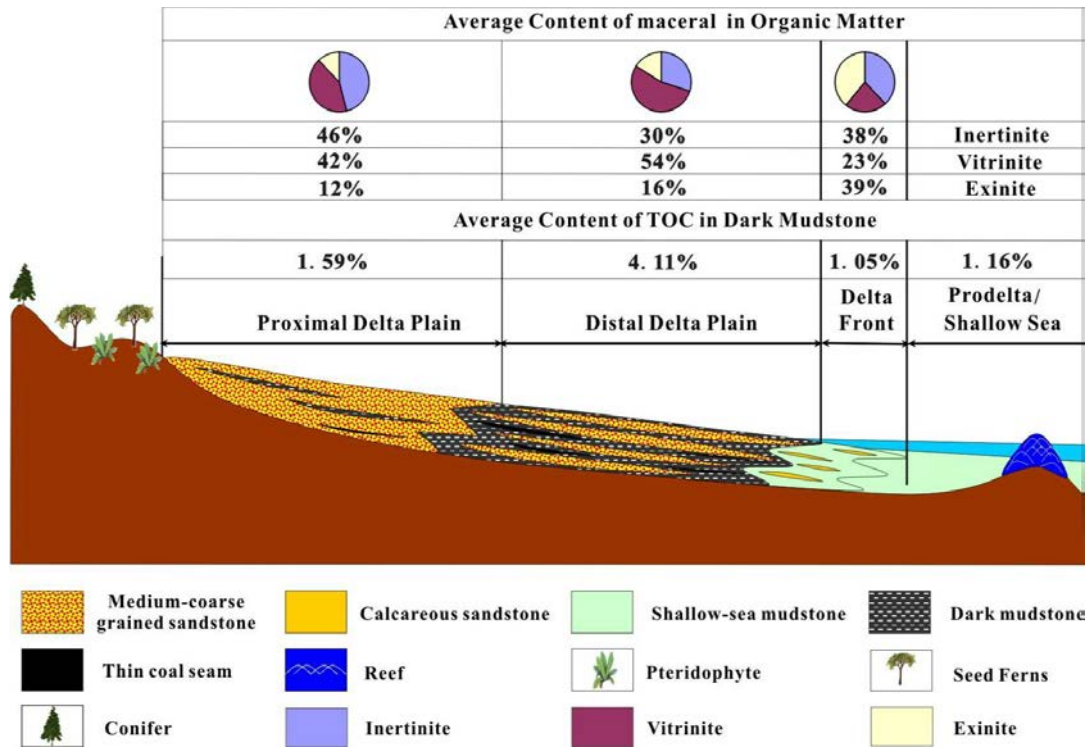


Figure 1 The distribution characteristics of TOM in Mungaroo delta



References

- [1] Parrish J T, Peterson F (1988). Wind directions predicted from global circulation models and wind directions determined from eolian sandstones of the western United States-a comparison. *Sedimentary Geology* .
- [2] Mutti M, Weissert H(1995). Triassic monsoonal climate and its signature in Ladinian-Carnian carbonate platforms (Southern Alps, Italy). *Journal of Sedimentary Research* .
- [3] Dubiel R F, Parrish J T, Parrish J M, et al (1991). The Pangaeon megamonsoon-evidence from the upper Triassic Chinle formation , Colorado plateau. *Society for Sedimentary Geology* .
- [4] Dolby J H, Balme B E (1976). Triassic palynology of the Carnarvon Basin, Western Australia . *Review of Palaeobotany and Palynology* .

Petrographic investigations of materials used in Gothic church tabernacle from the St. Elisabeth's Church, Wrocław, Poland

Katarzyna Zboińska¹, Mateusz Szadkowski, Wojciech Bartz
email: kzboinska@gmail.com

¹ University of Wrocław

Summary

We analyzed samples of natural rock and artificial plaster stone from Gothic church tabernacle located in the St. Elisabeth's Church, Wrocław (Poland). Our studies demonstrated that the natural rock is quartz arenite. This is a local material, used since the Middle Ages, quarried probably from the North-Sudetic Basin, and of Turonian or Coniacian age. Some parts of the tabernacle was made of artificial plaster stone. It differentiates into two groups: 1) mortars without a filler, which represent the original material from the fifteenth century and 2) mortars rich in a filler, which are the result of subsequent renovations of the monument.

Introduction

The object of our petrographic study was the late Gothic church tabernacle (Fig. 1) from St. Elisabeth's Church, Wrocław (Lower Silesia, Poland). It was built in the fifteenth century in the form of slender tower, high on about 16 meters. Its base was made of the natural sandstone, whereas the architectural details (like sculptures of the apostles or the finials) were made of the gypsum mortar (artificial plaster stone).

Due to turbulent history of Lower Silesia, numerous wars, fires and devastation of the church led to severe damages of the tabernacle. Macroscopically observed differences in the materials used for the reconstruction imply numerous and successive stages of the renovation. Thus, the aim of the study was the detailed petrographic characteristic of the materials used in the tabernacle and the attempt to differentiate between the original (Gothic) building material and secondary elements, added at a later time. Attempts were also made to determine provenance of used natural rocks.

Figure 1. Object of our petrographic research - church tabernacle from St. Elisabeth's Church in Wrocław, Poland.



Methods

For our studies we analyzed 5 samples of natural rock and 11 samples of mortar. They were studied by means of: 1) petrographic polarizing microscope (PPM), 2) computer image analysis (CIA) and 3) thermal analysis (DSC-TG). Using the petrographic microscope we assessed mineral composition and structure of the investigated samples. We also made grain-size analysis of natural rock samples. It was determined using JMicroVision software (Ronduit 2007). For each of the samples 150-250 grains were measured, then the histograms of grain size distributions were prepared.

Thermal analysis of mortars was done by means of the Perkin Elmer analyzer STA6000, at a temperature range 40 - 980°C, a heating rate of 10° C per minute.

Research results

Natural rocks, yellow to brownish in colour, were classified as quartz sandstones. They are dominated with quartz grains (over 90%), feldspar grains and lithic grains are subordinate. In all samples there is a pore-filling clay cement, accompanied with authigenic quartz overgrowths. Limonite-goethite locally appears as thin coatings on individual framework grains. Since the content of matrix is negligible, it allowed us to classify rocks as quartz arenites (Pettijohn et al., 1987).

The petrographic data obtained for samples of sandstone and the proximity of large deposits of raw material (quartz arenites) located in the Sudetes (SW Poland) suggest that the natural material represents the Cretaceous joint sandstone. These rocks occur in the Intra-Sudetic Basin (Kłodzko area) or North-Sudetic Basin (Bolesławiec area; Labus, 2011). Within these geological structures Upper Cretaceous sandstones occur in three levels (bottom, middle and top). The lower and middle levels are both Cenomanian and Turonian aged, the upper level of the Intra-Sudetic Basin is also Turonian, while the upper level of the North-Sudetic Basin is Coniacian. These sandstones have been widely used as a building and decorative material from the Middle Ages (Ehling 1999). Between different regions and levels there are differences in mineral composition and grain-size distribution (Ehling, 1999; Labus, 2011). For comparison purposes, the grain-size distribution obtained for each of the rock samples have been processed statistically. Hence the median ranges from 0,23 mm to 0,33 mm, the first quartile from 0,12 mm to 0,24 mm and the third quartile from 0,35 mm to 0,45 mm. This particular data set stays in good agreement with granulometric characteristic of sandstones described by Ehling (1999) as belonging to the middle and upper levels of the North-Sudetic Basin. This is confirmed by the analysis of the mineral composition of framework grain and binder. Based on a number of similarities we can assume that the rock material used in the tabernacle represents Turonian or Coniacian sandstones from the North-Sudetic Basin.

The majority of mortars represents artificial plaster stone, of which the details of tabernacle were made. Due to observed mineralogical differences they could be divided into two groups. The first are the predominant mortars, without filler, composed entirely of a colourless in plane-polarized light, fine-crystalline gypsum. The samples of the second group, less common, are characterized by the presence of abundant filler (quartz grains), cemented by microcrystalline to cryptocrystalline gypsum, light brown in plane-polarized light. Thermal analysis showed strong, doublet at 130-150°C, which should be interpreted as the effect of the thermal decomposition of gypsum (Ramachandran et al., 2002). In addition, in the case of samples of the second group, effects associated with endothermic effect accompanied by weight loss at about 350°C and over 600°C were visible. The latter results from the thermal decomposition of calcium carbonate, while the lower temperature effect presumably result from thermal decomposition of the plaster additives – organic substance.

Among the analysed samples, only one represents aerial lime mortar. It has a microcrystalline calcium carbonate (micritic) binder, strongly heterogeneous, containing numerous lime-lumps. Filler is composed of quartz, with less common feldspars, fragments of rocks and accessory minerals. The sparse charcoal occurs, being most likely the remnants of fuel used for calcination of lime.

Conclusions

Analyzed samples, taken from the Gothic church tabernacle, represent: 1) natural stone - quartz arenite with silica-clay binder, and 2) artificial plaster stone. Sandstone was classified as quartz arenite of Turonian or Coniacian age, coming from deposits of North-Sudetic Basin.

Samples of gypsum mortar without filler represent original Gothic material, whereas gypsum mortar with quartz filler and aerial lime mortar represent material from the later stages of the renovation.

Acknowledgements

The authors would like to thank Mr. Przemysław Gorek (Gorek Restauro Studio Conservation & Restoration of Fine Art) for providing research material for petrographic analysis.



References

- Ehling A. (1999). Die oberkretazischen Bausandsteine Schlesiens. Dissertation, Universität Hannover.
- Labus M. (2011). Parametry przestrzeni porowej jako determinanty podatności na wietrzenie surowców skalnych dolnośląskich piaskowców ciosowych. Wydawnictwo Politechniki Śląskiej.
- Pettijohn F. J., P.E. Potter, Siever R. (1987). Sand and sandstone. 2nd ed. Springer-Verlag.
- Ramachandran V.S, Paroli R. M., Beaudoin J., Delgado A. (2002). Handbook of thermal analysis of construction materials. Noyes Publications, William Andrew Publishing.
- Roduit, N. (2007). JMicroVision: un logiciel d'analyse d'images pétrographiques polyvalent. <http://www.jmicrovision.com>.



Microfacies and sea level fluctuation analyses of the uppermost Jurassic and Lower Cretaceous deposits in the Carpathian basement in the Ropczyce area (Poland)

M.Sc. Tomasz Krogulec, prof. Anna Wysocka, M.Sc. Paweł Zdanowski
email: tomasz.krogulec@student.uw.edu.pl
University of Warsaw

Summary

The main goal of described study were microfacies and sedimentological analyses of the uppermost Jurassic and Lower Cretaceous deposits in the Carpathian basement in the Ropczyce area (Poland, Podkarpackie province). Integrated data from core analyses, thin section and fossils identifications allowed for a detailed characteristic of the sedimentary environment (very shallow marine to marine) and creation of bathymetric curve for the Polish Basin during late Mesozoic transgression.

Introduction

The research was focused on the characterization of microfacies and sedimentological analyses of the uppermost Jurassic and Lower Cretaceous deposits in the Carpathian basement in the Ropczyce area (south Poland, Podkarpackie province). It was based on the drill core and thin sections from Zagorzyce 7 well (from 2862 m to 2697.5 m). The aim was to create high resolution microfacies and sedimentological analyses and determine bathymetric curve related to the thickness and estimated time of deposition (not to biostratigraphy) for the Polish Basin during late Mesozoic transgression.

Method

During the first stage, the research was focused on observations on the macro scale of Zagorzyce 7 drill core. Core length is 169.5 m. Observations made at this stage led to preliminary conclusions and made possible further stages of the research.

Second phase of studies was based on thin section analyses from the same depth as core from Zagorzyce 7 well. The number of samples amounted to 77. Thin sections had been previously acquired by the team from Polish Oil and Gas Company in the characteristic areas of facies variation (Zdanowski et al., 2001).

In addition, major groups of micro- and macrofossils have been identified as a support in the diagnosis of sedimentary settings.

Examples

The first part of examples used during the research comes from core (169.5 m) observation. These examples made it possible to determine lithology (limestones and dolomites interfingering with clayey sediments) and also to recognize sedimentary environments. On this basis it can be concluded that the main trend of bathymetric curve is deepening (in accordance with the global trend).

Microfacies analysis is a basic tool for the study of carbonate rocks. It allows for a very thorough investigation and detection of small changes in the condition of sedimentation, such as depth or salinity (Flügel, 2010).

In case of described research one can observe such microfacies as mudstone (Fig.1. A), wackestone, packstone, grainstone (Fig.1. C and D) and rarely bindstone (Fig.1. B). This variation is due to rapid response of shallow carbonate environments to small changes of relative sea level (Coe, 2002). Microfacies analysis served also as a tool to create a detailed lithological profile. It was supported by macro- and microfossils identification. Paleontological data facilitated recognitions of environmental energy and salinity during the sedimentation (Flügel, 2010), which was also a verification of findings from earlier stages of studies.

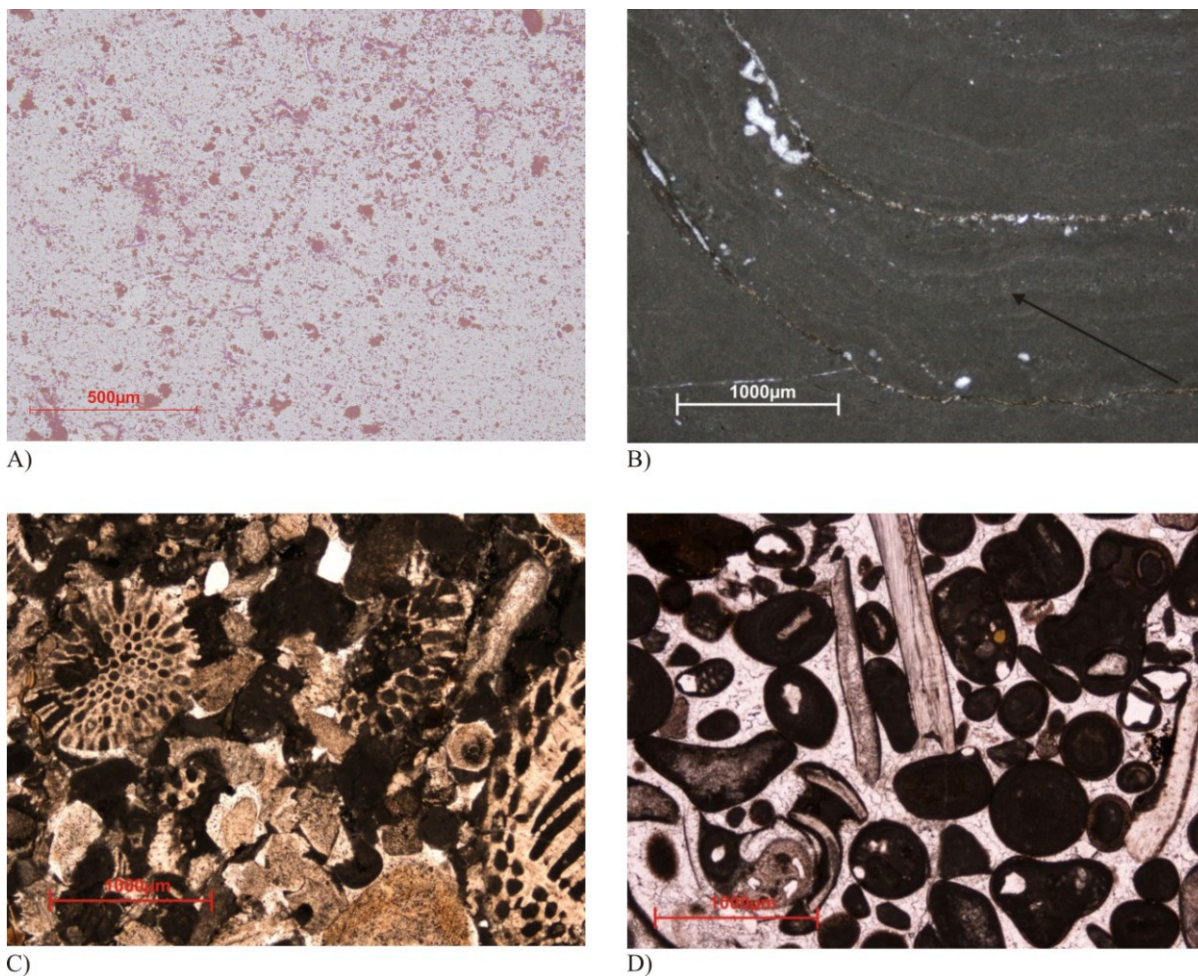


Figure 1 Microfacies from thin sections of uppermost Jurassic and Lower Cretaceous deposits in the Carpathian basement in the Ropczyce area (Matyja, et al., 2008); A) Mudstone (no sedimentary structures, small spots of dark pigment); B) Bindstone (small-scale lamination); C) Grainstone (Crinoid and Bryozoan); D) Grainstone (Ooids and Bivalves);

Conclusions

Integrated data from core analyses, thin section and fossils identifications from 2862 m to 2697.5 m depth of Zagorzyce 7 borehole shows high variability within the shallow marine sedimentary environments in the Polish Basin during the latest Jurassic and Early Cretaceous. In the case of described rocks, all types of microfacies of carbonate rocks (mudstone, wackestone, packstone, grainstone and rarely bindstone) can virtually be observed. Such variability allows to specify the sedimentological environment as very complex and rapidly changing – from lagoon to marine settings.

Analyzed data provide the basis for determining generalized bathymetric curve and its comparison with the global eustatic curve (Haq, 2008). The main trend and peaks of these two curves are very similar and show the deepening of the sedimentary basin during the latest Jurassic and Early Cretaceous time.

Acknowledgements

I would like to thank the Polish Oil and Gas Company (PGNiG SA) for providing data and substantive assistance during research. The research was funded from the budget of the University of Warsaw.



References

- Coe, A. (2002). *The Sedimentary Record of Sea-Level Change*, Cambridge. Flügel, E. (2010). *Microfacies of carbonate rocks*, Springer.
- Haq, B.U., Schutter, S.T. (2008). A Chronology of Paleozoic Sea-Level Changes, *Science*, 322: 64-68.
- Matyja, B.A., Barski, M. (2008). Rozpoznanie architektury i rozprzestrzenienia górn jurajskich budowli organicznych dla określenia czynników warunkujących występowanie mezozoicznych złóż węglowodorów południowo-wschodniej Polski, część I (unpublished).
- Zdanowski, P., Baszkiewicz, A. and Gregosiewicz, Z. (2001). Facies analysis of the uppermost Jurassic and the Lower Cretaceous deposits in the Zagorzyce region (southern Poland), *Przegląd Geologiczny*, 49:161-178.

Physical and chemical fluctuations of mineral springs from Slanic Moldova, Romania

Madalina Ciucu, Diana Hughineata, Florina Chitea
 email: madalinaelenaciucu@yahoo.ro

¹University of Bucharest

Summary

In a relative confined area (800*400m) an impressive number of groundwater types were documented to exist, most of them being spread along the Slanic River. Hazardous natural phenomena (landslides, rainfall regime, river erosion, earthquakes) as well as anthropogenic triggered hazards, caused by intense exploitation of the groundwater resources, has led to the decrease of the total number of water outlets which are nowadays in use. From the total number of 15 springs, during the monitoring time span (4 months), water samples were collected from a maximum of 9 locations. Some of these sources were waterless during the entire period, while others only occasionally.

Introduction

A total number of 15 springs are placed along an approximately 1km long pathway, on both sides of Slanic River. For the present study we documented the variability of water temperature ($^{\circ}\text{C}$) at the source, the activity of the hydrogen ion (pH), the electrical conductivity (σ) and the content of total dissolved solids (TDS) of the groundwater samples from Slanic Moldova area. Results were interpreted using data from literature. High chloride, as well as the springs with higher potassium content correlated well with the high electrical conductivity values locations determined by us. Hence, we considered that following the electrical conductivity parameter, we can obtain valuable information related to the groundwater source (deep or shallow), migration patterns, and the influence of the rainfall regime. Therefore, for the monitoring time span we also recorded the rainfall regime at Slanic Moldova.

Methods and results

The field measurements of temperature (Figure 1) indicated a variation of maximum 3.7°C . The cooler spring resulted to be Nr. 5 (8°C), while the higher temperature was recorded for spring Nr. 2 (11.7°C), at a surrounding atmospheric temperature of 14°C .

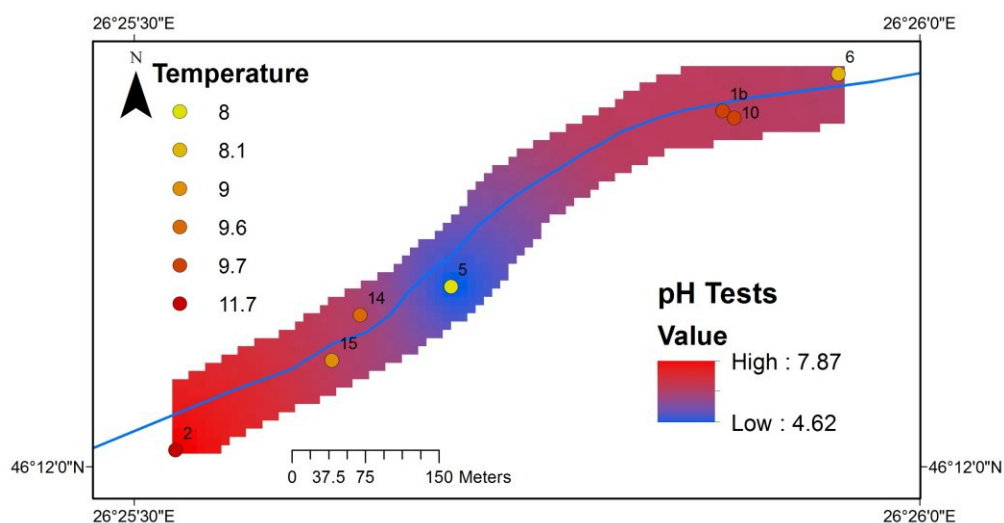


Figure 1 Variation of temperature and pH values for seven springs spread along Slanic River

Laboratory analyses of the electrical conductivity performed with a specific sensor showed wide chemical variations among the outflows encountered in the analyzed area: from a minimum of 0.57 dS/m (Spring Nr. 5) to a maximum of 7.19 dS/m (Spring nr. 1b) (Figure 2). The collected groundwater samples were also tested using a special sensor for TDS (total dissolved solids) determinations, providing up to +/- 5% accuracy. Lower electrical conductivity values correspond to smaller contents of dissolved solids.

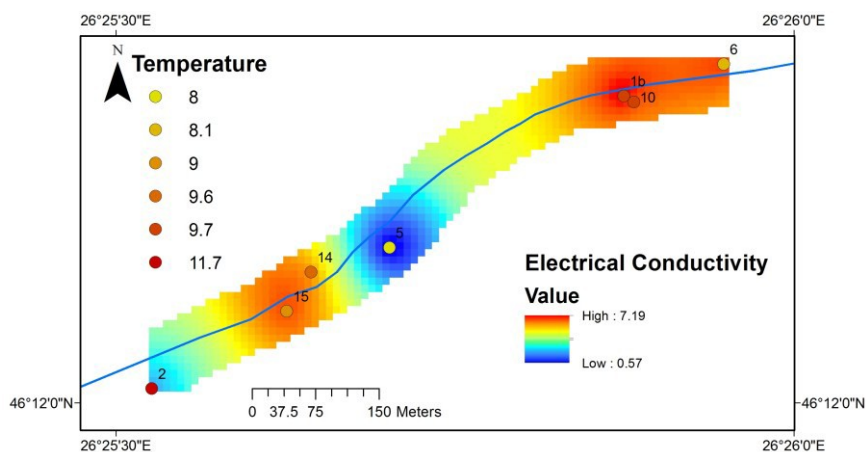


Figure 2 Variation of temperature and electrical conductivity values for several springs spread along Slanic River

Conclusions

The analyzed springs of Slanic Moldova can be classified as cold, low-discharge springs, and extremely diversified in terms of mineralization: naturally enriched in salts (7.59 ppt for Spring Nr. 1b), while others display very low mineralization (192 ppm for the acid – pH= 4.58 - Spring Nr. 5). The monitoring data sets obtained till now allow one to conclude that the measured chemical and physical parameters are influenced by the meteorological regime. Moreover, it is quite evident that the saline springs are supplied by deep sources, located in different hydrostructures, as suggested in Mitrofan et al., 2014. The influence of the geological formations from the aquifers is felt in the electrical conductivity results. The high electrical conductivities correlate well with the high chloride and potassium water contents.

A long – time monitoring program will be further developed in order to understand the space and time fluctuations of these water resources and their correlations with geohazards (seismic activity of Vrancea area) and with the rainfall regime influence.

Acknowledgements

Laboratory analyses presented in this paper were possible through the kind support of SEG/TGS - Field Camp Grant 2015, for the project entitled “Electrical Signatures of Groundwater - Student’s Geophysical Quest”

References

Mitrofan H., Marin C., Tudorache A., Visan M. (2014). Diagnosing Non-Meteorically Induced Variations in the Chemistry of Saline Springs of the Vrancea Seismic Area (Romania), Pure Appl. Geophys. 171 (2014), 2315–2338.



Mineralogical, geochemical and textural characterisation of siliciclastic deposits of Ulmet Valey, Romania

Alexandra CONSTANTIN¹, Constantin UNGUREANU¹, Erik Kuikman², Dan V. PALCU², Izabela MARIS¹

alexandra_kog@yahoo.com; ungureanuconstantin@yahoo.com; Eric_Kuikman@hotmail.com
d.v.palcu@uu.nl;
izabela@contentlogic.ro

¹ University of Bucharest, ²Utrecht University

Summary

Paratethys was a large epicontinental sea, a relict of the Tethys Ocean, which spanned from Western China to the Alpine Region in Europe. One of the most important events in its evolution occurred in the Middle Miocene and consisted of a complete faunal turnover from rich, fully marine ecosystems to poor brackish ones characterized by solely endemic species. The event that led to this change is known as the Badenian Sarmatian Extinction Event (BSEE) and there is as yet no agreement on its age or triggers. The challenges in understanding the BSEE are due mainly to the geographical coverage of the studied areas.

Introduction

The aim of this study is to describe as accurately as possible the characteristics of the depositional environment at the Badenian/Sarmatian boundary using sedimentological methodology (lithological and granulometric analysis), integrated with geochemical and mineralogical data. Using magneto-biostratigraphic data, we aim to provide a sedimentological, mineralogical and geochemical description of the changes recorded in the basin sediments, before, during and after the extinction event.

The studied area is located on the Ulmet Valley - Romania. We analyzed data from Eastern Paratethys which correspond to Carpathian Foredeep. The sedimentary sequence of Ulmet Valley consists of intercalations of centimetric layers of clays, silts and fine sands with plan – parallel laminations and stratifications, most of them being deep marine sediments with a high organic matter content.

Method and/or Theory

Grain-size analysis of Ulmet sequences were made with Horiba LA 950 laser granulometer, after removing the organic matter and the carbonates from the sediments. Geochemical analysis (XRF method) with Horiba – XGT-7000 was used to identify the major elements (Al, Fe, Mg, K, P, Si, Ca, S) and minor elements (V, Cr, Ni, Ti, Zr, Rb, Sr). The general mineralogical analysis and a more detailed one performed on the clay minerals, were conducted using a PANanalytical X'pert pro X ray diffractometer. The resulted data are in progress.

Examples (Optional)

Grain-size analysis of Ulmet sequences suggest that samples vary from fine sand to clay, with median between 5,719 and 7,434 Φ units. The frequency curves have an unimodal and bimodal character, and the size distribution shows moderately to poorly sorted sediments.

Geochemical analyses reveal the major elements and their distribution. The terrigenous material supply was identified using Ti/Al, Zr/Al and Si/Al ratios. In addition, the high Ti/Al and

Zr/Al ratios are considered as indicative of increased volcanic input, and were the main ratios used in correlation with these two depositional units. According to these results two anoxic levels were separated in the lower part and in the upper part of the sedimentary sequences. Estimating anoxic events was possible through applying the V/Cr, Ni/Al, Mn/Al, Al/(Al+Fe+Mn) ratios.

The organic matter content was measured by Loss on Ignition (LOI), and the obtained values range from 2.4 to 4.8%.

Furthermore, the age of the investigated sedimentary sequence was determined on the basis of magneto-bio-stratigraphy.

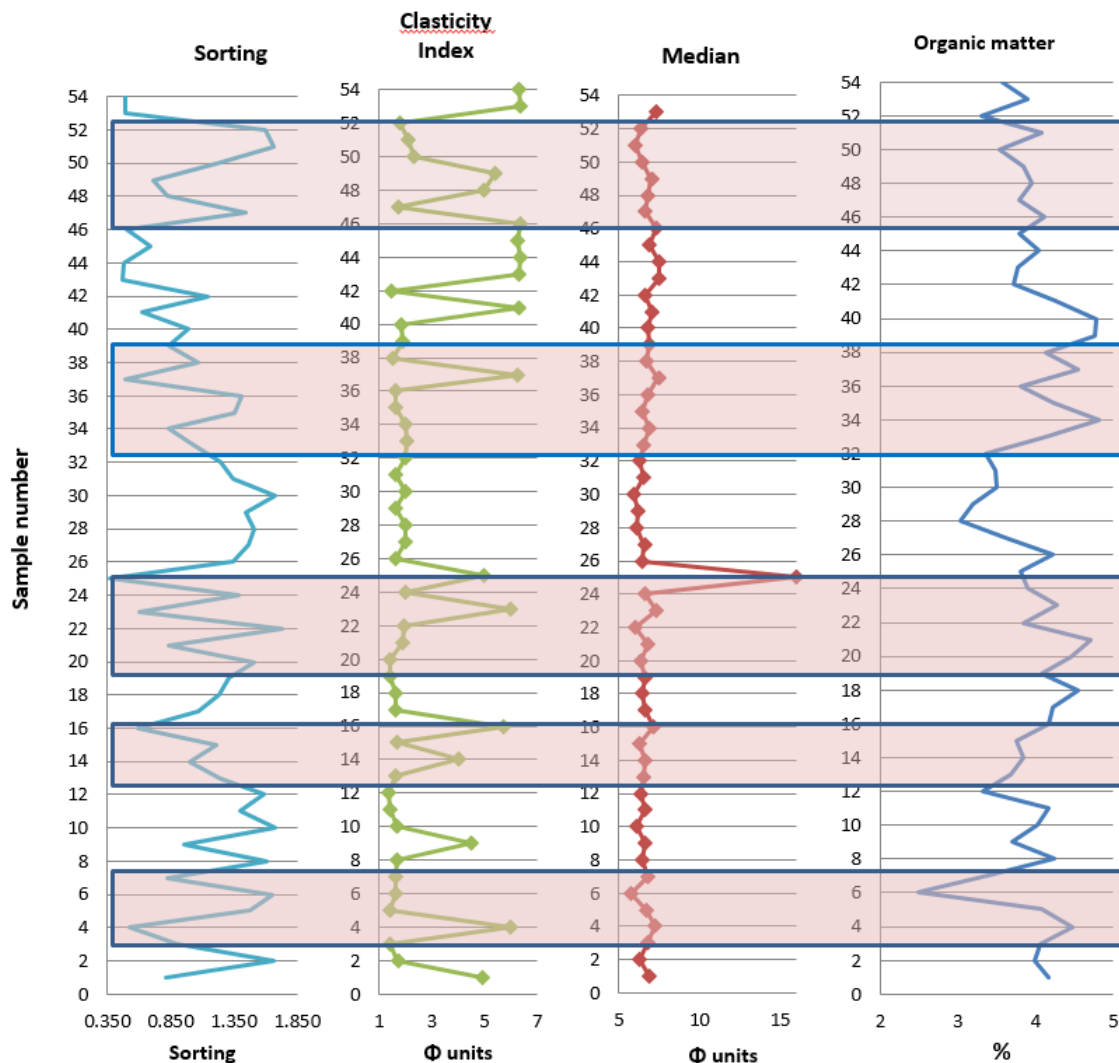


Figure 1 Correlation between sorting, clasticity index, median and organic matter

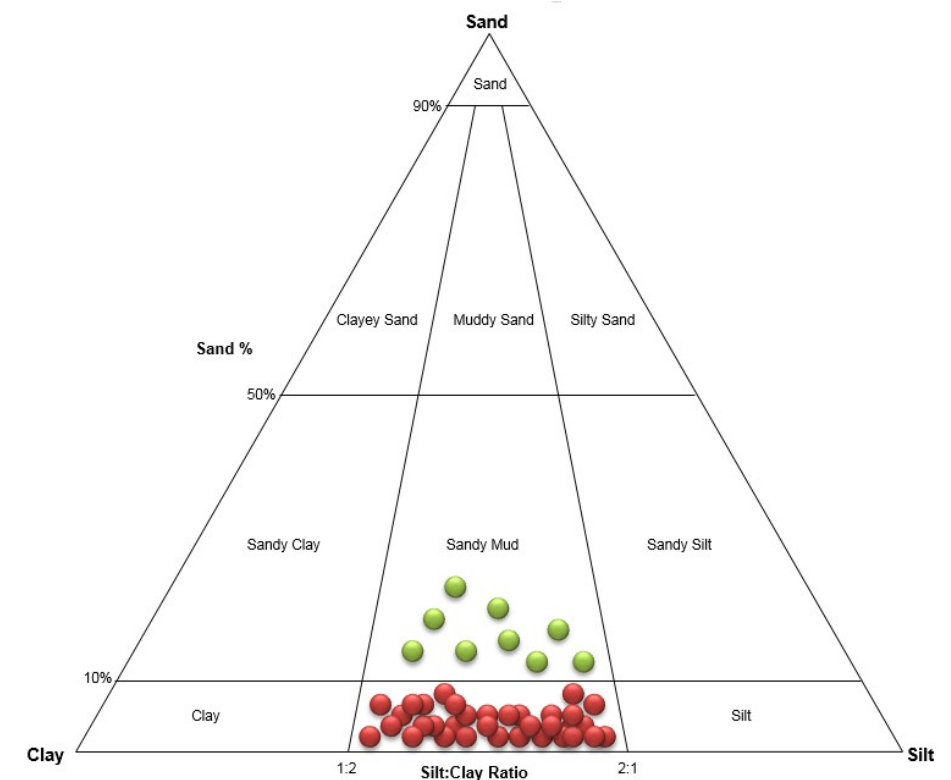


Figure 2 Textural classes of the analyzed samples (Folk, 1954)

Conclusions

The examined sediments belong to a deep marine environment, having a high concentration of organic matter, which suggest their accumulation into an anoxic and quiet environment.

Acknowledgements

Research has been carried out within the project “The evolution of Paratethys: the lost sea of Central Eurasia”, financed by NWO Council for Earth and Life Sciences (NWO).

References

- ANASTASIU N., JIPA D., (2000). Texturi si structuri sedimentare, Editura Universitatea din București
- PANĂ., (1966). Studiul depozitelor pliocene din regiunea cuprinsă între Valea Buzăului și Valea Bălăneasa. Institutul. Geologic, București 1966



Mid-Late Holocene evolution of a carbonate-clastic barrier bank, during changing sea levels (Shark Bay, Western Australia)

Giada Bufarale¹, Lindsay Collins
email: giada.bufarale@postgrad.curtin.edu.au
¹ Curtin University

Summary

To investigate the Mid-Late Holocene development of the Faure carbonate-clastic barrier bank complex (Shark Bay, Western Australia), remote sensing imagery analysis, acoustic profiles and sedimentological information have been combined, in order to correlate internal architecture, sediment bodies and lithofacies. By integrating these data with radiocarbon dating, information about the accumulation rates was obtained, together with an estimated age of bank onset and development.

The study demonstrated the interconnection between sediment body morphologies, seagrass related substrates and pre-existing topography and revealed that sea level fluctuations had largely controlled the hydrodynamic conditions of the bank, contributing to its evolution.

Introduction

Located approximately 800 km north of Perth (Western Australia), Shark Bay was registered as a World Heritage Property in 1991. Pre-Holocene topography, seagrass and sea level fluctuations have contributed to the evolution of the marine ecosystem of Shark Bay, and in particular to the growth of the Faure Sill, a well-developed carbonate-clastic barrier bank. The bank lies east-west across the axis of Hamelin Pool and L'Haridon Bight, restricting the water exchange between these southern embayments and Hopeless Reach (Figure 1). These environmental settings, associated with a semi-arid to arid climate, produced and preserve the metahaline and the hypersaline conditions in the Hamelin and L'Haridon basins, providing a basis for the development of a variety of biogenic and physical structures such as microbial communities (stromatolites) and oolitic shoals (Logan and Cebulski, 1970; Logan et al., 1974; Walker et al., 1988).

Methods and Theory

High-resolution shallow seismic profiles provided information on the thickness and acoustic characteristics of the subbottom deposits. To integrate and assess the results obtained with the geophysical survey, sediment cores were collected, logged and dated. Radiocarbon dating values were used to estimate the Mid-Late Holocene history and to create a stratigraphic model of bank.

The results indicated that the development of the Faure Sill has been controlled by three mechanisms: 1) pre-existing topography that shaped the initial deposition; 2) the seagrass, which have been produced and trapped a large amount of deposits during the entire Holocene time; 3) sea level oscillations, that significantly controlled the hydrodynamic conditions, influencing the erosion, transportation and deposition of the sediments. The development of the bank can be grouped in three sea level stages. The initial commencement can be traced back to the early Holocene transgression (no earlier than 8500 years BP, in lower but rising sea levels, Figure 1.1). The sediment accumulation peaked around 6800 years BP, in correspondence with the sea level maximum highstand (Figure 1.2) and, during the following fall to present level, the deposits continued to fill the available accommodation space (Figure 1.3-4).

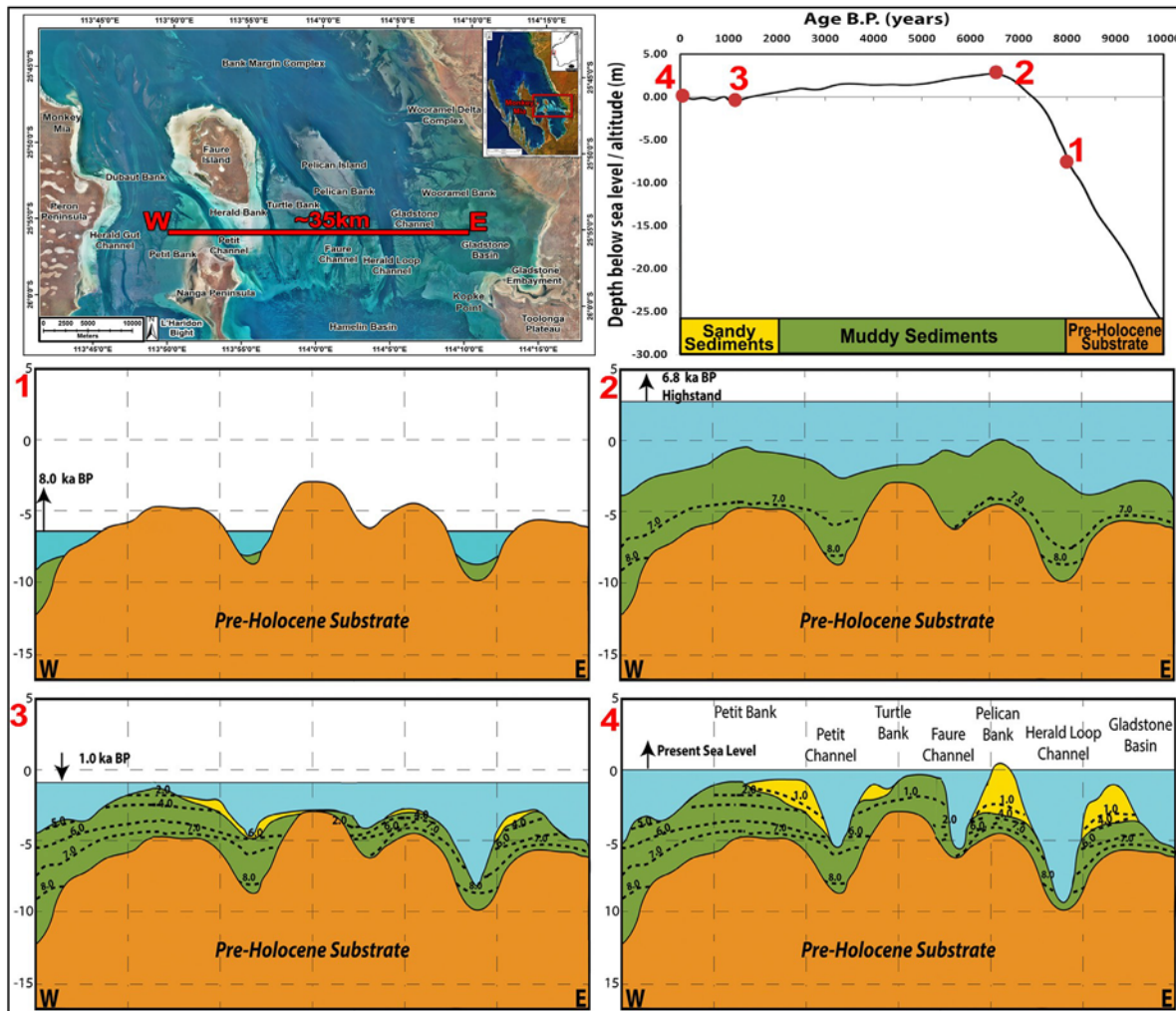


Figure 1 Top left corner: aerial view of the Faure Sill (mosaic of photos from Landgate, Western Australia. Insert image from Geoscience Australia) showing the study area and the locality names. Top right corner: Holocene sea level (Bufarale and Collins, 2015). 1-4: Reconstruction of the Holocene chronology of the Faure Sill, based on Bufarale and Collins, 2015. Dashed lines represent isochrones. The colours are a generalisation of the lithology. The arrows refer to the trend of the sea level. The profile is not to scale. The transect length is about 35 km, W–E oriented. On the vertical axis, the scale is in metres, 0 corresponds to the present sea level.

Conclusions

Through shallow seismic and sedimentological analysis, this study has characterized the Faure Sill in terms of its seismic architecture, facies, chronology and growth history, providing a better understanding of the sedimentological facies and geomorphological features of the bank.

Bufarale and Collins, 2015 is a fuller account of this work.



References

Bufarale, G. and Collins, L.B. (2015). Stratigraphic architecture and evolution of a barrier seagrass bank in the mid-late Holocene, Shark Bay, Australia. *Marine Geology* 359, 1–21.

Logan, B.W. and Cebulski, D.E. (1970). Sedimentary environments of Shark Bay, Western Australia. In: Logan, B.W., Davies, G.R., Read, J.F., Cebulski, D.E. (Eds.), *Carbonate Sedimentation and Environments, Shark Bay, Western Australia*. American Association of Petroleum Geologists Memoirs 13, pp. 1–37.

Logan, B.W., Read, J.F., Hagan, G.M., Hoffman, P., Brown, R.G., Woods, P.J., Gebelein, C.D. (1974). Evolution and diagenesis of quaternary carbonate sequences, Shark Bay, Western Australia. *American Association of Petroleum Geologists Memoir* 22, 358.

Walker, D.I., Kendrick, G.A., McComb, A.J. (1988). The distribution of seagrass species in Shark Bay, Western Australia, with notes on their

Sedimentary Facies Analysis, Cyclicity and Reservoir Characterization of the Northeastern Offshore Nile Delta (Ha'py Field Case Study)

Nada Amer, Darwish M., El Barkooky A., Sharaf E.

Email: nada.amer@hotmail.com

Faculty of Science, Cairo University

Summary

Ha'py Field is an excellent example to perform integrated stratigraphic setup, sedimentary facies and depositional environment analyses. Understanding the patterns of cyclicity and their distribution in time and space is crucial to build a realistic reservoir geological model. The studied reservoir unit belongs to the El Wastani Formation of the Late Pliocene age. The El Wastani Formation was deposited in shallow marine to partly restricted environment. Detailed sedimentologic study indicates that the reservoir unit includes repetitive sedimentary cycles of shallow marine shelf bar facies, representing the main reservoir, interbedded with flooding shale, non-reservoir, that act as cycle boundaries.

Introduction

The Nile Delta extends west to Burg El Arab on the Mediterranean coastal area and east to the Gulf of Tineh in north Sinai, Egypt. The region could be subdivided into four tectono-sedimentary provinces (EGPC, 1994); Northern Nile Delta province (including the eastern, the central and the western mini-basin), Southern Nile Delta province, Nile Delta Cone and Levant platform. The present study area (Ha'py Field) is located in the Ras El Barr Concession, in the northeastern portion of the offshore Nile Delta in the eastern mini-basin (Fig.1). Eight selected wells of the Ha'py Field were included in the present study. The main study interval of the Ha'py Field area is concerned with the Pliocene - Pleistocene sequence that includes Kafr El Sheikh and El Wastani formations (Sarhan et al. 1996).

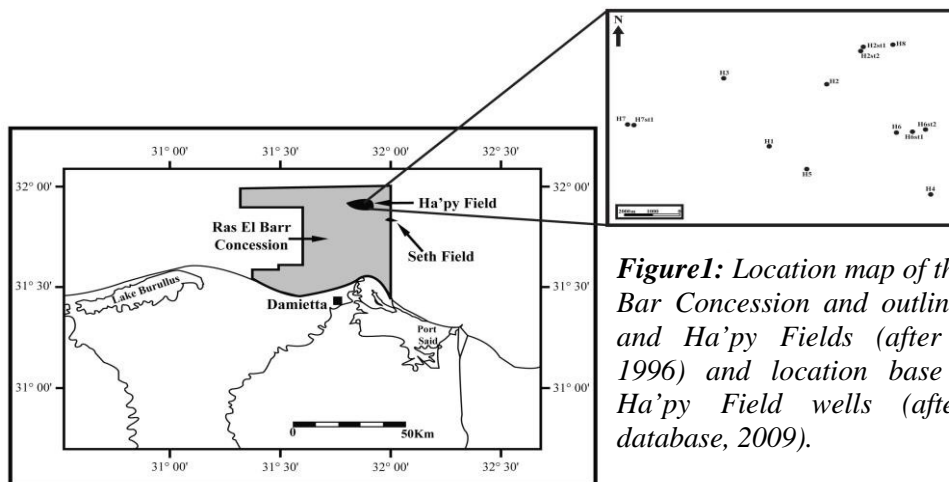


Figure 1: Location map of the Ras El Barr Concession and outline of Seth and Ha'py Fields (after Wigger, 1996) and location base map of Ha'py Field wells (after Bp database, 2009).

Method and Theory

The main target is to perform a detailed stratigraphic setup, sedimentary facies and depositional environment analyses as well as cyclicity patterns and their distribution in time and space in order to the buildup of a reservoir geological model. These are elaborated through the following steps:

- 1- Detailed lithological and palentological interpretations (Amer et al. 2013) being carried out by ditch cutting and core samples examination that were calibrated with the wireline logs responses for electrofacies characterization.

- 2- High resolution biostratigraphic analysis for a sequence stratigraphic interpretation. Cyclicity patterns and interpretation support the impact of the global sea level changes and local tectonic accommodation that controlled the studied reservoir distribution.
- 3- Petrographical study for selected thin sections in addition to X-ray Diffraction (XRD) and Scanning Electron Microscope (SEM) with EDAX.

Conclusion

The present detailed lithological and paleontological study indicates that all the studied sequences belong to the El Wastani Formation of the Late Pliocene age. This is contrary to the previous interpretation that considered the lower section of the studied wells is belonging to the Kafr El Sheikh Formation of Early Pliocene age (Bailey et al. 1999).

The lithological and paleontological interpretation proves that the studied interval of the El Wastani Formation could be subdivided into five sedimentary cycles (A, B, C, D and E). These five main sedimentary cycles could be distinguished in the third order cycle (3.7) and the lower part of (3.8) cycle that included in the Upper Pliocene - Early most Pleistocene (3.00-2.00 M.a), (Fig.2).

Scarcity of planktonic assemblages compared to the abundance of calcareous benthonics supports the deposition under shallow marine to partly restricted environment. This conclusion contradicts to the previous interpretation of open to deep marine channel and slumps (Bailey et al. 1999).

The reservoir unit consists of repetitive sedimentary cycles of one facies type in the form of shallow marine shelf sand bars. These sandstone bars were developed during the LST to TST systems tracts of the 3.7 third order cycle. The reservoir description of each sedimentary cycle was based on lithological, paleontological, petrographical analyses in addition to clay type identification using XRD analysis as well as pore spaces interpretation (SEM analysis).

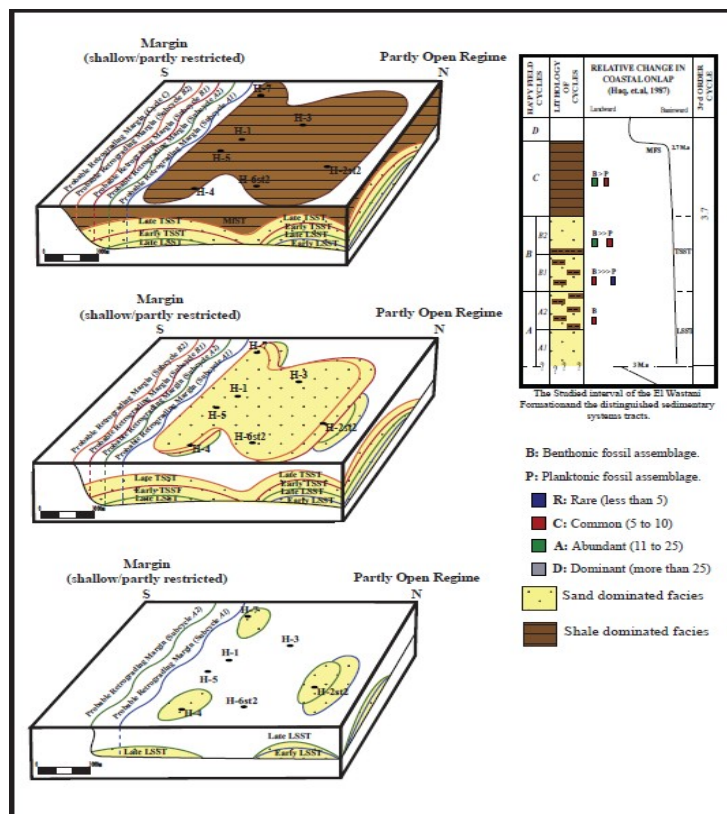


Figure 2: Cyclostratigraphic cartoon model (no vertical scale) of the study interval of the El Wastani Formation during the sea level rise of the 3.7 third order cycle.



References

- **Amer, N. M., (2013)** Sedimentary Facies Analysis and Cyclicality of Post-Miocene Sequences in the Northeast Offshore Nile Delta (Ha'py Field Case Study), M.Sc., Cairo University.
- **Bailey, I. W., Bryant, W. T., Wallace, M. G. and Shaheen W. S., (1999).** Pre-Development Reservoir Characterization of the Ha'py Field, Nile Delta, Egypt, AAPG Search and Discovery Article #90923, International Conference and Exhibition, Birmingham, England.
- **EGPC (1994)** Nile Delta and North Sinai; fields, discoveries and hydrocarbon potentials (a comprehensive overview), Egyptian General Petroleum Corporation, Cairo, Egypt, 387 p.
- **Sarhan, M.; Barsoum, K.; Bertello, F.; Talaat, M., and Nobili, M., (1996)** The Pliocene play in the Mediterranean offshore: structural setting and growth faults controlled hydrocarbon accumulations in the Nile Delta basin: A comparison with the Niger Delta basin, EGPC 13th Petroleum Conference, Cairo, Egypt, v. 1, p. 121 - 139.
- **Wigger, S. T.; Simpson, M. G.; Nada, H.; Larsen, M. J., and Haggag, M. (1996)** Ha'py Field, the result of Pliocene exploration in the Ras El Barr Concession, Nile Delta, EGPC 13th Petroleum Conference, Cairo, Egypt.



FORAMINIFERAL DISTRIBUTION IN A TROPICAL MESO-TIDAL ESTUARY ON THE SOUTH EAST COAST OF NIGERIA

Victoria I. Antia¹, Chimezie N. Emeka², Etie B. Akpan² and Edak E. Efiom¹

email: vikizbox@live.com

¹Faculty of Marine Science, University of Calabar, ²Department of Geology, University of Calabar

Summary

Fifty sediment samples collected from Qua-Iboe River estuary, Southeastern Nigeria, along 10 transects yielded nineteen foraminiferal species (fifteen benthics; four planktics). Bottom sediments were predominantly medium to very fine-grained sands. Salinity and temperature ranges were 6-14‰ and 24-29°C, respectively while the pH of bottom water varied from slightly acidic to slightly alkaline during the period of sampling. Two foraminiferal biofacies were distinguished: The upper facies, predominantly *Cyclaminna bradyi*; and the lower facies, mainly *Anomalina sp.* and *Bolivina sp.* Foraminiferal tests were sparsely distributed in the studied channel. Salinity and tidal strength greatly influenced foraminiferal distribution in the estuary.

Introduction

Estuaries are coastal sedimentary environments related to the Holocene rise in sea level. They are dynamic and dependent on tides, waves and fluvial processes. Interpretation of their ancient equivalents requires a detailed study of modern analogues. Microfossils such as foraminifera are sensitive indicators of environmental conditions (Alve and Goldstein, 2003) and their occurrence is controlled to a great extent by salinity, temperature, depth, dissolved oxygen, pH, amount of light, turbidity of water, availability of food and character of the bottom sediments (Kumar and Manivannan, 2001). Although relationships between physico-chemical parameters and foraminiferal distributions have been well established in many brackish-water settings in Nigeria (e.g. *et al.*, 1976; Aseez *et al.*, 1974; Dublin-Green, 1990; Ramanathan, 1981; Olayiwola and Odebo, 2011), little attention has been paid to the ways in which foraminifera respond to environmental parameters in Qua-Iboe River estuary, Southeast coast of Nigeria.

Dublin-Green (1990) investigated the distribution patterns of benthic foraminiferal fauna in the Bonny River estuary and attributed the complete dominance of *Textulariina sp.* in the upper and middle estuary to low pH of sediment. He observed that *Rotaliina sp.* which predominated the lower estuary, due to marine conditions prevailing at the mouth, was rare in the middle and upper estuary due to decreasing salinity and pH upstream. Ramanathan (1981) reported similar distribution along the Cross River estuary. Sediment distribution is highly controlled by energy regimes while foraminifera seem to respond to salinities and tidal exposures (Schröder-Adams, 2006). Foraminiferal assemblages serve as important signatures for recognizing various sedimentary environments.

The Qua Iboe River is a 155km long and 0.5 to 1km wide north-south trending river situated on the southeastern coast of Nigeria. Antia *et al.* (2012) distinguished two sedimentary facies, Upper and Lower for Qua-Iboe River estuary, based on grain size statistical parameters. In this present study, efforts have been made to correlate foraminiferal distribution with known environmental parameters and to establish a record of biofacies present within the estuary for better rock record reconstruction.

Method and/or Theory

Tidal current measurements were made using the Langragian method during Spring (13/9/2011), Mean (19/9/2011) and Neap (22/9/2011) at Qua-Iboe Mission and Mobil Jetty respectively. 50 bottom sediment samples were collected along 10 transects of 5 stations each. These were analysed for grain size parameters and foraminiferal content. Depth soundings were made at each station using an echo sounder, while physico-chemical parameters, such as pH, temperature, salinity and turbidity were measured in-situ, using a Hannah hand-held combo device, and a secchi disk.

Results and Discussion

Results obtained revealed that the estuary is meso-tidal with a maximum surface velocity of 0.99m/s at Spring Flood stage and 1.30m/s at the Spring Ebb stage; also maximum Spring Flood bottom tidal current velocity of 0.6m/s and maximum Spring Ebb current velocity of 1m/s, showing ebb dominance. The channel meanders, and is deepest towards the mouth, with a maximum depth of 10m. Sediments within the channel are predominantly poorly to moderately sorted fine and medium sand. Bottom water parameters include: temperature, which varies mainly between 26 and 28°C; turbidity principally ranging from 100cm to 180cm; pH between 6 and 8; and salinity mainly varying between 8 and 12ppt.

Distribution of foraminifera within the channel is presented in FIG. 1. Two foraminiferal biofacies were highlighted, on the basis of textural characteristics, coinciding with the upper and lower portions of the estuary. The upper portion with 10-70% mud content and a salinity range of 6-12 ‰ was associated with 15 species (13 benthics; 7 planktics). Higher numbers of agglutinated taxa were encountered in the upper estuary. The dominant species of the estuary, *Cyclamina bradyi*, with a relative abundance of 78% was recorded at depths of 2-4m interval of the upper estuary. The dominance of this species and general increase in diversity upstream can be attributed to the abundance of mud and deposition below the depth of tidal reworking. The lower portion with <10% mud content and a salinity range of 8-14 ‰ was associated with 2 calcareous species namely: *Anomalina sp.* and *Bolivina sp.* These species constitute less than 1% of the total population and are known to be good indicators of marine water incursion into the estuary. The decrease in species diversity at the lower portion of the studied channel is possibly due to strong winnowing by tidal current which carries both sediments and foraminiferal test into suspension, transporting them to quieter waters of the estuary. Tidal energy, salinity and mud content are important environmental parameters influencing foraminiferal distribution in the estuary.

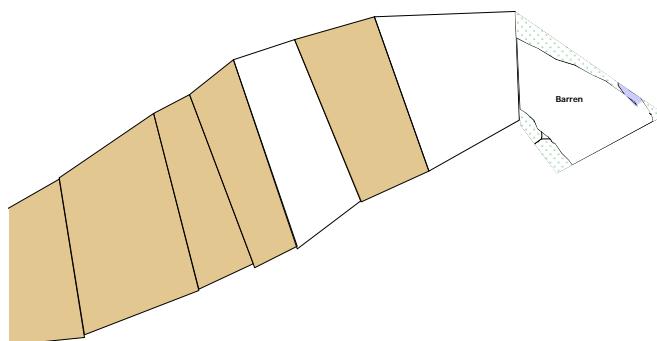


Figure 1: Foraminifera distribution in Qua Iboe River estuary

Conclusions

Qua Iboe River has been subdivided into 3 facies, based on sedimentary characteristics and foraminiferal distribution. The most numerically dominant foraminiferal species recognized for the studied estuary is *Cyclamina bradyi*. It shows a maximum occurrence in the upper portions of the estuary and decreases downstream towards marine waters where the salinity gradually becomes more stable. Planktonic species found in bottom sediments of Qua-Iboe River estuary are brought in by tidal energy while benthic species are controlled by tidal energy and salinity fluctuations.



References

- Alve, E. & Goldstein, S. T. (2003). Propagule transport as a key method of dispersal in benthic foraminifera. In E. Alve and S. T. Goldstein, *Dispersal, survival and delayed growth of benthic foraminiferal propagules*. *Journal of Sea Research*, 63, 36–51.
- Aseez, L. O., Fayose, E. A. & Omatsola, M. E. (1974). Ecology of the Ogun River estuary. In M. A. Olayiwola and M. O. Odebode, *Multivariate analysis of planktonic foraminiferal assemblage of Southwestern Nigeria's surface continental shelves' sediments*. *European Journal of Scientific Research*, 54, 84-101.
- Kumar, V. & Manivannan, V. (2001). Benthic foraminiferal responses to bottom water characteristics in the Palk Bay, off Rameswaram, southeastern coast of India. *Indian Journal of Marine Science*, 30, 173-179.
- Dublin-Green, C. O. (1990). The foraminiferal fauna of Bonny Estuary, Niger Delta: A baseline study. *Technical Paper of the Nigerian Institute of Oceanography and Marine Research*, 64, 1-27.
- Ramanathan, R. M. (1981). Ecology and distribution of foraminifera in Cross River estuary and environs off Calabar, Nigeria. *Journal of Mining Geology*, 18 (1), 154-162.
- Olayiwola, M. A. & Odebode, M. O. (2011). Multivariate analysis of planktonic foraminiferal assemblage of Southwestern Nigeria's surface continental shelves' sediments. *European Journal of Scientific Research*, 54, 84-101.
- Schröder-Adams, C. J. (2006). Estuaries of the past and present: A biofacies perspective. *Sedimentary Geology*, 190, 289–298.
- Antia, V. I., Emeka, N. C., Ntekim, E. E. U. & Amah, E. A. (2012). Grain size distribution and flow measurements in Qua-Iboe River estuary and Calabar River, South-East Nigeria. *European Journal of Scientific Research*, 67 (2), 223-239.



Growth and evolution of syn-sedimentary deltaic faults in Tomboy Field, Niger Delta

Omosanya K.O¹, Lawal, M.A^{2*}, Kaigama, U³

Email: kamaldeen.o.omosanya@ntnu.no

Department of Petroleum Engineering and Applied Geophysics, Norwegian Univ. of Sci. and Tech.¹;

University of Perugia²; Modibbo Adamawa University of Technology, Adamawa. Nigeria³

Summary

The faults in the study area developed through a combination of syn-sedimentary activity and blind/radial propagation of their tips. The syn-kinematic packages in the study area include rocks of the Agbada and Akata Formation, the Benin Formation is unfaulted and post-kinematic in nature. In addition, fault growth in the Tomboy Field is in agreement with both the isolated and coherent fault models. Reactivation is through dip linkage and are shown as displacement minima on t-z plots. In general, the faults geometry and propagation have influenced the compartmentalization of sedimentary units in the delta.

Introduction

Normal faults associated with deltas are involved in the formation of major traps for hydrocarbon reservoirs and may also isolate compartments in subsurface reservoirs (Bhattacharya and Davies, 2001). As normal faults can nucleate, propagate, and develop through either the coherent or isolated model (Figure 1). The several aspect of syn-sedimentary deltaic faulting such as nucleation, abandonment, reactivation, and growth remains unknown (Khani and Back, 2012). Hence, this study is aimed at assessing the growth and history of syn-sedimentary fault formed in a deltaic setting and how they fit into either the coherent or isolated model for fault growth. To achieve this aim, fault displacement plots such as displacement versus distance (t-x), displacement versus depth (t-z), expansion and growth indices are used to investigate the history of fault nucleation, propagation, segmentation, and linkage (*cf.* Omosanya and Alves, 2014).

Data and Methods

The data for this work is a pre-stack migrated (PSTM) seismic cube covering approximately 55 km² in water depth of 1000 to 2000 m in offshore Niger delta, Nigeria. Bin spacing, vertical and horizontal resolutions are 25 m x 25 m, 16 m, and 25 m, respectively. Seismic interpretation of thirteen (13) stratigraphic units and eight (8) faults were done to constrain the geometry and history of sedimentation in the field. Fault modeling was used to estimate angle of dip and direction of the dip. The orientation of the faults is graphically shown in rose diagram. Fault propagation and evolution were assessed using displacement plots and expansion indices. Fault throw was estimated on faults using seismic profiles (inlines) perpendicular to fault strike. The throw is the difference between hangingwall and footwall cut-offs. Expansion index (EI) is the ratio of thickness between the layers in the hangingwall to the thickness in the footwall of a fault (Pochat et al., 2009) while the growth index is calculated as the difference in thickness between the hangingwall and the footwall of an interval divided by the thickness of the interval in the footwall (Childs et al, 2003).

Results and Conclusions

Faults in the study area are rotational, non-planar listric normal faults, they are characterised by decreasing angle of dip with depth (Figure 1). On the hanging wall section, some of the faults have roll-over anticlines which were developed during fault activity. Fault movement is influenced by the shaly detachment, Akata Formation. As a consequence, the interpreted faults interacted with the whole of the Agbada Formation (H2 to H10) and are detached into the Akata Formation.

Along strike, the faults display complex throw-distance plots and are comprised of several segments. This is evidence that the faults are laterally linked along strike (Figure 2a). Furthermore, the throw (t) – depth (z) plots include M-type and skewed C-type (Figure 2b). Fault segments are linked at displacement minima. The complex combination of t-z profiles hints at reactivation through dip-linkage and polycyclic fault growth. In addition, the faults have combined expansion and growth

indices (Figure 2c), EI of > 1 suggest significant thickening of strata on the downthrown side of the faults while values of < 1 are associated with thinning of sediments in the hanging wall of the faults (Thorsen, 1963; Pochat et al., 2009). Conversely, GI of > 0.1 implies that the faults were buried beneath stratigraphic surfaces during their growth while $GI < 0.1$ indicates the faults grew to the surface and interacted with a free surface.

Hence, faults in the study area are not simply syn-sedimentary faults in terms of their growth and geometry but are developed through a combination of blind propagation of their tips (isolated model), syn-sedimentary activity (coherent model) and dip-linkage (reactivation).

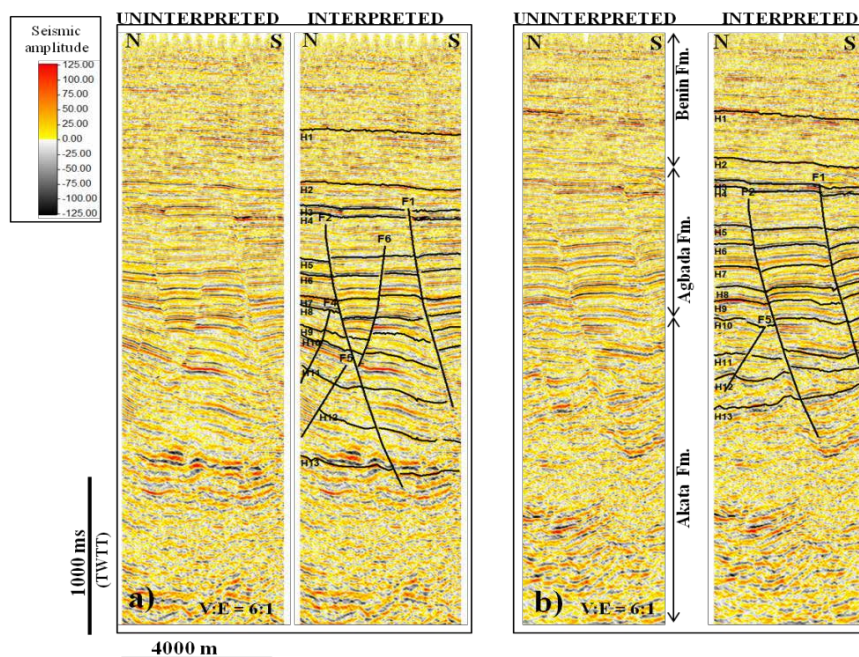


Figure 1: Interpreted faults are dip-slip normal faults that are detached into the shaly Akata Formation (H10) and are buried beneath at the Base Benin Formation (H2).

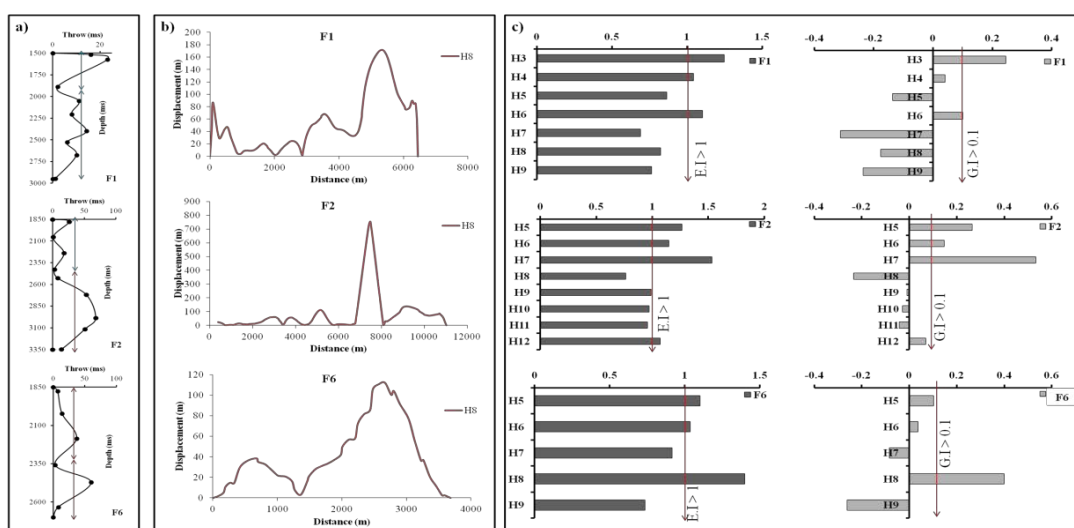


Figure 2: (a) Throw(t) vs. Depth(z) plots (b) Displacement(d) vs. Distance (x) plots show that faults in the study area have complex lateral segmentation (c) Plots of EI and GI . Faults have $EI > 1$ and < 1 and also GI of > 0.1 and < 0.1 .



References

- Bhattacharya and Davies, (2001). Growth faults at the Prodelta to delta front transition, Cretaceous Ferron Sandstone, Utah: *Marine and Petroleum Geology* 18, 525-534.
- Childs, C., Nicol, A., Walsh, J.J., Watterson, J., (2003). The growth and propagation of synsedimentary faults. *Journal of Structural Geology* 25, 633-648.
- Khani H. and Back S., 2012. Temporal and Lateral variation in the development of growth faults and growth strata in the western Niger delta, Nigeria. *American Association of Petroleum Geologists Bulletin* 96, 595-614.
- Omosanya, K.O. and Alves, T.M. (2014). Mass-transport deposits controlling fault propagation, reactivation and structural decoupling on continental margins (Espírito Santo Basin, SE Brazil). *Tectonophysics*.
- Pochat, S., Castelltort, S., Choblet, G., Van Den Driessche, J. (2009). High resolution record of Tectonic and Sedimentary Processes in Growth strata. *Marine and Petroleum Geology* 1350-1364.
- Thorsen, C.E., (1963). Age of growth faulting in the southeast Louisiana. *Transactions Gulf Coast Association of Geological Societies* 13, 103-110.

Subsurface structure of the saline hot spring in Krabi, Southern Thailand, from an integrated geoscientific investigation

Wipada Ngansom, Helmut Dürrast

email: p_wipada@hotmail.com

Prince of Songkla University, Hatyai, Thailand

Summary

Geological, geophysical, and geochemical investigations were carried out in the saline hot spring area of Krabi in southern Thailand. The purpose of this work was to determine subsurface geological structures related to the hot springs. Geophysical results show salty groundwater from ocean water intrusion in shallow sandstone aquifers. Hot waters are coming from depth, approximately at 200 m, based on geothermometers. Their flow is limited by shallow faults, which were delineated by geoelectrical measurements. Well data suggest that these faults restrict the flow of the hot waters but allow osmotic exchange of the salinity.

Introduction

Saline hot springs can be found in Khlong Thom District of Krabi Province, Thailand, about 814 km south of Bangkok or about 70 km southeast of Krabi city, at latitude 7° 54.199' North and longitude 99° 6.505' East (Figure 1). The site is located close to one of the tributaries of the Phela river system, which is connected to the Andaman Sea. Altogether 15 natural hot springs can be found, ten within the mangroves and five outside nearby. Latter ones have been developed for tourism. Hot spring sites cover an area of about 0.5 km² with surface exit temperatures from 41 to 47 °C.

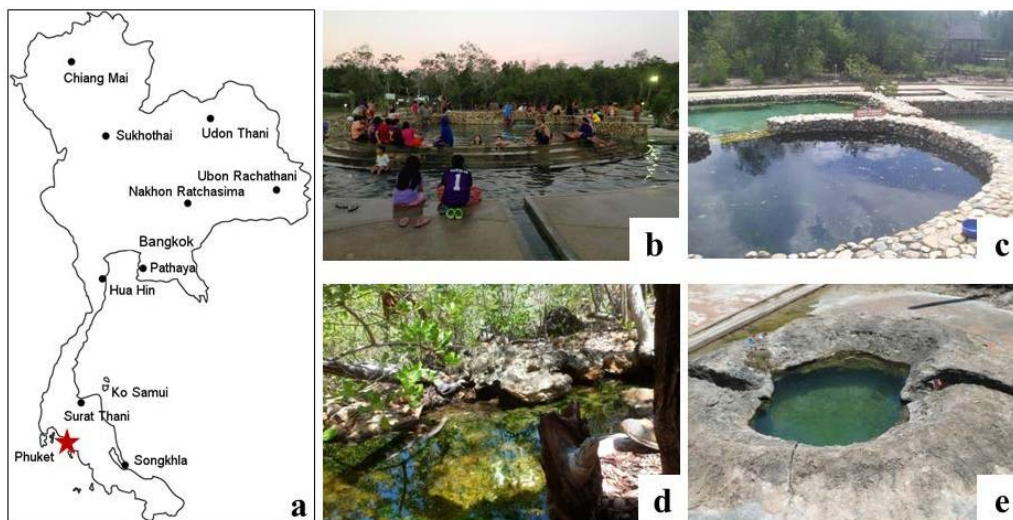


Figure 1 a) Location of the study area with saline hot spring; b) and c) man made structures for tourism, d) and e) natural hot spring sites with precipitated carbonate crust around.

Methods

In order to understand the subsurface structure of the saline hot springs a combination of geological fieldwork, geophysical surveys, geochemical analysis of water samples was applied. Altogether fifteen 1-D vertical electrical sounding measurements were carried out around the hot spring sites with an AB/2 of 100 to maximal 150 m in order to delineate the distribution of the hot waters in the shallow subsurface. Water samples from several wells were collected, its exit temperatures measured, and its geochemical composition determined in the laboratory of the Faculty of Science, Prince of Songkla University. Local offices were contacted for additional data and information available.

Results and Discussion

Almost all 1-D resistivity surveys show very low resistivity values (below 10 ohm-m) at relatively shallow depth, 5 to 20 m, in the southern and at 5 to 60 m in the northern part of the hot spring site (see Figure 2). However, further south low resistivity layers are phasing out, so that 500 m further away very low resistivity values could not be measured anymore. These low values can be correlated to saline groundwater and saline hot spring water in sandstone layers. Due to their salinity the VES method cannot distinguish between both. A 100 m-deep well drilled in the hot spring area shows only sandstone of different color, with upper layers weathered. Shallow wells, 30 to 50 m, south of the site show saline hot waters, whereas further away shallow groundwaters are salty but not hot anymore. In the western part of the hot spring site the horizontal distance between 46 °C salty groundwater in a well and salty water with normal temperature is only 150 m. In order to explain this a fault has been introduced between both sites (see Figure 2). In the western part another fault has been introduced based on significant differences in VES profiles at short horizontal distances, which could not be explained by normal stratigraphy. At all the natural hot spring sites carbonate crusts were found around with up to 1.2 meter thickness (see Figure 1), which supports the assumption that beneath the sandstone at depth there are limestone formations (see also Jonjana et al., 2012). The geochemical analysis of the hot waters show higher Ca content and about 7 km to the west limestone mountains can be found. From Na-K, Na-K-Ca, and K-Mg geothermometers a hot water reservoir depth of 200 m km can be inferred (Baioumy et al. 2015).

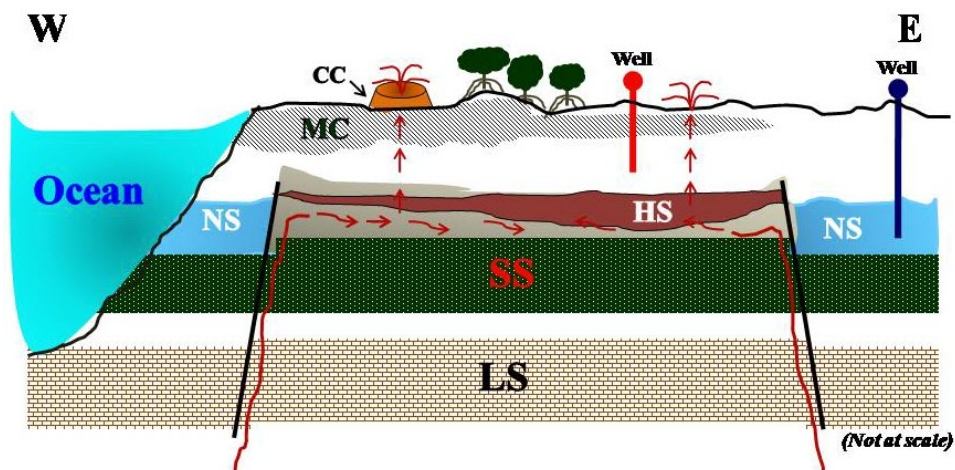


Figure 2 Schematic geological cross-section of the study area and geothermal system along a west-east profile; CC – carbonate crusts at hot spring sites, MC - black marine clay, NS - salty water of normal temperature, HS – salty hot spring water, SS - sandstone, and LS – limestone. Relative locations of some wells are shown.

Conclusions

Geophysical and geochemical investigations at the saline hot spring area in Krabi Province have shown that the hot water is coming from a deeper reservoir whereas the salty water is coming from the ocean via intrusion into shallow aquifers. The exchange might be osmotic through faults that have been delineated in the shallow subsurface. They also act as boundaries for the hot waters and by this restricting further flow into the aquifers, by this limiting the spatial extent of the hot spring area. The heat source of the hot waters has not been found yet and is likely outside the study area (see Nilsuwan, 2011).



References

- Baioumy, H., Nawawi, M. Wagner, K. and Arifin, M.H. (2015). Geochemistry and geothermometry of non-volcanic hot springs in West Malaysia. *Journal of Volcanology and Geothermal Research* 290, 12–22.
- Jonjana, S., Lohawijarn, W. and Dürrast, H. (2012). Geological structure and origin of the Kaochaison hot spring in Phattalung, Southern Thailand, *Songklanakar J. Sci. Technol.*, 34 (2), 231-239.
- Nilsuwan, U. (2011). Gravity and Magnetic Investigations of the Geothermal Hot Springs in Krabi, Southern Thailand. Master Thesis, Geophysics Program, Faculty of Science, Prince of Songkla University.



Chemical and textural variability within the Adamello tonalites: Implications for melt extraction from crystal mush

Alina Fiedrich¹, Olivier Bachmann¹, Chad Deering², Peter Ulmer¹
email: falina@student.ethz.ch

¹ETH Zurich, ²Michigan Tech

Summary

In order to better understand the link between volcanic and plutonic realms, quantitative textural analyses were performed on samples from the Adamello batholith, using scanning electron microscopy and electron backscatter diffraction. This textural information was coupled to bulk-rock geochemical analyses and phase maps to determine the amount of interstitial melt trapped in different parts of the batholith.

Introduction

Understanding the evolution of magmatic systems is one of the most prominent research topics in igneous petrology (e.g. Bachmann et al., 2007). Magma reservoir processes and the connection between volcanic and plutonic rocks, in particular, are of prime interest (e.g. Huber et al., 2012; Cashman & Sparks, 2013; Lipman, 2007; Annen, 2009; Glazner et al., 2008). The study of melt extraction from highly crystalline magma reservoirs (mush), which may lead to volcanic eruptions, is of interest for determining the timescales over which eruptible magma accumulates in the shallow crust and can aid in volcanic hazard assessment (Bachmann & Bergantz, 2008). The Adamello batholith in the Italian Alps represents a well-studied, well-exposed shallow-level pluton, consisting of four tonalitic superunits that are well-suited for research on internal magma reservoir processes.

Methods

Electron backscatter diffraction (EBSD)

Crystal structures can be used, complementary to trace element studies, to identify crystal cumulates and to trace processes operating in the crystal mush that led to melt extraction. Some indicators of crystal accumulation are magmatic foliation, oriented crystal clusters, and crystal bending. These indicators may be visible macroscopically in strongly compacted samples. However, EBSD (Fig. 1) proves helpful for samples with only faint textures; with only one thin section scan, foliation(s) and lamination(s) can be visualized. This quantitative textural data can be used to determine mechanisms of textural development (Meurer & Boudeau, 1998b). In addition, misorientation between neighboring crystals can be measured to determine the strength of fabric (e.g. Wheeler et al., 2001).

Energy-dispersive spectroscopy (EDS) scans

The quantification of the interstitial material is essential for the study of cumulates as it can be used to estimate the terminal porosity achieved during crystal-melt separation. This type of estimation was attempted by means of whole-rock geochemistry and trace element modeling in layered mafic intrusions by several researchers (Meurer & Boudreau, 1998a and references therein); however, utilizing simple light microscopy determining the extent of late overgrowth on minerals and the amount of inter-cumulus material could not be achieved. Here, phase maps (Fig. 2) are used to estimate the amounts of cumulus crystals, inter-cumulus material, and late overgrowth. Quartz, alkali feldspar, and low-An plagioclase are assumed to crystallize last in these tonalitic rocks. The percentage of low-An plagioclase is quantified by means of An-binning based on Al/Si net count ratios. Phenocrystic quartz is excluded based on CL images.

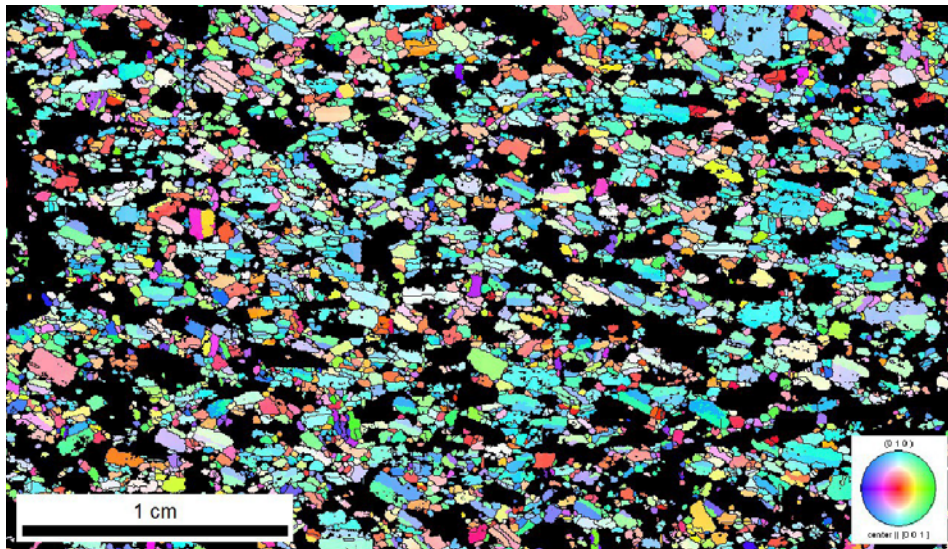


Figure 1 EBSD orientation map on a foliated quartz-diorite from Adamello, color-coded according to crystal orientation with respect to long axis. Only plagioclase crystals are displayed in color.

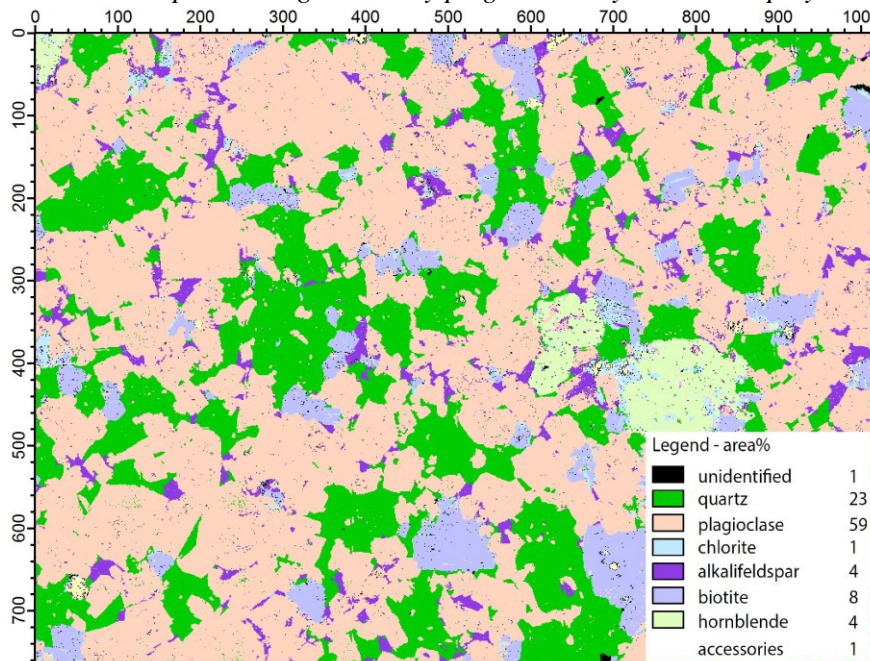


Figure 2 EDS thin section scan of an unfoliated tonalite sample from Adamello, processed to a phase map in iSpectra. Major phases are plagioclase, quartz, biotite, hornblende, and alkali feldspar.

Conclusions

Expected outcomes are a correlation between compactions, expressed as textural “maturity”, and percentages of interstitial material, as well as evidence for silicic crystal mush. Some parts of the batholith that exhibit strong magmatic foliation and little interstitial material can unambiguously be identified as cumulates; while others that possess no crystal orientation and much interstitial material are interpreted to be frozen liquids. Both orientation and phase maps can be applied to various fields in petrology.



References

- Annen, C. (2009). From plutons to magma chambers: Thermal constraints on the accumulation of eruptible silicic magma in the upper crust. *Earth and Planetary Science Letters* 284.3, 409–416.
- Bachmann, O., Bergantz, G. (2008). The magma reservoirs that feed supereruptions. *Elements* 4.1, 17–21.
- Bachmann, O., Miller, C., De Silva, S. (2007). The volcanic-plutonic connection as a stage for understanding crustal magmatism. *Volcanology and Geothermal Research* 167.1, 1–23.
- Cashman, K., Sparks, R. (2013). How volcanoes work: A 25 year perspective. *Geological Society of America Bulletin* 125.5-6, 664–690.
- Glazner, A., Coleman, D., Bartley, J. (2008). The tenuous connection between high-silica rhyolites and granodiorite plutons. *Geology* 36.2, 183–186.
- Huber, C., Bachmann, O., Dufek, J. (2012). Crystal-poor versus crystal-rich ignimbrites: A competition between stirring and reactivation. *Geology* 40.2, 115–118.
- Lipman, P. (2007). Incremental assembly and prolonged consolidation of Cordilleran magma chambers: Evidence from the Southern Rocky Mountain volcanic field. *Geosphere* 3.1, 42–70.
- Meurer, W., Boudreau, A. (1998a). Compaction of igneous cumulates part I: geochemical consequences for cumulates and liquid fractionation trends. *The Journal of geology* 106.3, 281–292.
- Meurer, W., Boudreau, A. (1998b). Compaction of igneous cumulates part II: Compaction and the development of igneous foliations. *The Journal of geology* 106.3, 293–304.
- Wheeler, J., Prior, D., Jiang, Z., Spiess, R., Trimby, P. (2001). The petrological significance of misorientations between grains. *Contributions to Mineralogy and Petrology* 141.1, 109–124.



Primary results on geochemistry of copper slags from Kondratów and Leszczyna, SW Poland

Katarzyna Kadziolka¹, Jakub Kierczak
email: katarzyna.a.kadziolka@gmail.com

¹University of Wrocław

Summary

Slags are important source of knowledge about technological process of metal smelting. Analyzes based on the historical samples from Kondratów and Leszczyna provided first actual data on the character of metal production in this part of North Sudetic Basin. Deposits of Cu ores found in the area are related to Zechstein copper deposits (Lower Permian) that appear in SW Poland. Electron microprobe and X-ray diffraction spectroscopy have been used for recognition of chemical and mineralogical (phase) composition of slags. Collected samples revealed certain differences what led to conclusions about various smelting technology conducted on both sites.

Introduction

Kondratów and Leszczyna are situated in Lower Silesia, southwestern Poland. This region is known for its rich copper ores that have been excavated since Middle Ages. There are several main geological units distinguished within this area but only two of them are associated with rich Cu ores: Fore-Sudetic Monocline in the north, and North Sudetic Basin in the south. This units are orientated NW-SE and situated north from Sudetes Mountains and Sudetes Foreland, within Silesian Lowland. Deposits of Kondratów and Leszczyna are located in the North Sudetic Basin.

Ores were formed in Lower Permian. Cu deposits are associated with slate marls (which means they are strata-bound type) and are of relatively low quality presenting the highest Cu content of less than 2%. Nevertheless its fairly easy extraction resulted in the fact that the ore was mined willingly.

First evidence of the copper mining presence and existence of smelting facility come from the late Middle Ages. Based on archaeological research it has been proven that ores have been exploited since 17th century (Stolarczyk 2012). Obtained ore has been processed and remelted in a nearby smelters what resulted in a long-term accumulation of smelting production wastes. As a consequence the region of Kondratów and Leszczyna is nowadays rich in those industrial sludge in the form of slags.

Method

Samples were obtained in the area of Kondratów and Leszczyna and it have occurred in two characteristic forms – of porous and massive slag blocks. Both of those samples were collected in order to check whether smelting process in both localities was similar and of an equal age.

Chemical and phase composition of slag has been identified with few spectroscopy methods. Main research methodology has not yet been established and there are numerous methods used, usually dependently on equipment availability. In this research results were obtained using electron microprobe and X-ray diffraction spectroscopy.

Results

Analyzed samples present two different types of slag but both are composed of: silica, lime, alumina and iron with a small amount of potassium and magnesium. There were clear differences in the quantitative composition of the main ingredients of which the most common are: SiO₂, CaO, Al₂O₃ and Fe₂O₃. Slags from Leszczyna contain respectively 46,96% SiO₂, 19,20% CaO, 17,96% Al₂O₃, 3,31% Fe₂O₃ whereas slags from Kondratów: 45,98% SiO₂, 16,97% CaO, 11,6% Al₂O₃, 14,40%

Fe₂O₃. Clear discrepancies between those chemical components are first sign of a different smelting process and its efficiency since there is 2991 ppm of Cu in slags from Leszczyna and about six times more – 19239 ppm in slags from Kondratów. As copper slags emerged as a result of smelting copper ores – Cu was a eligible element that was supposed to be extracted in the largest possible quantity.

Major phases are represented by silicates (e.g., leucite, pyroxene) and silicate glass.

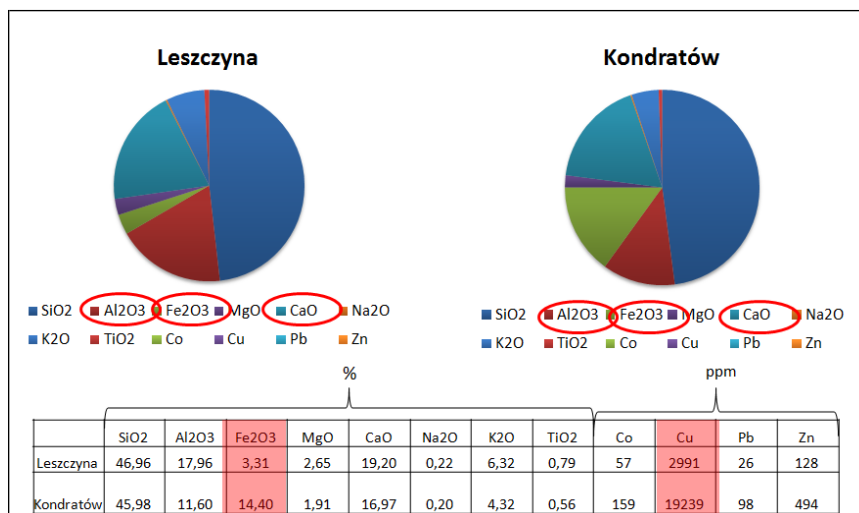


Figure 1 Main chemical components in slags from two localities. Most important differences are highlighted with red colour.

Conclusions

Despite close location, preliminary research conducted on the slags from Kondratów and Leszczyna allowed to conclude that smelting technology on both sites differed. Basing on chemical composition it seems that slags from Kondratów are remnant of substantially worse production technology as big amount of desired element (Cu) has been left in a waste product.

Acknowledgements

I would like to acknowledge and thank to my scientific supervisor – dr Jakub Kierczak – who allowed me to engage in the research, but as well as dr Tomasz Stolarczyk from Copper Museum in Legnica for help and allowing access to the samples.

References

Stolarczyk, T. (2012). Wyniki badań archeologicznych dawnego górnictwa i hutnictwa miedzi na terenie Pogórza Kaczawskiego i Rudaw Janowickich w 2012 r. Zeszyty Legnickie, 33, 207-239.

APPLIED GEOPHYSICS

TUESDAY, 14 July

Session A 10:15-11:30

Charimen: Małgorzata Drwiła, Christian von Hebel

10 : 15	Determination of seismic wave attenuation based on acoustic full waveforms	Eryk Święch
10 : 30	Crustal S-wave velocity structure beneath Cameroon Volcanic Line (CVL) and adjacent regions from Ambient Noise Tomography	Ojo Adebayo Oluwaseun, Ni Sidao, Li Zhiwei
10 : 45	A Novel algorithm for boundary analysis	Fikret Dogru, Emre Timur, Coskun Sari
11 : 00	Seismic geomorphology of the Lobed-channel System of Upper Miocene Huangliu Formation, DF-1/2 Block, Yinggehai Basin, Northwestern South China Sea	Haoran Liu
11 : 15	Mapping of bedrock discontinuity using resistivity and seismic imaging techniques at El- Obour city, Egypt.	Samir, A., El-Kenawy, A., Gmail, Kh. and Abd El- Raouf, A.

Session B 12:30-13:30

Charimen: Filip Bolesta, Andrey Konkov

12 : 30	Analysis of seismic reflection data recorded in the desert areas (Ghadames, Libya)	Hamdi Elagieli
12 : 45	Aftershock Prediction Map of New Zealand Using Wavelet Based Multi-scale Analysis	Vishnu Srivardhan
13 : 00	The Development of a Channel-system in a tropical Carbonate Slope Environment and the Influence of Syn-sedimentary Deformation, Browse Basin, Australian North-WestShelf	L. Rinke-Hardekopf, L. Reuning, S. Back, J. Bourget
13 : 15	A new sorbent for arsenic (As) removal in contaminated groundwater sites	Olusegun K. Abass, S.Q Kong



Determination of seismic wave attenuation based on acoustic full waveforms

Eryk Święch

email: swiech@agh.edu.pl

AGH University of Science and Technology

Summary

The loss of elastic energy to the medium can be quantified by the quality factor Q . Acoustic full waveforms log from Winna – Góra - 1 borehole were used to estimate P – wave quality factor. Interpretation of acoustic full waveforms was performed for the one pair of waveforms. The most important part in the interpretation of the data is manual picking of P wave arrival, calculation of semblance function and picking anomalies of P wave on amplitude spectrum. Using data from interpretation of acoustic full waveforms quality factor Q was calculated.

Introduction

Attenuation of elastic waves is the phenomena of that manifests itself by the decrease of amplitudes along with time and distance, where the wave is recorded in reference to source point. Attenuation is inelastic process, where we observe constant loss of seismic energy as a result of inelastic deformations. One of the reason why attenuation occurs is redistribution of energy connected with heterogeneity of rocks. Fractures, lithological boundaries, faults and other heterogeneities cause generation of new waves at the expense of the energy of the incident wave. Another reason for attenuation of elastic waves are losses of energy, caused by high - temperature internal friction. Interaction between grains and fluids penetrating pore space of rocks, result in losses of energy at the expense of created heat [Barton, 2007].

In case of seismic measurements in highly fractured zones it seems, that the greatest influence on the attenuation of seismic wave is related to absorption resulted from internal friction on the surfaces of microcracks etc. This is the view presented by Barton in reference to deformation state of medium that allows for displacement of contact area. In such conditions we observe significant impact of friction on stress level [Barton, 2007].

As a fundamental measure of attenuation is assumed [Tonn, 1989]:

a. Attenuation coefficient α

$$\alpha = \frac{l}{\Delta l} \left[\ln \left(\frac{A_1}{A_2} \right) - \ln \left(\frac{G(z_1)}{G(z_2)} \right) \right] \quad (1)$$

where:

A_1, A_2 – amplitudes of selected phase of the wave,

Δl – tool length,

$G(z_1), G(z_2)$ – geometrical spreading factor of the wave towards closest and furthest receivers.

b. Quality factor Q

$$Q = \frac{-\pi(T_{pj} - T_{pi})f}{\ln \left(\frac{W_2}{W_1} \right)} \quad (2)$$

where:

f – wave frequency,

T_{pj} – time of the first arrival of P wave on acoustic full waveforms recorded on more distant receiver

T_{pi} – time of the first arrival of P wave on acoustic full waveforms recorded on closer receiver,

W_1, W_2 – amplitude spectrum of the wave, calculated for signal recorded on both receivers

Method

Several different approaches for determination seismic wave attenuation exists. One of them is calculation attenuation of seismic waves using acoustic full waveforms. This method is based on the measurement of velocity of the seismic wave travelling through geological formation.

Instrument used for the measurements is equipped with transmitter (emitting acoustic wave) receivers. Modern devices used for this kind of measurements are equipped with at least one transmitter and two receivers [Paillet et al., 1992].

Interpretation of acoustic full waveforms (Fig. 1) was performed for one pair of wave acoustic images WF1-WF4, that corresponds to the greatest distance between receivers.

Conducted interpretation was based on:

- Picking times of the first arrivals of P and S wave, on both chosen receivers, e.g. WF1-WF4
- Calculating the semblance function
- Picking anomalies of P and S waves on the amplitude spectrum of the signal

As measure of attenuation, quality factor Q was used. It was calculated with usage of equation 2.

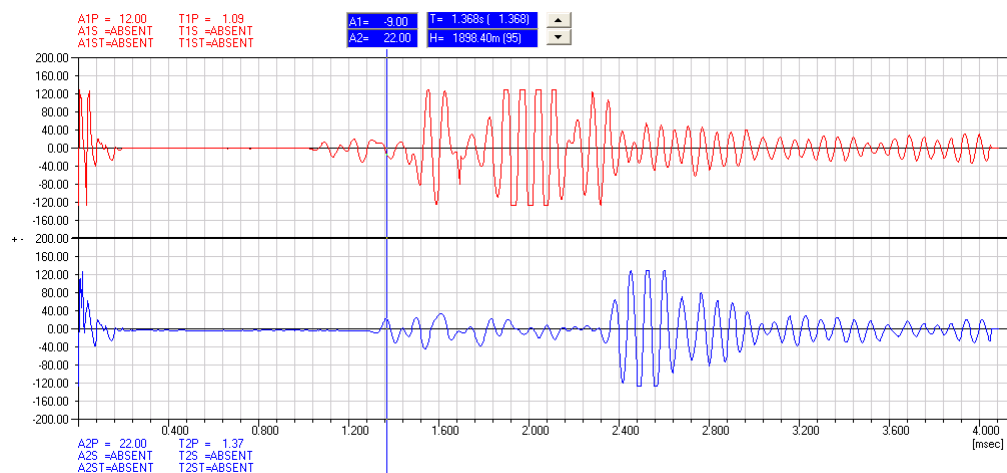


Figure 1 Acoustic full waveforms data, set WF1 – WF4, record nr. 95

Conclusions

Conducted analysis, proved that attenuation, measured in terms of quality factor Q is highly dependent on lithology.

Quality factor was calculated for 9 stratigraphic intervals from 116 to 3520 m. The lowest value for Q , so the biggest attenuation is observed in Rotliegend strata. The smallest attenuation, so the highest value for Q is in J1 strata.

Further analysis is required for more precise identification of P and S wave on acoustic full waveforms both in time and frequency domain.

Surface layer was not the subject of analysis in this study but it seems to be very reasonable to calculate quality factor also for this zone, since it is believed that this zone is highly attenuated.



References

Barton N. (2007): Rock Quality, seismic velocity, attenuation and anisotropy. Taylor & Francis.

Paillet F. L., Cheng C. H. & Pennington W. D. (1992). Acoustic-waveform logging – advances in theory and application. *The Log Analyst*, 32, 3, 239-257.

Tonn R. (1989). Comparison of seven methods for computation of Q. *Physics of the Earth and Planetary interiors*, 55, 259 – 268.

Crustal S-wave velocity structure beneath Cameroon Volcanic Line (CVL) and adjacent regions from Ambient Noise Tomography

Ojo Adebayo Oluwaseun¹, Ni Sidao² and Li Zhiwei²

¹School of Earth and Space Sciences, University of Science and Technology of China, Hefei, China

²State Key Laboratory of Geodesy and Earth's Dynamics, Institute of Geodesy and Geophysics, Wuhan, China

Summary

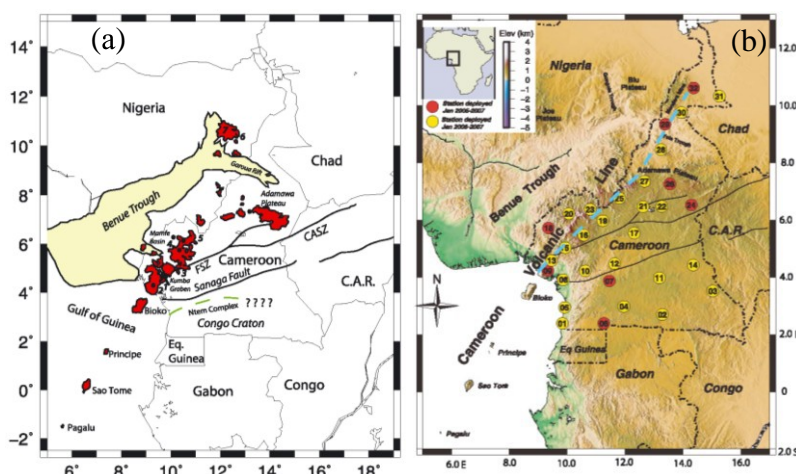
Rayleigh wave group and phase velocity dispersion curves were extracted from ambient seismic noise and jointly inverted for 3-D shear wave structure of the crust beneath Cameroon. We find that (1) a low velocity anomaly is evident along the CVL and Mamfe basin in the upper crust; (2) the Crust is thinner in the southern part of the CVL and near the Garoua Rift. (3) The Ntem Complex is imaged as a high velocity zone and a boundary can obviously be inferred between it and the Pan African Oubanguides belt.

Introduction

The Cameroon region corresponds to a complex geologic unit which hosts major geologic features such as the Cameroon Volcanic Line (CVL), Central Africa Shear Zone (CASZ), Benue Trough, Adamawa Plateau, Congo Craton and several other diverse tectonic structures as shown in Figure 1(a).

Figure 1: (a) Simplified geological map of the study area. Volcanic areas of the CVL are shown in red. The approximate northern boundary of the Congo Craton is shown with a green dashed line, and the small solid circles show approximate location of xenolith occurrences. FSZ, Fouban shear zone; CASZ, Central African shear zone. The approximate locations of the Etinde, Cameroon, Manengouba, Bamboutos, Oku and Mandara mountains are shown by numbers 1–6, respectively, and the Biu Plateau is shown with the number 7.

(b) Colour elevation map showing seismic station locations (After Tokam et al., 2010)



Cameroon Volcanic Line (CVL) consists of chain of volcanoes that do not exhibit an age progression. Its origin has been a subject of considerable debates. To resolve its evolution, the crustal and upper mantle structure beneath the CVL and other regions in Cameroon has been studied by a number of researchers using various techniques ranging from passive to active seismic methods and Potential Field methods. Recent studies include that of Tadjou et al. (2009); Tokam et al. (2010); Reusch et al. (2010, 2011); Gallacher and Bastow (2012); Koch et al. (2012); Elsheikh et al. (2014); De Plaen et al. (2014) and Noel et al. (2014) among others.

Surface wave tomography from ambient noise becomes an effective tool for crustal velocity structure studies, which uses the cross correlation of seismic noises to estimate Green function between pairs of seismic stations. The first application of this method by Sabra et al. (2005) and Shapiro et al. (2005) in Southern California revealed that geologic features such as sedimentary basins and large igneous batholiths could be reliably imaged. The method has been applied to investigate the crustal structure in many regions of the world. With the joint inversion of Rayleigh wave group and phase velocity dispersions across 32 broad-band seismic stations (Figure 1b), we investigate the crustal 3-D shear wave velocity structure beneath CVL and adjacent regions. New insights into the structure of the crust across Cameroon are presented in this study.

Data and Methodology

We use vertical component of continuous broadband data with sampling frequency of 1Hz recorded during the year of 2006 by the Cameroon Broadband Seismic Experiment, which consisted of 32 portable broad-band seismometers across Cameroon (Figure 1b).

The data processing method presented in Bensen et al. (2007) were used to process the waveforms. In summary, after removing instrument responses and filtering, waveforms are converted to 1-bit amplitude time series. Daily cross correlations of noise records between all station pairs are computed and data for same station pair are stacked over a period of one year to obtain inter-station Noise Correlation Functions (NCF) which is often dominated by fundamental mode Rayleigh waves. The positive and negative time lags are averaged for each station pair to obtain symmetric component of the NCF's in order to improve the signal-to-noise ratio (SNR). Dispersion measurements are extracted by multi-filter method (Herrmann, 2013), and only NCF with high SNR and inter-station distance greater than three-times are used in the inversion. Group and phase velocity tomography are conducted on a grid of $0.5^\circ \times 0.5^\circ$ at periods ranging from 5 to 29 s using the Fast Marching Method (FMM) (Rawlinson and Sambridge, 2005).

The group and phase velocity estimates are jointly inverted as a function of depth. The 3-D shear wave velocity model which reliably extends to a depth of about 36 km highlights tectonic features apparent at the surface.

Results and Conclusion

The 3-D shear wave velocity models revealed the large-scale velocity anomalies of $\sim 2 - 4\%$ which clearly indicate the sedimentary basin, chain of volcanoes, Plateau and cratonic blocks. A low velocity anomaly is revealed across the CVL. The Mamfe basin is imaged as a low velocity zone from the surface to ~ 12 km depth beneath a thin oceanic crust imaged as high velocity zone at deeper crustal depth. The Ntem Complex is imaged as a high velocity zone deep to a depth of 32 km and subsequently underlain by a low velocity zone. It indicates that the crust is relatively thick at this region. The Garoua Rift initially imaged as a low velocity zone is underlain by high velocity zone at a depth of ~ 26 km. Generally, with the improved data coverage in this study, a better topographic results (Figure 2) of crustal structure is provided, which is also consistent with previous studies in this area.

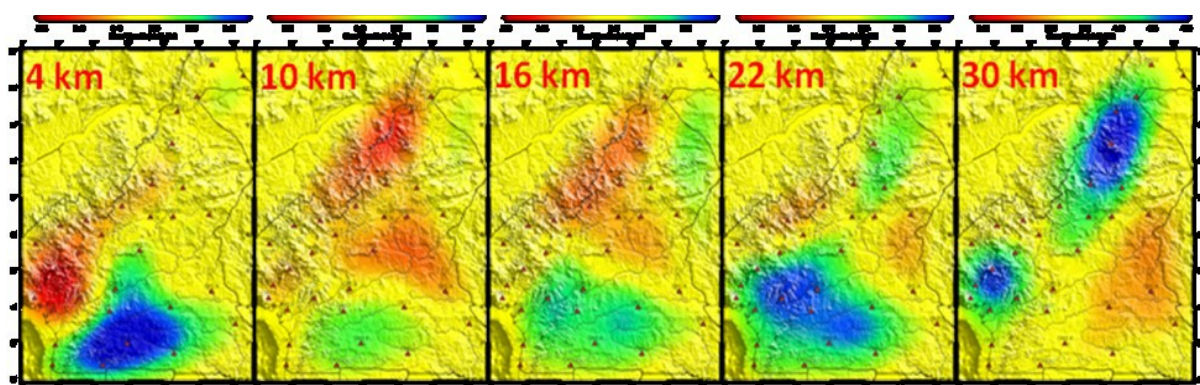


Figure 2: 3-D Crustal S-wave Velocity Structure beneath Cameroon Volcanic Line (CVL) and Adjacent regions for 4, 10, 16, 22 and 30 km.

Acknowledgement

The first author's PhD study is supported by the CAS-TWAS President's PhD Fellowship. Seismic data was provided by IRIS Data Management Center.



References

- Bensen, G.D., Ritzwoller, M.H., Barmin, M.P., Levshin, A.L., Lin, F., Moschetti, M.P., Shapiro, N.M. & Yang, Y., (2007). Processing seismic ambient noise data to obtain reliable broad-band surface wave dispersion measurements, *Geophys. J. Int.*, **169**, 1239–1260.
- DePlaen, R.M., Bastow, I.D., Chambers, E.L., Keir, D., Gallacher, R.J. and Keane, J. (2014). The Development of Magmatism along the Cameroon Volcanic Line: Evidence from Seismicity and Seismic Anisotropy. *Journal of Geophysical Research: Solid Earth*, **119**, 4233-4252.
- Elsheikh A. A., Gao S. S., Liu K. H. (2014). Formation of the Cameroon Volcanic Line by lithospheric basal erosion: Insight from mantle seismic anisotropy. *Journal of African Earth Sciences* 100 (2014) 96–108.
- Gallacher, R. and Bastow, I. (2012). The Development of Magmatism along the Cameroon Volcanic Line: Evidence from Teleseismic Receiver Functions. *Tectonics*, **31**, TC3018.
- Herrmann, R. B. (2013). Computer programs in seismology: An evolving tool for instruction and research, *Seism. Res. Lettr.* 84, 1081-1088.
- Koch, F., Wiens, D., Nyblade, A., Shore, P., Tibi, R., Ateba, B., Tabod, C. and Nnange, J. (2012). Upper Mantle Anisotropy beneath the Cameroon Volcanic Line and Congo Craton from Shear Wave Splitting Measurements. *Geophysical Journal International*, **190**, 75-86.
- Noel, E.O.P., Marcelin, M.P. and Bekoa, A. (2014). Crustal Structure and Seismogenic Zone of Cameroon: Integrated Seismic, Geological and Geophysical Data. *Open Journal of Earthquake Research*, **3**, 152-161.
- Rawlinson, N. and Sambridge M. (2005). The fast marching method: An effective tool for tomographic imaging and tracking multiple phases in complex layered media, *Explor. Geophys.*, **36**, 341-350.
- Reusch A. M. , Nyblade A. A., Tibi R., Wiens D. A., Shore P. J., Bekoa A., Tabod C. T. and Nnange J. M. (2011). Mantle transition zone thickness beneath Cameroon: evidence for an upper mantle origin for the Cameroon Volcanic Line. *Geophys. J. Int.* (2011) 187, 1146–1150.
- Reusch, A., Nyblade, A., Wiens, D., Shore, P., Ateba, B., Tabod, C. and Nnange, J. (2010). Upper Mantle Structure beneath Cameroon from Body Wave Tomography and the Origin of the CVL. *Geochemistry, Geophysics, Geosystems*, **11**, Q10W07.
- Sabra, K.G., Gerstoft, P., Roux, P. & Kuperman, W.A.. (2005). Extracting timedomain Green's function estimates from ambient seismic noise, *Geophys. Res. Lett.*, **32**, L03310, doi:10.1029/2004GL021862.
- Shapiro, N.M., Campillo, M., Stehly, L. & Ritzwoller, M.H. (2005). High resolution surface wave tomography from ambient seismic noise, *Science*, **307**, 1615–1618.
- Tadjou, J., Nouayou, R., Kamguia, J., Kande, H. and Manguelle-Dicoum, E. (2009). Gravity Analysis of the Boundary between the Congo Craton and the Pan-African Belt of Cameroon. *Austrian Journal of Earth Sciences*, **102**, 71-79.
- Tokam, A.P.K., Tabod, T.C., Nyblade, A., Julià, J., Wiens, D.A. and Pasyanos, M.E. (2010). Structure of the Crust beneath Cameroon, West Africa, from the Joint Inversion of Rayleigh Wave Group Velocities and Receiver Functions. *Geophysical Journal International*, **183**, 1061-1076.



A NOVEL ALGORITHM FOR BOUNDARY ANALYSIS

Fikret DOGRU¹, Emre TIMUR¹, Coskun SARI¹

email: fikretjfm@gmail.com

¹Dokuz Eylul University

Summary

Edge detection and edge enhancement techniques play a crucial role in interpreting potential field data. There have been various edge detection applications to gravity data in order to determine the edges of subsurface structures in geophysics. The edge detection methods comprise analytic signal, total horizontal derivative (THDR), theta angle, tilt angle, hyperbolic of tilt angle (HTA), normalised total horizontal gradient (TDX) and normalised horizontal derivative (NTHD). In this study, a new edge detection procedure is proposed, called the normalized tilt angle of theta map (NTATM) technique. The sufficiency of the NTATM method is indicated utilized using two synthetic models and a bouguer gravity data set from city of Erzurum (Turkey) and its surroundings.

Introduction

Gravity and magnetic anomalies are essential to geophysical approaches to geologic mapping (Pilkington and Keating, 2010). Boundaries detection of causative sources is one of the most important stages in the modeling of gravity anomalies (Bournas and Baker, 2001; Ardestani and Motavalli, 2007). Accurate detection of source shape coordinates is becoming the main goal for interpretation and therefore enhanced methods are acquiring an increasing revival in data interpretation (Bournas and Baker, 2001). There are various procedures that have been engaged to attain edge detection, for example, analytic signal (AS), tilt angle (TI), theta map (TH) and etc. (Arisoy and Dikmen, 2013). Miller and Singh (1994) introduced a tilt derivative (TA) filter to detect edge (Hoseini et al., 2013). Verduzco et al (2004) suggested total horizontal derivative of the tilt angle (THDR) to improve edge detection process (Pilkington and Keating, 2004; Cooper and Cowan, 2006). Wijns et al (2005) introduced the usage of theta angle which is supported the AS to magnetic and gravity interpretation (Nejati Kalateh and Roshandel Kahoo, 2012). In this research, as a new approach, we employed a normalized tilt angle of theta map method (NTATM) for detecting gravity source boundaries. Before the field studies, two theoretical studies were carried out and the results were compared with those obtained by the usual methods of edge detection such as tilt angle and theta map. After that, the NTATM operator was applied to a data set collected from the city of Erzurum in Eastern Turkey.

The NTATM Method

A number of methods have been proposed to make subtle anomalies more visible. The first filter developed for this purpose was the tilt angle (Miller and Singh, 1994), which is the ratio of the vertical derivative to the absolute value of the horizontal derivative of the magnetic field. The tilt angle produces a zero value over the source edges. Wijns et al (2005) introduced the theta map (θ), which is the normalization of the THDR by the AS. The theta map delineates model edges well, but the response of deeper bodies is diffused; consequently, it does not produce the expected sharp gradient over the edges. We suggest the use of the tilt angle of the theta map (NTATM) as an edge detector. The NTATM is the normalization of the amplitude of the theta map by the tilt angle.

Field Study

The field example of NTATM method shown in Figure 1.

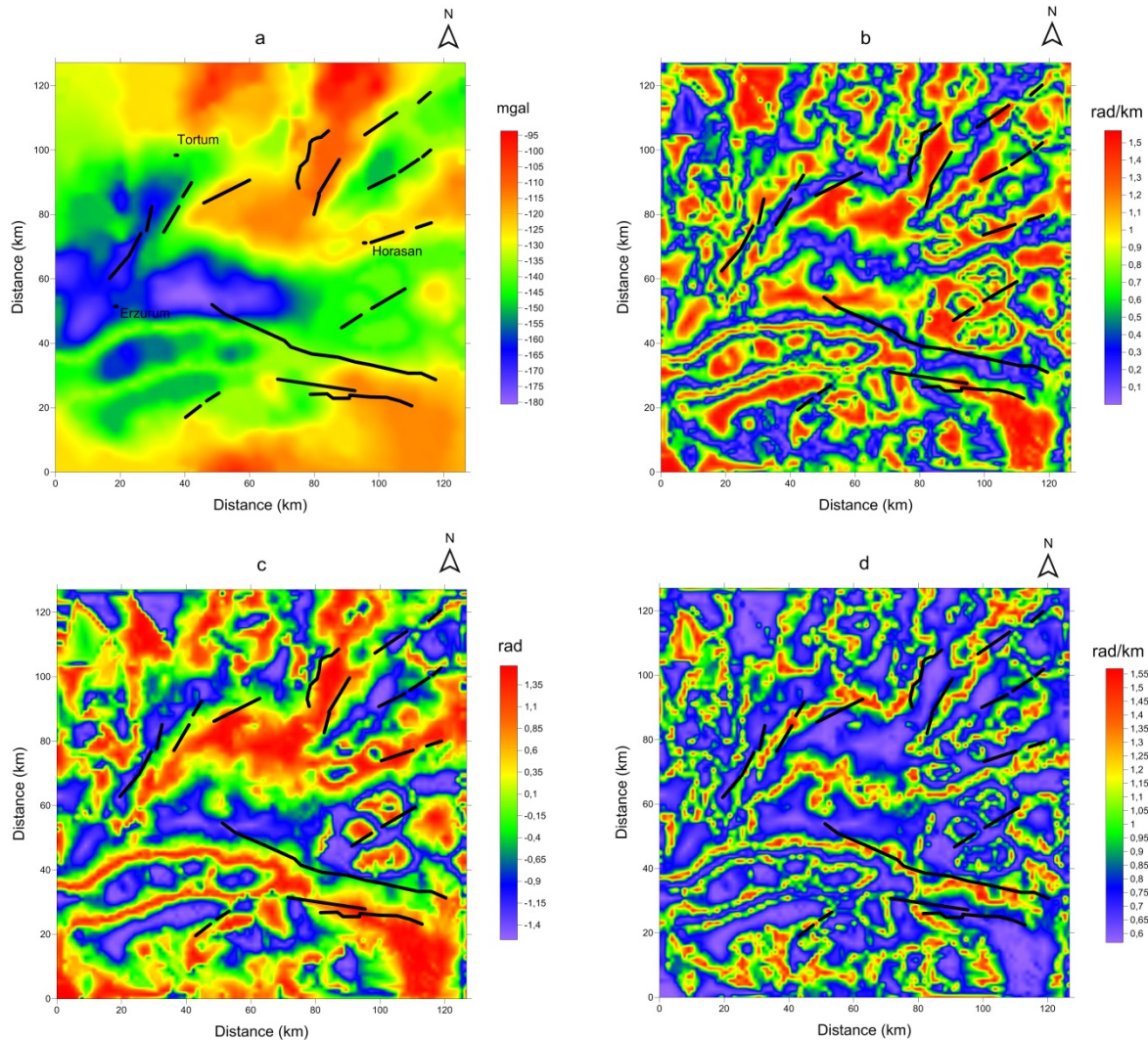


Figure 1 Bouguer gravity anomaly and analysis results: (a) Bouguer gravity anomaly of Erzurum and its surroundings, (b) the results of theta map, (c) the result of tilt angle, (d) the result of the NTATM. Black lines indicate the major faults in the study area.

Conclusions

As a conclusion, the results of the NTATM method are in good agreement with the results of tilt angle and theta map applications. The results show that the NTATM method gives the maximum values where only the edges of buried structure exist. The anomalies represented with red colour are clearly in alignment with the major structural features of the study area. Therefore, it is determined that the NTATM method can be applied as an applicable method for boundary analysis purposes.



References

- Ardestani V.E. and Motavalli H., (2007). Constraints of analytic signal to determine the depth of gravity anomalies. *Journal of Earth & space physics*, 33(2), 77-83.
- Arisoy, Muzaffer Ozgo., and DikmenUnal., (2013). Edge Detection of Magnetic Sources Using Enhanced Total Horizontal Derivative of the Tilt Angle, *Bulletin of the Earth Sciences Application and Research Centre of Hacettepe University*, 34 (1), pp 73-82.
- Bournas, Nasreddine, and Baker, Haydar Aziz., (2001). Interpretation of magnetic anomalies using the horizontal gradient analytic signal, *Annali di Geofisica*, 44 (3), pp 506-526.
- Cooper, G.R.J., and Cowan, D.R., (2006). Enhancing potential field data using filters based on the local phase. *Computers and geosciences*, 32(10), pp 1585-1591.
- Hoseini Asil, R., (2013). Depth estimation using a tilt derivative map from gravity gradient data, M.Sc. Thesis, Hamedan Branch, Islamic Azad University, p.70.
- Kalateh, Ali Nejati., and Kahoo, Amin Roshandel., (2012). Edge detection of potential field data using Theta maps, *Iranian journal of geophysics*, 7(1), pp 24-33, (Persian version).
- Miller, H.G., and Singh, V., (1994). Potential field tilt: a new concept for location of potential field sources. *Journal of Applied Geophysics*, 32, pp 213-217.
- Pilkington, M., and Keating, P., (2004). Contact mapping from gridded magnetic data: a comparison of techniques, *exploration geophysics*, 35, pp 206-311.
- Pilkington, M., and Keating, P., (2010). Geologic applications of magnetic data and using enhancements for contact mapping, *EGM international workshop Adding new value to electromagnetic, gravity and Magnetic methods for exploration*, Capri, Italy, pp 11-14.
- Verduzco, B., Fairhead, J.D., Green, C.M., and MacKenzie, C., (2004). New insights into magnetic derivatives for structural mapping. *The Leading Edge*, 23(2), pp 116-119.
- Wijns, C., Perez, C., and Kowalczyk, P., (2005). Theta map: edge detection in magnetic data, *Geophysics*, 70(4), pp 39-43.

Seismic geomorphology of the Lobed-channel System of Upper Miocene Huangliu Formation, DF-1/2 Block, Yinggehai Basin, Northwestern South China Sea

Haoran Liu¹

Email: cugharrison@email.com

¹China University of Geosciences, Wuhan

Summary

This note aims at documenting the depositional architecture of lobed-channel system and figuring out the effects on the morphology of channels and lobes. The specific goals of applying seismic morphology to the study of lobed-channels in the deep-water Yinggehai Basin are to (1) examine spatial and temporal morphometric trends of elements in lobed-channel system (2) assess the effects on channel and lobe architecture.

Introduction

Several deepwater basins have developed in the northern South China Sea (SCS) margin (Zheng et al., 2009; Dorrik and Mayall, 2000). Yinggehai Basin is a Cenozoic petroliferous basin developing in the western region of the northern SCS continental shelf (Figure 1). And thin beds reservoirs are widely distributed in this basin. The study areas, DF-1/2 blocks are located in the southwest of mud diapir structure zone in the central depression, with a total area of 1048 km² (Fig. 1). Several thin-bed lobed channel systems formed in Low System Tract of Huangliu Formation in DF-1/2 blocks. Although some previous works have concerned the sequence stratigraphy of the Yinggehai basin fill, the depositional architecture and evolution of thin bed reservoirs, especially the lobed-channel system, have rarely been investigated, with substantial potential remaining.

Method

This study utilizes software GEOSID typically designed for spatial analysis of deep-water sedimentary elements. In 3D seismic survey area, four fifth-order sequences in first member of Huangliu formation are identified in an interval using well and seismic data (Zeng, 2004). Firstly, seismic inversion and 90° phasing of seismic data convert seismic traces to pseudolithologic logs that may indicate the geometry of sandstone reservoir units (Zeng, 2005). After frequency division processing from 15HZ to 55HZ, seismic sequence boundaries T301 and T31 change less and keep consistent on the seismic profile. Then we extract a data volume in every 5 HZ within Bandwidth spectrum of 15 to 55 HZ in both DF-1 and DF-2 block. This intends to choose the best matching relationship between seismic event and logging curve (GR) according to different frequencies data volume in the same section. 45HZ seismic data is the best volume to use seismic data in high-order sequence study. Finally, stratal slicing makes it possible to interpolate and extrapolate well-data-derived sequence and identify submarine fan, channel fill and lobes.

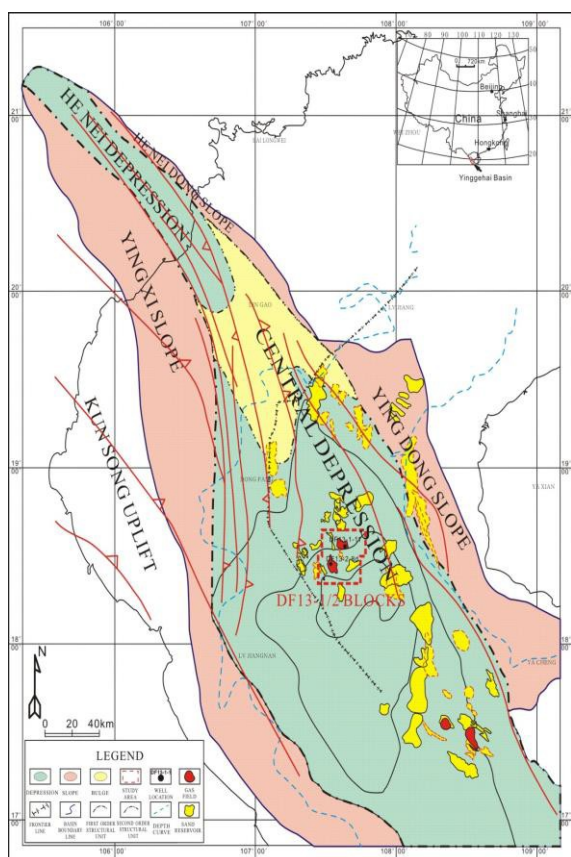


Figure 1. Location of study area DF-1/2 in Yinggehai Basin

Results

Seismic facies difference of lobes and channels are recognized at Fig.2-I in DF-1 block. Eastern part of Part A show linear black amplitude and RMS value is relative lower, which represents muddy lobes. Two short linear channels are recognized by low RMS value and black positive amplitude in the north. Part B represents a low system deep water fan, which inside includes five channels. B1, B2 and B3 are the branch channels and B4, B5 are the main channels. As for the geometry, B1, B2, B3 are straight and shallowly incised, and they show a tendency to form lobes along their pathways. B4 are highly sinuous, architecturally complex, and deeply incised, and they appear bank confined. Lobes are composed dominantly of thin-bedded fine sand and silt, with some clay.

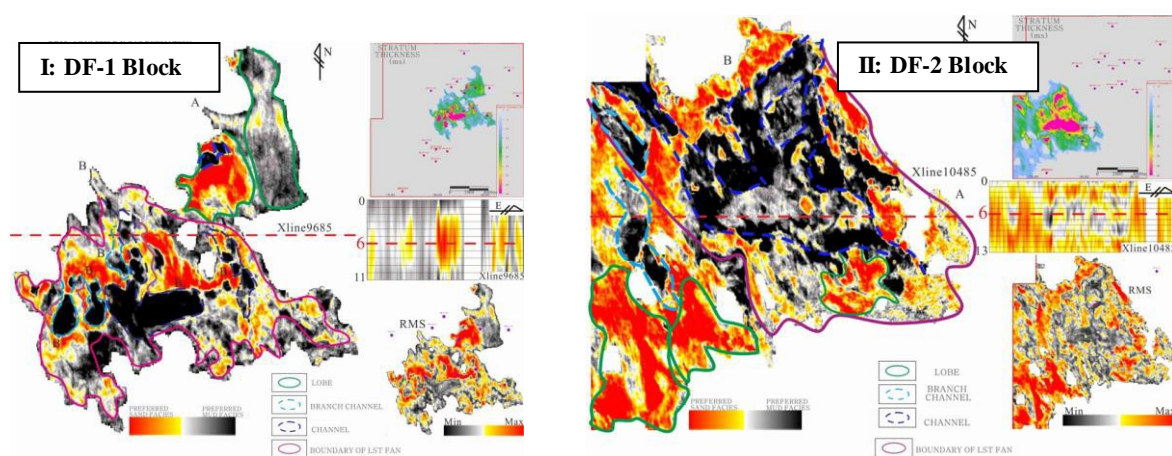


Figure 2. I : Strata slice (RMS) of DF-1 Block which is divided into Part A and B and confined as channelized lobe system; **II :** Strata slice (RMS) of DF-2 Block which is divided into Part A and B and confined as lobed channel system

Lobes and channels are best recognized at Fig.2-II in DF-2 Block. Part A shows negative amplitude (red) and RMS value is middle, which stands for submarine fan. Northwest of Part B distributes three linear red negative amplitude, which are surrounded by black positive amplitude and RMS value are lower. They are recognized as the main channels. Southwest of Part B appears two fan-shape negative amplitude (red) and RMS value is relative high, which is consider as isolated lobes.

From DF-1 to DF-2, channel depths decrease and channels are deeply incised. Moreover, meanderbelts widen, and sinuosities increase. This sudden change in meander-belt size and channel sinuosity and depth is clearly associated with the channel response to the relative sea level change. Moreover, DF-1 block has high gradient but gentle slope, which mainly distributes depositional lobes and relatively low sand-ground ratio. But DF-2 block establishes low gradient but steep slope, which mostly indicates braided channels and high sand-ground ratio.

Conclusions

Collectively, DF-1 block has high gradient but low slope. Because of the relative shallow sea level, debris from the west provenance incised weakly. Content of shale is larger than sandy sediment in DF-1 block, which distributes multiple small scattered lobes. However, DF-2 block has low gradient but high slope. Because of the relative deep sea level, debris from the west provenance incised strongly. Content of sand is larger than muddy sediment, which distributes braided incised channels. Main channel incised strongly but braided channel incised weakly and distribute on the multi-phase lobes.



References

Dorrik, A. V. S., Mayall, M., 2000. Deep-Water Sedimentary Systems: New Models for the 21st Century. Marine and Petroleum Geology

Zhang, G. C., Mi, L. J., Wu, S. G., Braaksma, H., 2007. Deepwater Area—The New Prospecting Targets of Northern Continental Margin of South China Sea. Acta Petrolei Sinica, 28(2): 15–21 (in Chinese with English Abstract)

Zeng H L and Hentz T F. 2004. High-frequency sequence stratigraphy from seismic sedimentology: applied to Miocene, Vermilion Block 50, Tiger Shoal area, offshore Louisiana [J]. AAPG Bulletin.

Zeng H L and Backus M M. 2005. Interpretive advantages of 90°-phase wavelets: Part 1 — Modeling. Geophysics.



Mapping of bedrock discontinuity using resistivity and seismic imaging techniques at El-Obour city, Egypt

Samir, A., El-Kenawy, A., Gemail, Kh. and Abd El-Raouf, A.
email: amr_geoscience@yahoo.com

¹Zagazig university, Faculty of science, Geology Department

Summary

Fracture and fault zones often constitute an engineering hazard in many regions of the new urban cities such as in the northern part of El-Obour city, Egypt. The present aim is to map and understand problematic conditions due to discontinuity of limestone bedrocks. Resistivity and refraction seismic imaging surveys were carried out to achieve this goal. The inverted sections of the both techniques revealed that a sharp contact between clayey with sandy clay soils and sandy limestone bedrock could be noticed running N-S along the axis of the surveyed area. A good matching 2D resistivity and seismic results was obtained and calibrated using borehole results to reflect the importance of integration between the applied techniques to get useful and better information on delineating contact and faults for engineering purpose.

Introduction

A geological discontinuity is a boundary between two units that is identified on the basis of a compositional, textural, structural, or temporal difference between units (Howe, 1997). Fracture and fault zones and vertical contents often constitute an engineering hazard. They can be identified geophysically by the contrasting properties of the fracture zone itself, irrespective of the rock types brought together by the fault movement. Such features are often sub-vertical and therefore difficult to locate by drilling, even when the boreholes are closely spaced (McDowell et al., 2002).

The 2D electrical resistivity method is most suitable for interpreting geological structures in subsurface while seismic method is valuable for mapping depth of bedrock and fracture zones but fail to indicate the depth or dip direction of the zone as 2D resistivity method. Thus, integration of seismic refraction and 2D electrical resistivity method will give useful and better information on delineating contact and faults for engineering purpose. 2D resistivity imaging is one of the geophysical methods often applied in an early stage of ground investigations to get a first-order idea of the shallow lithologic discontinuity (Dahlin et al., 1999; Rønning, 2003; Ganerød et al., 2006 and Gemail, 2015). Thus, the objectives of present works are to map and understand problematic subsurface bedrock and verify the features based on borehole exploration data using resistivity and seismic imaging techniques.

Methodology

The field survey was executed through two gradual stages. First, 1D Schlumberger resistivity soundings were measured to map the distribution of near surface layers. According to 1D survey, two localities were chosen for 2D resistivity and one location for seismic refraction profiling (Fig. 1). The joint implementation of these methods are necessary in order to enhance the resolution of the survey, as each method presents different sensitivity and resolution, according to the physical properties of different materials. Resistivity and refraction seismic profiles were measured perpendicular to the contact between the high and low relief areas, which indicated from the 1D electric data interpretations. Resistivity and seismic refraction profiles were correlated with boreholes data that inline and nearest to the survey lines

Results and discussion

To visualize the horizontal and vertical variations surveyed area, the interpreted resistivities with depths from 1D sounding were used to create a 3D model of the entire area (Fig. 1a). This model shows three geoelectric layers comprising the clay/sandy clay topsoil resistivity varies from 10 to 200 Ohmm and thickness ranges from 0.5 to 1.5 m; sandy limestone bedrock (resistivity varies from 10 to 250 Ohmm and thickness ranges from 5 to 9 m); clay and clayey sand (resistivity varies from 1 to 15 Ohmm and thickness ranges from 5 to 8 m).

Figure (1b, c and d) shows the comparison of 2D resistivity for profiles P₁ and P₂ using dipole-dipole and seismic refraction section crossing the bedrock discontinuity. The inverted sections of P₁ and P₂ (Fig. 1b and c) show well-defined vertical contacts in the middle parts between distances 110-170m and 35 and 95m, respectively. These profiles clearly illustrate the lateral and in depth changes in the surface of sandy limestone bedrock which changes dramatically to loose sand and clay rich soils (low resistivity) towards the both profiles boundaries. The conductive anomalies in the western side of P₁ and P₂ extend crossing the road to cover the whole area as indicated from the boreholes. These low resistivities are related to the unconsolidated and water-saturated sandy clay with high clay and natural water content in the western side. The image of P₂ (Fig. 2 c) shows rapid changes on the bedrock surface as well as the thickness of above sandy clay layer, which may indicate vertical discontinuities or local faults,

The seismic cross section P₁ (Fig. 1d), was measured in the central resistive block to assess the quality of sandy limestone bedrock. This section shows four layers indicates and displays an average depth of 26 m. The first layer is the top soil with low velocity (0.4–0.6 Km/s and 0.5-1.5m thick) then follows by a relatively high-velocity layer of fractured sandy limestone (0.7–1.2 Km/s and 5m thick). The third layer is characterized by the velocities in the range of 1.4–2.1 Km/s which represents by water saturated clay layer with thickness of about 8 m and underlain by basal layer of hard sandy limestone bedrock with velocity of 2.2-3.3 Km/s.

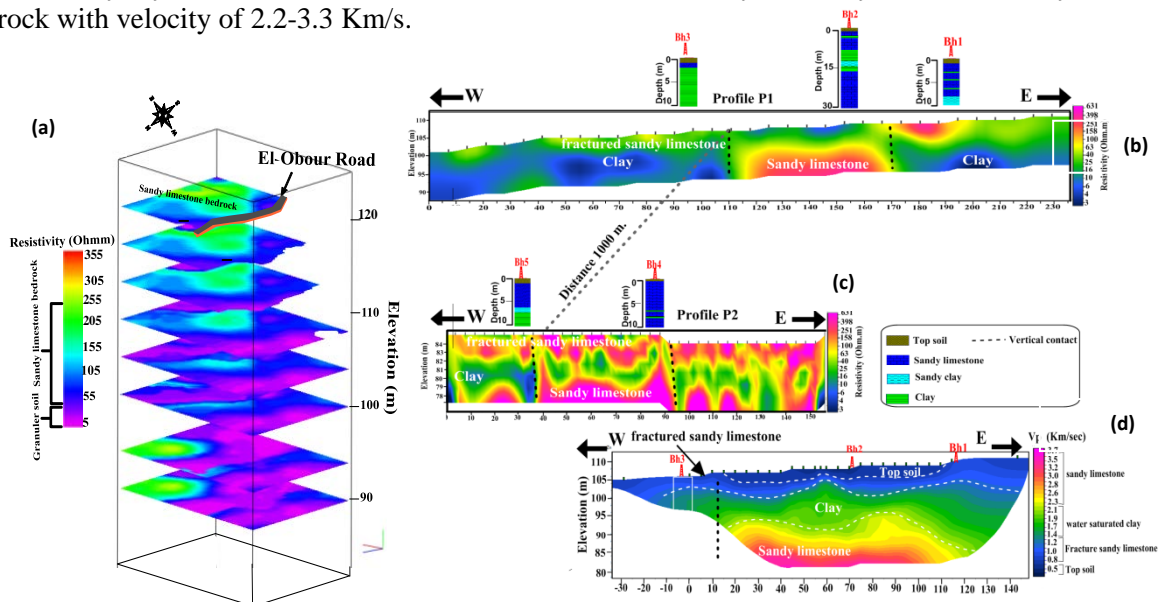


Figure 1 (a) 3D diagram for 1D sounding and (b and c) 2D dipole dipole inverted sections for profiles p1 and p2 and (d) seismic refraction cross section.

Conclusion

A good matching 2D resistivity and seismic refraction results was obtained and calibrated using borehole results which shows that these techniques are appropriated to be applied in near surface mapping of foundation bedrock which can further substantiates and compliments borehole data and others physical mapping. The engineering geologic zone characterization using resistivity and refraction seismic imaging, is economic, fast and efficient for engineering purposes and thus it is very useful for civil engineering investigations. According to the resistivity and p-wave velocity distributions, sharp contact between the granular soil and sandy limestone bedrock could be noticed running N-S along the axis of the surveyed area. This indicates that great care must be taken when designing the foundation system along the bedrock discontinuity and in the undeveloped western part.

Acknowledgement

The authors wish to thank the Egyptian Academy of Scientific Research and Technology for finance support that was extended for the present research work



References

- Dahlin, T., Bjelm, L., and Svensson, C. (1999). Use of electrical imaging in site investigations for a railway tunnel through the Hallandsås Horst, Sweden: *Quarterly Journal of Engineering Geology*, 32, 163-172.
- Ganerød, G. V., Rønning, J. S., Dalsegg, E., Elvebakk, H., Holmøy, K., Nilsen, B. and Braathen, A. (2006). Comparison of geophysical methods for sub-surface mapping of faults and fracture zones in a section of the Viggja road tunnel, Norway: *Bull Eng Geol Env*, 65, 231 – 243.
- Gemail, Kh. (2015). Application of 2D resistivity profiling for mapping and interpretation of geology in a till aquitard near Luck Lake, Southern Saskatchewan, Canada: *Environ. Earth Sci*, 73, 923-935
- Howe, R. (1997). Geologic Contacts: *Journal of Geoscience Education*, Vol. 45, 1997, 133-136.
- Rønning, J. S., Dalsegg, E., Elvebakk, H., & Storrø, G. (2003). Characterization of fracture zones in bedrock using 2D resistivity, 9th EEGS European Meeting, Prague.
- McDowell, P. W. and others. (2002). *Geophysics in engineering investigation*. CIRIA C562, Westminster, London.



Analysis of seismic reflection data recorded in the desert areas (Ghadames, Libya)

E. Hamdi

Hamdi.a.elagieli@gmail.com

¹ University of Bucharest, Dept. of Geophysics, Bucharest

Summary

Ghadames area is located in the north-west of Libyan desert. The loose sand bed with large thickness has a strong influence on the attenuation of seismic waves, and the sand dune also has some influence on the stacking velocity and statics. In this study, I analyze a dataset recorded along a linear profile in Ghadames area. The standard processing combined with the trace editing of the shot gathers provided us a seismic section in which the false geological structure, introduced by the sand dune crossed by the seismic profile, disappeared.

Introduction

The goal of the seismic data processing is to eliminate/suppress all noise, coherent or random, and to present the reflections on the seismic section with the greatest possible resolution (Dobrin, 1976). Non Seismic Objects or obstacles are encountered during seismic surveys, which pose practical difficulties in placement of source or receiver or both along the planned layout (Roa et al., 2006). To solve the problems of unconsolidated sand related noise and attenuation, (Gu Yanbin et al. 2006) have approached processing technique to compensate for seismic attenuation of incompact sands and to obtain correct velocity profile.

In this study, I analyze a 2D seismic dataset acquired over an area covered by sand dunes. The propagation of the reflected waves is influenced by the source positions in the vicinity of the sand dune. Various strategies are tested to remove/attenuate the effect of non-linear source line on the wave propagation.

Description of seismic data acquisition

The Ghadames area is covered by sand dunes with various elevation profiles. The seismic profile crossed such a dune. Because of the type of seismic source (Vibrois), the source positions were shifted from the linear profile in the vicinity of the sand dune (Figure 1). The seismic energy was generated in points spaced at 25 m. The sweep frequency was 10-70 Hz. Two sweeps per shot point were generated. The distance between the shot point and the first geophone on both sides of the shot point was about 120 m, in order to avoid the recording of strong spatially aliased coherent energy. The geophone spacing was equal to 25 m. The maximum number of channels/record was 200. Time sampling interval is 4 ms.

Description of the data analysis

I analyzed the seismic records using a standard processing flow from industry. The dataset contains a number of 209 shot gathers. The geometry was computed for a linear profile. The static corrections were computed and applied for a final datum of +460 m and a replacement velocity of 4200 m/s. The effect of the sand dune cannot be attenuated by applying static corrections because the source points are not linear with the receiver line (Figure 2). Trace muting was applied to remove the noise above the first arrivals. The coherent noise was removed by f-k filtering, frequency band-pass filtering (14-60 Hz) and spiking deconvolution (Figure 2). The Normal Move-Out (NMO) correction was applied using stacking velocities from interactive velocity analysis performed on common-depth-point (CDP) gathers. One way to remove the effect of the sand dune on the stacked section is to kill the traces where this effect is too strong (not shown here). In this way, I improve the continuity of the reflections on the stacked section (not shown here). The remaining time shifts after the application of

static corrections are responsible for the false structure seen on the stacked section under the sand dune.

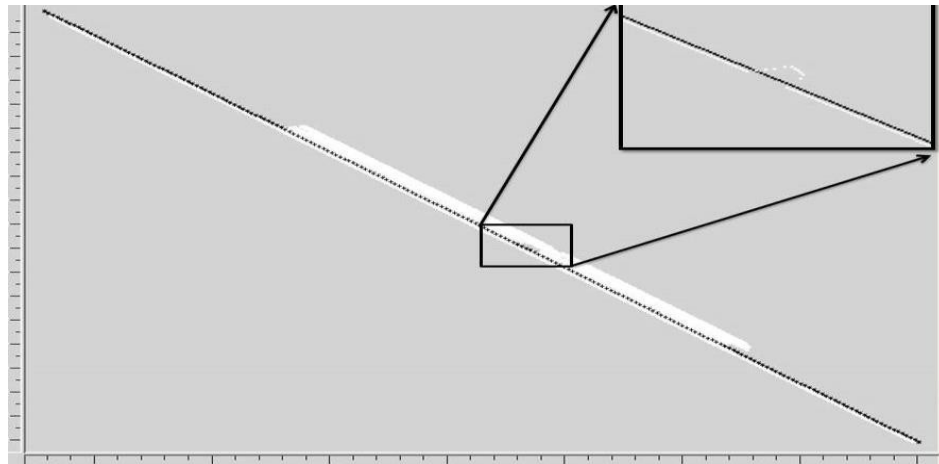


Figure 1 Receiver (black stars) and CDP (white stars) positions; upper rectangle – shifted source positions (white stars), receiver positions – black stars.

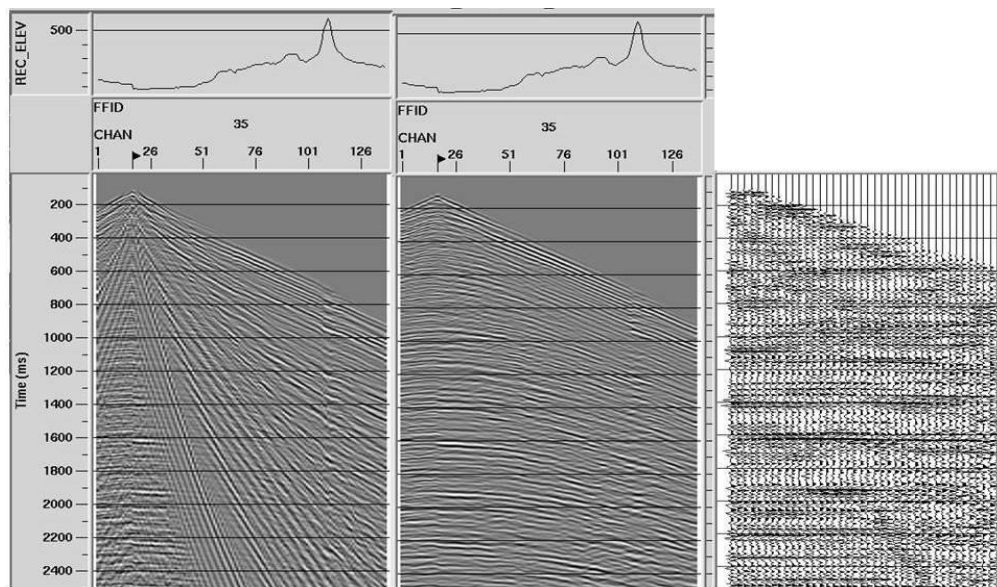


Figure 2 Raw (left) and filtered (center) shot record; NMO-corrected CDP gather.

Conclusions

I analyzed a seismic reflection dataset recorded in a desert area (Ghadames area). The designed acquisition parameters were locally changed in order to avoid the sand dune crossed by the seismic profile. Standard processing of this data combined with trace editing provided us a stacked section where the effect of the sand dune is completely eliminated. The false interesting geological structure observed on the stacked section after standard processing disappeared after the trace editing of the shot gathers.

Acknowledgments

The author thanks to Dr. Lili Panea for her support in the performing of this study.



References

A. K. Roy* and R. V. S. Murthy, (2006). Negotiation with NSO (Non Seismic Object) – 2D Land Seismic Surveys. ONGC Ltd., Chennai, India.

Dobrin, M. B. , (1976) . Introduction to Geophysical Prospecting . Mc Graw – Hill Book Company , New York .

Gu Yanbin and Dai Xiaoyun, (2006). Desert seismic data processing technology from desert surface. SEG.



Aftershock Prediction Map of New Zealand Using Wavelet Based Multi-scale Analysis

V. Srivardhan
email: vardhan.sri@gmail.com
Indian School of Mines

Summary

The b value of earthquakes is a useful indicator to predict the occurrence of future aftershocks in a given region. Wavelet based multi-scale analysis of earthquakes is used in this study to determine the b value. Repeated earthquakes were analyzed between 2007 and 2014 for New Zealand with magnitude greater than 4.0 and an aftershock prediction map was generated. Results showed that the stable b value levels for the entire island varied between 0.41 to 0.76. Aftershocks keep occurring until the b value of the earthquake typically approached this stable b value of the region.

Introduction

Earthquakes are strong ground motions that has the potency to cause massive loss to life and property. It is a challenge that humanity faces today to predict their occurrence and prevent such large-scale destruction. The b value has been used in the past to predict the occurrence of earthquakes and their magnitudes (Okal et al, 1994). The Gutenberg-Richter Law and Omori Law have been used to determine the b value and predict earthquakes (Hirose et al, 2011; Kagan, 2010). Spatial and temporal variations of b value have been recorded in the past and the magnitude of earthquake occurrences has been related to these events (Parsons 2007; Midha 2012; Nuannin et al, 2012, Sorbi et al, 2012). The b value has been found to be influenced by many factors through laboratory experiments and notably dependent on, heterogeneity, rheology, thermal gradient, and the stress conditions of the subsurface in a given region (Mogi 1962; Scholz 1968; Wyss 1973; Bayrak et al, 2013). In this study a demonstration using wavelet based multi-scale is used to find the b value of earthquakes in New Zealand, and is used to prepare an aftershock prediction map.

Theory

The continuous wavelet transform of a time series is defined by Equation 1. Here $f(t)$ is the time series, φ is the mother wavelet, $W(x,y)$ are the wavelet coefficients, while x and y represent the scale and translation parameters. The scale factor is inversely proportional to the frequency of the signal. The translation factor controls the shifting of the window function or the mother wavelet when analyzing the time series (Polikar 1996).

$$W(x,y) = \frac{1}{\sqrt{|x|}} \int_{-\infty}^{\infty} f(t) \varphi\left(\frac{t-y}{x}\right) dt \quad (1)$$

The variance in the wavelet coefficients for the variance in the scale factor is calculated and is called the Holder exponent, denoted by H . It is related to the fractal dimension D which in turn is related to the b value through the following relations expressed as Equation 2 and 3. Wavelet based multi-scale analysis of earthquakes has been carried out in the past by (Dimri et al., 2005; Srivardhan and Srinu, 2014).

$$2D = 5 - H \quad (2)$$

$$b = \frac{c * d}{3.0} \quad (3)$$

The factor c is dependent on the nature of the subsurface rocks and is usually taken as 1.5 (Dimri 2000), but for crystalline rocks it is taken as 3.0. In this analysis the scale factor was varied between 1

and 4.4 for obtaining best results and the Symlet-2 and Daubechies-2 family of wavelets gave the best results as compared with other wavelets.

Case Study

Wavelet based multi-scale analysis of earthquakes in New Zealand was performed and more than 25 different earthquakes with magnitudes greater than 5.5 were analyzed by 9 stations with earthquakes occurring between 2007-2014 (May 2014) using Equations 1, 2, and 3. It was assumed that the area surrounding the epicenter with a 10 km radius enclosing the receiver station was part of a zone where there was not much geologic variations. The position of the epicenters and the receiver stations are indicated in Figure 1(a). The mainshock and its corresponding aftershocks occurring in a zone were repeatedly analyzed until there were no aftershocks occurring there. Based on this analysis a stable b value map of the entire country was prepared and represented in Figure 1(b). This map gives us the criteria for aftershocks to stop occurring. Tremors keep occurring until the stable b value designated for that zone is attained after which the tremors stopped.

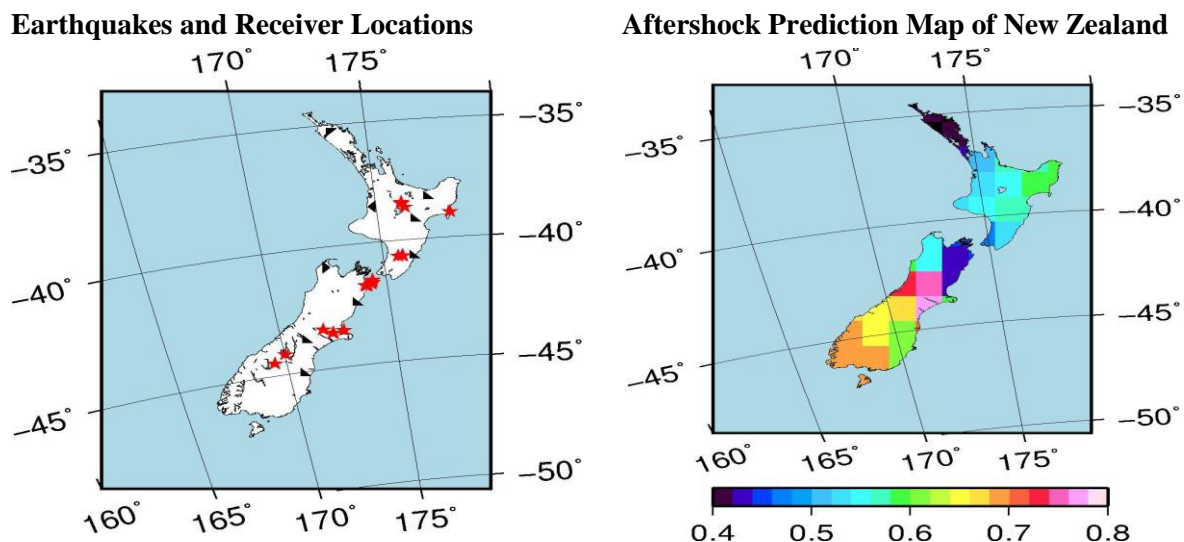


Figure 1: (a) The black triangles show the position of the receivers and the red stars depict the epicenters of the earthquake. (b) The stable crustal b value zonation map of New Zealand.

Conclusion

The multi-scale analysis of earthquakes suggests that there is a characteristic stable crustal b value of every region. But this stable state is perturbed during the onset of an earthquake and they occur repeatedly with the change in b value, until the region once again goes back to its stable state. An aftershock prediction map helps us in understanding these values. From Figure 2, it can be interpreted that for New Zealand the stable crustal b values varied between 0.41 to 0.78. The changes in b value during earthquakes are manifested as changes in various physical properties, most notably heterogeneity, rheology, thermal gradient, and the stress conditions of the subsurface. Aftershock prediction maps help in understanding the stable nature of b values of a region and the results of the analysis can be further improved by considering more events and more stations. Moreover wavelet based multi-scale analysis requires a limited dataset as compared with conventional methods as demonstrated in this study.



References

- Bayrak, Y., Yadav, R. B. S., Kalafat, D., Tsapanos, T. M., Çınar, H., Singh, A. P., Bayrak, E., Yılmaz, S., Öcal, F. and Koravos, G. (2013). Seismogenesis and earthquake triggering during the Van (Turkey) 2011 seismic sequence. *Tectonophysics*, 601, 163-176.
- Dimri, V. P. (Ed.). (2000). *Application of fractals in earth sciences*. CRC Press.
- Dimri, V. P., Vedanti, N. and Chattopadhyay, S. (2005). Fractal analysis of aftershock sequence of Bhuj earthquake—a wavelet based approach. *Current Science*, 88(10), 1617-1620.
- Hirose, F. and Maeda, K. (2011). Earthquake forecast models for inland Japan based on the GR law and the modified GR law. *Earth Planets and Space*, 63(3), 239.
- Kagan, Y. Y. (2011). Random stress and Omori's law. *Geophysics Journal International*, 186(3), 1347-1364.
- Midha, P. (2012). Multifractal Analysis of Seismicity of Kutch Region (Gujarat). *Proceedings of the 9th Biennial International Conference & Exposition on Petroleum Geophysics*, pp. 1–382.
- Mogi, K. (1962). Magnitude-frequency relationship for elastic shocks accompanying fractures of various materials and some related problems in earthquakes, *Bulletin of the Earthquake Research Institute*. University of Tokyo, vol. 40, pp. 831–883.
- Nuannin, P., Kulhánek, O. and Persson, L. (2012). Variations of b-values preceding large earthquakes in the Andaman–Sumatra subduction zone. *Journal of Asian Earth Sciences*, vol. 61, pp. 237-242.
- Okal, E. A. and Romanowicz, B. A. (1994). On the variation of b-values with earthquake size. *Physics of the Earth and Planetary Interiors*, 87(1), 55-76.
- Parsons, T. (2007). Forecast experiment: Do temporal and spatial b value variations along the Calaveras fault portend $M \geq 4.0$ earthquakes? *Journal of Geophysical Research: Solid Earth* (1978–2012), 112(B3).
- Polikar, R. (1996). *The wavelet tutorial*.
- Scholz, C. H. (1968). The frequency-magnitude relation of microfracturing in rock and its relation to earthquakes. *Bulletin of the Seismological Society of America*, 58, 399–415.
- Sorbi, M. R., Nilfouroushan, F. and Zamani, A. (2012). Seismicity patterns associated with the September 10th, 2008 Qeshm earthquake, South Iran. *International Journal of Earth Sciences*, pp. 1-9.
- Srivardhan, V. and Srinu, U. (2014). Potential of Fractal Analysis of Earthquakes through Wavelet Analysis and Determination of b Value as an Aftershock Precursor: A Case Study Using Earthquake Data between 2003 and 2011 in Turkey. *Journal of Earthquakes*, 2014.
- Wyss, M. (1973). Towards a physical understanding of the earthquake frequency distribution. *Geophysical Journal of the Royal Astronomical Society*, vol. 31, pp. 341–359.

The Development of a Channel-system in a tropical Carbonate Slope Environment and the Influence of Syn-sedimentary Deformation, Browse Basin, Australian North-West-Shelf

L. Rinke-Hardekopf¹, L. Reuning, S. Back, J. Bourget

email: Lucian.Rinke-Hardekopf@rwth-aachen.de

¹ RWTH Aachen University, Energy & Mineral Resources Group

Summary

High-resolution 3D seismic analysis of a Miocene tropical carbonate platform and its slope system of the Browse Basin on the Australian North-West-Shelf documents well-developed channel-systems in front of one of the largest Neogene barrier reefs. A detailed geomorphologic investigation of this channel-system from reef initiation via a mature barrier reef stage to a stage of decay and death of the barrier reef is presented. The last stage displays the appearance of a deep-water, 10 km long channel-levee complex.

Introduction

The Miocene succession of the Browse Basin on the Australian North-West-Shelf hosts one of the largest Neogene tropical barrier reef systems. This barrier reef was established during the middle Miocene and ultimately drowned during the late Miocene. The growth architecture and development of this system was recently investigated by Rosleff-Soerensen et al. (2012) and Rosleff-Soerensen et al. (2014). We present a high-resolution 3D seismic investigation of the coeval slope system. The study was carried out on the partially overlapping 3D seismic surveys Snarf 3D, which covers the platform to slope stratigraphy, and the Brecknock 3D survey, which mostly covers the carbonate platform. Each survey is processed in Shell European zero-phase polarity convention for seismic reflections with a sample rate of 4 ms. While the Snarf 3D survey covers an area 1271 km² with a lateral resolution of < 20 m, the Brecknock 3D survey covers an area 845 km² with a lateral resolution of < 14 m, leading to a total areal coverage of 2116 km².

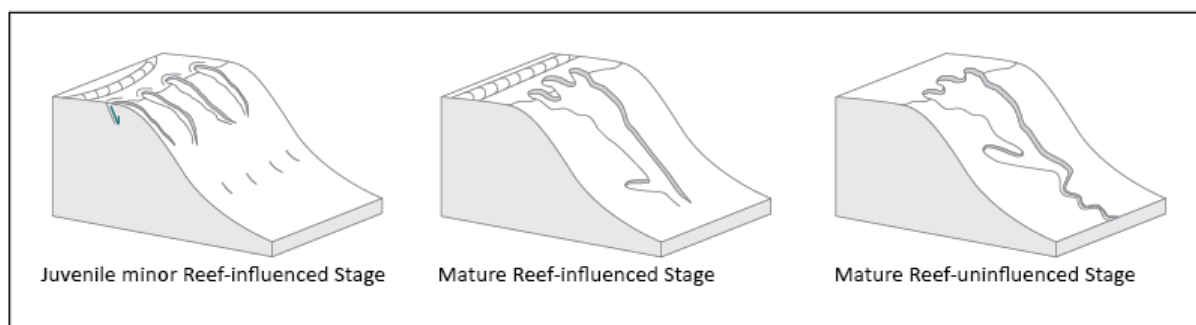
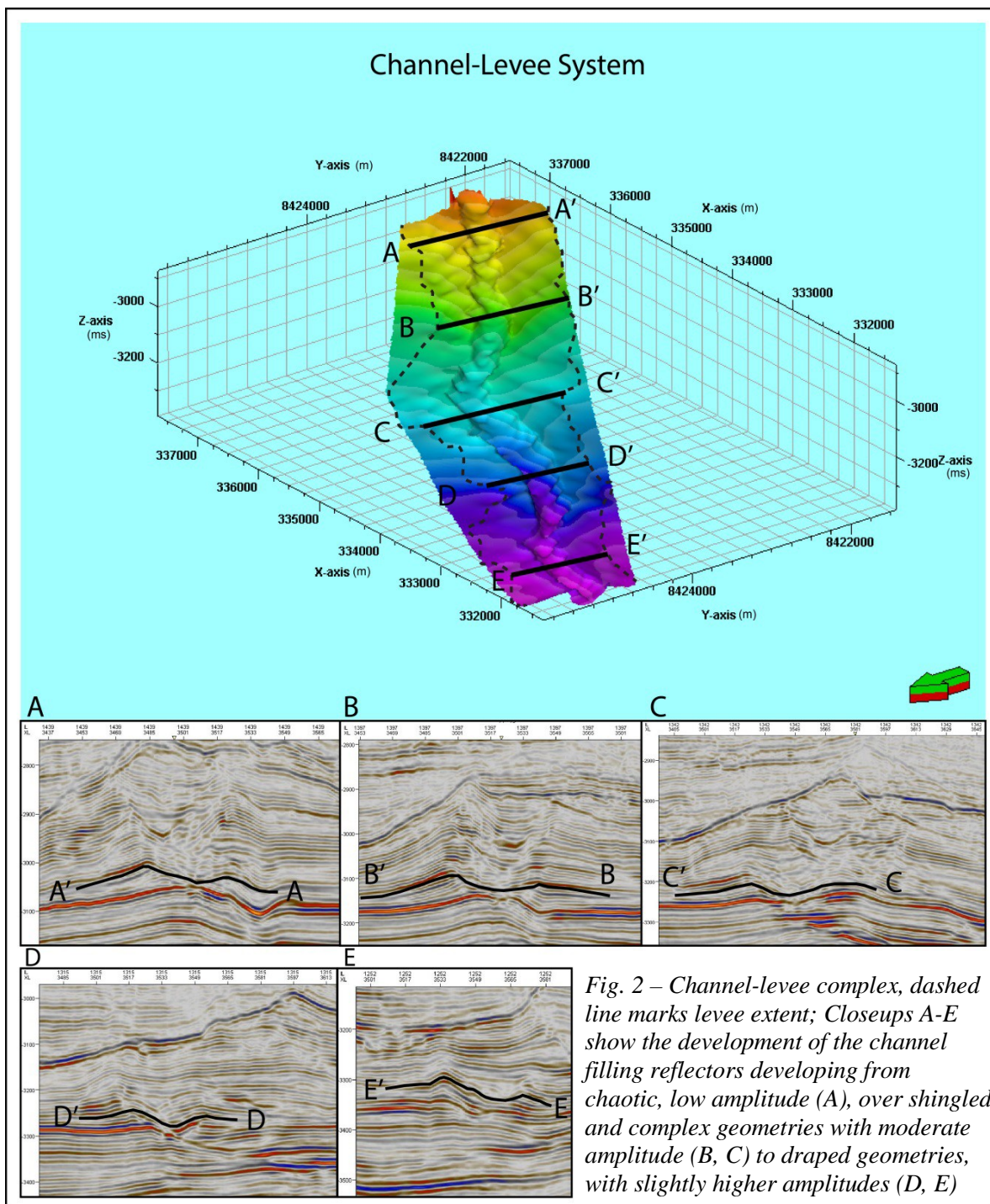


Fig. 1 – A: Juvenile minor reef-influenced stage and clinoform-breakpoint parallel fractures; B: Mature reef-influenced stage with merged tributaries; C: Mature reef-uninfluenced stage with a channel-levee system in the lower slope area

Channel systems and channel-levee complexes have been widely studied in deep-sea siliciclastics, however very few studies exist regarding their existence in carbonate settings (e.g. Mulder et al., 2012), especially if associated with a tropical barrier reef (e.g. Puga-Bernabéu et al., 2011). We present a detailed seismic-geomorphological description of the development of such channel systems from an early (Fig. 1A) to a mature stage in which single tributaries have partially merged (Fig. 1B, 1C). Additionally, we show a detailed description of a 10 km long deep-water channel-levee complex with levee widths of up to 850 m and varying channel filling reflectors (Fig. 2).



Syn-sedimentary deformation structures are known from numerous high-relief carbonate platforms across the world. Syn-sedimentary fractures and faults commonly show steep dips, and are typically associated with growth strata (e.g. Resor and Flodin, 2010). They can be caused by differential compaction through the progradation and aggradation of a steep-sloped margin leading to shear-stress concentration and lastly to brittle normal-faulting. In the study area, an extensive network of syn-sedimentary fractures and small faults with a throw of up to a few tens of m is located adjacent to the clinoform break-point in direct vicinity to channel heads and may control their initiation (Fig. 1A). Channel fills and syn-sedimentary fractures potentially form conduits for fluid migration and hence are important for the understanding of hydrocarbon reservoirs in carbonate slope systems.

Conclusions

We conclude that channel initiation is possibly directly linked to the progradation and aggradation of the carbonate platform, which leads to stress concentration on the clinoform breakpoint leading to brittle deformation. The developing syn-sedimentary normal faults document weaknesses at the platform to slope transition and act as predecessors for channel-systems. Channel development takes place under the influence of the barrier reef, located landward of the clinoform breakpoint. This is further displayed in the development of the channel-levee complex, which only occurs after reef drowning.

References

- Mulder, T., Ducassou, E., Eberli, G., P., Hanquiez, V., Gonthier, E., Kindler, P., Principaud, M., Fournier, F., Léonide, P., Billeaud, I., Marsset, B., Reijmer, J., P., P., Bondu, C., Jousseaume R., Pakiades, M. (2012): New insights into the morphology and sedimentary processes along the western slope of Great Bahama Bank, *Geology*, Vol. 40, p. 603-607, DOI: 10.1130/G32972.1
- Resor P., G., Flodin, E., A. (2010): Forward Modeling synsedimentary Deformation associated with a prograding steep-sloped Carbonate Margin, *Journal of Structural Geology*, Vol. 32, p. 1187-1200, DOI: 10.1016/j.jsg.2009.04.015
- Rosleff-Soerensen, B., Reuning, L., Back, S., Kukla, P. (2012) Seismic geomorphology and growth architecture of a Miocene barrier reef, Browse Basin, NW-Australia, *Marine and Petroleum Geology*, Vol. 29, p. 233-254, DOI:10.1016/j.marpetgeo.2010.11.001
- Rosleff-Soerensen, B., Reuning, L., Back, S., Kukla, P. (2014): The response of a basin-scale Miocene barrier reef system to long-term, strong subsidence on a passive continental margin, Barcoo Sub-basin, Australian North West Shelf, *Basin Research*, p. 1-21, DOI: 10.1111/bre.12100

A new sorbent for arsenic (As) removal in contaminated groundwater sites

Olusegun K. Abass^{1,2}, S.Q Kong¹
segunabass@iue.ac.cn

¹ State Key Laboratory of Biogeology and Environmental Geology, School of Environmental Studies, China University of Geosciences, Wuhan, 430074, P. R. China

² Institute of Urban Environment, Chinese Academy of Sciences, Xiamen, 361021, PR China

Summary

Arsenic, a ubiquitous metalloid is found both in terrestrial and aqueous environments and could be released into groundwater by various redox processes. In this study, magnetic nanoscale Fe–Mn binary oxides loaded on zeolite (FMOZ), a new sorbent is produced by an improved precipitation method; and is easily separated from water by an external magnetic field after arsenic removal. With a BET surface area of 340 m²/g, the removal efficiency of FMOZ for arsenic is greater than 99.0% at groundwater pH values. FMOZ exhibits strong adsorption affinity for arsenic and is a promising adsorbent for arsenic removal in contaminated groundwater.

Introduction

Arsenic is a widely distributed element in atmosphere, soils, and natural waters. It occurs as a major constituent in more than 200 minerals of the earth's crust (1). The primary source of arsenic in the environment originates from weathering of arsenic (As) bearing rocks. However, factors including the desorption and dissolution of naturally occurring As bearing minerals is generally considered as the principal source of As contamination in groundwater (2, 3). Arsenic can be found in variety of solid phases including component of volcanic glass in volcanic rocks, co-precipitated with metal oxides (especially iron oxides), adsorbed onto clay-mineral surfaces, or associated with sulfide minerals and organic carbon. Long-term exposure to high levels of As in drinking water is associated with various skin lesions, cardiovascular diseases, diabetes, neuropathies, as well as cancers of several organs (4).

To combat this menace, adsorption processes are utilized because of its cost effectiveness. Unfortunately, the agglomeration of nanomaterials and the efficiency of most adsorbents have remained technical bottlenecks that hamper their wide application (5). Hence, in this study, magnetic nanoscale Fe–Mn binary oxides loaded on zeolite (FMOZ); a new sorbent, is produced by improved precipitation method and used to investigate the adsorption behavior of As(III) and As(V) on FMOZ. The key process controlling arsenic removal on FMOZ, the spontaneity and thermodynamic feasibility of the adsorption process were investigated.

Material and Method

We synthesize magnetic nanoscale Fe–Mn binary oxides loaded on zeolite (FMOZ) using hydrothermal technique to produce FMOZ nanomaterials by a continuous and gentle stirring of 1.0 g polyvinylpyrrolidone (PVP, K-30) dissolved in 150 mL deionized water (DI water) and kept at 70 °C for 1 h.

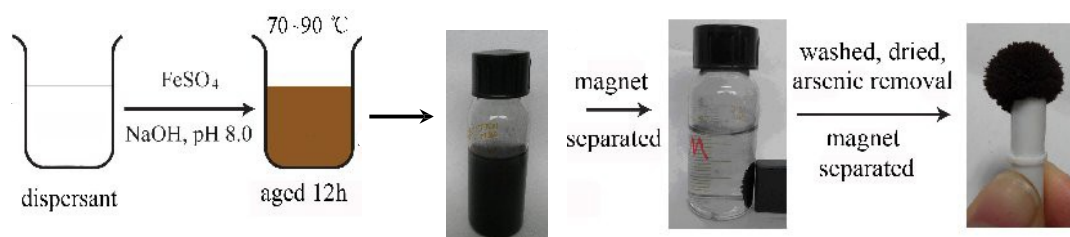


Figure 1 One pot synthesis of FMOZ magnetic nanoparticles and its arsenic removal capability

The resulting solution was added to 0.44–2 g zeolite and 13.9 g $\text{FeSO}_4 \cdot 7\text{H}_2\text{O}$, then mixed thoroughly. One milliliter of 4.0 M NaOH was dropped into the mixture to generate a green-colored suspension. After 5 min, 100 mL aqueous solution containing 1.77 g KMnO_4 was sprayed on the reaction solution to produce a dark brown precipitate, which was aged for 12 h (Fig. 1). Finally, the resulting solid powder were washed six times using DI water and ethanol alternately, followed by vacuum drying inside an oven at 50 °C. Arsenic removal experiments were carried out by reacting arsenic solutions with FMOZ suspensions in synthetic groundwater. The supernatant was analyzed for As(V) and As(III) and total arsenic in aqueous phase. At the same time, another suspension sample was dissolved in 2M HCl solution to determine the concentration of total As(V) and As(III) and total arsenic in the whole FMOZ suspensions. Afterwards the concentrations of adsorbed As(III) and As(V) on FMOZ and in aqueous solution were calculated.

Results and discussion

Arsenic removal on FMOZ: We characterized sample of FMOZ by SEM-EDX analysis after As(V) and As(III) removal. Elemental analysis shows that arsenic was adsorbed onto FMOZ. This result suggested that almost all As(III) was adsorbed on FMOZ in a very short period, and then converted to As(V) gradually on the surface of FMOZ with a moderate reaction phase. The produced As(V) was detectable in solid phase and was not released to the aqueous phase.

From Fig. 2b, It can be observed that wt% of arsenic (0.15%) derived from As(V) adsorption was lower than that derived from As(III) adsorption (0.29%), which implies As(III) has a higher adsorption. In comparison to other adsorbents reported in the literature (6, 7), the magnetic FMOZ nanoparticles showed a higher adsorption rate, particularly for arsenite. As reported elsewhere, the adsorption of arsenic on activated alumina required 2 days to reach equilibrium (8).

Since the

adsorption on the present magnetic FMOZ nanoparticles was achieved in less than 30 min, this holds promise for practical industrial application (Fig. 2a).

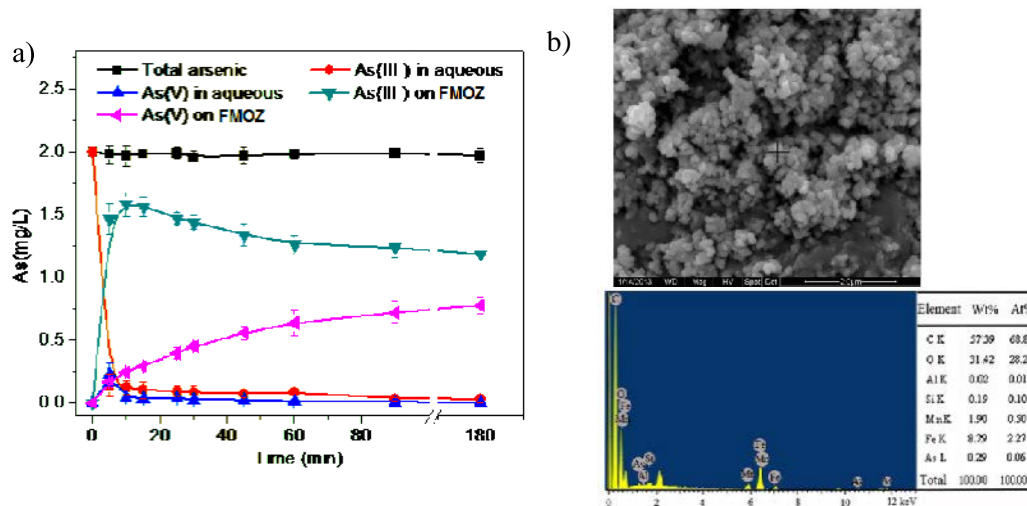


Figure 2a & b Arsenic adsorption experiment at pH 7 (Arsenic int. conc. = 2mg/l) and SEM-EDX analysis of As-removal on FMOZ

Conclusions

In this study, we observed that the kinetic rates and maximum adsorption capacities of FMOZ for As(III) were higher than As(V). The adsorbed arsenic on FMOZ could be separated from solution using a magnet due to FMOZ magnetic property. Hence, this new adsorbent is expected to have potential applicability in the removal of arsenic from contaminated groundwater.



References

1. Bissen M & Frimmel FH (2003) Arsenic — a Review. Part I: Occurrence, Toxicity, Speciation, Mobility. *Acta hydrochimica et hydrobiologica* 31(1):9-18.
2. Matschullat J (2000) Arsenic in the geosphere — a review. *Science of The Total Environment* 249(1-3):297-312.
3. Polizzotto ML, *et al.* (2006) Solid-phases and desorption processes of arsenic within Bangladesh sediments. *Chem Geol* 228(1-3):97-111.
4. Zhu YG, Williams PN, & Meharg AA (2008) Exposure to inorganic arsenic from rice: a global health issue? *Environ Pollut* 154(2):169-171.
5. Kong S, Wang Y, Hu Q, & Olusegun AK (2014) Magnetic nanoscale Fe–Mn binary oxides loaded zeolite for arsenic removal from synthetic groundwater. *Colloids and Surfaces A: Physicochemical and Engineering Aspects* 457:220-227.
6. Lin S, Lu D, & Liu Z (2012) Removal of arsenic contaminants with magnetic γ -Fe₂O₃ nanoparticles. *Chemical Engineering Journal* 211-212:46-52.
7. Shi R, Jia Y, & Wang C (2009) Competitive and cooperative adsorption of arsenate and citrate on goethite. *Journal of Environmental Sciences* 21(1):106-112.
8. Lin T-F & Wu J-K (2001) Adsorption of Arsenite and Arsenate within Activated Alumina Grains: Equilibrium and Kinetics. *Water research* 35(8):2049-2057.

poster presentations

APPLIED GEOPHYSICS

TUESDAY, 14 July, 16:30-17:30

Personal attendance required

Gravity and Magnetic Studies in the Aegean Sea	Ezgi Erbek, M.Nuri Dolmaz
Geophysical investigation on buried 19th century orthodox churchyard in Sosnowiec	Maciej J. Mendecki, Michał Glazer, Dawid Surmik
Geophysical investigation of Babia Góra peak	Barbara Bieta, Michał Glazer, Maciej J. Mendecki, Wojciech Dobiński
Practical aspects of field Gamma Ray Spectrometry - new insights	Lidia Zenkner
Comparison of geophysical methods: GPR and ERT in the study of permafrost based on chosen case studies	Magdalena Mita, Anna Piątek
ERT Surveys over anthropogenic void of known dimensions	Damian Kula
Geological and geophysical analysis of Upper Cretaceous rocks - a case study of the Mięchów Trough (SE Poland)	Aleksandra Stachowska
Geophysical research of waste dump from Zn-Pb processing	Mateusz Dariusz Raciok
Geophysical investigation of former iron mine in Cisna, SE Poland.	Ewa Janowska, Radosław Kaczmarzyk
The diagnostics of soil liquefaction when saturated with water based on the measurements data of Rayleigh surface wave characteristics	Andrey Konkov, Sergey Manakov, Andrey Lebedev
Electrical borehole imaging method used for investigation of open-hole located in Moldavian Platform	Saleh Gabriel
Usage of numerical modelling for determination of stress change in seam overburden during longwall face advance in locations of installed stress measu	Alice Hastikova
Horizontal stiffness of Brno clay measured by seismic cross-hole method	Richard Malát, Josef Rott
Detrended Fluctuation Analysis of Geophysical Well log Data of Bombay Offshore Basin, India	D. Subhakar, E. Chandrasekhar
Study of error propagation in NMR measurements' inversion	Tamás Lukács, Virág Darányi, László Balázs
Magnetotelluric inversion in the seismo-active West-Bohemia region	Radek Klanica, Josef Pek



Gravity and Magnetic Studies in the Aegean Sea

Ezgi ERBEK¹, M.Nuri DOLMAZ¹

email: ezgierbek@sdu.edu.tr

¹Department of Geophysical Engineering, Suleyman Demirel University, 32260, Isparta, Turkey

Summary

Aegean Sea has intensity seismic activity. Earthquakes of which focal depth reaches up to 200 km are seen in southwest of Turkey and Aegean Sea. Deep focus earthquakes indicate that African plate plunges beneath Aegean plate. Aegean Volcanic Arc and its vicinity are characterized with negative magnetic (~ -60 nT), positive free-air (~ 120 mGal), and high heat flow anomalies (~ 110 mW/m²). Trench area is represented with low heat flow (20-40 mW/m²), negative free-air (~ -80 mGal) anomalies. Obtained progressively upward continuation maps (5, 10, 15, 20 kms) of potential field data imply the deep structure of the study area.

Introduction

The Aegean volcanic arc is one of the most important geological structures of the Alpine-Himalayan orogenic belt. This volcanic arc is represented by active subduction of African plate beneath Aegean/Anatolian plates. A lot of work (geological and geophysical) has been done by various researchers and the results are shown that diverse structures such as trench, subduction zone, seamounts, oceanic basins have been occurred in Aegean Sea and Mediterranean (Papazachos and Comninakis, 1971, 1977; Papazachos, 1990; Kalyoncuoğlu et al., 2011, 2013; Erbek and Dolmaz, 2014).

The study area is located between the longitudes of 24.5°-30.5° E and the latitudes of 34.5°-38.5° N (Fig.1). Earthquakes of which focal depth reaches up to 200 km and the biggest 7 magnitude reaches up are seen in southwest of Turkey and Aegean Sea. In Aegean Sea, two geophysical profiles with approximately NW-SE trending and in the length of 300 km constitute (Fig.1). Profiles that have 50 km wide contain earthquake data, curves of bathymetry (km), heat flow (mW/m²), magnetic (nT), free air and Bouguer gravity anomaly (mGal). With the interpretation of these profiles the relation between earthquake data and heat flow and also the disruptive mass of magnetic and gravity data in subsurface of Aegean Sea are aimed to explain.

Method

In this study, earthquakes occurred between the years 1964 and 2014 are obtained from International Seismological Centre (ISC) earthquake catalog. Using earthquake data, focal depth and distance graphics were constituted (Fig. 2). In this work, reduce to pole correction (RTP) was applied to magnetic anomaly and obtained anomaly values were drawn a square grid with a spacing of 5 km using standard Kriging method. For RTP, angle of declination was applied assuming 4° and angle of inclination was taken 57°. Upward continuation method is applied to separate a regional anomaly resulting from deep sources from the observed magnetization and gravity. Using this method, upward continuation maps of magnetic and gravity data for different heights were calculated (5, 10, 15 and 20 kms).

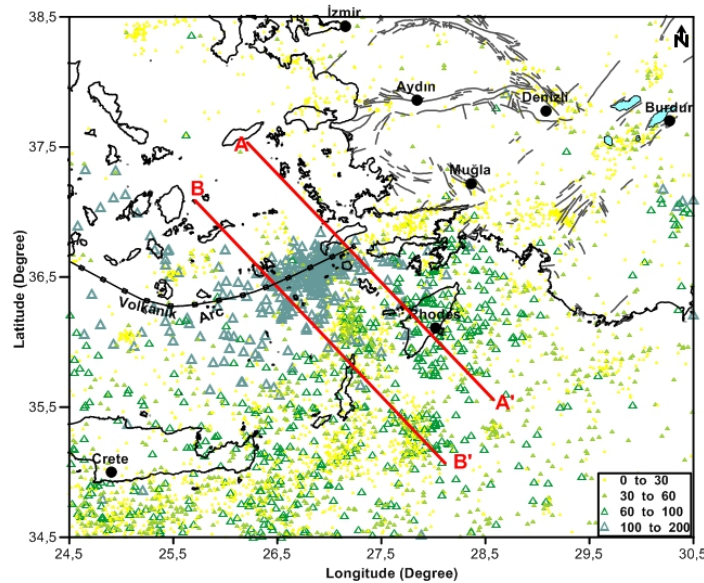


Figure 1 The map is shown that the study area and focal depths of earthquakes occurred between the years 1964 and 2014.

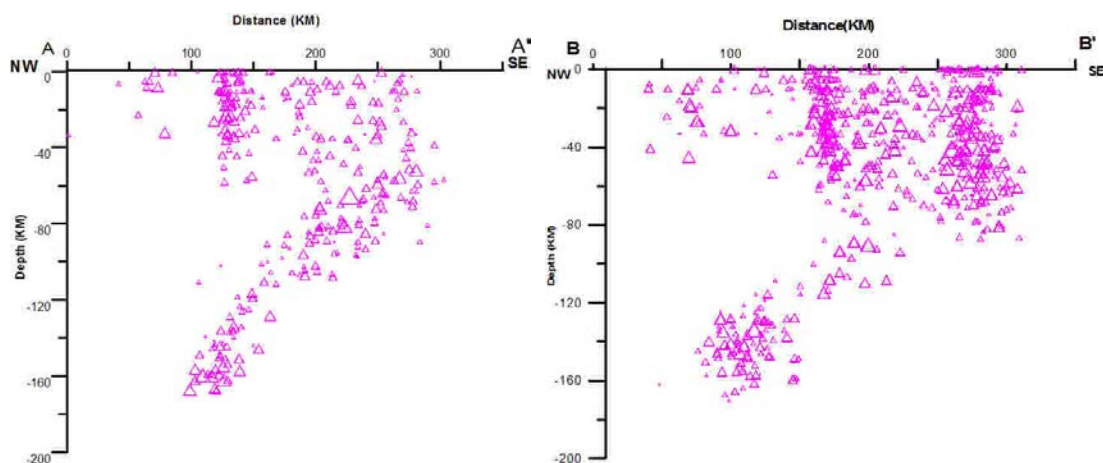


Figure 2 Focal depths and distance graphics for each profiles.

Conclusions

In the area corresponding to the distance between 80 and 250 km on profiles the intensity of deep-focus earthquakes are observed (Fig.2). It is the signal of subducting African plate's plunge. This area where deep-focus earthquakes is situated is on Aegean Volcanic Arc and its northern part. The area is characterized with curves of negative magnetic anomaly (~ -60 nT), positive free-air (~ 120 mGal) and gravity anomaly (~ 250 mGal). Curve of high heat flow anomaly (~ 110 mW/m²) on the profiles about 100 km indicates Aegean Volcanic Arc is located edge section of Africa plate. Based on earthquake data, slope of subducting plate is found average value of 35°. Trench is represented with curves of low heat flow (20-40 mW/m²), not anomaly including magnetic (0 nT), negative free-air (~ -80 mGal) and negative Bouguer (~ 130 mGal) anomaly. Upward continuation of magnetic data is indicated that remarkable anomaly is located northeast of Crete. Obtained progressively upward continuation maps (5, 10, 15, 20 kms) of potential field data imply the deep structure of the study area. Upward continuation maps (20 km) of magnetic data having maximum values (170 nT) takes attention a huge causative body in northeast of Crete.



References

- Erbek, E. ve Dolmaz, M.N., 2014. Geophysical researches (Gravity and Magnetic) of the Eratosthenes Seamount in the Eastern Mediterranean Sea, *Acta Geophysica*, 62,4,762-784.
- Kalyoncuoglu U.Y., Elitok O, Dolmaz M.N., Anadolu N.C., 2011. Geophysical and geological imprints of southern Neotethyan subduction between Cyprus and the Isparta Angle, SW Turkey. *J Geodyn*, 52,70–82.
- Kalyoncuoglu, U.Y., Elitok, O. ve Dolmaz, M.N., 2013. Tectonic implications of spatial variation of b-values and heat flow in the Aegean region, *Mar Geophys Res*, 34, 59–78.
- Papazachos, B. C. ve Comninakis, P. E 1971. Geophysical and tectonic features of the Aegean arc., *J. Geophys. Res.*, 76, 8517–8533.
- Papazachos, B. C. ve Comninakis, P. E., 1977. Modes of Lithospheric interaction in the Aegean area: Biju– Duval, B. And Montadert, L. (eds.), *Structural History of the Mediterranean basins*, Editions Technip, Paris, 319 – 332.
- Papazachos, B. C. 1990. Seismicity of the Aegean and the surrounding area, *Tectonophysics*, 178, 287–308.



Geophysical investigation on buried 19th century orthodox churchyard in Sosnowiec

Maciej J. Mendecki¹, Michał Glazer¹, Dawid Surmik¹

email: maciej.mendecki@us.edu.pl

¹ University of Silesia in Katowice, Poland

Summary

Geophysical surveys were carried out in order to find the churchyard graves and the foundations of the Orthodox Church in the city of Sosnowiec, Southern Poland. Resistivity Imaging method and conductivity measurements were applied to map the foundation plan and the location of the graves sketch. The resistivity studies showed anomalies changes with depth of the investigated objects while the EM measurements allowed to present horizontal changes in the conductivity map.

Introduction

Maczki is a district of Sosnowiec, located in the southeastern corner of the city. During the Partitions of Poland, in the half of 19th century Maczki (in these times called “Granica”, means in polish “border”) was a borderline between the Austrian-Hungarian Empire and the Russian Empire. Maczki, as part of Russian Empire, became the great transfer station complex at that time with the Warsaw–Vienna Railway station, the customs house, hostels and the Orthodox Church with surrounded cemetery. The complex existed up to the beginnings of the communism period in Poland. According to locals, the Church was pulled down in 1950 and all decors and sacral furnishings were deported by the communists (Szcupak 2002). The churchyard was levelled and there is a football court at present, covering the foundations and the graves.

The aim of the study was to find the accurate positions of the Orthodox Church foundations and the graves located around the Church. The studied object are present in the Quaternary muds and sands, deposited here as a fluvio-glacial sediments of the Biała Przemsza River (Lewandowski & Zielinski 1990).

Methods

The fundamental physical law used in resistivity and electromagnetic (EM) surveys is general Ohm’s law that governs the flow of current in the ground. The equation for Ohm’s Law in vector form for current flow in a continuous medium was given by many authors (e.g. Sumner 1976, Telford et. al. 1990; Schön 1996, Milsom 2003). General Ohm’s Law states that current density is proportional to conductivity of the medium and electric field intensity. In geophysical practice, electric field potential is measured during resistivity surveys and electromagnetic field is measured by conductometers in EM surveys (Schön 1996, Milsom 2003) which allowed to obtain the 2D vertical cross-section and the conductivity maps. In presented research ABEM Terrameter LS was applied on 5 parallels profiles with 40m length. The conductometers surveys were carried out to map horizontal changes of conductivity on the rectangle plane with dimensions of 35 m x 50 m. In presented study Geonics EM-38 conductometer was used.

Electromagnetic survey results

EM measurements carried out to up to depth of 0.5 m from surface. Figure 1 shows the change in real and imaginary component. On both maps the fundamentals of the Orthodox Church can be noticed, particularly on the imaginary map. In contrast, the expected graves areas also marked strongly on the imaginary map. Red circles represent relatively stronger EM responses of the ground which are probably more distinct tombs. Colour scales are presented as relative values with respect to the electromagnetic background of the ground.

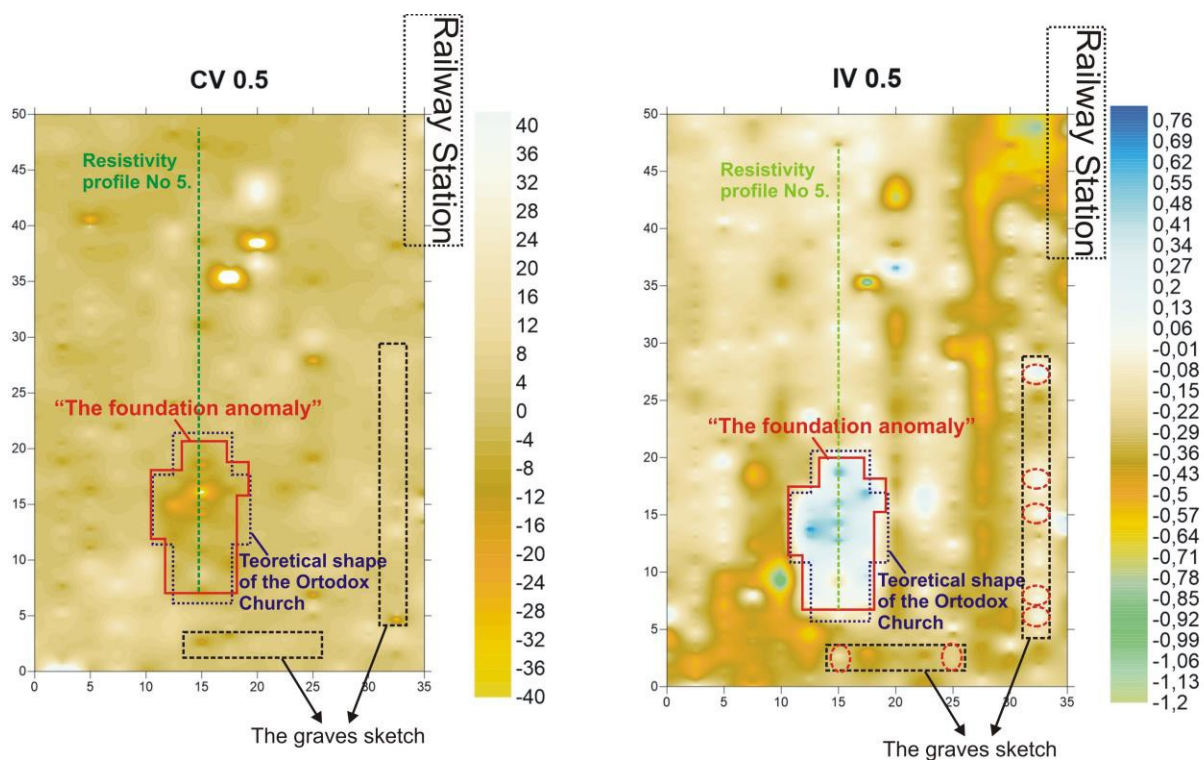


Figure 1 EM measurements result present as maps of real part (*left*) and imaginary part (*right*).

Resistivity Imaging results

The five resistivity profiles were processed in the RES2DINV software and presented as a 3D image of the study area. However, only the fifth profile is shown in Figure 2 which passes over the center of EM anomaly. The results indicate the presence of low resistivity anomalies (the values between 0 – 600 Ohmm, blue colour) which are probably related to the presence of the foundations of the Orthodox Church. This anomaly is a change in the vertical direction what can indicated the additional presence of the crypt. Additional anomalies are observed between 25 and 35 meter which could be natural or anthropogenic. There is possibility that the unknown objects are remains of the Church and it requires further study.

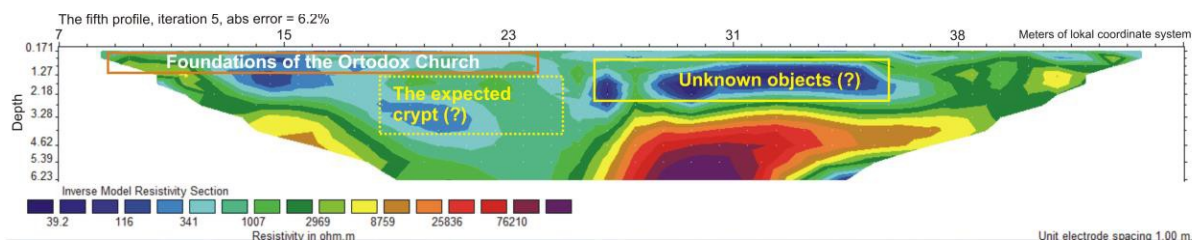


Figure 2 2D resistivity imaging result of the fifth profile.

Conclusions

The studies showed geoelectrical research efficiency in archaeological issues. Test results will be used by the local community to protect old graves localities and their exhumation by the relevant services under archaeological supervision. Further direct researches are required to solve the unknown anomalies on both data sets.



References

Lewandowski, J., Zieliński, T. (1990). An age and genesis of the deposits of fossil valley of Biała Przemsza river (Silesian Highlands) [Wiek i geneza osadów kopalnej doliny Białej Przemszy (Wyżyna Śląska).] Biuletyn Państwowego Instytutu Geologicznego, 364, 97-126 (in Polish)

Milsom, J. (2003). Field Geophysics. The Geological Field Guide Series. Wiley, England, 3rd ed.

Schön, J.H. (1996) Physical Properties of rocks, Pergamon.

Sumner, J.S. (1976) Principles of induced polarization for geophysical exploration, Elsevier, Amsterdam.

Szczupak, W. (2002). Maczki, which were the border. A historical monography. [Maczki, które były Granicą. Monografia historyczna] WDR „Progres”, Sosnowiec 2002. ISBN 83-87543-13-6 (in Polish).

Teleford, W.M., Geldart, L.P. and Sheriff, R.E. (1990) Applied Geophysics, 2nd ed. Cambridge University Press, Cambridge.

Geophysical investigation of Babia Góra peak

Barbara Bieta¹, Michał Glazer¹, Maciej J. Mendecki¹, Wojciech Dobiński¹

email: barbara.bieta@wp.eu

¹ University of Silesia in Katowice

Summary

Resistivity imaging survey was carried out on the peak of Babia Gora, which is one of the highest (1725 m a.s.l.) isolated mountain massif in the Outer Western Carpathians in Poland. The study allowed to identify shallow geological structures in NW-SE direction. The layers of flysch formations marked on the resistivity cross-section shows distinct inclination in the Southern direction.

Introduction

Babia Gora is an isolated mountain massif located on the border between Poland and Slovakia and the highest peak in the Western Beskidy Mountains (elevation 1.725 m above sea level). So far, only a few research has been conducted regarding the geology of Babia Gora. The Babia Gora massif mainly consists of Alpine Orogeny flysch, uplifted and folded in the Miocene. The strongly erosion-resistant Magura sandstones, interbedded with shale and less resistant sandstone, constitute the Babia Góra peak, above approximately 1 000 m (Łajczak 2014).

In contrast, The presented geophysical survey is the first deep geophysical research on this area. The main aim of study in the Babia Góra peak was an attempt to detect with sufficient accuracy geological structures by application Resistivity Imaging (RI) method. The IR profile (Figure 1) was carried out in the Eastern sub-peak area and was directed towards the NW-SE.

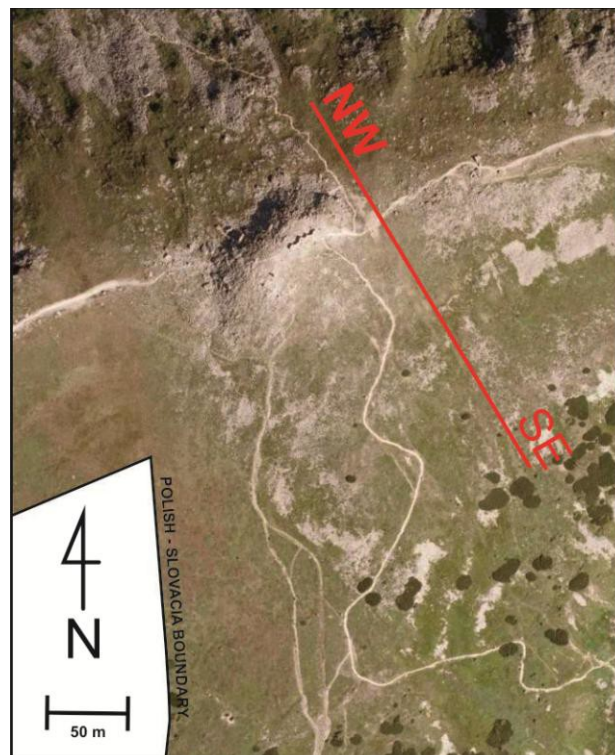


Figure 1 Location of the study profile on the Babia Góra peak which is visible on the upper left side of the profile.

Resistivity Imaging Method

The resistivity method is one of the oldest geophysical survey techniques applied in the geological surveys (Loke 2013). The purpose of such electrical surveys is to determine the subsurface resistivity distribution by making measurements on the ground surface. From these measurements, the true resistivity values of the subsurface layers can be estimated. The ground resistivity as well as the penetration depth is related to various geological parameters such as the mineral and fluid content, porosity and degree of water saturation in the rock. The fundamental physical law used in resistivity surveys is Ohm's Law that governs the flow of current in the ground (Dobinski et al. 2008, Loke 2013). The survey was performed by using the ABEM Terrameter LS which measured apparent resistivity on NW-SE profile. The profile-line consists of three cables with 5-meter electrode spacing and both Schlumberger and dipole-dipole arrays were used to obtain the mixed data set resistivity cross-section. The raw data were processed in the RES2DINV software with the smooth-constrained least squares inversion algorithm (Olayinka & Yaramanci 2000, Loke et al. 2003, Loke 2013).

Resistivity Imaging Result

The resistivity cross-section presented in figure 2 shows geological interpretation of geophysical prospecting. The flysch layers can be distinguished as a rock complex dipping in the Southern direction. Probable relative high resistivity anomalies are sandstone layers interbedded by low resistivity shale rocks. The thinnest layer is located directly under the surface and corresponds to weathered flysch rock. Discordances, directly under the debris, may be associated with stronger erosion and natural fracturing processes that occurred on the outskirts of flysch layers in shallow upper part of the peak. Unknown water drainage also plays important role in this structures and influences the shown resistivity model. The observed layers discontinuity require therefore further studies. However, their presence is probably caused by the Miocene folding processes which strongly had occurred in this area.

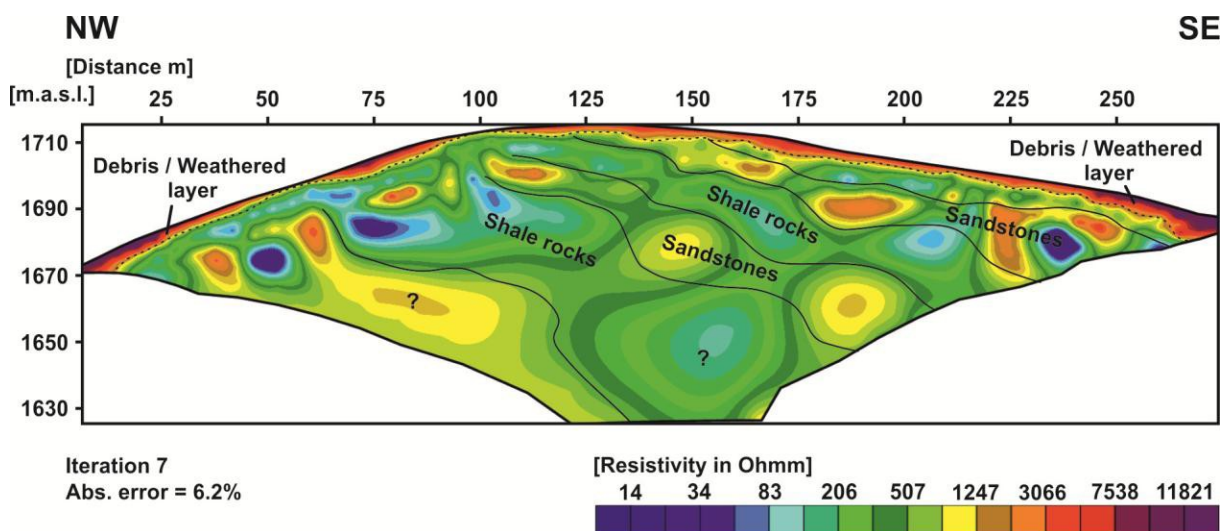


Figure 2 Resistivity cross-section from the Babia Góra peak.

Conclusions

The performed geophysical survey allowed to show the shallow geological structures of the Babia Góra peak. The interpretation indicated that the flysch complex dips in Southern direction and several layers of different resistivity values could be distinguished. Further studies are required to create a more precise geophysical model of this interesting mountain.



References

- Dobinski, W., Zogala, B., Wziątek, K., Litwin, L. (2008). Results of geophysical surveys on Kasproy Wierch, the Tatra Mountains, Poland. (In:) Applied Geophysics in Periglacial Environments, C. Hauck, C. Kneisel (eds). Cambridge University Press, 126-136.
- Gądek, B. (2012). Debris slopes ventilation in the periglacial zone of the Tatra Mountains (Poland and Slovakia): The indicators. Cold regions Science and Technology, 74-75, 1-10.
- Loke, M.H., Acworth, I., Dahlin, T. (2003). A comparison of smooth and blocky inversion methods in 2d electrical imaging surveys. Exploration Geophysics 34, 182-187.
- Loke, M.H. (2013) Tutorial: 2D and 3D electrical imaging survey. [online access: 13th January, 2015: www.geotomosoft.com].
- Łajczak A. (2014). Relief development of the Babia Góra massif, Western Carpathian Mountains. Quaestiones Geographicae 33,1, 89–106.
- Olayinka, O.I., Yaramanci, U. (2000). Use of block inversion in the 2-D interpretation of apparent resistivity data and its comparison with smooth inversion. Journal of Applied Geophysics 45, 63–81



Practical aspects of field Gamma Ray Spectrometry – new insights

Lidia Zenkner¹, Wojciech Kozłowski¹

email: lidia.zenkner@uw.edu.pl

¹ University of Warsaw

Summary

This study discusses the influence of outcrop conditions on the results of spectral gamma ray field analysis and provides methodology of SGR measurements, enabling minimization of this impact.

Introduction

Total natural gamma radiation has long been used in subsurface correlations and to determine the lithology in boreholes (Rider 2002). What is more, gamma-ray peaks are treated as an indicator of maximum flooding surfaces in siliciclastic successions (Hesselbo 1996), which are very important boundaries in sequence stratigraphy. Contrary to total gamma radiation, the spectral gamma radiation analysis allows determination of absolute abundances of main radioactive elements in rocks: K, U and Th (Rider 2002). In the last few decades this method has increasingly been used in paleoenvironmental studies of wide range of rock types both in boreholes and outcrops.

For outcrop measurements, portable spectral gamma detectors are widely used. Most often measurements are performed directly in the outcrop. However, the ubiquity of gamma radiation in the environment constitutes supposed threat to the reliability of the results. To assess whether the field conditions somehow affect the SGR analysis, results of measurements performed both directly in the outcrop wall (Outcrop Wall Measurements - OWM) and using a lead shield for individual rock samples (Shielded Samples Measurements – SSM) have been compared.

Methods

The measurements have been performed in the 5.3-meter thick succession of Silurian graptolitic shales in the Bardo-Stawy locality (Holy Cross Mountains, central Poland). SGR measurements by the portable gamma-ray spectrometer *Gamma Surveyor II* (GF Instruments, Brno, Czech Rep.) were 3 minutes long. First we examined each layer directly in the outcrop wall. After each outcrop measurement, we removed approx. 5-cm thick package of shale (with a weight of 6 kg) from the outcrop into plastic bag and placed it in the lead shielded box together with the detector. All shielded measurements were performed in one place at a distance of 6 meters from the outcrop.

Results and Discussion

SGR data obtained from the outcrop wall (Fig. 1, B) diverged significantly from those derived from the shielded samples (Fig. 1, A). Differences in the placement and magnitude of SGR peaks were striking. The largest divergence was observed in marginal parts of the profile, especially in the uppermost fragment, where the distance from the soil, plant cover and weathered rocks was small. Depth of investigation of scintillation gamma detectors is estimated at 10-20 cm (Rider 2002). Hence, the tool register signal not only from the examined rock layer, but also from the surrounding objects. Thus, presence of other sources of radiation in close proximity to studied rocks can affect the SGR signal.

Extremely high values of radiometrically determined potassium (eK) from OWM in *acuminatus* and *cyphus* sector of the outcrop (Fig. 1, B) are interpreted as an effect of clay contamination due to nearby presence of soil layer. Clay minerals containing potassium, mainly of the illite group, are commonly present in the rock waste (Deconinck et al. 2003). Thorium, as an insoluble element, tends

to concentrate in soil during weathering processes (Hesselbo 1996). Therefore, high eTh values in OWM of uppermost part of the profile (Fig. 1, B) are most likely related to the nearby soil. Uranium, in turn, can be stored in organic humus (Ebbs et al. 1998), which constitutes the top of soil profile. What is more, plants can uptake small amounts of U from soil and store it in their tissues (Singh et al. 2005). This effect seems to be responsible for high values of eU in OWM from *cyphus* sector (Fig. 1, B). From the other hand, eU from OWM, contrary to eK and eTh, did not show significant disagreement with data from SSM in the upper *acuminatus* sector (Fig. 1). It can be caused by the high solubility of uranium in aerobic conditions (Lüning & Kolonic 2003). This part of the profile was located near the brook, so it could be periodically submerged and uranium was leached away from the soil, while K-bearing clay minerals and Th remained in place due to their insolubility. Other factor leading to different anomalies in OWM of lower and uppermost part of the profile is probably different lithology of underlying and overlying rocks (radiolarian cherts and sandstones, respectively), which provide different rock waste.

Standard deviation (σ) of the ratio of ROI-Total [cps] and Dose Rate [nGy/h] is 1.11 for SSM and 1.62 for OWM (Fig. 1). Higher result in OWM means that the influence of the background radiation was stronger, while the shielding maximized the alteration of wavelength of background radiation by Compton scattering effect (background photons were counted as total gamma counts but not recognized as specified elements) (see: Rittersdorf 2007).

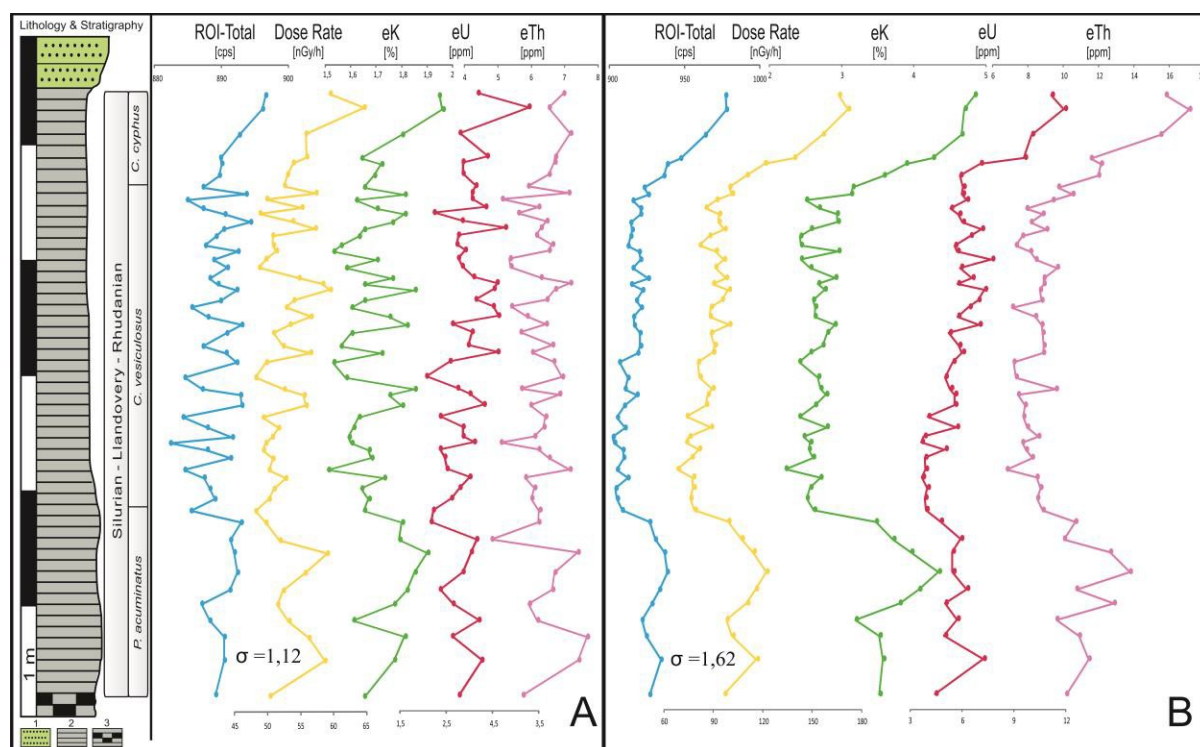


Figure 1 Spectral gamma ray logs for the measurements performed in lead shield (A) and outcrop wall (B). Lithology: 1-sandstones; 2-shales; 3-radiolarian cherts. Further explanations in the text.

Conclusions

According to our study, field conditions appear to potentially affect the results of SGR measurements and lead to misinterpretations. Particularly vulnerable are those parts of the profile that are in the immediate vicinity of the soil, plants and rock waste. According to the above, use of partial shielding in field SGR measurements is recommended, especially when the condition of the outcrop differs significantly along the profile.



References

- Deconinck, J.-F., Hesselbo, S. P., Debuisser, Averbuch, O. N., Baudin, F., Bessa, J. (2003). Environmental controls on clay mineralogy of an Early Jurassic mudrock (Blue Lias Formation, southern England). *International Journal of Earth Sciences*, 92, 255–266.
- Ebbs, S. D., Brady, D. J., & Kochian, L. V. (1998). Role of uranium speciation in the uptake and translocation of uranium by plants. *Journal of experimental botany*, 49(324), 1183-1190.
- Hesselbo, S. P. (1996). Spectral gamma-ray logs in relation to clay mineralogy and sequence stratigraphy, Cenozoic of the Atlantic margin, offshore New Jersey. *Proceedings of the Ocean Drilling Program: Scientific results*, 150, 411–422.
- Lüning, S. & Kolonic, S. (2003). Uranium spectral gamma-ray response as a proxy for organic richness in black shales: applicability and limitations. *Journal of Petroleum Geology*, 26, 153-174.
- Rider, M. (2002). *The Geological Interpretation of Well Logs*. 2nd ed., 67-86.
- Rittersdorf, I. (2007). Gamma ray spectroscopy. *Nuclear Engineering & Radiological Sciences*, 18-20.
- Singh, S., Malhotra, R., & Bajwa, B. S. (2005). Uranium uptake studies in some plants. *Radiation measurements*, 40(2), 666-669.



Comparison of geophysical methods: GPR and ERT in the study of permafrost based on chosen case studies

Mita Magdalena¹, Piątek Anna¹
email: magdalenamita@gmail.com

¹ University of Silesia, Faculty of Earth Sciences

Summary

The presented researches are an overview of the strengths and limitations of two geophysical methods: Ground-Penetrating Radar (GPR) and Electrical Resistivity Tomography (ERT) in permafrost occurrence investigation based on chosen case studies. Authors attempted to compare parameters and factors of geophysical techniques: depths ranges, horizontal and vertical resolutions, types of land forms which can be taken into account during the measurements, etc., basing on scientific paper review of selected issue.

Introduction

Permafrost is a physical state, which is defined as soil or rocks whose temperature is 0°C or below. This condition must persist for at least two consecutive years (Permafrost Subcommittee, 2005). Permafrost is defined only by thermal conditions. Local climate change may be responsible in this case for thawing, which may even lead to disappearance of permafrost (Dylikowa et al., 1992). Permafrost thickness is varied and can range from few meters up to 1 kilometer. Permafrost can be successfully investigated using geophysical methods, particularly Ground-Penetrating Radar (GPR) and Electrical Resistivity Tomography (ERT) thanks to its characteristic properties e. g. the dielectric constant or electrical resistivity values difference between the water and the ice.

Permafrost manifests diversity - from continuous permafrost, through discontinuous to sporadic. This diversity is associated with climatic and topography conditions, such as air temperature, solar radiation, surface energy exchange, altitude and slope rating (Dylikowa et al., 1992; Haeberli 1992; Haeberli et al., 1993). According to W. Haeberli (1993), one of the most important factors affecting the distribution of permafrost is change of air temperature with the altitude above sea level.

Methods and Theory

Ground-Penetrating Radar (GPR) is an electromagnetic method which basic principle is emission of electromagnetic pulse by transmitting antenna through the geological or anthropogenic medium. The electromagnetic pulse may be refracted, reflected or dumped. The converted wave after reflection is recorded by the receiving antenna. Obtained results are shown in profile data which is called an echogram. The necessary factor to register useful information is the dielectric constant between two objects. Recently, GPR method is used more often in geological research, also for the investigation and detection of permafrost (e. g. Sass, 2007; Hauck, 2013).

Electrical Resistivity Tomography (ERT) or Resistivity Imaging is a geoelectric method based on measurements of distribution of apparent resistivity over geological medium. The basis of this method is tracking changes in electric field with electrodes supplied by direct current. Furthermore, data is processed with inversion methods to obtain resistivity models which presents study area in 2D. A priori geological structure information of study area improves a choice of appropriate parameters which allow in the inversion processes to select the best resistivity models. In recently years, Electrical Resistivity Tomography method became more popular than Vertical Electrical Soundings (VES) or Electrical Profiling (EP), especially for detection of permafrost (e. g. Hauck and Kneisel, 2006; Onaca et al. 2013).



Figure 1 Permafrost distribution in the Northern Hemisphere [after Romanowsky V. E. et al. (2007) adapted from Brown et al. (1997)]

Conclusions

Geophysical methods are non-invasive techniques which provide physical properties measurements of geological or anthropogenic medium. The most effective approach to obtaining information about the subsurface structure of permafrost is the application of several geophysical methods at the same location. The usage of geophysical methods requires careful approach, both in research planning, field selection and execution. Interpretation should take into account the specific conditions of measurements, the local morphology and land cover. The interpretation must be supported by modeling, which can facilitate choice among possibilities and propose a final interpretation of the study.

Ground penetrating radar (GPR) has been used widely in permafrost studies for identifying the boundaries of permafrost and its distribution (e.g., Moorman et al., 2003; Angelopoulos et al., 2013) and characterizing ground ice structures (e.g. Moorman et al., 2003; De Pascale et al., 2008).

Electrical resistivity tomography (ERT) has also been extensively applied in permafrost studies (e.g. Hauck and Vonder Mühl, 2003; Maurer & Hauck, 2007), which focused mainly on mountain permafrost. It has also been applied for monitoring of permafrost in solid rock walls (Krautblatter & Hauck, 2007) and for the study of structure and composition of a tidewater glacier push moraine (Kristensen et al., 2009).

The ERT method requires contact between the ground and examined geological medium. The advantage of GPR is that measurements can be conducted without grounding and the system is relatively lightweight.



References

- Angelopoulos, M. C., Pollard, W. H. and Couture, N. J. (2013). The application of CCR and GPR to characterize ground ice conditions at Parsons Lake, Northwest Territories. *Cold Regions Science and Technology*.
- De Pascale, G. P., Pollard, W. H. and Williams, K. K. (2008). Geophysical mapping of ground ice using a combination of capacitive coupled resistivity and ground-penetrating radar, Northwest Territories, Canada. *Journal of Geophysical Research*.
- Dylikowa et al. (1992), Permafrost terminology: Polish translation. *Biuletyn Peryglacjalny*.
- van Everdingen, R. O. et al., *Glossary of Permafrost and Related Ground Ice Terms*. (2005). Permafrost Subcommittee.
- Haerberli, W. (1992). Construction, environmental problems and natural hazards in periglacial mountain belts. *Permafrost and Periglacial Processes*.
- Haerberli, W. Gouodong, C., Gorbunov, A. P. and Harris, S. A. (1993). Mountain permafrost and climatic change. *Permafrost and Periglacial Processes*.
- Hauck, C. and Vonder Mühl D. (2003). Inversion and interpretation of two-dimensional geoelectrical measurements for detecting permafrost in mountainous regions. *Permafrost and Periglacial Processes*.
- Hauck, C. and Kneisel, C. (2006). Application of capacitively-coupled and DC electrical resistivity imaging for mountain permafrost studies. *Permafrost and Periglacial Processes*.
- Hauck, C. (2013). *New Concepts in Geophysical Surveying and Data Interpretation for Permafrost Terrain*. *Permafrost and Periglacial Processes*.
- Krautblatter, M. and Hauck C. (2007). Electrical resistivity tomography monitoring of permafrost in solid rock walls. *Journal of Geophysical Research*.
- Kristensen, L., Juliussen, H., Christiansen, H. H. and Humlum, O. (2009). Structure and composition of a tidewater glacier push moraine, Svalbard, revealed by DC resistivity profiling. *Boreas*.
- Maurer H. and Hauck C. (2007). Instruments and methods: Geophysical imaging of alpine rock glaciers. *Journal of Glaciology*.
- Moorman, B. J., Robinson, S. D. and Burgess, M. M. (2003). Imaging Periglacial Conditions with Ground-Penetrating Radar. *Permafrost and Periglacial Processes*.
- Onaca, A. L., Urdea, P. and Ardelean, A. C. (2013). Internal structure and permafrost characteristics of the rock glaciers of Southern Carpathians (Romania) assessed by geoelectrical soundings and thermal monitoring. *Geografiska Annaler: Series A, Physical Geography*.
- Romanovsky, V. E., Gruber, S., Instanes, A., Jin, H., Marchenko, S. S., Smith, S. L., Trombotto, D. and Walter, K. M. (2007). Frozen Ground, Chapter 7, In: *Global Outlook for Ice and Snow*, Earthprint, UNEP/GRID.
- Sass, O. (2007). Bedrock detection and talus thickness assessment in the European Alps using geophysical methods. *Journal of Applied Geophysics*.



ERT Surveys over anthropogenic void of known dimensions

Barbara Bieta¹, Michał Glazer¹, Damian Kula¹,
email: contact@damiankula.pl; Barbara.bieta@gmail.com
¹University of Silesia in Katowice

Summary

Over the sewage well which dimensions were known were made 2 ERT parallel profiles and additional one crossing them. Observed anomalies fit to real dimensions of the well. There were also Depth-of-Investigation Index method used which is a complementary method for interpretation of the ERT.

Introduction

ERT method is a commonly used method during surveys that aims to recognize the structure of land from few meters to a more than a dozen of meters. Geophysical surveys often have to deal with different types of voids both anthropogenic and natural ones. The aim of surveys is to check how the

Presented surveys are planned to check the dimensions of anomaly caused by a sewage well after complete inversion process. During the experiment there were made 3 ERT profiles as presented on fig. 1.

Method and/or Theory

Resistivity surveys were performed on a single cable with 21 take-outs. There were designated 3 profile lines as shown on Fig.1. Line 1 and line 3 were parallel to each other and there were 1 m of distance between them. Line 2 was crossing line 1 and 3 around the centre of each one. During the surveys there were used 1m electrode spacing and Wenner-Schlumberger measurement protocol.

The inversion of resistivity data was carried out in Res2Dinv x64 ver. 4.03.13 software. There were also used depth of investigation(DOI) index method for purposes of estimation prepared resistivity models reliability. The method is based on comparing two resistivity models derived from the same dataset. The difference between models are reference models in inversion process. Recovered DOI value for a single model cell according to Oldenburg and Jones (2007), modified by Deceuster et al. (2014) can be calculated using:

$$R_{AB}(x, z) = \frac{|\log_{10} q_A(x, z) - \log_{10} q_B(x, z)|}{|\log_{10} q_A - \log_{10} q_B|}$$

Where:

- $q_A(x, z)$ and $q_B(x, z)$ are cell resistivity values obtained from the first and second inversion
- q_A and q_B are values of resistivity of uniform reference models

After inversion and preparing DOI index maps there were conducted interpretation of obtained cross-sections and comparison of anomalies size to dimensions of the sewage well.

Conclusions

The dimensions of anomaly differ a little from dimensions of the well both in width and height. Maps of DOI Index indicates that inversion process relied mostly on obtained data. Anomalies of DOI values were observed mostly at the bottom of each cross section where density of obtained data points is lowering. Observed anomalies of resistivity are slightly wider than the width of well most likely due to spacing that was used during the surveys. Height of high resistivity anomalies might be determined by occurrence of liquid in the well.

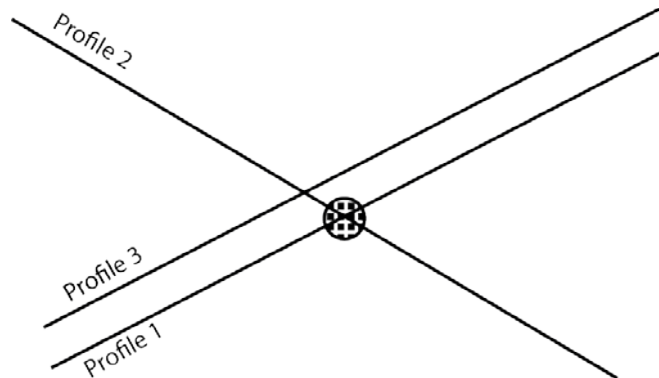


Figure 1 Sketch of profile lines prepared during the surveys. The circular shape stands for a sewage well's hatch.

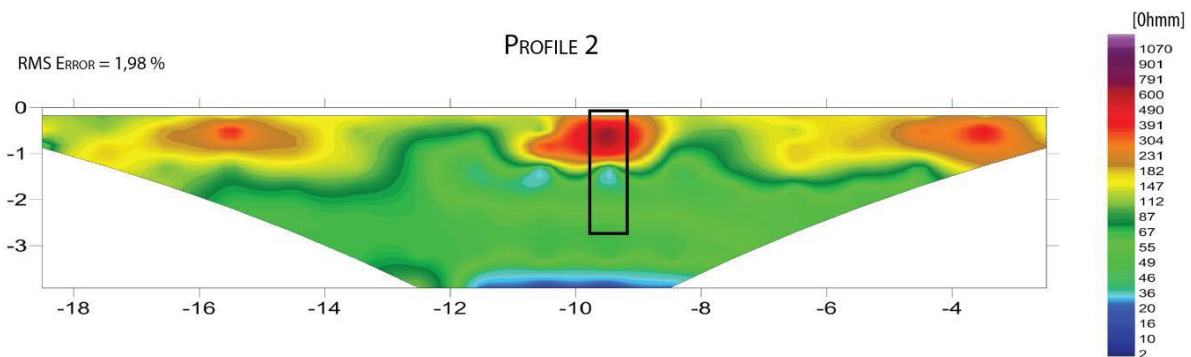


Figure 2 The resistivity cross-section from profile 2.



References

1. Deceuster, John, et al. "A modified DOI-based method to statistically estimate the depth of investigation of dc resistivity surveys." *Journal of Applied Geophysics* 103 (2014): 172-185.
2. Kirsch, R., ed. 2009. *Groundwater Geophysics. A Tool for Hydrogeology*, 2nd ed., Springer 2009
3. Mieszkowski R., Kowalczyk S., Barański M., Szczepański T., Zastosowanie metod geofizycznych do rozpoznania powierzchni stropowej gruntów słabo przepuszczalnych oraz stref rozluźnienia w korpusie zapory ziemnej., *Zeszyty Naukowe Instytut Gospodarki Surowcami Mineralnymi i Energią PAN.*, nr 86., 2014r., str. 172
4. Oldenburg D. W., Jones F.H.M., (2007) *Inversion for Applied Geophysics; Learning resources about geophysical inversion*, University of British Columbia: Geophysical Inversion Facility, <http://www.eos.ubc.ca/ubcgif/iag/index.htm> (Website accessed 26.04.2014)
5. Pasierb B. ,Techniki pomiarowe metody elektrooporowej. , *Czasopismo Techniczne, Zeszyt 23*, Wydawnictwo Politechniki Krakowskiej 2012r.
6. Rudzki M., Zastosowanie metody elektrooporowej do lokalizacji struktur krasowych ., *Geofizyka Toruń Sp. Z o.o. , str. 2-4*



Geological and geophysical analysis of Upper Cretaceous rocks - a case study of the Miechów Trough (SE Poland)

Aleksandra Stachowska¹, Łukasz Słonka
email: a.stachowska@student.uw.edu.pl

¹ Faculty of Geology, University of Warsaw

Summary

The Cretaceous of the southern Miechów Trough (SE Poland) was studied based on well-data, 2D seismic profile, and all new and archival available data. Facies relationship, structural geometry and influence of tectonics on sedimentation in the Late Cretaceous were recognised. The geological and geophysical data demonstrated syntectonic control on sedimentation. Late Cretaceous reactivation of older faults is recognised.

Introduction

The Miechów Trough (SE Poland) is a SE part of the Szczecin–Łódź–Miechów Synclinorium (Pożaryski, 1974). During the Late Cretaceous the area of the Trough was a marginal part of the Polish epicontinental basin. The ?Albian–Cenomanian part (Hakenberg, 1978) is mostly siliciclastic (conglomerate, sandstone and glauconitic sand). It is followed by the Turonian through to Maastrichtian carbonate (limestone, marl and opoka) dominated succession. The Cretaceous is also clearly two-fold in respect of the completeness of its record. The ?Albian–Santonian part is characterized by numerous unconformities with associated stratigraphic gaps (Walachczyk, 1992); the overlying Campanian–Maastrichtian part is relatively uniform and stratigraphically complete.

The main aims of the study are: (1) recognition of facies and structural geometry of the Upper Cretaceous in the southern part of the Miechów Trough; and (2) revealing the relationship between sedimentary and tectonic processes in the area, during the Late Cretaceous.

Method

New and archival data from outcrops (sedimentological and paleontological observations) and well-logs (e.g. Jawor, 1970; Heller & Moryc, 1984) are used in geological and geophysical analyses. Both outcrops observations and borehole data provide, however, only localized images of the structures. To reveal the structural geometry between boreholes, seismic profile is used. Only Upper Cretaceous part of the profile used is discussed in this study.

In the first step of the interpretation of 2D seismic profile, the depth of well-data was calibrated to time seismic data. For interpretation of rock complexes and for construction of synthetic seismograms (Fig 1) the well-log data from Zagość-2 (data: GR- natural gamma-ray, DT- acoustic log, RHOB – density log, RC – reflection coefficients) were used. Subsequently, faults and seismic horizons (which are also geological boundary; e.g. stratigraphic gap, facies changed) were determined. The geological interpretation was made in 5-5-92K section (Fig 2).

Results

Seismic cross-section (Fig 2) depicts two positive tectonic structures (anticlines) and several normal and reverse faults. Identified thickness variations of seismic horizons allowed to identify the influence of tectonics on sedimentation during the Late Cretaceous. The increasing thickness of some horizons indicates a regional subsidence stage, whereas decreasing thickness indicates inversion stage and uplift (Krzywiec *et al.*, 2009).

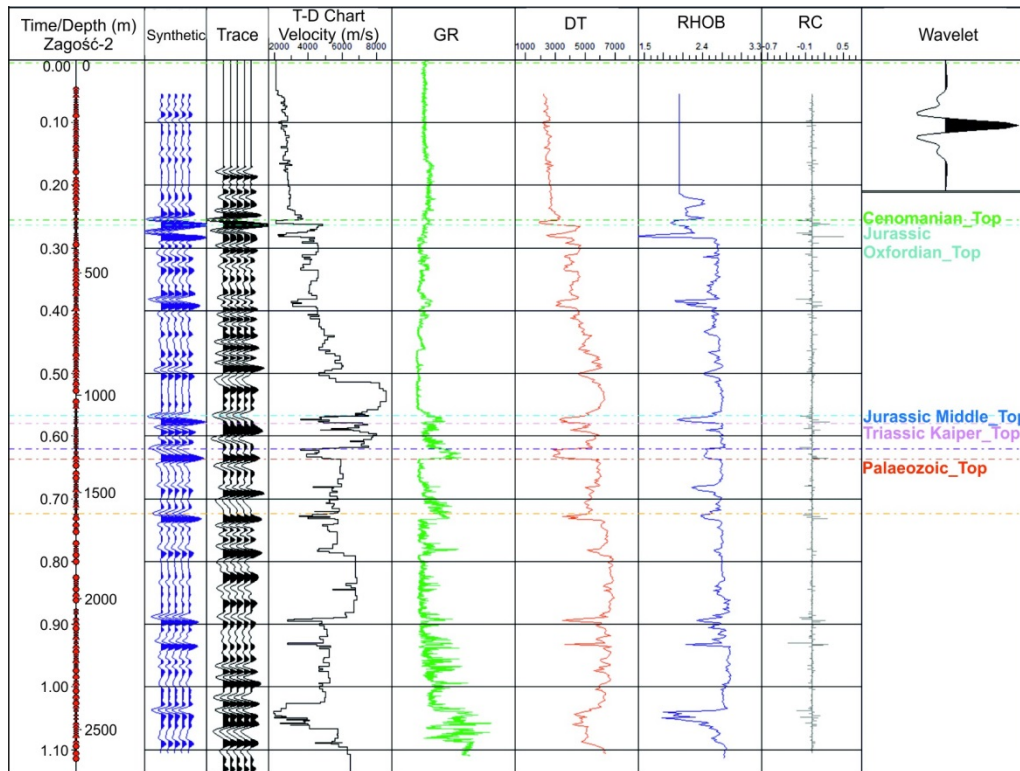


Figure 1 Synthetic seismograms for Zagość-2 well

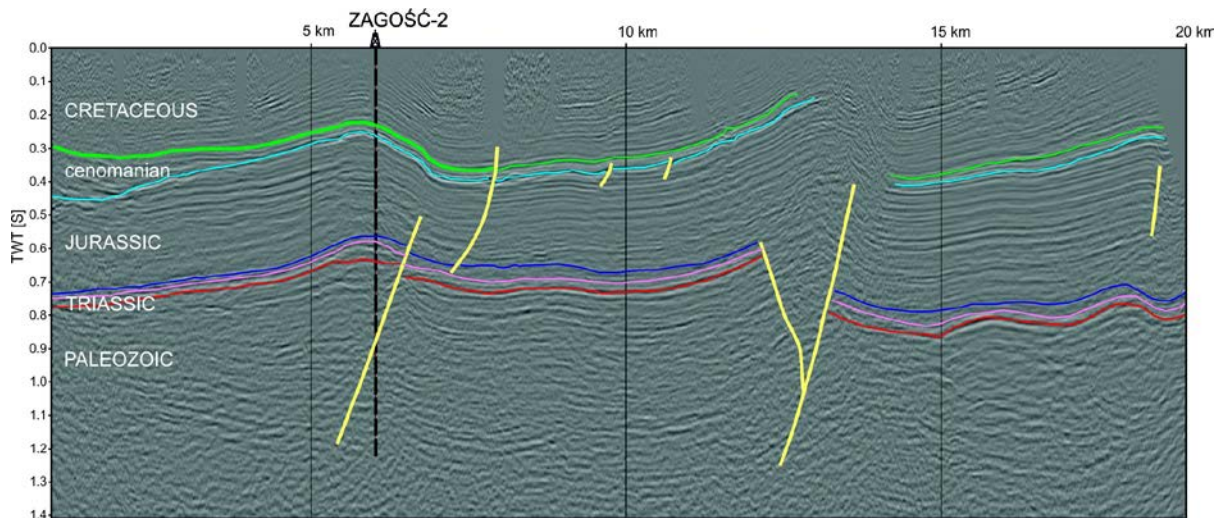


Figure 2 Structural interpretation on 5-5-92K seismic profile

Conclusions

The results of geological and geophysical interpretation proved that sedimentation during the Late Cretaceous in the study area was partly controlled by syntectonic movements. Late Cretaceous reactivation of older faults is demonstrated.

Acknowledgements

We would like to thank PGNiG company and San Leon Energy for providing seismic and borehole data. Kingdom® software used for cross section interpretation was provided by IHS.



References

Hakenberg, M. (1978). Albian – Cenomanian palaeotectonics and palaeogeography of the Miechów Depression, northern part. *Studia Geologica Polonica*, 58: 1-104. [In Polish]

Heller, I. and Moryc, W. (1984). Stratygrafia utworów kredy przedgórza Karpat. *Biull. PIG*. 346, 24: 1-46.

Jawor, E. (1970). The structure of the deep substratum in the region east of Cracow. *Acta Geologica Polonica*. 20, (4): 709-769. [In Polish]

Krzywiec, P., Gutowski, J., Walaszczyk, I., Wróbel, G. and Wybraniec, S. (2009). Tectonostratigraphic model of the Late Cretaceous inversion along the Nowe Miasto-Zawichost Fault Zone, SE Mid-Polish Trough. *Geological Quarterly*. 53, (1): 27-48.

Požaryski, W. (Red). (1974). *Budowa Geologiczna Polski, IV*. Wydawnictwo Geologiczne. Warszawa.

Walaszczyk, I. (1992). Turonian through Santonian deposits of the Central Polish Uplands; their facies development, inoceramid paleontology and stratigraphy. *Acta Geologica Polonica*. 42, (1-2): 1-40.



Geophysical research of waste dump from Zn-Pb processing

Raciok M., Brom A., Kondracka M.

email: mateuszraciok@gmail.com

¹ University of Silesia, Faculty of Earth Science, Sosnowiec, Poland

Introduction

The areas of mining and smelting non-ferrous metal such as zinc and lead carried out large-scale processing of ore flotation which generate significant amounts of waste rich in iron sulfides and various mineral phases containing heavy metals and metalloids. The environmental impact of deposition of lead and zinc processing waste is associated mainly with the issue of emission of heavy metals (heavy metals - HM) and sulphates ions cause pollution of air, soil, water and organisms (Girczyk J., Sobik-Szołtysek J., 2002)

This paper presents geophysical research of post-industrial waste dump from Zn-Pb processing. The studies were performed in Southern Poland - at waste dump located in Ruda Śląska and Bytom. Both waste dumps were studied using geoelectrical method - electrical resistivity tomography (ERT). Examination site in Ruda Śląska was formed as a result of activity of Hugo Steelworks between 1812 and 1932. It is assessed that about 1 860 000 m³ volume of waste was stored on the area of 8.5 ha (Jonczy, I. 2006).. In Bytom two millions of tons post-flotation waste have been accumulated in studied tailings pond on area of 19 ha. The waste dump was formed in 1926 to 1970 by mining and metallurgical plant "ZGH Orzeł Biały". Piled up wastes are characterized by high lead and zinc concentration. Different waste of Zn-Pb processing has different electrical, physical and chemical properties. Electrical resistivity of waste depends on various factors, including heavy metal content, the nature of solid constituents, water content, degree of water saturation, electrical conductivity of the pore fluid and temperature. The aim of this study is to characterize the electrical resistivity of waste from Zn-Pb processing in different areas in Poland.

Method and/or Theory

By measuring the resistance of the ground along the profile the tomography method obtained a two-dimensional (2-D) electrical resistivity images. All tomography surveys were carried out using 41 electrodes connected to a multi-core cable and to the central switching system. Each of used electrodes had the same spacing between them. During a measurement four electrodes were chosen at each time for resistance measurement, two of them were current electrodes, another were potential ones. Wenner-Schlumberger electrode configuration was used in order to combine accurate horizontal coverage of the ground, good depth penetration and good signal-to-noise ratio (Loke and Barker 1996). Spacing between electrodes during measurement in Ruda Śląska and Bytom was 1.2 m and 0.5 m respectively.

Examples (Optional)

There are two section examples presented below. The first section (fig. 1) presents the results from Bytom. Tailing pond has homogenous structure. However, it divided into two parts: near surface layer with higher electrical resistivity and deeper part of tailing pond with lower values of electrical resistivity. The higher electrical resistivity is related with soil layer which covered the waste dump as a part of its reclamation. The thickness of this layer is about 1 m. The difference between upper and lower layers is also probably caused by hypergenetic processes occurred in the waste dump. Acid drainage of raining waters results in changes in chemical composition of tailings. Near surface this process caused washed out the metals what is reflected in the reduction of the electrical resistivity with depth. Waste resistivity varies from 8Ωm to 110Ωm.

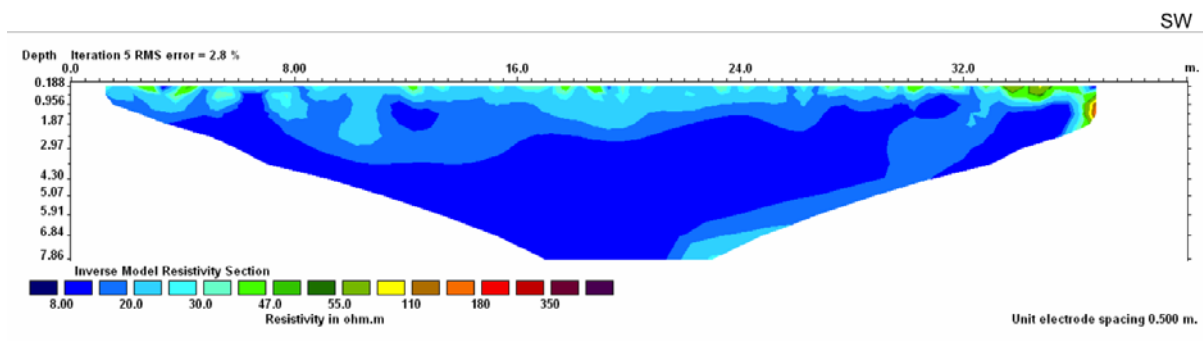


Fig.1. 2-D electrical resistivity image for Bytom

The second section (fig. 2) presents the results from Ruda Śląska. The waste dump can be divided into three zones.

The upper part is characterized by lower electrical resistivity (from 415 to 1114 Ωm). In the middle of section there is a high-resistive layer (from 1900 to 16 000 Ωm). Thickness of this part is about 5,5 [m]. Underlying layer is also characterized by lower electrical resistivity (the same like first layer). High electrical resistivity may result from type of deposited waste.

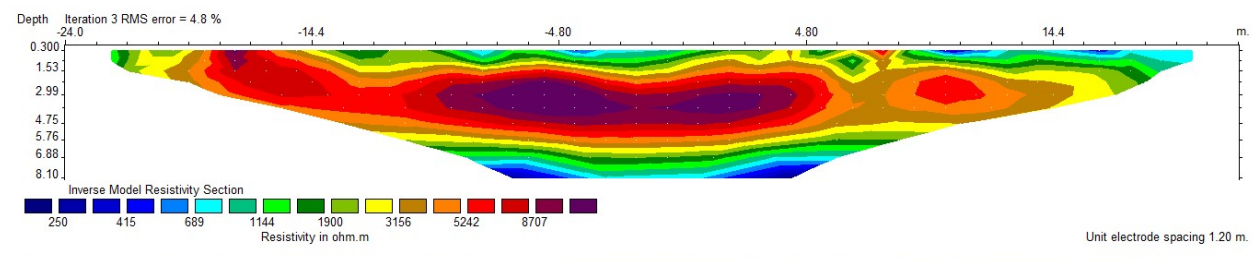


Fig.2. 2-D electrical resistivity image for Ruda Śląska

Conclusions

Different waste production processes causes various electrical resistivity image of studied waste dumps. Post-flotation waste are described by low electrical resistivity (8 Ωm to 110 Ωm). Electrical resistivity of metallurgical waste varied from 250 to 16 000 Ωm . Electrical resistivity shows variations in chemical and physical properties of waste. Contrast between electrical resistivity of waste and geological settings can be used to monitor direction of environment pollution using geoelectrical methods. Resistivity measurements are essentially non-destructive methods, quick and cheap methods which can provide particularly important information about ground and water pollution, information about changing chemical composition of waste and mechanical properties of embankment. In the future geoelectrical research will be extended with other geophysical methods and geochemical analysis allowed indicating the direction of contamination caused by acid and sulfate waters flowing from the studied waste dump.



References

Chodyniecka L., Haber T., 1995, *Procesy hipergeniczne w zwałowiskach odpadów poflotacyjnych po produkcji cynku i ołowiu*, *Rudy i Metale Nieżelazne* R. 40, Vol. 6: 184-189

Girczys J., Sobik-Szołtysek J., 2002, *Odpady przemysłu cynkowo-olowiowego*, seria Monografie nr 87, Wydawnictwo Politechniki Częstochowskiej, Częstochowa

Jonczy, I. 2006. *Charakterystyka mineralogiczno-chemiczna zwałowiska odpadów poprodukcyjnych huty cynku i ołowiu w Rudzie Śląskiej – Wirku oraz jego wpływ na środowisko*. Monografia, Gliwice, Wydawnictwo Politechniki Śląskiej.

Kondracka M., 2013, *Wpływ składowisk odpadów górniczo - hutniczych rud Zn – Pb na zanieczyszczenie gruntów w świetle badań geofizycznych*, praca doktorska, Uniwersytet Śląski, pp. 1- 206.

Geophysical investigation of former iron mine in Cisna, SE Poland

Ewa Janowska¹, Radosław Kaczmarzyk
 email: ewa_janowska@wp.pl
¹ University of Silesia

Summary

The protection of cultural relics and industry is a peculiar obligation to the heirs of our ancestors. Not only should it be of paramount importance for local people but this is also the overriding issue of the whole population. It is obvious that because taking care of historic buildings or monuments of nature is complicated and time consuming we must find the way in which we can protect something that is not discernible at first glance.

The Research was aimed to find the “Róża” iron mine location from the nineteenth century, formerly owned by the Fredro family. The study were carried out to determine a possible course of the mine. the study area was the Mochnaczka – Jeleni Skok belonged to the Bieszczady mountains , located in the village of Cisna.

Introduction

Cisna area is consist of Carpathian flysch which is interbeds of sandstones, marl, shale and mudstones. The regional structure is represented by the Menilite-Krosno Series, which is typical marginal deposits of the cretaceous and paleogene sediments. Geoelectrical and refraction SEISMIC method. Were apply because of non-invasive survey.

Method and/or Theory

LUND Imaging System was used to perform geoelectrical measurements with a 5-meter electrode spacing and Sand dipole-dipole systems were applied to three profile: Pe 1 - length of 500 m, Pe 2 - with a length of 200m, Pe 3 - profile with a length of 100m. Seismic refraction method were carried out by PASI equipment over ps1 profile - 115 m long.

Data interpretation was performed in the RES2DINV program and SeisImager program. Figure 2 presents the inversion result for Pe 1 profile. On the figure 2 the potential location was marked where iron mine could be find.

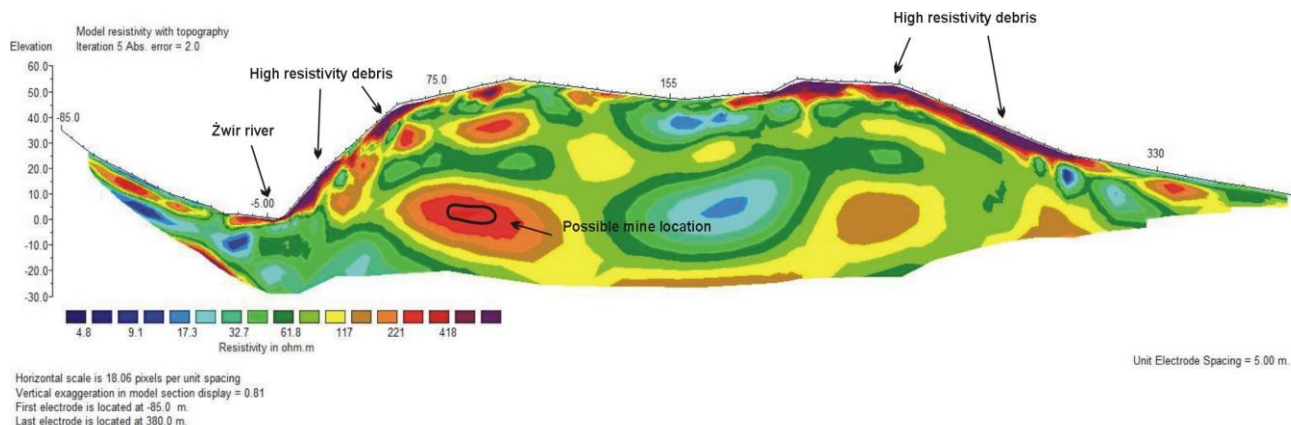


FIG.1. Inversion results of Pe 1 profile.

Low resistance values of the 8-36 Ω m may indicate the shales, the values of 37-100 Ω m may indicate sandstones. However, the marked anomaly corresponds to the assumptions of sought tunnel. It is relatively high resistivity in relation to the surrounding - can result from high filler resistance inside



the tunnel. The anomalies appear above the selected location of mine may indicate cracks in the layers lying above - may be caused by the same phenomenon backfill a tunnel.

Based on the analysis of the results can be seen significant similarity in the resulting cross-sectional profile of Pe 3 and Ps 1 that were made on the same profile (position), so they are the most comparable and reliable. Both sections showed a significant anomaly of resistance and the propagation velocity of seismic waves. The anomaly is located on approx. 60 meter measuring profile and approx. 5-6 meters below the surface. It is moved by approx. 10 meters in relation to the expected entrance to the "Rose" mine. Most likely, the corridor is overwhelmed.

Conclusions

- Geophysical research realized on 26-29 March 2015 in the village of Cisna showed a probable location of adit "Rose" the nineteenth century iron ore mine.
- Applied geophysical methods - geoelectric and seismic method - showed a good correlation measurements result.
- The results indicate the presence of mining tunnels "Rose" in the Mochnaczka- Jeleni Skok mountain.
- Estimated location of mine was partially selected on measurement field.
- Presumably location of the entrance to the tunnel must be revised.
Most likely, the entrance to the tunnel is moved by 10 meters in relation to the expected entrance to the mining tunnel.
- To obtain assurance as to the location of entry and the course of adit is recommended additional geophysical measurements - using geoelectrical and conductivity methods. They show a high compatibility during the results correlation.



References

Gruszczyński et al. (1996). Bieszczady - słownik historyczno-krajoznawczy. Stanisław Kryciński, Warsaw

Loke M.H.(2000). Electrical imaging surveys for environmental and engineering studies. M.H. Loke

Ślącza et al. (2008) Regionalizacja tektoniczna Polski - Karpaty zewnętrzne i zapadlisko przedkarpackie . Przegląd Górniczy

Malata T. (2005) Warstwy menilitowe w kamieniołomie w Krościenku.

Wiąłow O.S.(1967) Niektóre ogólne rozważania o tektonicznych strefach w Karpatach i o ich nomenklaturze. Rocznik Polskiego Towarzystwa Geologicznego

The diagnostics of soil liquefaction when saturated with water based on the measurements data of Rayleigh surface wave characteristics

Andrey Konkov¹, Sergey Manakov, Andrey Lebedev
email: magister44@yandex.ru

¹ Institute of Applied Physics

Summary

This work is aimed to describe effects of saturation with liquid on soil's behavior and constitution. Special attention was given to estimation of nonlinear parameters of soil. Effects of hysteresis nonlinearity in dependence "force versus displacement" were observed and discussed as well.

Introduction

The high content of liquid can lead to dilution of dispersive soil, therefore the diagnostics of the degree of saturation with moisture is of interest while predicting the phenomena associated with the development of its instability. In their numerous studies (Konkov et. al., 2012, 2013, 2014) authors have demonstrated the possibility of remote diagnostics of liquid content based on the analysis of the frequency dependence of the Rayleigh wave velocity and the ratio of longitudinal horizontal and vertical projections of displacement.

Experiment and Processing

In the summer of 2014 at the test area it was conducted the experiment devoted to the study of effects associated with the instability of soil when it was saturated with liquid. 2 weeks before the experiment's fulfilment there was dug a 20 cm wide and 50 cm deep trench, in which a hose with holes was embedded. The hose was connected to the water supply network through the water meter (with one end). The second end of hose was shut.

The photo from the experimental site is shown in Fig. 1. The receiving antenna consisting of geophones was placed on the surface, along the hose line. Each antenna element represented a pair of geophones with horizontal and vertical polarizations. The vibrator was set at a distance of 1 m from the nearest pair. To measure the force applied two accelerometers were mounted on the vibrator's plate and reaction mass respectively. The vibrator was excited by the signal with linear frequency modulation in the bandwidth from 3 to 430 Hz. During the saturation of the soil with water the medium's response was being continuously recorded. Each measurement lasted 1.536 s. Upon completion of the experiment the soil lost its stability, what led to the loss of vibrator's vertical position. Examination of experimental site revealed the fact that the water did not leak outside the scope of ditch, where the ground was close to the liquid state. The photo of vibrator after the loss of soil's stability is shown in the inset of Fig. 1.



Figure 1 Photo from the scene of the experiment. The inset shows the position of vibrator after the loss of soil's stability.

To extract the Rayleigh wave from the wave packet recorded by receiving system the signal from geophones underwent the double Fourier transformation in order to obtain the spatio-temporal spectrum (F-K spectrum (Hatton et. al., 1986; Yilmaz, 2001)). Such transformation was executed separately for sensors with vertical and horizontal polarization. On the F-K spectrum there was being found the characteristic which meets the Rayleigh wave. In such a manner the phase velocity was being determined. The projections ratio was calculated by division of absolute values of spectral quantities for geophones with horizontal and vertical polarization. So, the Rayleigh wave properties were determined in a bandwidth from 20 to 100 Hz.

Results and Discussion

In order to determine nonlinear parameters of the soil it was conducted the analysis of signals received from accelerometers mounted on vibrator. One of them was fastened to the plate that was in contact with ground. Second accelerometer was mounted on the reaction mass. Supporting mass was connected to the plate by spring. The resonant frequency of vibrator was 16 Hz. Based on the data obtained from accelerometers it was determined the relation between harmonic force applied to the soil and the displacement (Averbakh et. al., 2008). Fig. 2 shows temporal evolution of this dependence on the frequency of 216 Hz while liquid saturated the soil. The delay associated with radiation losses of energy is excluded. The horizontal axis represents the displacement of the plate. The vertical axis represents the magnitude of force exerted on ground by the vibrator. Blue color corresponds to the dependence obtained before the launch of experiment, red - a few minutes before the loss of soil's stability, green - 3 seconds before the vibrator's "fall". In all three cases the hysteresis nonlinearity can be observed. Also, we can conclude that with the increase of the amount of liquid in soil the hysteresis nonlinearity disappears, but before falling-down it appears again. Presumably, the nonlinearity is dictated by the hysteresis of interaction between granules of the soil (Averbakh et. al., 2014). By increasing the amount of liquid in pores, the concentration of stresses in the contact area decreases. In such a case the nonlinearity reduces. At the end of experiment the dynamic soil's destruction takes place. As the result the hysteresis dependence "force versus displacement" reappears.

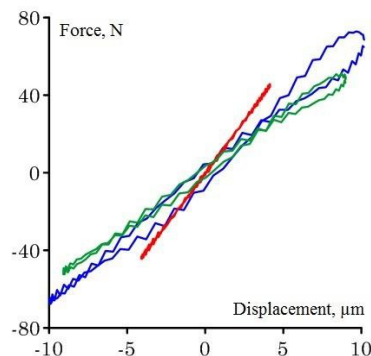


Figure 2 The dependence between the displacement of the vibrator's plate and the force acting on the ground.

The results of this study can be applied in the construction prospecting, as well as in solving the problems pipelines leakage location.

Acknowledgements

The reported study was partially supported by RFBR, research projects No.14-02-00695, 15-05-08196, 15-45-02450, 14-05-31249.



References

Konkov, A., Lebedev A., and Manakov S. (2012). The Near Surface Profiling based on the Rayleigh Wave Dispersive Properties for Vector Displacement: Near Surface Geoscience 2012 — 18th European Meeting of Environmental and Engineering Geophysics, EAGE, Extended abstract, DOI: 10.3997/2214-4609.20143332.

Konkov, A., Lebedev A., and Manakov S. (2013). Subsoil characterization with use of acoustical methods. Official publication of congress “TECNIACÚSTICA 2013” — 44th Spanish Congress on Acoustics and Iberian Encounter on Acoustics “TECNIACÚSTICA 2013”.

Konkov, A., Lebedev A., and Manakov S. (2014). Rayleigh Wave Dispersive Properties of a Vector Displacement as a Tool for P- and S-wave Velocities Near Surface Profiling, in W. Freedon, M. Z. Nashed, T. Sonar, eds. Handbook of Geomathematics (2nd edition). DOI: 10.1007/978-3-642-27793-1_98-2.

Hatton, L, Worthington, M.H., and Makin, J. (1986). Seismic data processing: theory and practice. Blackwell Scientific.

Yilmas, Ö. (2001). Seismic Data Analysis: Processing, Inversion and Interpretation of Seismic Data. SEG.

Averbakh, V., Lebedev, A., Maryshev, A., and Talanov, V. (2008). The diagnostics of unconsolidated media acoustic properties in the field conditions. Acoustical Physics 54(4).

Averbakh, V., Bredikhin, V., Lebedev, A., Manakov, S. (2014). Nonlinear acoustic spectroscopy of a rock sample and a granular medium. The book of abstracts of Forum Acusticum, Krakow, Poland, 7-12 September 2014.



Case Study: Electrical borehole imaging method used for investigation of open- hole located in Moldavian Platform (Romania)

Saleh GEBRIEL

Salehali479@yahoo.com

University of Bucharest, Dept. of Geophysics, Bucharest

Summary

This case study focuses on borehole measurements from high-resolution Compact Micro-Imager CMI data along with other standard open hole logs which were acquired in well A. This well is located in Moldavian Platform which is considered the oldest platform unit from Romanian territory. I started the interpretation with dips picking using sinusoidal features detected on oriented images, the results being presented as "tadpole" plots with different dip patterns and then I analyzed the dip patterns to identify a variety of geological attributes such as structural dip, faults, unconformities and fractures. I have also used borehole breakouts to estimate the contemporary tectonic stress.

Introduction

Electrical borehole imaging is basically a map of rock resistivity at the borehole wall (George Asquith and Daniel Krygowski , 2014) .The raw data acquired by an electrical imaging tool is a series of microresistivity curves, These form the matrix which is processed into an image(Malcom Rider, 2002). In this case study I have used data measured by using Compact Micro-Imager (CMI) tool in a well located in the Moldavian Platform which represents the south-western part of the East European Platform. The age of this unit is Middle Proterozoic time. The Moldavian platform consist in a metamorphic basement with granitic intrusions and a mostly horizontal sedimentary cover. Sedimentary cover corresponds to the tectonic stability phase when only positive and negative epigenetic movement took place there where three major cycles of marine transgressive and regressive which generated the sedimentary megacycles forming the sedimentary cover deposit. The total thickness of sedimentary cover varies from few hundreds of meters to more than 6000 meters, increasing East towards West and from North towards South(Mutihac, V., Stratulat, M.I., Fechet, R.M , 2002).

The primary purpose of this study is to perform a basic structural analysis of the CMI image to identify bedding , fractures, unconformities and faults by measuring the dip and azimuth of planar features by using "*Interactive Petrophysics*" log interpretation software.

Data – processing parameters:

I examined pre-processed data and there were no major areas of the tool momentarily sticking and pulling. Depth Domain Speed Correction was applied to the raw data. The deviation of the well was minor and it ranged from 0.242° to 0.882° .

To visualize the image logs, I used two types of image color designation.The static image was generated by assigning the highest and lowest resistivity values from the entire logged interval of the well. The dynamic image was normalised using a 1 m window to enhance the log quality and increase the geological and structural features resolution.

Structural & Sedimentological Analysis

All data was interactively picked over the entire borehole. All dips are oriented to True North, the magnetic declination for the studied area being 5.12° E. In addition, to help in the

interpretation and final presentation Dual Laterolog formation resistivity, Neutron, Density and sonic logs were used .

In this study the results of dip picking are presented in "tadpole" plots (Figure 1). I analyzed the dip patterns to identify a variety of geological features, for instance the green patterns symbols represent the hand-picked parallel and thin laminations of *SHALE* which representing regional dip. Red patterns symbols "increasing dip with depth" represent *FAULT* .abrupt change in dip and/or direction, representing *UNCONFORMITIES*.

Bedding statistical analysis overall structure shows two dominant dip directions towards NNE and SSW. While Cross-Beddings statistical analysis overall structure shows two dominant dip directions towards N , ESW and SW.

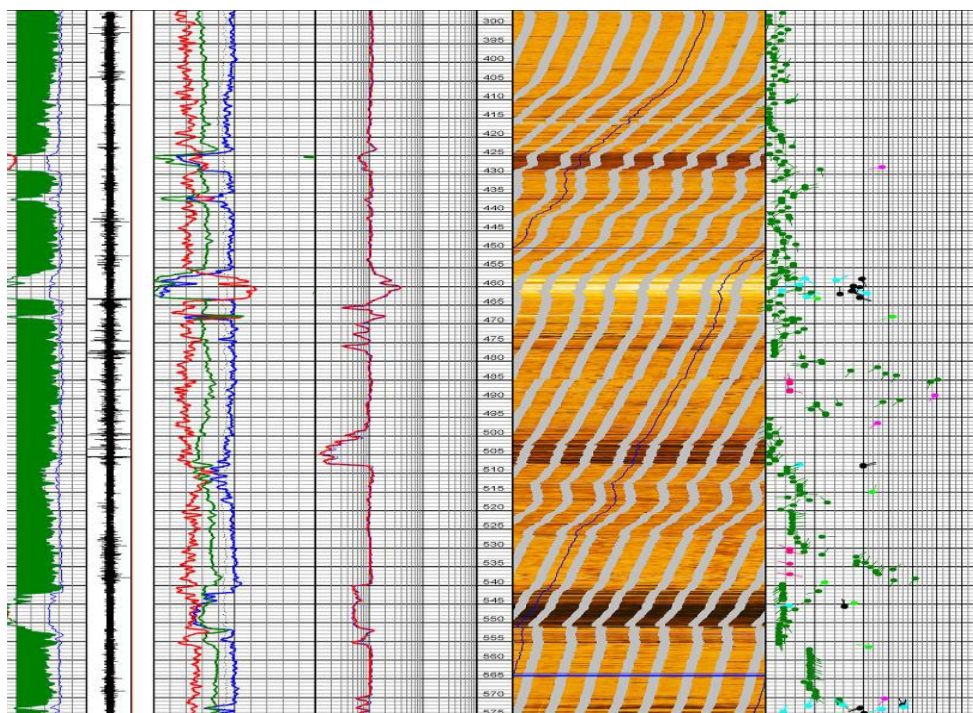


Figure 1: CMI interpretation summary (interval 386.0-582.0 m)

Conclusions

To sum up, Compact Micro-Imager CMI data used together with other standard open hole logs have been used to identify a variety of geological features such as shale sequences, clean sands with cross bedding, faults and unconformities in a well located in Moldavian platform - Romania. Important borehole breakout was observed on Imaging, such features being important indicators of horizontal stress.

Determination of sediment transport direction within depositional systems paleocurrent analysis is based on the orientation of cross stratification structures. However, at least 2 wells are needed for the determination of paleocurrent directions.

Acknowledgments

The author express his gratitude to Prof. Dr. Bogdan NICULESCU for his good advice and support for this study.



References

Malcolm Rider (2002). The Geological Interpretation of Well Logs. Rider-French consulting Ltd

George Asquith and Daniel Krygowski (2004). Basic Well Log Analysis . American Association of Petroleum Geologists

Mutihac, V., Stratulat, M.I., Fechet, R.M. (2004). Geology of Romania. Didactic and Pedagogical Publishing House, Bucharest, Romania, ISBN 973-30-1013-8.

Usage of numerical modelling for determination of stress change in seam overburden during longwall face advance in locations of installed stress measuring devices CCBO(M)

Alice Hastikova¹, Jaroslav Zdvorak
 email: alice.hastikova@ugn.cas.cz

¹ Institute of Geonics AS CR, v.v.i.

Summary

CCBO(M) - Compact Conical-Ended Borehole Overcoring (Monitoring) is the method of determination of stress or continual measuring of stress change in the rock massif. Strain gauges located at the surface of conical shape measuring device allow determination of full stress tensor in idealized point in the rock massif. Stress changes induced by longwall face advance of coal seam in deep coal mine are presented and compared with the results obtained by numerical modelling in 3D space. The differences between IN-SITU and model results are discussed with the introduction to the future work taken into account.

Introduction

CCBO(M) is the method of stress determination in the rock mass (Kang 2000) and stress changes monitoring in the rock mass (Stas et al. 2011; Soucek et al. 2013). ISRM (International Society for Rock Mechanics) declared the method to be the one of suggested method for rock stress determination (Sugawara and Obara 1999). This method allows to determine the full stress tensor for idealized point in the rock massif.

The stress tensor determination by this relief method depends on theory of elasticity and is subjected to laws of homogeneity and isotropy. Practical experience shows these conditions of the surrounding of the measuring device don't meet the theory requirement. Hence conditions of homogenous, isotropic and elastic responding surrounding media are used to simulate the case of IN SITU monitoring. The differences between the results may indicate how to set up the model to get results closer to the reality.

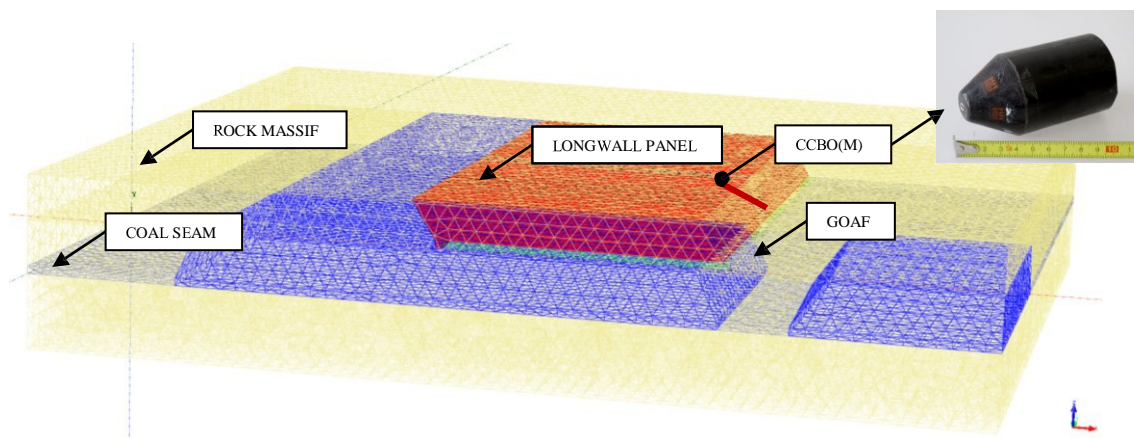


Figure 1 Basic concept of model geometry

Method

After drilling the borehole with conical shape at the end of it, CCBO probe is installed and the following overcoring of the surrounding media of installed probe allows the media to relax the stress by deformation response and individual deformations are measured by gauges situated at the conical surface of the probe.

The method of evaluating stress tensor using CCBO(M) measuring device is semi-analytical observing rules of Hooke's law and Kirsch solution for stress around holes in surrounding media of homogenous and isotropic character. The stress tensor itself is determined from matrix of compliance which represents individual relationship between these rules and also contains numerically evaluated deformation response relationships for geometrical shape of cone which is under individual component of unit tensor load. Following these presumptions it is possible to determine stress tensor and final principle stresses with their directions.

The case of determination stress tensor IN SITU and following stress changes during longwall face advance was modelled using Finite Element Method via software Midas GTS 3D. Linear elastic material model was used to obtain trends of principal stress changes and their directions during longwall face advance. The basic geometry can be seen in figure 1.

Results

Figure 2 introduces IN SITU and model results of principle stress change depending on longwall face advance. Principle stress changes of each longwall face advance are determined from stress tensor changes measured by CCBM probe or determined from stress tensors obtained from numerical modelling.

Comparing trends of stress changes depending on longwall face advance loses its important without evaluations of directions of each component of principal stresses, hence these are presented in figure 2 on the right. Interrelation between directions proves the incompatibility.

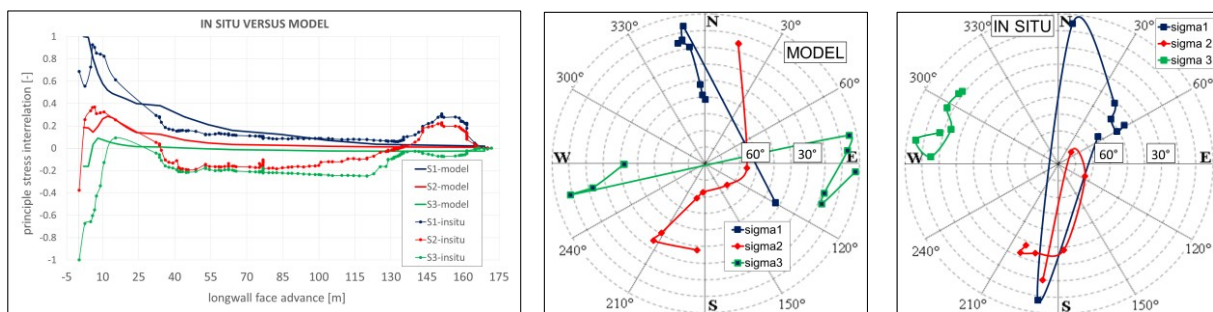


Figure 2 IN SITU versus model results of stress changes depending on longwall face advance (left: interrelation of principle stress change; right: directions of principle stresses)

Conclusions

From the comparative results presented in this paper it is clear some modifications have to be made. The principle focus is to upgrade semi-analytical solution for determination of stress tensor – using the method CCBO(M) from homogenous and isotropic media to inhomogeneous and anisotropic one. Ideas of the way of solving the problem will be introduced.

From modelling experience it can be stated that simulating of the weight of overburden in high depths doesn't meet the reality loading. Hence different simulating of initial status to the model should be used. Prestress loading conditions by defining of the initial stress tensor (obtained from CCBO method) to the surrounding meshes could be the starting point for the future work and then correlation of the input material properties to converge absolute values of the principal stresses may be followed.



References

Kang, S.S. (2000). Measurement and interpretation on stress history of a limestone deposit. Kumamoto University.

Soucek, K., Konicek, P., Stas, L., Waclawik, P. (2013). Experimental approach to measure stress changes in rock ahead of longwall mining faces in Czech coal mines. The University of Wollongong.

Stas, L., Knejzlik, J., Palla, L., Soucek, K., Waclawik, P. (2011). Measurement of Stress Changes Using a Compact Conical-ended Borehole Monitoring. ASTM International.

Sugawara, K. and Obara, Y. (1999). Draft ISRM suggested method for in situ stress measurement using the compact conical-ended borehole overcoring (CCBO) technique. Springer



Horizontal stiffness of Brno clay measured by seismic cross-hole method

Richard Malát, Josef Rott, Martin Krupička, Jan Vilhelm
e-mail: richardmalat@gmail.com
Faculty of Science, Charles University in Prague

Summary

The paper deals with the estimation of the horizontal shear wave velocities that are one of the essential parameters for assessing of G_0 shear modulus. Investigated location is situated in Brno city consisted of so-called “Tegel” clay using a seismic cross-hole method. The obtained values were compared with laboratory results. The in-situ shear wave velocities for the depth 6 – 13 m vary between ca. 314 – 396 m/s. The results do not fully agree with laboratory measurements.

Introduction

Brno clay Tegel is the lower-badenian (~ 14,3 – 14,8 Ma) calcareous infill of the Carpathian foredeep. The liquid limit reaches in average 75 %, plastic limit 38%. As the clay is not perfectly homogenous, inclusions of gypsum and limonite, as well as tectonic fracturation can locally occur. Mechanical behaviour of Tegel clay is influenced by inherent stiffness anisotropy with higher stiffness, e.g. higher shear and Young moduli (and horizontal shear waves) in the direction of the horizontal sedimentation plane. The shear modulus for very small strain in the direction parallel to the sedimentary plane G_{pp0} is one of the inherent stiffness parameters characterising anisotropic (transversely isotropic) material.

Method and results

The cross-hole measurement was carried out using seismograph Terraloc Mark 6 with electrodynamic source BISSH, pulse generator IPG (Geotomographie GmbH) and receiver Geospace GS14-L9 (3 receivers for each coordinate). During each measurement the pneumatic load device inflates and leans against the wall in the unsupported borehole. The cross-hole method applied in Brno-Slatina locality included 2 boreholes. The borehole “V1” was equipped with generator of waves and in the second borehole “V2” the receiver was installed. The boreholes are in the distance of about 5 m. The local coordinate system was chosen in such a manner that point (0;0;0) agrees with the position of head of borehole V1, the head of borehole V2 is located at (5;0;0). 3 receivers were oriented parallel with coordinate axis: The receiver No. 1 in the z-direction, No. 2 in the x-direction, No 3 in the y-direction. For each of the depths 6, 8, 11, 12 and 13 m below the ground surface, a single electromagnetic impact pulse was generated in the horizontal direction. The time of arrival of the horizontally polarized shear wave at receiver No. 2 was interpreted using the visualization software REFLEX®. Resulting values are in Tab. 1.

During isotropic triaxial testing, horizontally trimmed undisturbed clay samples from the depth of 21 and 24 m were equipped by the oscillating piezoelectric bender elements. Again, the time of arrival of the polarized shear wave was measured and the shear wave velocity was evaluated consequently.

Depth (m)	V_{pp0} (m.s ⁻¹)
13	396
12	375
11	314
8	318
6	394

Table 1 Measured data with evaluated values of shear wave velocities V_{pp0} .

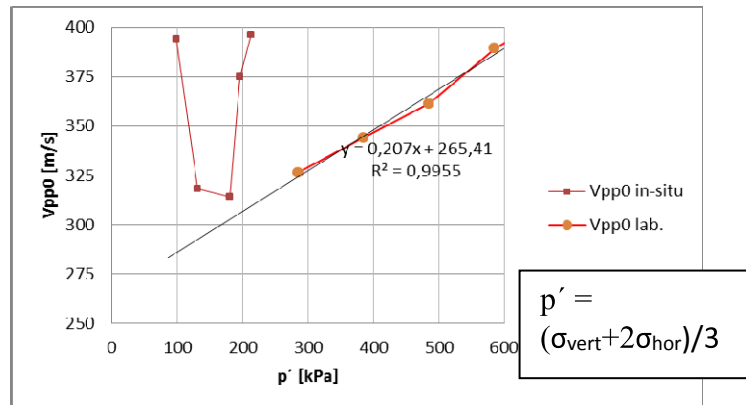


Figure 2 Comparison of field and laboratory data (sample from the depth of 21 m).

Discussion

The shear wave velocity V_{pp0} and therefore the horizontal modulus G_{pp0} depends clearly on mean effective stress which is the generally accepted assumption based on laboratory measurements. The behaviour of laboratory sample responds to this idea (see Fig. 2). This dependence is not observed in case of V_{pp0} assessed from the in-situ measurement, as the values significantly fluctuate. This can be possibly explained either by influence of “scale effect” and/or by the presence of stiffer inclusions in massif and local tectonically disturbed zones. However, field measurement shows generally higher values compared to the laboratory. This fits to the initial assumption of minimal soil disturbance caused by the field methods.

It is believed that Tegel is over-consolidated. Therefore, coefficient of earth pressure at rest K_0 and corresponding mean effective stress p' for various depths is very hard to estimate. However, back-analysed value of K_0 in the vicinity of Královo Pole tunnel complex indicated $K_0 = 0.75$ in the depth of 23 m (Rott et al. 2015) and this value was adopted for the purposes of the Fig. 2.

Conclusion

Shear wave velocities V_{pp0} evaluated from the field test and in the laboratory show relatively good agreement. The fluctuations and differences can source from various reasons like “scale effect” or non-homogeneity of investigated strata. Laboratory samples are disturbed during sampling and preparation for laboratory measurement, which may be not a negligible aspect as well.

Acknowledgements

The authors thank to the project of the Czech Science Foundation GAČR 14-32105S for its support.

References

- Rott, J.; Mašín, D.; Boháč, J.; Mohyla, T.; Krupička, M. (2015). Evaluation of K_0 in stiff clay by back-analysis of convergence measurements from unsupported cylindrical cavity. Acta Geotechnica (in print).
 Filipický, D. (2012). Měření rychlostí seismických vln ve dvojici vrtaných sond. Závěrečná zpráva, INSET, s.r.o.



Detrended Fluctuation Analysis of Geophysical Well log Data of Bombay Offshore Basin, India

D. Subhakar and E. Chandrasekhar
Email: subhakar17@gmail.com

Department of Earth Sciences, Indian Institute of Technology Bombay, Mumbai, India-400076

Summary

In this paper, we discuss the results of Detrended Fluctuation Analysis (DFA), applied to geophysical well log data to delineate depth to the tops of reservoir zones. We have considered gamma-ray, sonic and neutron porosity logs of three different wells: A, B and C, located in western offshore basin, India. We have implemented the DFA algorithm by operating different windows varying in length 1.5 m to 30 m in sliding window method to determine the scaling exponents as a function of depth. The scaling exponents thus obtained were contoured to identify the depths to the tops of reservoir zones.

Introduction

Correct interpretation of geophysical well log data sets is essential to determine the spatial location of the hydrocarbon reservoir zones. Over the past few decades, advanced mathematical and signal processing techniques have been progressively developed to facilitate improved understanding of well log data for reservoir characterization. Chandrasekhar and Rao (2012 and references therein) used wavelet transformation to identify the depths to tops of reservoir zones. More recently, Hernandez et al (2013) employed detrended fluctuation analysis (DFA) for facies identification. It was Peng et al (1994), who first provided the required mathematical details for DFA technique, when they applied it to study DNA sequences. In the present work, we applied the DFA technique to gamma-ray log, sonic log and neutron log of data of three different wells, A, B and C, located in the western offshore basin of India, to delineate the depth to tops of the reservoir zones.

Methodology

Detrended Fluctuation Analysis (DFA) facilitates to study the intrinsic self-similarities in non-stationary signals, such as well-logs, by determining the scaling exponents in a modified least-square sense. Estimation of scaling exponents through DFA requires converting a signal, say, $x(t)$, to an unbounded process through integration, which unfolds the presence of long-range power law correlations in the signal. The integrated series generated from the signal is given by

$$y(m) = \sum_{i=1}^m [x(i) - \bar{x}]$$
 where \bar{x} is the mean of the signal and 'm' denotes the total number of data points. The obtained integrated series is then divided into p windows, each of length k , to determine

the average fluctuations corresponding to each window, as
$$F_k(p) = \sqrt{\frac{1}{k} \sum_{i=1+(p-1)}^{k+(p-1)} (y(i) - y_k(i))^2} \cdot y_k(i)$$

designates the 1st order least squares trend in each window. The thus obtained $F_k(p)$ and the window length, k , form a power law relationship, given by $F_k(p) \approx k^\gamma$. γ , defined as $\log F_k(p) / \log k$ represents the scaling exponent and is attributed to the centre of the window. Next, the window is shifted by one unit and the scaling exponent is again calculated. This exercise is repeated till the end of the data is reached. The end result of this sliding window method provides the scaling exponent values as a function of depth.

Various window lengths in the range of 1.5 m - 30 m with an increment of 0.75 m were used to calculate the scaling exponents. The increment in window sizes is chosen so as to have a better resolution of subsurface formation zones. Figure 1 shows a contour plot of scaling exponents determined for gamma-ray logs wells A, B and C as a function of window length k and depth. Since the entire operation of sliding window method carried out with various window sizes is analogous to

translation and dilation process in continuous wavelet transformation, it was possible to represent the obtained scaling exponents in the form of contour plot as shown in Fig. 1 for delineation of depths to the tops of subsurface formation zones with adequate resolution.

Results and Discussions

The main oil and gas reserves (pay zones) are L-I, L-II, L-III (limestone) and S-I (sandstone). The deepest and largest L-III pay zone is the most important of all the pay zones. L-I and S-I are gas reservoirs (see Chandrasekhar and Rao (2012) for more lithological details). Shales generally show high natural gamma-ray content compared to the limestones and sandstones. Accordingly, at the shale-limestone boundary and at the shale-sand boundary, the average fluctuations and thereby the scaling exponents corresponding to gamma-ray logs increases. As the sands in the study area are not clean, the depth location of S-I zone in well A is not quite discernible from gamma-ray log.

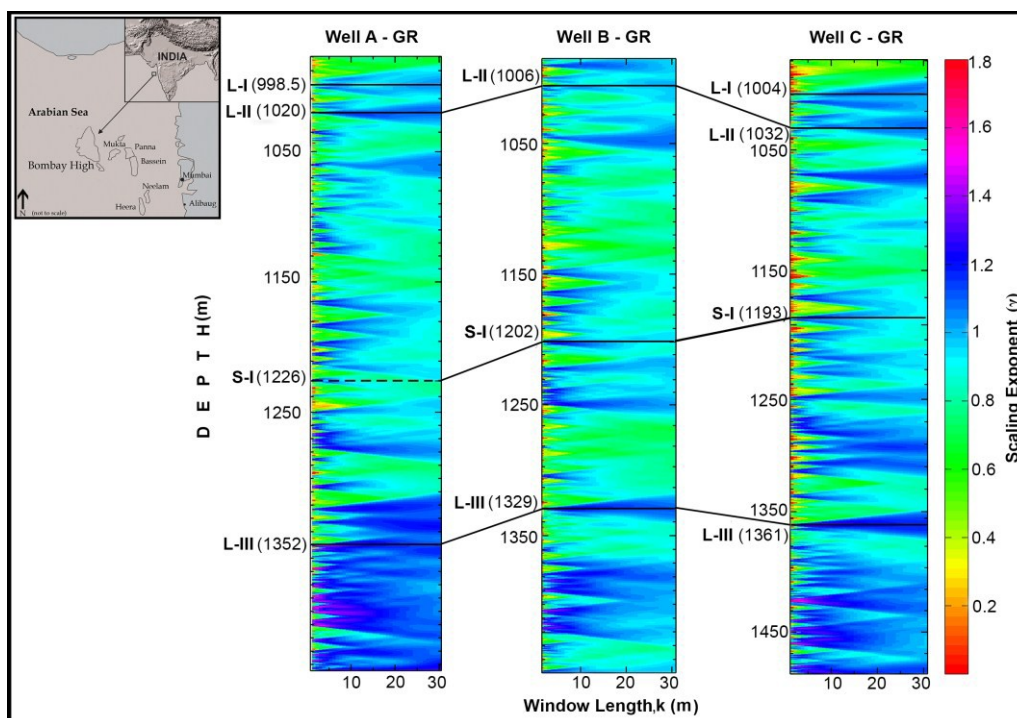


Figure 1 Contour plots of scaling exponents corresponding to gamma-ray logs of wells A, B and C of various window lengths depicted as a function of depth. Dashed line indicates the probable depth location of S-I as inferred from wavelet analysis results of Chandrasekhar and Rao (2012). Inset depicts the geographic location of the wells (indicated by arrow) in western offshore basin, India.

The depth locations of pay zones could also be clearly delineated in the contour plots of sonic (DT) and neutron logs (not shown here). In case of sonic (DT) logs, as the interval transit time is less in limestone and sand reservoirs compared to the shales, the scaling exponent values increase at these boundaries of lithological transition. In case of the neutron logs, the hydrogen index of the shales is higher than that of limestones and sandstone reservoirs due to the presence of bound-water in them. Accordingly, the scaling exponents are increased at these boundaries, clearly depicting the transition in the subsurface lithology.

Conclusions

DFA has been proved to be an efficient mathematical technique to delineate the subsurface reservoir boundaries in geophysical well log data, using scaling exponent as the diagnostic parameter. The results match well with those reported using wavelet analysis (Chandrasekhar and Rao, 2012).



References

- Chandrasekhar, E. and Rao, V. E. (2012) Wavelet analysis of geophysical well-log data of Bombay offshore basin, India. *Math. Geosci*, **44**, doi:10.1007/s11004-012-9423-4, 901–928.
- Hernandez-Martinez, E., Jorge X.Velasco-Hernandez, Teresa Perez-Muñoz and Jose Alvarez-Ramirez. (2013) A DFA approach in well-logs for the identification of facies associations. *Physica A*, **392**, <http://dx.doi.org/10.1016/j.physa.2013.07.052>, 6015-6024.
- Peng, C. K., Buldyrev, S. V., Simons, M., Stanley, H.E., and Goldberger, A. L. (1994) Mosaic organization of DNA nucleotides. *Phys. Rev. E*, **49**, 1685–1689.



Study of error propagation in NMR measurements' inversion

Tamás Lukács¹, Virág Darányi¹ and László Balázs¹

email: lukacs.tom@gmail.com

¹Department of Geophysics and Space Sciences, Eötvös Loránd University

Summary

Nuclear magnetic resonance (NMR) is a powerful tool in not only hydrocarbon exploration but subsurface water exploration. The results of such NMR measurements are very sensitive to the signal to noise ratio (SNR) since regularisation parameters used during the inversion process are highly dependent on SNR. The purpose of this study is to set up an estimation of the optimal regularisation parameters of the inversion, in order to provide the fittest, smoothest but still the optimal solution for the transversal relaxation time (T_2) distribution

Introduction

NMR is based on the fact that certain nuclei possess magnetic moment therefore interacting with external magnetic fields. In geophysics we use proton since it has the highest gyromagnetic ratio and it is very common. Hence the protons' atomic environments are very different in water and in hydrocarbons, in certain cases the fluidum characterization is also possible. In most cases geophysical NMR gives a reliable estimation of water content and T_2 distribution. The aim of inversion is to give a solution for the transversal relaxation time's distribution T_2 , which carries information about fluidum properties. Several formulae for permeability and hydraulic conductivity of fluids have been derived based on T_2 so it is a direct method to estimate the mentioned petrophysical attributes (Timur – Coates equation, SDR model, [1]).

Method

In our analyses we used synthetic data to simulate an ideal NMR experiment. We hid a double - peaked Gaussian T_2 distribution with realistic values (at 20 ms and 150 ms) into an exponential curve which stood for the ideal FID (Free Induction Decay) of the experiment. This was inverted with an iterative Gauss – Newton minimalisation method (as it is described in [2]). Hence this is an ill-posed problem we needed to use smoothing methods to stabilize the solution ([3]). All program codes were implemented and ran in MATLAB. After the basic situation we started to load the signal with Gaussian white noises with known amplitude to observe how the solutions answer to the noise. These investigations were conducted with various SNR levels, namely SNR= 1000, 100, 50, 15, 10 and 5 beside the noise-free basic situation.

An example can be seen in *Figure 1* and *Figure 2*. In this case the SNR was 15 (the calculated SNR was 15.12). The solution (red line) gave back the two-peaked distribution nicely, and the variance shows (blue dotted lines) how the curve is reliable at that certain point. The amplitudes are quite unreliable which indicates that the shape of the curvature is unreliable which has undesirable effects on derived parameters such as permeability ([1]).

Also the correlation matrices of the solutions were calculated and investigated. The strong diagonal elements show that the neighbour elements are in strong correlation because the

almost similar T2 values have almost equal amplitudes. The bell shape towards the higher elements indicates that the higher order terms are less reliable. The size and angle of the bell are important to compare the cases.

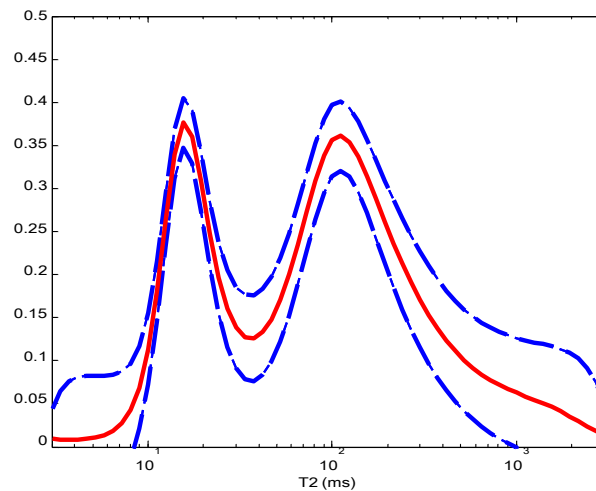


Figure 1 This is the T2 distribution of an inversion with SNR=15. The red line represents the T2 distribution from the inversion and the blue dotted line is the variance of the solution.

Also the correlation matrices of the solutions were calculated and investigated. The bell shape towards the higher elements indicates that the higher order terms are less reliable. The size and angle of the bell are important to compare the cases.

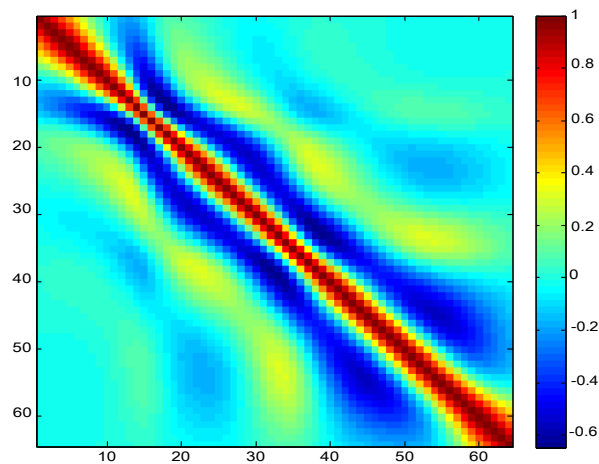


Figure 2 The correlation matrix of the T2 distribution from the inversion. The axes show the number of model parameters' elements respectively.

Conclusions

The SNR dependency of such measurements were investigated and the strong relation has been demonstrated. An empirical relation for SNR and regularisation parameters has been defined. Also for an exemplary derived parameter's variance has been calculated for each case.



References

- [1] Behroozmand, A. A., Keating, K., Auken E. (2014) A Review of the Principles and Applications of the NMR Technique for Near-Surface Characterization, *Surveys in Geophysics*, Volume 36, Issue 1, pp.27-85
- [2] Günther T., Rücker, C. (2006), A general approach for introducing information into inversion and examples from dc resistivity inversion, Ext. Abstract, EAGE Near Surface Geophysics Workshop. 4.-6.9.2006
- [3] Borgia, G. C., Brown, R. J. S., Fantazzini, P. (2000) Uniform-Penalty Inversion of Multiexponential Decay Data, *Journal of Magnetic Resonance*, **147**, pp 273-285.



Magnetotelluric inversion in the seismo-active West-Bohemia region

Radek Klanica^{1,2}, Josef Pek²

email: klanicar@natur.cuni.cz

¹Faculty of Science, Charles University in Prague

²Institute of Geophysics, Czech Academy of Sciences, Prague

Summary

West-Bohemia seismo-active region (Central Europe) can be characterized by earthquake swarms and high CO₂ flow of mantle origin. The periodically occurring earthquakes reach seismic magnitudes M_L of up to 5 and have hypocentres at depths from 5 to 25 km. One possible hypothesis is that the earthquakes are linked to fluids which can play a substantial role in their origin. Fluids (or paleofluids) are generally characterized by low resistivities and can be thus localized by geoelectric magnetotelluric measurements.

Introduction

Magnetotelluric method is an electromagnetic induction method with a large depth range, which can be increased simply by widening the spectrum range of the sounding periods. As a source of the induction in the Earth, magnetotellurics uses variations of the natural electromagnetic field. This passive source of the induction is the main advantage of the method because it makes it independent of the source-receiver distance, which is a limiting factor in methods of the applied geophysics. The shadow side of the method is that natural electromagnetic fields are relatively weak compared to the industrial electromagnetic noise, and a lot of problems with strong noise are typical of natural data processing in cultural areas.

Many authors proved that fluids are linked to earthquakes and their origin (Rawat, 2014; Gürer, 2007). Due to large depth of these fluids, magnetotellurics is the only geoelectric method, which has the potential of detecting them. Fluids always act as a high conductivity (low resistivity) zones, so I made an attempt to find them in the West-Bohemia seismo-active region.

Method

I used magnetotelluric data collected by the Institute of Geophysics in 2001. The data were obtained with three different sampling frequencies: 4096 Hz, 64 Hz and 2 Hz. 10 temporary magnetotelluric stations were set up in the area of interest. For noise reasons, the time series were measured mainly during nights. Once I processed data, I found a strong influence of cultural noise, especially for lower frequency data obtained with the sampling frequencies of 64 Hz or 2 Hz. High frequency data were relatively clean, so I hoped that the data inversion could bring some useful results for at least shallow depths.

I tried to collect as much information as possible about the geology of West-Bohemia before the inversion. The whole area is located in the Bohemian Massif, in the Saxothuringian unit. Most of the investigated area is covered by the Vogtland-Saxony Paleozoic Unit, which is built by cambrian-ordovician phyllites with various mineralogical composition. At some places, inclusions of quartzite or black shales are found (Chlupáč et al., 2011). The direction of the main faults in the area is N-S, and calculations of the regional electromagnetic strike prove it for most of the MT sites.

I carried out the inversion of the magnetotelluric data by employing the Reduced Basis Occam – REBOCC software (Siripunvaraporn & Egbert, 1999). The program can be used for a 2D inversion of magnetotelluric data, and is fast even for huge data sets, because of a really efficient implementation

of the forward problem. I calculated the inverse models for the TE and TM modes (transversal electric/magnetic) separately. Finally I calculated the TE+TM mode, which uses the impedances from both the NS and EW directions simultaneously.

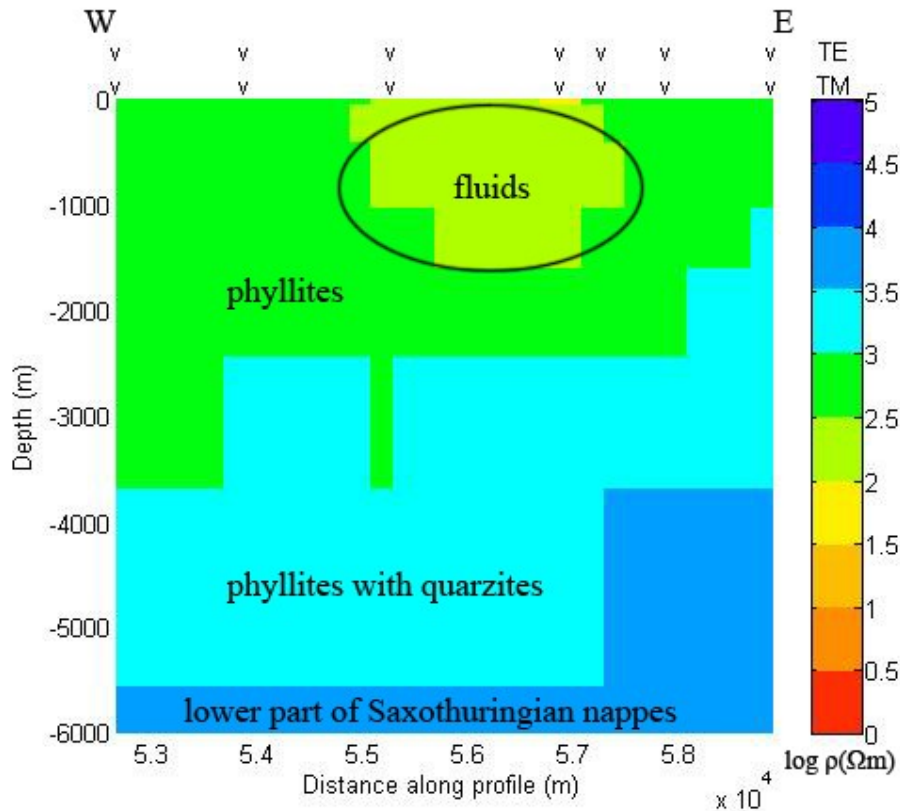


Figure 1 Result of a 2D inversion in TE+TM mode on a W-E profile. From the depth of 4-5 km, the data are strongly damaged by cultural noise and a link to the geology settings is unsure. A large relatively conductive zone can be caused by fluids, which has been already suggested by DiMauro et al.(1999).

Conclusion

From the results of TE+TM mode, a large low resistivity zone with resistivity between 100-300 Ωm can be seen. This is surprise since the metamorphic phyllites should have higher resistivities of the order of thousands of Ωm . The lower resistivity zone can be caused by fluids. Their direct relation to the earthquakes is, however, arguable because the earthquakes hypocenters are located at depths between 5 and 25 km. Thickness of phyllites is referred in geology literature from 3 to 4 km, gravity studies suggest that it can be 5 or 6 km. Due to the strongly damaged time series by the cultural noise, we can trust resistivity to a depth of about 4 km only. Below this depth, the interpreted resistivities are most likely due to the noise effects in the data, but they may also reflect some influence of the geology.



References

- Di Mauro, D., Volpi, G., Manzella, A., Zaja, A., Praticelli N., Červ, V., Pek, J. and De Santis A., 1999, Magnetotelluric investigations of the seismically active region of Northwest Bohemia: preliminary results, *Annali di Geofisica*, 42, 39-48.
- Gürer, A., Bayrak, M., 2007, Relation between electrical resistivity and earthquake generation in the crust of West Anatolia, Turkey, *Tectonophysics* 445, 49–65.
- Chlupáč, I., Brzobohatý, R., Kovanda, J., Stráník, Z., 2011, *Geologická minulost České republiky*, Praha-Academia, 436 s. ISBN 978-80-200-1961-5.
- Rawat, G., et al., 2014, Electrical resistivity cross-section across the Garhwal Himalaya: Proxy to fluid-seismicity linkage, *Tectonophysics* 637, 68-79.
- Siripunvaraporn, W., Egbert, G., 1999, *Reduced Basis Occam (REBOCC) Inversion Version 1.0 for Two-dimensional Magnetotelluric data*, College of Oceanic and Atmospheric sciences, Oregon state university.

OIL&GAS & SEISMICITY

WEDNESDAY, 15 July

Charimen: Jana Voroňáková, Seweryn Tlalka

1 0 : 1 5	Partial gas saturation effects on fracture-induced seismic anisotropy: A rock physics insight from experimental observations	Kelvin Amalokwu
1 0 : 3 0	AVO analysis of detecting submarine gas hydrate in lower Fangliao Basin, Taiwan	Welayaturromadhona, How Wei Chen
1 0 : 4 5	Geological controls on the gas hydrate system of Lower Fangliao canyon, offshore southwest Taiwan	Feisal Dirgantara, Andrew Tien-Shun Lin, Char-Shine Liu
1 1 : 0 0	Tuning experiments show that gas can be hidden, as well as revealed, in seismic data	Bonita Barrett-Crosdil
1 1 : 1 5	Distribution of petrophysical parameters in diverse types of pore space in the Main Dolomite marginal zone of the Wielkopolska platform	Pawel Wandycz
1 1 : 3 0	Comparison of marine CSEM data acquisition system by Occam inversion: analysis the effect of water depth	Zhenwei Guo, Hefeng Dong, Åge Kristensen
1 1 : 4 5	The use of seismic attributes for fault identification in the X field, Indonesia	Iqbal Fauzi Aditama



Partial gas saturation effects on fracture-induced seismic anisotropy: A rock physics insight from experimental observations

Kelvin Amalokwu¹
email: ka1c12@soton.ac.uk

¹ University of Southampton

Summary

Seismic wave propagation is known to be sensitive to the presence of aligned fractures (anisotropy) and to partial gas saturation but their combined effects are still poorly understood. Recent laboratory experimental studies have shown interesting frequency-dependent saturation effects on seismic anisotropy in rocks containing aligned fractures. Our experimental observations could be explained by combining a frequency-dependent fractured rock model and a frequency-dependent partial saturation model. Using the modelling approach adopted for explaining our experimental observations, we will present a numerical study showing possible effects of partial gas saturation on seismic anisotropy at seismic frequencies.

Introduction

Studies have shown that seismic waves are strongly affected by the presence of partial gas saturation and by the presence of aligned fractures, the latter causing seismic anisotropy. This sensitivity makes it possible (in theory) to obtain fracture and fluid information from seismic data. The combined effect of both is still poorly understood as little work has been done on partial saturation effects in fractured rocks. P-wave anisotropy and shear wave splitting (SWS) are commonly used methods for fractured rock characterisation (Crampin 1985, Lynn et al. 1996, Sayers and Rickett 1997). In anisotropic rocks fluid compressibility can affect shear wave propagation (Brown and Korringa 1975), causing fluid-dependent shear wave splitting. P-wave anisotropy in fractured rocks is also known to depend on saturating fluid (Bakulin, Grechka, and Tsvankin 2000). This fluid-dependent seismic anisotropy could be used as a diagnostic tool to infer the saturation properties of fractured reservoirs (e.g., Qian et al. 2007).

Fluid-dependent seismic anisotropy has been observed both in field data and laboratory experiments and has been shown to be frequency dependent due to wave induced fluid flow mechanisms. The presence of partial gas saturation is also known to affect elastic waves in a frequency-dependent way. Recent experimental results showed interesting water saturation (S_w) effects on SWS at oblique angles and P-wave anisotropy (Amalokwu et al. 2015). These effects could be explained by combining a frequency-dependent partial saturation model and a frequency-dependent fractured rock model.

Using the modelling approach we adopted for explaining the experimental data, we present a numerical study showing possible effects of partial gas saturation on seismic anisotropy at seismic frequencies.

Method and results

There is a lack of suitable frequency-dependent theoretical models for elastic wave velocities in partially saturated fractured rocks. Using the same method as Amalokwu et al. (2015) we combine two models to give some insight into the possible mechanisms in our experiments. We combine the fractured rock model of Chapman (2003) and the partial saturation model of White (1975). The stiffness tensor, C_{ijkl} , given by Chapman (2003) relating the contributions from the isotropic elastic tensor (C^0 , with Lamé parameters, λ and μ), C^1 (pores), C^2 (microcracks) and C^3 (fractures) scaled by the porosity (Φ_p), microcrack density (ϵ_c) and fracture density (ϵ_f) is of the form:

$$C_{ijkl} = C_{ijkl}^o - \Phi_p C_{ijkl}^1 - \varepsilon_c C_{ijkl}^2 - \varepsilon_f C_{ijkl}^3 \quad (1)$$

This model is not designed for partial saturation, so in the elastic tensors, we replace all terms apart from the fracture correction, with the Lamé parameters λ^o and μ^o obtained from the model of White (1975) for each water saturation value. The Lamé parameters λ^o and μ^o from White's model already contain porosity effects, and as shown by Chapman et al. (2003), ε_c can be set to zero in high porosity rocks which would make the contribution from C^2 zero. We now have an equation of the form:

$$C_{ijkl} = C_{ijkl}^{iso}(\lambda^o, \mu^o) - \varepsilon_f C_{ijkl}^3; \quad (2)$$

where the term C_{ijkl}^{iso} is obtained from the Lamé parameters λ^o and μ^o calculated using the model of White (1975), after which the fracture correction C^3 from the model of Chapman et al. (2003) is applied.

Figure 1a shows the modelling result for the isotropic response to partial saturation at different frequencies calculated using White's model and Figure 1b shows the results for the P-wave anisotropic parameter after applying a fracture correction. The modelling results were calculated using blank rock properties from Amalokwu et al. (2015) as input for White's model (with a gas patch radius of 2 cm), with vertically aligned fractures (causing HTI symmetry) with an aspect ratio of 0.01 and a fracture density of 7%. We will present results showing the effects of partial gas saturation on the anisotropic parameters ε , γ , and δ (see Thomsen 1986), SWS at oblique angles and we will also repeat the analysis of Rüger and Tsvankin (1997) to see how the P-wave reflectivity responds.

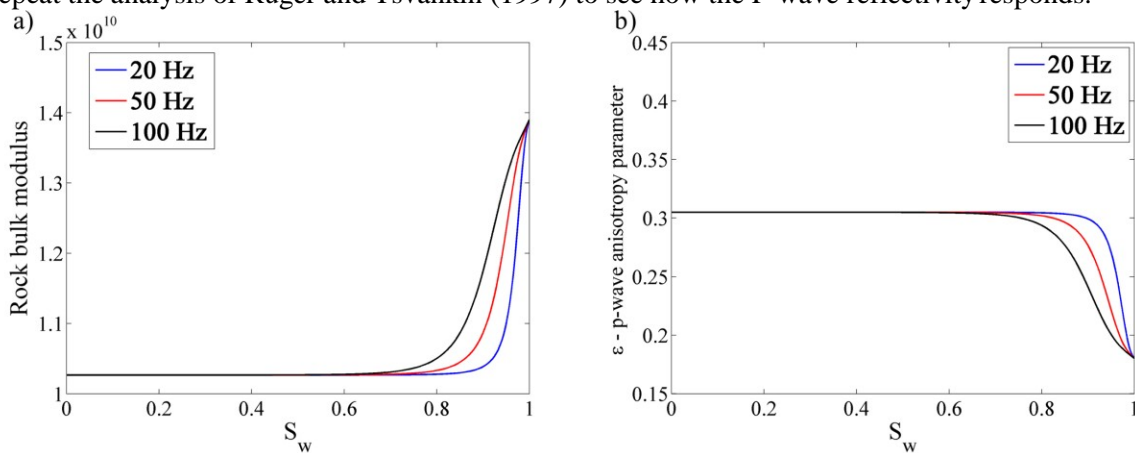


Figure 1. a) Bulk modulus versus water saturation (S_w) using White's model b) P-wave anisotropy parameter versus S_w after applying fracture correction to Figure 1a.

Conclusions

A numerical study of partial gas saturation effects on fracture-induced seismic anisotropy at seismic frequencies is presented using a modelling approach that was used to gain insight into novel experimental observations. The results show partial gas saturation could have a frequency-dependent effect on seismic anisotropy which could potentially be exploited for improved characterisation of fractured reservoirs containing gas.

Acknowledgements

We wish to thank the sponsors of the BGS Edinburgh Anisotropy Project for supporting this work which forms part of the PhD studies of Kelvin Amalokwu under a NERC-NOC-BGS PhD studentship.



References

- Amalokwu, K., M. Chapman, A. I. Best, J. Sothcott, T. A. Minshall, and X.-Y. Li. 2015, Experimental observation of water saturation effects on shear wave splitting in synthetic rock with fractures aligned at oblique angles. *Geophysical Journal International*, **200**, no. 1,17-24. doi: 10.1093/gji/ggu368.
- Bakulin, A., V. Grechka, and I. Tsvankin. 2000, Estimation of fracture parameters from reflection seismic data—Part I: HTI model due to a single fracture set. *Geophysics*, **65**, no. 6, 1788-1802. doi: 10.1190/1.1444863.
- Brown, R., and J. Korrinda. 1975, On The Dependence Of The Elastic Properties Of A Porous Rock On The Compressibility Of The Pore Fluid. *GEOPHYSICS*, **40**, no. 4, 608-616. doi: doi:10.1190/1.1440551.
- Chapman, M., S. Maultzsch, E. Liu, and X.-Y. Li. 2003, The effect of fluid saturation in an anisotropic multi-scale equant porosity model. *Journal of Applied Geophysics*, **54**, no. 3–4,191-202. doi: <http://dx.doi.org/10.1016/j.jappgeo.2003.01.003>.
- Crampin, S. 1985, Evaluation of anisotropy by shear-wave splitting. *GEOPHYSICS*, **50**, no. 1,142-152. doi: doi:10.1190/1.1441824.
- Lynn, H. B., K. M. Simon, C. R. Bates, and R. V. Dok. 1996, Azimuthal anisotropy in P-wave 3-D (multiazimuth) data. *The Leading Edge*, **15**, no. 8,923-928. doi: doi:10.1190/1.1437392. doi:10.1190/1.1437392.
- Qian, Z., M. Chapman, X. Li, H. Dai, E. Liu, Y. Zhang, and Y. Wang. 2007, Use of multicomponent seismic data for oil-water discrimination in fractured reservoirs. *The Leading Edge*, **26**, no. 9,1176-1184. doi: doi:10.1190/1.2780789.
- Rüger, A., and I. Tsvankin. 1997, Using AVO for fracture detection: Analytic basis and practical solutions. *The Leading Edge*, **16**, no. 10,1429-1434. doi:10.1190/1.1437466.
- Sayers, C. M., and J. E. Rickett. 1997, Azimuthal variation in AVO response for fractured gas sands. *Geophysical Prospecting*, **45**, no. 1,165-182. doi: 10.1046/j.1365-2478.1997.3180238.x.
- Thomsen, L. 1986, Weak elastic anisotropy. *Geophysics* **51**,1954-1966.
- White, J. E. 1975, Computed seismic speeds and attenuation in rocks with partial gas saturation. *Geophysics*, **40**, no. 2,224-232. doi: 10.1190/1.1440520.



AVO analysis of detecting submarine gas hydrate in lower Fangliao Basin, Taiwan

Welayaturromadhona, How Wei Chen

email: wela_wel@yahoo.com

Institute of Geophysics, National Central University

Summary

Amplitude versus offset (AVO) analysis provides an accurate method to identify gas hydrate and possible occurrence mechanism. A bottom simulating reflector (BSR) which sub-parallel to the seafloor topography with reverse polarity compare to sea-floor reflection is a helpful hint to identify the presence of gas hydrate. Preliminary studies indicate that BSR responses show a Class III AVO effect. AVO analysis is performed on reflection event around TWT 2250 mili-second can be observed with indication of gas supply from below show distinct AVO anomaly. The AVO anomalies were identified from both gradient analysis and intercept and gradient cross-plot and also from AVO attributes. The gradient curve shows Class III AVO response indicating the free gas beneath a high velocity layer, in this case, gas hydrate.

Introduction

An AVO analysis can be used to locate gas hydrates. The existence of gas hydrate in lower Fangliao Basin can be confirmed by AVO analysis. AVO refers to the dependency of the seismic amplitude with the distance between the reflection coefficient and the angle of incidence. Areal distribution of hydrate can be easily identified through AVO attributes. Amplitude preserved seismic data processing with compensation of geometrical spreading loss were required and to avoid artificial influence on the waveform. The study area is located in the lower Fangliao Basin (Figure 1). The AVO analysis is based on the seismic reflection studies for MCS937-10 data. The acquisition system included a 84-channel with 447 shots. The number of channels we the shot interval and the channel interval were 25 m and 12.5 m, respectively. The record length used was 6 s and sampling rate was 1 ms.

Method and Theory

Gas hydrates are crystalline solid that form from low molecular weight gases (usually methane) and water under conditions of low temperature, high pressure, and gas saturation (Sloan, 1990). The presence of natural submarine gas hydrates is commonly inferred from the widespread occurrence of a strong seismic Bottom-Simulating Reflector (BSR) at depths corresponding approximately to the base of methane hydrate stability field which is the most widely used indicator of the presence of gas hydrate accumulations beneath the seabed (Kvenvolden and Barnard, 1983).

The main thing that is needed to the seismic processing are both seismic amplitude preservation and detailed velocity analysis. The processing sequences included spherical divergence correction, bandpass filtering, detailed velocity analysis, normal moveout correction and CDP stacking. The pre-stacked data has been used in order to preserve the true reflection amplitude for AVO analysis. The seismic velocity analysis was performed by using semblance and velocity panel in order to get an accurate seismic velocity information. Detailed velocity analysis were made for every 20 CDP and also AGC (automatic gain control) was applied before velocity analysis which is useful for identifying and picking velocity values of the weak reflectors. Gas hydrates were identified along survey lines. The conclusive results indicating the BSR were found which vary in depths from 0.4 to 0.5 s beneath the seafloor. This depths closely approximate the base of the methane hydrate stability field. The seafloor multiple appears 2 s below the seabed.

Results and Discussions

The gradient curve shows the Class III AVO response which is indicated by negative amplitude and it increase negatively with increasing offset, indicative of free gas beneath a high velocity layer, in this case, gas hydrate. The AVO graph response is displayed in the form of the curve which will provide the relationship between changes in the reflected signal amplitude with offset. The AVO curve shows the behavior of the reflected signal amplitude to the offset by Aki & Richard approximations. The AVO graph response is actually conducted in CDP 774 and TWT 2250 ms where there is a strong indicator for the presence of BSR due to an AVO anomaly. The result of multiplying between intercept (A) with gradient (B) can be used to observe the appearance of AVO anomaly. An increase in amplitude of the offset indicated in positive AVO response. Pseudo poisson ratio is the sum of intercept (A) and gradient (B). The positive value indicates a high pseudo poisson ration value, which indicates the presence of gas prospects. Normal incidence reflectivity or intercept is the reflection coefficient at zero offset, while the gradient is a variation of the amplitude of the offset. Crossplot between normal incident reflectivity (intercept) on X-axis and gradient on Y-axis is used to determine the classification based on Rutherford and William (1989). This classification is likely showing the indication that gas sand are beyond the background trend in the form of ellipse. By creating crossplot between intercept and gradient around CDP 774, indicates the Class III AVO response.

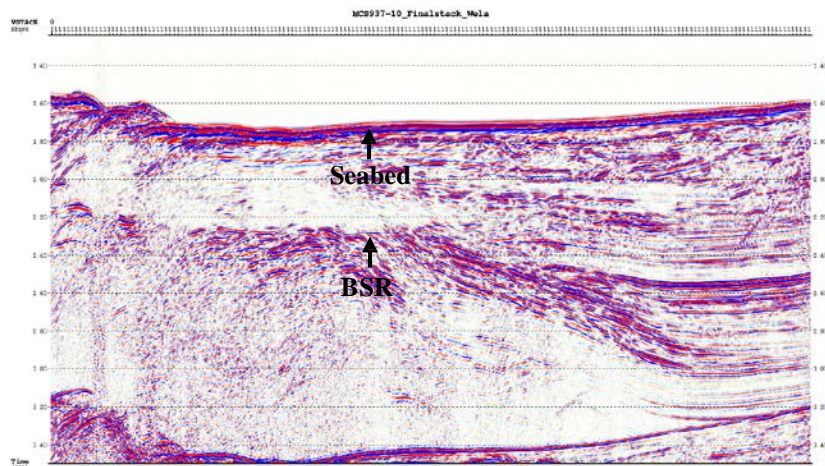


Figure 1 Processed, interpreted two-way travel time seismic section MCS937-10 showing the BSR associated with the bottom of the hydrate stability zone (HSZ)

Conclusions

In conclusion, it is demonstrated that the location of the BSR associated with the bottom of the hydrate stability zone can be located at lower Fangliao Basin using an AVO analysis method. Based on the results, the appearance of AVO anomaly can be identified in CDP 774, TWT 2250 ms. The product of $A*B$ and pseudo poisson ratio $A+B$ shows positive value that indicates the presence of free gas. The AVO anomaly in the target zone has been classified as Class III anomaly with negative amplitude and will be increasingly negative by increasing offset. Crossplot of intercept versus gradient shows marked separation of anomalous points from background trend which has been identified as Class III AVO anomaly based on Rutherford & William classification.

Acknowledgments

The authors are really thankful to National Science Council of Taiwan and National Taiwan University for providing the data and also all members of Computational Seismology and Visualization Research Group NCU for assistance in order to accomplish this study as well as the guidance or encouragement.



References

- Kvenvolden, K.A. and Barnard, L.A., 1983. Hydrates of Natural Gas in Continental Margins. In: J.R. Watkins and C.L. Drake (Editors), *Studies of Continental Margin Geology*. AAPG Mem., 34:631-640
- Rutherford, S., and Williams, R., 1989. Amplitude versus offset variation in gas sands. *Geophysics* 54, 680-688
- Sloan, E. D., Jr., 1990. *Clathrate Hydrates of Natural Gases*, 641 pp., Marcel Dekker, New York.



Geological controls on the gas hydrate system of Lower Fangliao canyon, offshore southwest Taiwan

Feisal Dirgantara^{1,2}, Andrew Tien-Shun Lin¹, Char-Shine Liu³
email: fdirgant@gmail.com

¹ Institute of Geophysics, National Central University, Zhongli, Taiwan, ROC

² TIGP – Earth System Science Program, Academia Sinica, Nangang, Taiwan, ROC

³ Institute of Oceanography, National Taiwan University, Taipei, Taiwan, ROC

Summary

The geologic setting of Lower Fangliao canyon offshore southwest Taiwan exerts specific controls on the formation of bottom-simulating reflectors (BSRs) and the inferred shallow distribution of gas hydrates. Six distinct seismic facies, which include convergent-symmetrical, convergent-baselapping, chaotic, parallel-draping, convergent-conformable, and free-reflection facies, have been recognized in the area. These facies are interaction consequences of mud diapirism, sedimentary dispersal, and regional convergent tectonics and their influences to gas hydrate system. The gas hydrate zonation is characterized by (1) high amplitude reflections with the similar phase of seafloor indicating possible porous turbidite sands reservoir in the gas hydrate stability zone (GHSZ); (2) polarity reversal of BSRs suggests negative reflection coefficient with higher impedance gas hydrate accumulated sands overlays lower impedance free-gas accumulated sand; (3) those strong reflections usually locate at migration pathways for gas-bearing fluids; and (4) strong reflections on the side of mud diapirs (e.g flank drags) and above buried mud diapir indicate presence of gas hydrate. Vertical venting governed by mud tectonics is the key to induce biogenic and/or thermogenic gas seepages, which later will be accumulated and trapped as gas hydrate.

Introduction

Gas hydrate is a naturally occurring frozen compound formed when water and gas combine at high pressure and relatively low temperature conditions. For decades, gas hydrates have been discussed as a potential resource, particularly for countries with limited access to conventional hydrocarbons or a strategic interest in establishing alternative, unconventional gas reserves.

Widely distributed BSRs have been observed in the area offshore of southwestern Taiwan where the active accretionary complex meets with the passive China continental margin (Chi et al. 1998), such as in Lower Fangliao canyon. Central Geological Survey of Taiwan has proposed the canyon as one of gas hydrate drilling prospects. Understanding the gas hydrate system within the vicinity is essential towards successful drilling campaign. This study is a part of larger geological and geophysical investigations aiming at a full assessment of gas hydrate potentials as possible future energy source. Results of study are then incorporated within larger geological and geophysical frameworks, thereby contributing to a better understanding of gas hydrates potential off southwest Taiwan.

Method

Gas hydrate play-types in Lower Fangliao canyon is associated with gas seepages related to mud tectonics in upper continental slope of Taiwan orogenic wedge. Multi-channel seismic reflection profile (MCS-937) used in this study was processed at the Institute of Oceanography, National Taiwan University under standard seismic data processing procedure. Seismic facies analysis, which has been widely used to study basin evolution and depositional processes in slope basin environments (Weimer et al., 1998; Brown et al., 2004), was applied to final time-domain stacked seismic section.

Results

Gas hydrate system in Lower Fangliao canyon (Fig. 1) is characterized by (1) high amplitude reflections with the similar phase of seafloor indicating possible porous turbidite sands reservoir in the gas hydrate stability zone; (2) polarity reversal of BSRs suggests negative reflection coefficient with higher impedance gas hydrate accumulated sands overlays lower impedance free-gas accumulated sand; (3) those strong reflections usually locate at migration pathways for gas-bearing fluids; and (4) strong reflections on the side of mud diapirs (e.g flank drags) and above buried mud diapir indicate presence of gas hydrate. There are six distinguishable seismic facies, which reflect the combined influence of mud diapirism, sedimentary dispersal, and regional convergent tectonics in intraslope basin as convergent-symmetrical, convergent-baselapping, chaotic, parallel-draping, convergent-conformable, and free-reflection facies. Biogenic and/or thermogenic gas seepages are facilitated by mud tectonics.

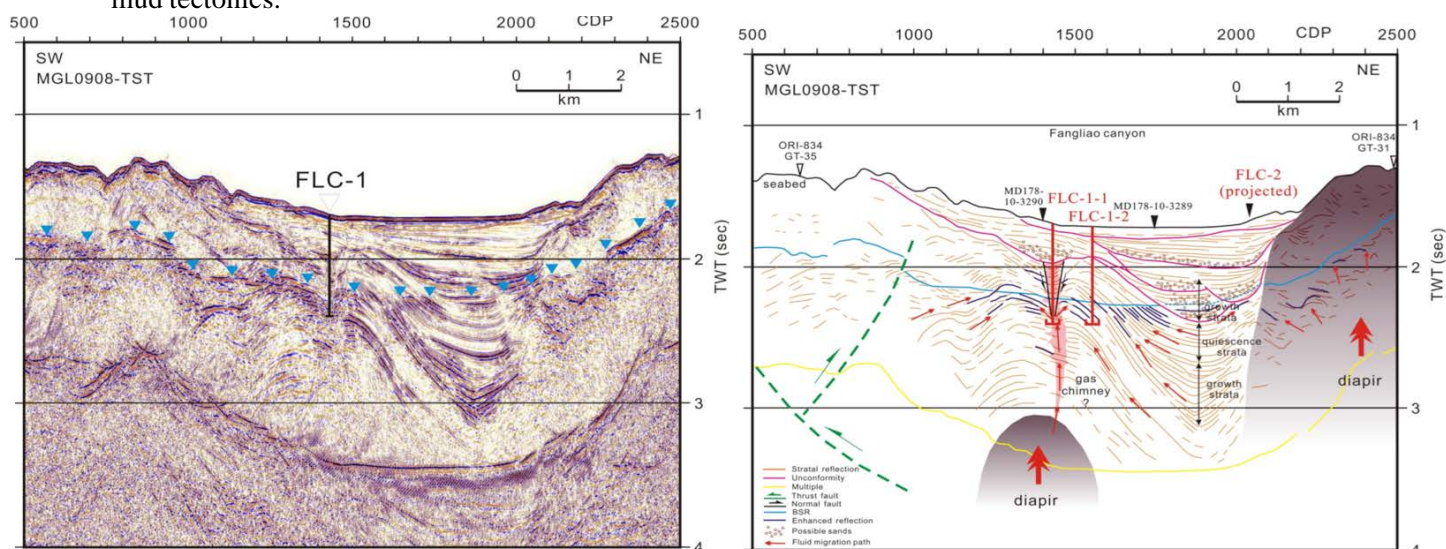


Figure 1. Gas hydrate system example in Lower Fangliao canyon based on seismic section (left) and interpreted section (right). Buried mud diapiric anticline governs the migration pathways for both biogenic and thermogenic gas seepage. Strong reflection above buried anticline is a local gauge of authigenic carbonate, an indication of gas seepage. Growth strata are sedimentary deposition related to syn-intrusion of mud. Quiescence strata are sedimentary deposition related to post-intrusion of mud. Targeted drilling prospects are shown as FLC-1-1 and FLC-1-2. Details of symbols are shown in legend.

Conclusions

The intraslope basin of Lower Fangliao canyon is a result of interaction among mud diapirism, sedimentary dispersal, and regional convergent tectonics. This is shown by six perceptible seismic facies as convergent-symmetrical, convergent-baselapping, chaotic, parallel-draping, convergent-conformable, and free-reflection facies. Within the environs, gas hydrate system is likely controlled by mud tectonics, which promotes the migration of biogenic and/or thermogenic gas leakage, thus accumulated and trapped as gas hydrate at shallower depth.

Acknowledgements

The authors would like to acknowledge the great help and discussion from members of Basin Research Group, Institute of Geophysics, National Central University. Seismic sections are provided by Prof. Char-Shine Liu from Institute of Oceanography, National Taiwan University. We wish to thank SEG Travel Grant for sponsoring author's accommodation and lodging during convention.



References

Brown Jr., L.F., Loucks, R.G., Trevino, R.H., Hammes, U. (2004). Understanding growth-faulted, intraslope subbasins by applying sequence-stratigraphic principles: examples from the south Texas Oligocene Frio formation. *AAPG Bulletin* 88, 1501–1523.

Chi, W.C., Reed, D.L., Liu, C.S., Lundberg, N. (1998). Distribution of the bottom-simulating reflector in the offshore Taiwan collision zone. *Terrestrial, Atmospheric and Oceanic Sciences* 9, 779–794.

Weimer, P., Varnai, P., Budhijanto, F.M., Acosta, Z.M., Martinez, R.E., Navarro, A.F., Rowan, M.G., McBride, B.C., Villamil, T., Arango, C. (1998). Sequence stratigraphy of Pliocene and Pleistocene turbidite systems, northern Green Canyon and Ewing Bank (offshore Louisiana), northern Gulf of Mexico. *AAPG Bulletin* 82, 918.



Tuning experiments show that gas can be hidden, as well as revealed, in seismic data

Bonita Barrett-Crosdil¹, Dr. Dei Huws
email: bonitabarrettcrosdil@gmail.com
¹Bangor University

Summary

False positive and false negative gas signatures pose a serious problem to seismic interpreters as the implications of drilling into a gas pocket can be disastrous. We demonstrate with the use of normal incidence synthetic seismograms that tuning can produce “gas-like” signatures without gas (false positives) at bed thicknesses other than the regularly-quoted ‘tuning thickness’ of $\frac{1}{4} \lambda$. Furthermore, gas signatures can be hidden (false negative) at $\frac{1}{4} \lambda$; even at high gas saturation. There is a requirement for better discrimination between true and false signatures in industry and this study highlights the importance for further research in this area.

Introduction

Shallow gas is widely distributed in shallow marine sediments throughout the world and represents a significant engineering hazard, particularly in shallow drilling activity. Fortuitously, gas is often apparent on normal incidence seismic data in the form of amplitude and phase anomalies, making it possible for hazard risk maps to be drawn-up and mitigation strategies to be adopted. However, it is known that the attribution of such anomalies to shallow gas can be ambiguous. Anomalies are said to represent *false positive* gas signatures in cases where gas is apparently evident on the seismic record but is not encountered during drilling. This potentially leads to extensive and costly well deviations. Less common, but more significant, are *false negative* gas signatures - whereby gas is not evident on the seismic data, but *is* encountered during drilling. It is clear that there is a strong requirement in industry to be able to discern between true and false gas signatures.

To make the shallow gas interpretation more robust, Amplitude-Versus-Offset methods may be applied (which were previously developed for reservoir analysis). However, this approach requires multichannel seismic data with the required offset. In engineering site investigation studies of the shallow section, this is often not the case. Yet there have been recent cases of shallow gas being encountered even during relatively shallow geotechnical drilling. For such site investigation, interpretation of seismic reflector amplitude and phase for normal incidence energy is still the prime means of assessing the presence of shallow gas; and the problem of false positive and false negative responses is an ambiguity that relies heavily on experience and geological knowledge to ameliorate.

This study uses a synthetic seismogram approach where seismic unit data are input in primitive form (porosity, grain mineralogy, pore fluid composition etc.) so as to produce model reflection series. The properties / thicknesses of the seismic units are varied in order to investigate the circumstances under which false gas signatures may be produced. In this way, the *tuning* phenomenon is tested; a feature commonplace in the North Sea, where thin sediment beds and anomalies litter the shallow section. In the tests, bed thickness is thought of in terms relative to the insonifying wavelength. In the literature, $\frac{1}{4}$ -wavelength (λ) is often quoted as the ‘tuning thickness’ whereby there is maximum construction of a signal (Widdes, 1973; Chung & Lawton, 1990). Construction is known to induce gassy signatures; however, we hypothesise that certain ground models could induce a gassy signature at bed thicknesses of other than $\frac{1}{4} \lambda$, and that a gas signature can also be hidden by the effect of tuning.

Method

The model takes the primitive layer data and uses Gassmann’s rock physics equations (1951) to predict p-wave velocity. The Gassmann approach assumes that the transmitting medium comprises three components: the frame, matrix (grains) and pore space. The output acoustic impedances are applied to the Zoeppritz (1919) normal incidence solution to generate a reflection series that is subsequently

convolved with a 60Hz Ricker wavelet. Transmission losses are incorporated, since these are critical in determining response (even in processed field data). No noise, incoherent or coherent, is introduced into the data and so the various noise-reducing data-processing functions are also omitted. This way we could ensure that any anomaly present was purely a lithological effect and not a processing artifact. The model was validated against real commercial data from the Peon gas field, North Sea.

Results

Taking a non-gassy ground model of alternating sand and clay, the bed thickness was reduced from 1λ to $1/8\lambda$. The regularly-quoted ‘tuning thickness’ was supported, whereby a gassy signature was induced at $1/4\lambda$. It was found that the false positive gas signature could also be induced at $1/2\lambda$ when the porosity of the sand and the clay is set to extreme values (60% and 20% respectively). However, when gas was introduced into the model, the signal is no longer enhanced at $1/4\lambda$; instead it is completely hidden and a false negative gas signature is produced. When gas was introduced into peat layers, replacing the clay, the gas signatures are again hidden, but this time at $1/8\lambda$ instead of $1/4\lambda$. Various gas saturations were tested in these ground models, and all were hidden with tuning at $1/4\lambda$. In reality, $1/4\lambda$ could represent a sediment layer that is several metres thick and from seismic data, it is not possible to determine the volume or pressure of the gas that could be present. A wedge model that shows the hiding of gas from $1/4\lambda$ to $1/6\lambda$ is presented in *Figure 1*.

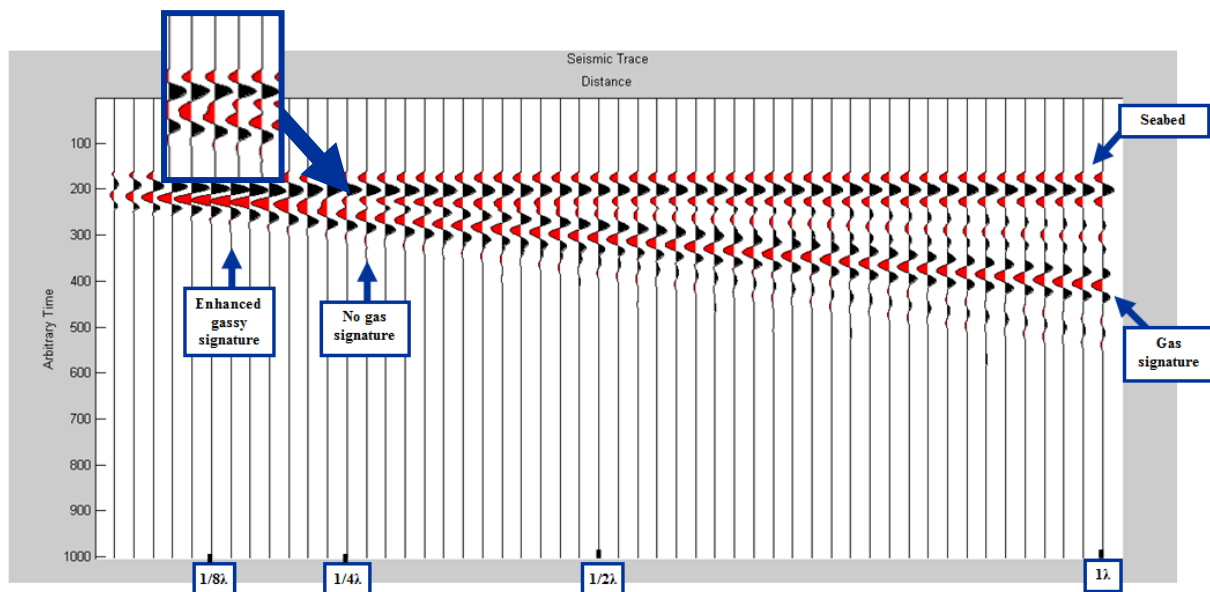


Figure 1. In the form of a wedge model, the bed thickness of a ground model of alternating sand and clay with gas in the third layer is reduced from 1λ to $\sim 1/24\lambda$ from right to left.

Conclusions

The ease of inducing both false positive and false negative gas signatures in different ground models at unexpected bed thicknesses has been shown. Shallow site investigation depends on semi-quantitative risk analysis based on amplitude and phase response; these results provide a clear illustration of the potential pitfalls in such an approach. This work comes in advance of the review of tuning research by SEG to be published August 2015 (Zeng & Marfurt, *unpubl. (2015)*).

Acknowledgements

The author would like to thank Statoil (Dag Lundqvist) for their support, advice and provision of data.



References

- Chung, H., & Lawton, D. (1990). Some properties of thin beds. CREWES Research Report.
- Gassmann, F. (1951). Über die elastizität poröser medien. Vierteljahrsschrift der Naturforschenden Gesellschaft in Zurich, **96**, 1–23.
- Widess, M.B. (1973). How Thin is a Thin Bed? *Geophysics*, **38**, 1176-1180.
- Zoeppritz, K. (1919). Erdbebenwellen VII. VIIb. Über Reflexion und Durchgang seismischer Wellen durch Unstetigkeitsflächen. Nachrichten von der Königlichen Gesellschaft der Wissenschaften zu Göttingen, Mathematisch-physikalische Klasse, 66-84.



Distribution of petrophysical parameters in diverse types of pore space in the Main Dolomite marginal zone of the Wielkopolska platform

Paweł Wandycz, Grażyna Semyrka, Roman Semyrka
email: pawel.wandycz@gmail.com

AGH-University of Science and Technology, Faculty of Geology, Geophysics and Environmental Protection, Department of Fossil Fuels

Summary

Three types porosity were recognized within the main dolomite unit in south-western part of Polish Lowland: intergranular porosity (I), fracture porosity (II) and intergranular/fracture porosity - dual porosity (III) (Semyrka et.al.,2008). Petrophysical parameters that play major role in accumulation and migration of hydrocarbons differ in each recognized porous space type (Semyrka et.al, 2014). The best reservoir parameters are found in the rock samples with intergranular type or porous space.

Introduction

From the of point of view of the hydrocarbon prospection, it is very important to precisely describe petrophysical parameters of the reservoir rocks within different types of the porous space. Petrophysical parameters that are responsible for the migration and accumulation of hydrocarbons might differ much within different types of porous space (Levorsen, 1972). The aim of the study is both quantitative and qualitative analysis of the petrophysical parameters of the recognized types of porous space in the main dolomite unit in the south- western part of Polish Lowland. In the studied area main dolomite sediments are reservoir rocks both for oil and gas accumulation. Sedimentation of this unit took place in two major depositional environments: carbonate platform , and the slope of the carbonate platform. Within these zones sediments of the main dolomite are recognized as boundstones, mudstones and grainstones (Słowakiewicz, Mikołajewski, 2011).

Method and/or Theory

Research was conducted on the 85 rock samples with usage of the mercury porosimeter. It allowed authors to describe petrophysical parameters such as: effective porosity - k_e (%), bulk density ρ_o (g/cm^3), matrix density - ρ_s (g/cm^3), average capillary - Φ (μm) and specific surface area - S (m^2/g). The quantitative analysis of the capillary pressure curve allowed authors to distinguish genetic types of the porous space that are present in the main dolomite sediments. Three major types of porosity were recognized: intergranular porosity (I) (fig. 1), fracture porosity (II) and intergranular/fracture porosity - dual porosity (III) (Semyrka et. Al., 2008).

In the intergranular type of pore space we observe higher capacity of the rock for accumulation of the hydrocarbons, but due to high specific surface area the fluid flow is limited. Rocks with fracture porous type usually have smaller effective porosity, so they how small capacity for accumulation, but due to a very low specific surface area, we observe better conditions for fluid flow (Semyrka, 2013a).

Conclusions

Within both recognized depositional zones the intergranular/fracture (III) porous type is dominant, it was recognized in 55% of all rock samples. Intergranular (I) and fracture (II) porous type were recognized in 26% and 19% of the rock samples respectively. The best parameters for accumulation

of hydrocarbons are observed within the rocks with intergranular (I) type of porous space with average effective porosity $k_{ef} = 9.06\%$, But very high average value of specific surface area ($S = 0.87 \text{ m}^2/\text{g}$) shows that the conditions for fluid flow are limited. The least resistance for fluid flow was observed in intergranular/fractured type of porous space, where the specific surface area is very low ($S = 0.20 \text{ m}^2/\text{g}$).

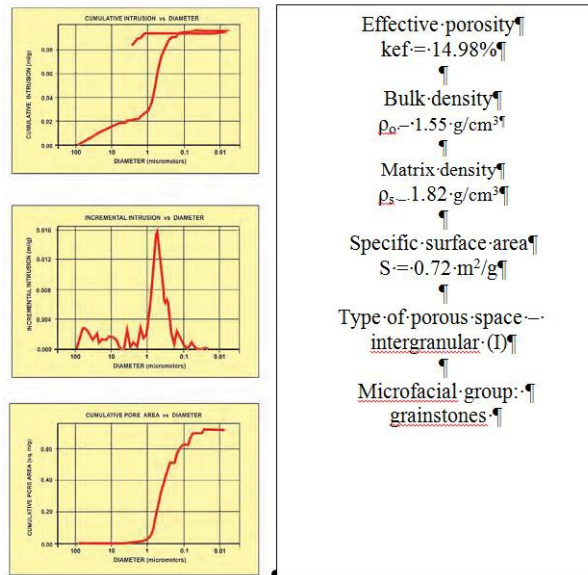


Figure 1 The results of the analysis with usage of mercury porosimeter for rock sample from well Leszczyny – 1, at depth 3239.95m – type of porous space (I).

Acknowledgements (Optional)

The presented results come from the research project founded by National Center for Science (NCN), titled “Znaczenie procesu stylolityzacji dla ropogazonośći utworów węglanowych dolomitu głównego.” ODW – 0601/B/P01/2011/40 (AGH nr 18. 18. 140. 083) led by dr. inż Grażyna Semyrka



References

Semyrka G., Semyrka R., Wandycz P., 2014 Rozkład parametrów petrofizycznych w zróżnicowanych typach przestrzeni porowej dolomitu głównego brzeżnej strefy platformy wielkopolskiej Wiadomości Naftowe i Gazownicze 7, 9-13

Semyrka R., 2013 (a) – Jakościowa i ilościowa charakterystyka petrofizyczna subfacji dolomitu głównego w strefach paleogeograficznych, Gospodarka Surowcami Mineralnymi.

Semyrka R., Semyrka G., Zych I., 2008 – Zmienność parametrów petrofizycznych subfacji dolomitu głównego zachodniej strefy półwyspu Grotowa w świetle badań porozymetrycznych, Kwartalnik AGH, Geologia 2008, t. 34. z. 3, Kraków, 445 - 468.

Słowakiewicz M., Mikołajewski Z. (2009). Sequence stratigraphy of the Upper Permian Zechstein Main Dolomite carbonates in Western Poland: a new approach. Jour. Petrol. Geology, 32: 215-234

Comparison of marine CSEM data acquisition system by Occam inversion: analysis the effect of water depth

Zhenwei Guo*; Hefeng Dong; Åge Kristensen
Zhenwei.guo@ntnu.no

¹ Norwegian University of Science and Technology, Norway

Summary

Recently, there has been a rapid development of the marine controlled source electromagnetic (CSEM) method for hydrocarbon exploration. The purpose of this study is to compare SeaBed Logging (SBL) and towed streamer EM on water depth effect by a number of simple inversion cases. In this paper, we compare these two data acquisition methods in both deep and shallow water environment by employing Occam's inversion method. As a results, SBL data acquisition system has an advantage in deep water, by contrast, towed streamer EM system has an irreplaceable excellent resolution and dense data.

Introduction

During the past ten years, there has been a rapid development of the marine controlled source electromagnetic (CSEM) method for hydrocarbon exploration. The EM field propagates through the water layer and into the subsurface, and the measurements at the receivers can be used to determine the resistivity at different locations and depths (Eidesmo et al., 2002; Ellingsrud et al., 2002.). Two CSEM data acquisition systems which are called SeaBed Logging (SBL) system and towed streamer Electromagnetic (EM) system are applied in hydrocarbon exploration.

Several methods for removing the airwave components have been proposed to extend deep water to shallow water (Amundsen et al., 2006; Maaø and Nguyen, 2010). As normal, marine CSEM data were analyzed by plotting electric field amplitude versus source-receiver offset. Mittet (2008) presented a modified version of normalized amplitude ratio. The modified ratio is calculated using both the amplitude and the absolute phase of the electromagnetic fields so that it is possible for this method to be used in very shallow water. Using the modified normalized amplitude ratio, he transformed the phase change to an anomalous amplitude. Using the up-down decomposition, the sensitivity to the subsurface resistors could be enhanced by the modified normalized amplitude ratio (Amundsen et al., 2006). Mittet and Morten (2012) defined a measure of sensitivity to marine CSEM to determine whether a hydrocarbon reservoir can be detected and whether it can be successfully represented.

In this paper, we employ Occam's inversion for marine CSEM data. The CSEM data inversion results are influenced by water depth in two marine CSEM data acquisition methods: SeaBed Logging (SBL) and towed streamer EM acquisition. We compare these two data acquisition methods in both deep and shallow water environment.

Simple layer forward model for synthetic data

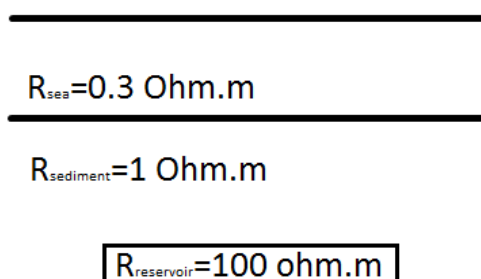


Figure 1 The model used for the analysis of the response from a thin resistive layer embedded in a conductive background medium. The modelled reservoir was set to be 3 km wide and 100

m thick and is located at 2 km depth. The water resistivity was set to be $0.3 \Omega\text{m}$, the formation resistivity $1 \Omega\text{m}$, and the reservoir resistivity $100 \Omega\text{m}$. Data were modeled in the models with varying water depth 300 m and 700 m, with frequencies 0.25 Hz and 0.75 Hz for both acquisition systems.

For our basic cases, the 2D isotropic target is designed as depicted in Figure 1. A reservoir is embedded into a background sediment. Both the sediments and the reservoir are isotropic. The reference model has the same background but does not include the reservoir block.

Reservoir sensitivity index variation with water depth

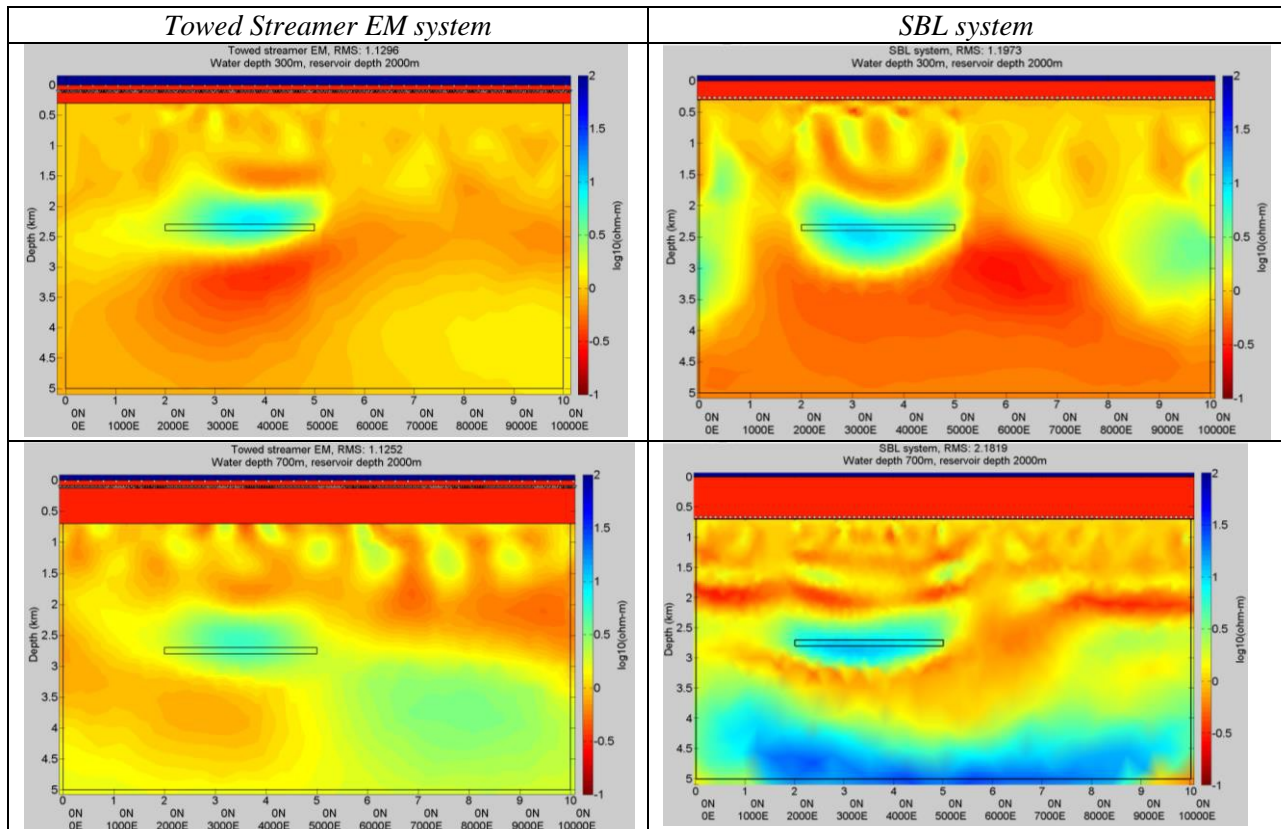


Figure 2 Inversion results for the two different data acquisition systems. Left panels: towed streamer; Right panels: SBL acquisition. Water depth: 300 m (upper panel), and 700 m (lower panel).

The inversion results are summarized in Figure 2 and the differences between the towed streamer EM system and the SBL system are able to be effectively and efficiently distinguished. In shallow water case, the resistivity image from towed streamer EM system inversion has a resolution and sensitivity advantage due to enormous data. In contrast, in the deep water case, the attenuation of a diffusive field in the water caused a increasing the signal to noise ratio with increasing water depth. The deeper the water depth was, the better inversion results could be given by the SBL system.

Discussion and Conclusion

In these comparison tests, we did not consider the effects when the resistivities were changed. We only tested the data acquisition system in various the water. From the simple model test, we observe that both of two data acquisition methods have a very high sensitivity and resolution at the shallow reservoir case. For the deep reservoir, towed streamer EM system has an advantage at the shallow water. By contrast, SBL has an advantage in the deep water.

Acknowledgements

We would like to thank P. A. Olsen., A. K. Nguyen. and E. Causse for discussing on the inversion results and J. Midgley for giving advice on the noise floor.



References

Amundsen, L., L. Løseth, R. Mittet, S. Ellingsrud, and B. Ursin. (2006) Decomposition of electromagnetic fields into upgoing and downgoing components: *Geophysics*, **71**(5), G211–G223.

Eidesmo, T., S. Ellingsrud, L. M. MacGregor, S. Constable, M. C. Sinha, S. Johansen, F. N. Kong, and H. Westerdahl. (2002) Seabed logging (SBL), a new method for remote and direct identification of hydrocarbon filled layers in deepwater areas: *FirstBreak*, **20**, 144–152.

Ellingsrud, S., T. Eidesmo, S. Johansen, M. C. Sinha, L. M. MacGregor, and S. Constable. (2002) Remote sensing of hydrocarbon layers by seabed logging (SBL): Results from a cruise offshore Angola: *The Leading Edge*, **21**, 972–982.

Johan Mattsson, Peter Lindqvist, Robert Juhasz, and Erik Björnemo. (2012) Noise reduction and error analysis for a Towed EM System. *SEG Technical Program Expanded Abstracts 2012*: pp. 1-5.

Maaø, F., and A. K. Nguyen. (2010), Enhanced subsurface response for marine CSEM surveying: *Geophysics*, **75**(3), A7–A10, doi: 10.1190/1.3377054.

Rune Mittet. (2008) Normalized amplitude ratios for frequency-domain CSEM in very shallow water: *First break*, **26**, P47-54.

Rune Mittet and Jan Petter Morten. (2012), Detection and imaging sensitivity of the marine CSEM method. *Geophysics*, **77**(6), E411-E425.



The use of seismic attributes for fault identification in the X field, Indonesia

Iqbal Fauzi Aditama¹, Mawar Indah Nursina²

email: iqbalf.173@gmail.com

¹ Bandung Institute of Technology, ²Petrochina International Jabung Ltd.

Summary

In the Jabung Block, South Sumatra Basin, the oil and gas are produced mainly from Talang Akar Formations. The main objective of the study was to detect and mapping of faults on the Lower Talang Akar Formation using seismic attributes (variance and Ant Tracking). Variance attribute can preserve the fault structural more detail on inline intersection and Ant Tracking attribute more clearly to visualization mapped fault on time slice intersection. Consistency results between mapped faults and the regional geology means the mapped fault is appropriate. The integration of the attributes has increased confidence in the seismic mapping of the fault.

Introduction

The onshore portion of the X Field is in the Jabung Block of the South Sumatra Basin. The field is approximately 250 km south of Singapore. The South Sumatra Basin are one of the most prolific oil-productive areas found to date in Southeast Asia. In the South Sumatra Basin, the oil and gas are produced mainly from Talang Akar Formations. The main objective of the study was to detect and mapping of faults on the Lower Talang Akar Formation (LTAF) using seismic attributes.

Regional Geology

The South Sumatra Basin is located to the east of the Barisan mountains and extends into the offshore areas to the northeast and is regarded as a foreland (back-arc) basin bounded by the Barisan mountains to the southwest, and the pre-Tertiary of the Sunda Shelf to the northeast (Darman and Sidi, 2000).

The sediments of the Talang Akar Formation generally grade from a fluvial depositional regime at the base, through a deltaic to shallow marine regime upward. The main oil producing (about 70%) reservoirs in South Sumatra Basin are the Oligocene-Miocene sandstones of the Talang Akar Formations.

Seismic Attribute

Variance, which measures the degree of dissimilarity, is applied to enhance lateral changes of seismic data due to changes of geologic conditions (Sukmono, 2006). This attribute is used to extract edge volume from an input seismic volume.

Ant tracking is used to extract faults from pre-processed seismic volume. The pre-processing could be chaos or variance combined with structural smoothing. The "Ants" will try to extract features in the attribute corresponding to expectations about the faults.

Methods

The seismic attributes that used for identifying fault are variance and Ant Track. All of the analysis was in the time scale. The time slice intersection that used are in the specific value based on the data. From the check shot result, the position of LTAF was concentrated at time slice 1700 ms. The top boundary was Upper Talang Akar formation (UTAF), at time slice 1550 ms and the bottom boundary was basement (BSMT) at time slice 1750 ms.

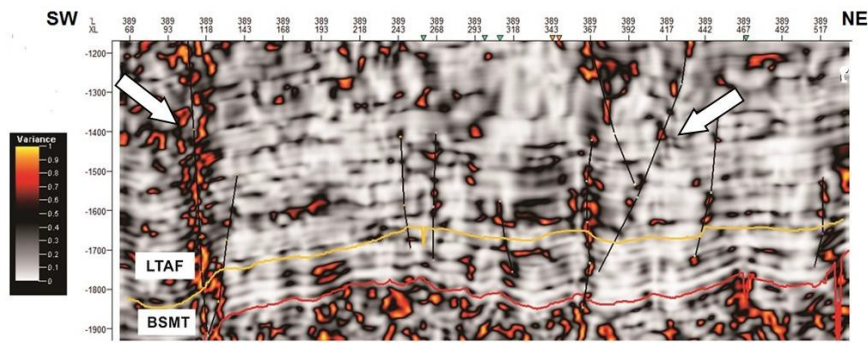


Figure 1 Mapped faults of variance attribute on inline 389

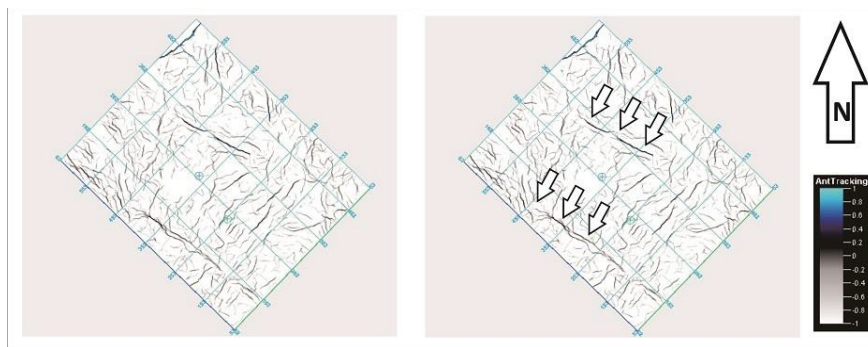


Figure 2 Time slice of Ant Tracking attribute at 1700 ms with arrow to marked main faults

Results and Discussion

Figure 1 shows that variance attribute can preserve the fault structural more detail on inline intersection. Figure 2 shows that Ant Tracking attribute more clearly to visualization mapped fault on time slice intersection. Figure 1 and Figure 2 show that main fault (marked by white arrow) have an align NW-SE. The mapped faults and regional geology based the structural map of Sumatra show a consistency results.

Conclusion

The integration of variance attribute and Ant Tracking attribute has been successfully applied to detect and mapping of faults on the Lower Talang Akar Formation in X Field. Fault structures can be identifying more effectively with the aid of seismic attributes. The integration of the attributes has increased confidence in the seismic mapping of the fault.

References

- Darman, H and Sidi, F. H. (2000). An outline of the geology of Indonesia, Indonesian Association of Geologists.
- Sukmono, S., Santoso, D., Samora A., Waluyo W., Tjiptoharsono, S. (2006). Integrating seismic attributes for reservoir characterization in Melandong Field, Indonesia, The Leading Edge, SEG, 532-538.

OIL&GAS & SEISMICITY

WEDNESDAY, 15 July, 14:30-15:30

Personal attendance required

Application of the Source-Scanning Method to West-Bohemia Swarm Earthquakes	Vojtěch Lávička, Václav Vavryčuk
Well Log Analysis of Gas Hydrates Bearing Region: Green Canyon, Gulf of Mexico and Mt. Elbert, North Slope Alaska	Srishti Ashish
Seismic attenuation of P waves and tectonic implications of Banda arc-Indonesia	Andreea Chiriac
Permian lacustrine Oil shale-shale oil system:Lucaogou Formation Shales in southern margin of Junggar Basin	HuangXiaoyi
Tectonic regime transition from extension to transtension in the Dongying Sag, BohaiBayBasin, China	XuYi
The estimation of reservoir and lithological properties of Productive Series Kirmaky Suite of Pirallahi oil-gas field	Shikhova Leyla
An attempt to determine the relationship between acoustic impedance and TOC for Shale Gas exploration in Poland Baltic Basin	Monika Kasperska, Kamil Cichostępski
Similarities between earthquake swarms in West Bohemia, the Czech Republic and those of the Reykjanes peninsula, Iceland	Martin Labuta
Application of MASW in ground analysis.	Artur Marciniak
Applicability of VSP to estimate laterally varying fracturing direction in reservoirs	Ivan Karpov, Sergey Gorshkalev, Dmitriy Vishnevskiy
Shale Volume Estimation Using Factor Analysis and Neural Network	V. Srivardhan, S. K. Pal
Imaging primaries and internal multiples in elastic media	Carlos Alberto da Costa Filho, Matteo Ravasi, Andrew Curtis
Hydrocarbon Charging History for Reservoir in the Northeastern Baiyun Sag, Pearl River Mouth Basin: Constrained by Fluid Inclusion Data	Jin Chen
Microseismicity Imaging of Underground Discontinuities around the mining vicinity, Witwatersrand Basin, South Africa	S.B. Mngadi, R. J. Durrheim
Challenges for microseismic monitoring acquisition optimization	Georgy Loginov



Application of the Source-Scanning Method to West-Bohemia Swarm Earthquakes

Vojtěch Lávička^{1,2}, Václav Vavryčuk²
email: lavicka@natur.cuni.cz

¹ Charles University in Prague, Faculty of Science

² Institute of Geophysics, Czech Academy of Sciences, Prague

Summary

We performed a series of tests with synthetic data as well as real data to assess the capability of the source-scanning method (Kao & Shan 2004) to determine rupture parameters of micro-earthquakes in the West-Bohemia region (Fischer et al. 2010). The results of the source-scanning method are compared with those obtained using analysis of directivity of the P and S waves.

Introduction

Stacking methods became recently used in prospection and hydraulic fracturing monitoring as well as in earthquake seismology. We applied these methods to locate the hypocenters of earthquakes and to determine rupture parameters of the source process.

Method

We used a method called source-scanning (Kao & Shan 2004) or time-reverse imaging (Artman et al. 2010). We constructed a dense subsurface grid of candidate point seismic sources. We calculated travel time for each pair of a grid point and a seismic station. We shifted waveforms back in time by the calculated travel time and stacked the shifted waveforms of all stations. The sum is called the brightness function (Kao & Shan 2004). This function depends on both space and time and can be used for locating the hypocenters and for mapping the space-time distribution of seismic sources (Kao & Shan 2004). Advantageously, accurate phase picking is not required; we only need to set up roughly a stacking window with the direct P phase.

Example

We tested the method on selected M3+ earthquakes of the 2008 West-Bohemia earthquake swarm. We used seismograms recorded by the West Bohemia Seismic Network stations. Their sampling rate is 250 Hz (Fischer et al. 2010). We used 1D velocity model by Málek et al. (2000, 2005) which was modified in order to produce smooth gradient velocity model appropriate for ray-tracing techniques.

We compared the hypocenter location obtained by time-reverse stacking with the hypocenter location obtained from P-phase picks and the hypocenter location adopted from Vavryčuk (2011).

We made a series of tests with synthetic data as well as real data using a variety of data preprocessing techniques, e.g. data with and without a normalization, stacking of waveform envelopes of velocities as well as displacements, fixed time window length for all records as well as time window length that covers just the duration of the first pulse of the particular waveform. We compared the obtained brightness functions in order to find an optimum way of data preprocessing.

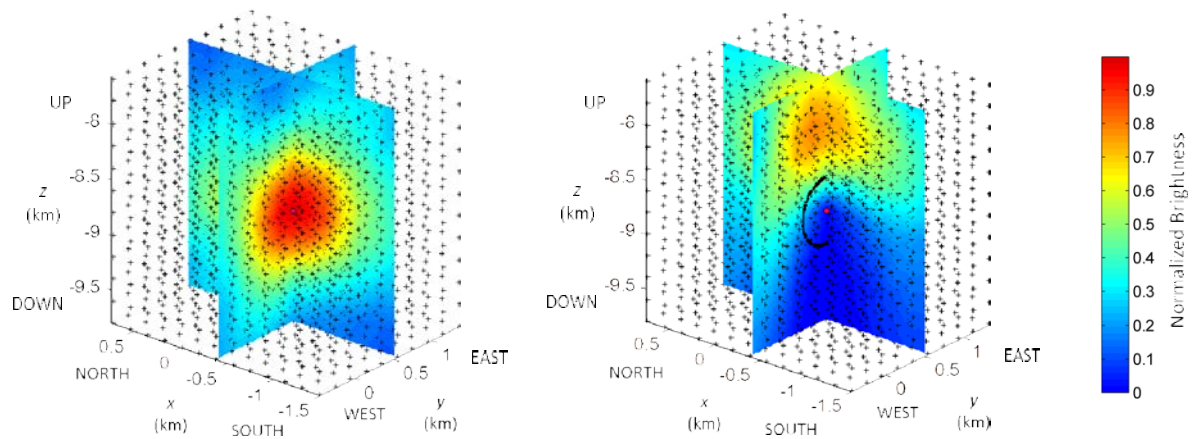


Figure 1 The brightness function for a synthetic waveform. Left: the origin time, right: 80 ms after the origin time. A pulse with shape of a sine function and length of 160 ms, which has its maximum at the calculated arrival time, was used for all stations. The arrival times corresponded via the calculated travel times to the hypocenter marked by the red spot in the middle. Grid points are marked by the small black crosses. The S wavefront radiated from the hypocenter is plotted as the black circle.

Acknowledgements

We thank the WEBNET group of the Institute of Geophysics of the Czech Academy of Sciences for providing the data used in this study. The work was supported by the Grant Agency of the Czech Republic, Grant No. 210/12/1491.



References

- Artman, B., Podladtchikov, I., Witten, B. (2010). Source location using time-reverse imaging. *Geophysical Prospecting*, 58(5), 861–873.
- Fischer, T., Horálek, J., Michálek, J., Boušková, A. (2010). The 2008 West Bohemia earthquake swarm in the light of the WEBNET network. *Journal of Seismology*, 14(4): 665–682.
- Kao, H. and Shan, S.-J. (2004). The Source-Scanning Algorithm: mapping the distribution of seismic sources in time and space. *Geophysical Journal International*, 157(2): 589–594.
- Málek, J., Janský, J., Horálek, J. (2000). Layered Velocity Models of the Western Bohemia Region. *Studia Geophysica et Geodaetica*, 44(4), 475–490.
- Málek, J., Horálek, J., Janský, J. (2005). One-dimensional qP-wave velocity model of the upper crust for the West Bohemia/Vogtland earthquake swarm region. *Studia Geophysica et Geodaetica*, 49(4), 501–524.
- Vavryčuk, V. (2011). Detection of high-frequency tensile vibrations of a fault during shear rupturing: observations from the 2008 West Bohemia swarm. *Geophysical Journal International*, 186, 1404–1414.



Well Log Analysis of Gas Hydrates Bearing Region: Green Canyon, Gulf of Mexico and Mt. Elbert, North Slope Alaska

Srishti Ashish¹, How-Wei Chen²

Email: srishti.ashish@hotmail.com, hwchen@ncu.edu.tw

¹National Central University, Jhongli City, Taiwan

²National Central University, Jhongli City, Taiwan

Summary

This paper illustrates the use of TechLog as a tool to process Well Logs from Gas Hydrates bearing regions, to quantify and estimate gas hydrates for successful exploration.

Introduction

Occurrence of gas hydrate has been found worldwide in the continental shelf, marginal seas and polar region. As interest in gas hydrate as a potential energy resource continues to grow, the need for accurate assessments of the amount of gas stored in gas hydrate at the accumulation or basin scale becomes more important [1]. Potential gas hydrate production is strongly dependent on a number of reservoir parameters, including the areal extent of the gas hydrate occurrence, reservoir thickness, reservoir porosity and the degree of gas hydrate and free gas saturation. The distribution and saturation of gas hydrate can be determined by seismic imaging and interpretations. Three most difficult reservoir parameters to be determined are the porosity, degree of gas hydrate and free gas saturation [2]. To get these parameters it is necessary to have the following information: - lithology, acoustic velocity, density, porosity, fluid type, saturation which can be obtained by well logs. Well log processing for oil and gas reserves is customary but processing for gas hydrates becomes relatively advanced. In recent years, a growing number of deep sea drilling expeditions have been dedicated to locating marine gas hydrates and understanding the geologic controls on their occurrence.

This has led to execution of gas hydrate research drilling and down hole logging programs. Out of those programs the two most studied and comprehensive datasets are those from Mt. Elbert North Slope Alaska and Green Canyon, Gulf of Mexico. The Mount Elbert well was designed as an advanced recent downhole wireline logging program with the planned acquisition of cores, well logs, and downhole reservoir pressure test data [3]. The Gulf of Mexico Joint Industry Project Leg II conducted its drilling operations in the eastern Green Canyon on the upper continental slope of Texas and Louisiana, where near-surface geology is dominated by active salt tectonics and rapid sea level-driven sedimentation. Salt diapirs are common on the upper slope [4]. The mobile salt has extensively fractured the overlying sediments with regional growth faults and associated fault types. These faults act as conduits for the migration of hydrocarbons from deep layers to shallow sections. Three sites were drilled during this leg GC955-I, GC955-H, GC955-Q out of which GC955-H penetrated a thick gas-hydrate-filled fracture sand section representing the complete range of gas hydrate reservoir conditions encountered during the GOM JIP Leg II [5].

Method

The purpose of this paper is to review the responses of well logs to the presence of gas hydrates, at Mt. Elbert (ME), North Slope Alaska and Green Canyon (GC), Gulf of Mexico and carry out well log processing and analyses and interpretation. This is done by using the software package TechLog - Quanti. Evaluation is done by optimizing simultaneous equations between tools, response parameters and formation component volumes described by one or more interpretation models. The information consists of a set of tools, or equations; a set of formation components, or volumes, and a set of

constraints. Implicitly response parameters and other global and model-specific parameters are derived from the log curves, background geological information, and confirmed using crossplots.

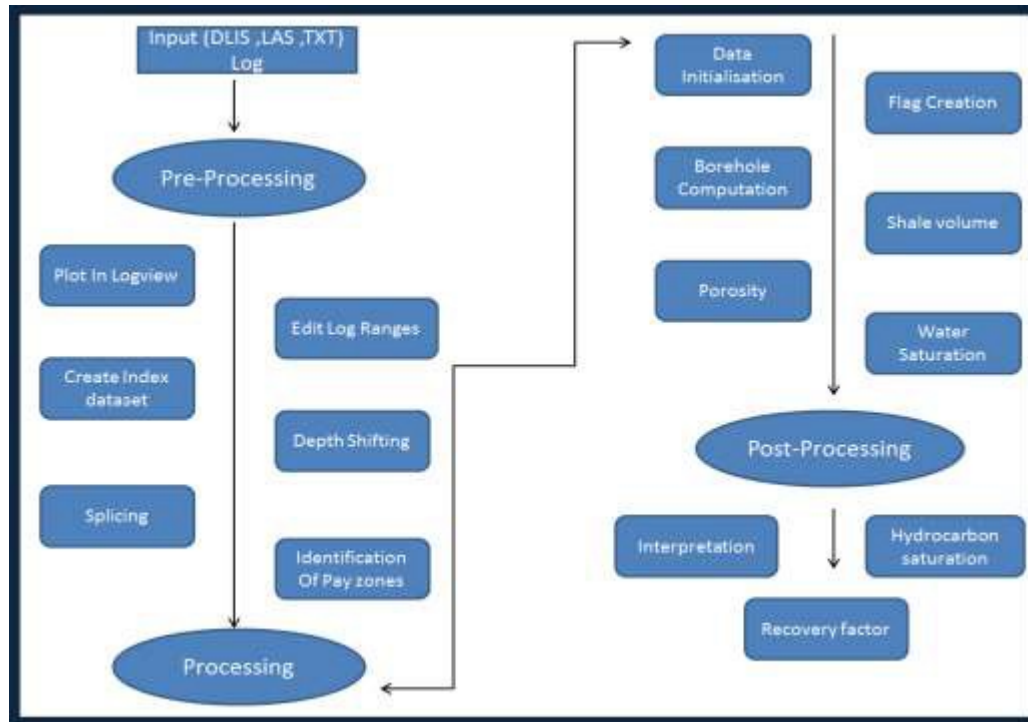


Figure 1: Steps to carry out the Well Log Processing using TechLog.

Conclusion

At the Mt.Elbert gas hydrates production is identified at two stratigraphic sections bearing reservoir-quality sandstone between 2016-2060ft and 2136-2180ft .Both zones displayed gas-hydrate saturations with values between 60% and 75%. At Green Canyon Gulf Of Mexico three sites were drilled GC955-I, GC955-H, GC955-Q and thick gas-hydrate-filled sand reservoir section has been discovered within the depth interval of 1300~15fbsf. At GC955-Q Gulf Of Mexico gas hydrates bearing zones are identified as shaly sand zones between 1360-1400 fbsf and 1417-1427 fbsf with GH saturations with values varying between 20% to 70 % with occurrence of free gas . At GC955-H Gulf Of Mexico gas hydrates bearing zones are identified as mud rich zones with sand reservoirs between 1360-1440 fbsf , 1460-1469 fbsf and 1470-2186 and 1470-2186 with GH saturations varying between 70~80% with presence of Gas hydrates rich reservoirs.. The description of the existing well log evaluation techniques used to characterize porosities and water saturation in gas hydrate bearing reservoirs is also included in this paper.



References

- [1] Collett, T., Johnson, A., Knapp, C., Boswell, R., 2009. Natural gas hydrates e a review (Chapter 1). In: Collett, T., et al. (Eds.), Natural Gas Hydrates e Energy Resource Potential and Associated Geologic Hazards. AAPG Memoir, vol. 89,p. 74.
- [2] Collett, T., Boswell, R., Frye, M., Shedd, W., Godfriaux, P., Dufrene, R., McConnell, D., Mrozewski, S., Guerin, G., Cook, A., Jones, E., Roy, R., 2010. Gulf of Mexico Gas Hydrates Joint Industry Project Leg II: Operational Summary. DOE-NETL. <http://www.netl.doe.gov/technologies/oilgas/publications/Hydrates/2009Reports/OpSum.pdf>.
- [3] Inks, T., Lee, M., Agena, W., Taylor, D., Collett, T., Hunter, R., Zyrianova, M., 2009. Prospecting for gas hydrate accumulations using 2D and 3D seismic data, Milne Point, North Slope, Alaska. In: Collett, T.S., Johnson, A., Knapp, C., Boswell, R. (Eds.), Natural Gas Hydrates; Energy Resource Potential and Associated Geologic Hazards. AAPG Memoir, vol. 89, pp. 1–29.
- [4] Ruppel, C., Boswell, R., Jones, E., 2008. Scientific results from Gulf of Mexico gas hydrates Joint industry Project Leg I drilling: introduction and Overview. J. Mar.Pet. Geol. 25 (8)
- [5] Boswell, R., Collett, T.S., Frye, M., Shedd, McConnell, D., Shelander, D., 2012a. Subsurface gas hydrates in the northern Gulf of Mexico. Journal of Marine and Petroleum Geology 34,



Seismic attenuation of P waves and tectonic implications of Banda arc- Indonesia

Andreea Chiriac¹

email: andreea_chiriac93@yahoo.com

¹University of Bucharest

Summary

Amplitude spectral ratio method has been used to compute the attenuation factor Q_p in the Banda Sea region. P and pP waves from teleseismic recordings have been investigated from eight major-depth events, located in Northern Indonesia. Most of the seismic stations are based in Asia and Eastern Africa. The results show a correlation between low Q_p values and aseismic or shallow earthquakes zones and between high Q_p values and slabs dipping in the subduction zone. Despite the general distribution on low values of attenuation factor, the setting of Wetar zone slab rupture can be marked on the map.

Introduction

The Banda subduction zone is located at the contact of Eurasia, Australia and Pacific plates and it is believed to have one of the most complex tectonics on Earth (Das, 2004). The motion of plate tectonics in Eastern Indonesia is described by a northward direction of Indo-Australian Plate and a westward direction of the Pacific Plate. One of the most outstanding features of this region is the dipping of adjacent subduction zones in different directions, being the result of a roll-back type subduction.

In previous studies, the geometry of the slab system and slab detachment beneath the Banda Sea has been built through relocated earthquakes hypocenters (McCaffrey 1989; Das 2004; Sandiford 2008). Seismic gaps have been observed in this region beneath Wetar zone where volcanism ceased at about 3 Ma and beneath Timor trench, at different depths.

In order to investigate the lateral seismic gaps between the Java, Timor, Seram trenches and Banda Basin, the contour map of the P waves attenuation factor has been compared with relocated hypocentres from 10000 events occurred between 2012 and 2015.

Methodology

Vertical records of digital waveforms have been web-requested from eight events listed in IRIS Data Base (Incorporated Research Institutions for Seismology). Time arrivals of P and pP phases have been observed in PITSA (Programmable Interactive Tool for Seismic Analysis). In order to evaluate the natural logarithm of the amplitude spectra and the wave energy, window lengths of 256 points for 20 Hz recordings, 512 points for 40 Hz and 50 Hz and 1024 points for 100 Hz, have been used for both P and pP waves. Fourier transformations have been applied for each window and pP-P pairs have been subtracted. On the new graphic results, frequency windows between 0.1 and 1.8 Hz have been applied in order to compute the absolute value of the regression line slope. The attenuation factor Q_p has been evaluated using the spectral ratio method, related to Roth et al. (1999), by obtaining the difference between time arrivals t_{pP} and t_P multiplied by π and divided by the absolute value of the slope.

Using the University of Carolina seismic travel time calculator TauP Toolkit, geographical coordinates for pP phase piercing the crust have been attached as attributes near Q_p . With these values, a contour map of Q_p has been created. As interpolation method, minimum curvature has been chosen and restrictions on interpolating values, where no data can be found, have been applied.

ArcGIS (Esri) and Surfer (Golden Surfer) have been used to create the graphic support.

Results

Relocated hypocenters show several lateral gaps between Java trench and Timor trench (Figure 1), but also in Wetar zone. A 3D scatter of the hypocenters shows a seismic gap along Wadati-Benioff zone beneath Wetar and between 300 and 500 km depth, beneath Java trench zone.

Low Q_P shows a general correlation with lateral seismic gaps, but also with the lack of intermediate depth events or deep events. High Q_P is correlated with high densities of events. Northern to Wetar zone a decreasing value of Q_P overlaps on the area of low density of events, increasing northward with the number of events.

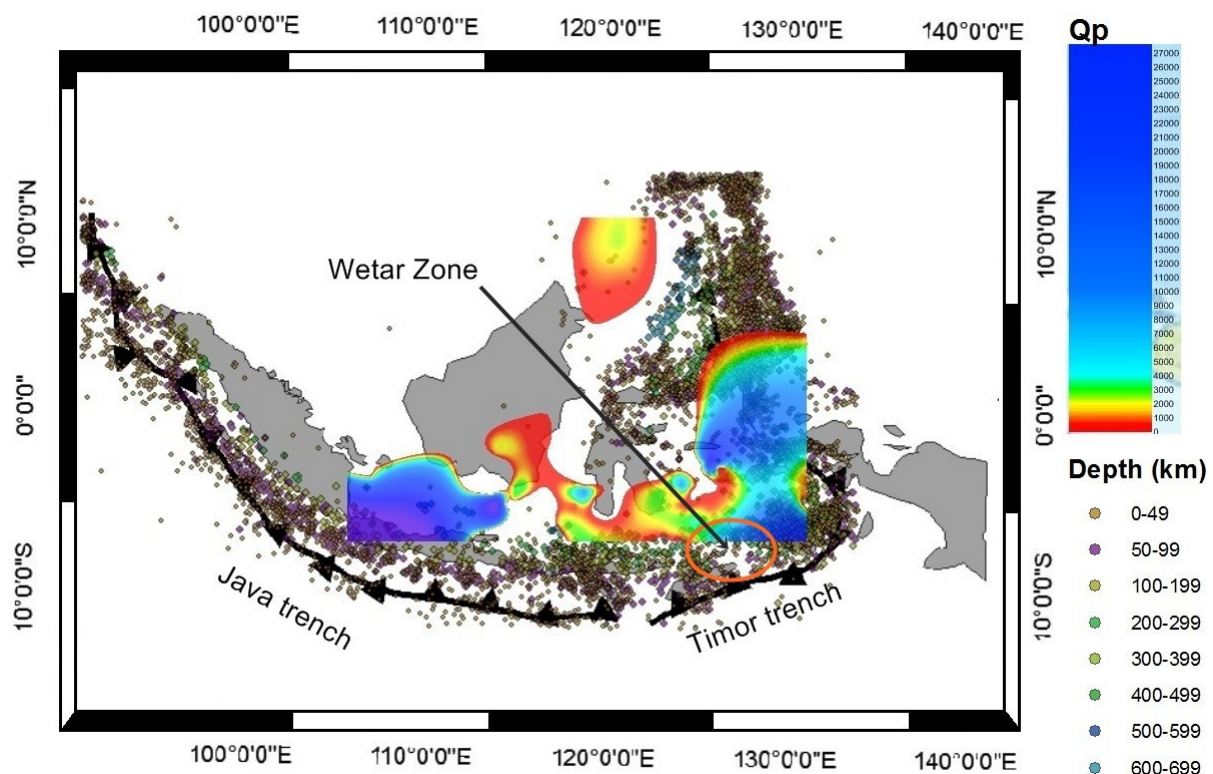


Figure 1 Hypocenters relocated along Java, Timor and Seram trench and Q_P contour map overlapped on Banda Basin. Events database downloaded from IRIS.

Conclusions

Depending on the difference of time between pP and P phase waves and linear regression slope, Q_P factor is highly sensitive in changing the frequency range for which the absolute value of the slope is computed. A frequency panel for a digital waveform could provide an expected result, but it is not the best choice for the other seismograms. Therefore, it is challenging to find an appropriate frequency window of which values can be related with the seismic Earth models.

Comparing the results, the amplitude spectral ratio method used to obtain the attenuation factor Q_P gives an accurate tool in locating subducting slabs. Lateral seismic gaps from relocated hypocenters support the idea of two trenches along Sunda and Banda Arc. In-depth seismic gaps could explain possible slab ruptures.

For further studies, more seismic records should be processed in order to fill the uncover areas.



References

- DAS, S. (2004). Seismicity gaps and the shape of the seismic zone in the Banda Sea region from relocated hypocenters. *J. Geophys. Res.*, Vol. 109
- IVAN, M. (2006). Attenuation of P and pP waves in Vrancea area- Romania. *Journal of Seismology*
- McCAFFREY, R. (1989). Seismological constrains and speculations on Banda arc tectonics. *Netherlands Journal of Sea Research*, Vol. 24 (2/3), p. 141-152.
- ROTH, E.G., WIENS, D.A., DORMAN, L.M., HILDEBRAND, J. & WEBB, S.C. (1999). Seismic attenuation tomography of the Tonga-Fiji region using phase pair methods. *J. Geophys. Res.*, Vol. 104, p.4795-4809.
- SANDIFORD, M. (2008). Seismic moment release during slab rupture beneath the Banda Sea. *Geophys. J. Int.* Vol. 174, p. 659-671



Permian lacustrine Oil shale-shale oil system: Lucaogou Formation Shales in southern margin of Junggar Basin

Huang, X. Y., Li, S.P.
hxcug529@163.com

Faculty of Earth Resources, China University of Geosciences, 430074-Wuhan, China

Summary

Lacustrine organic-rich shales have been gaining increasing attention in the field of non-conventional exploration. In this research, we mainly test specific indicator parameters of organic geochemistry such as Organic matter abundance (total organic carbon content, TOC), types, maturity of the shales and the test the Oil content in Lucaogou Formation, evaluating the hydrocarbon potential, revealing the prospect of application in the field of non-conventional oil and gas resources in the future. These specific indicators can provide the basis for organic-rich shales in the studied area and the comprehensive utilization of energy resources in the future.

Geological setting

Junggar Basin is a petroliferous basin with the development of lacustrine source rock, locating in the northern of Xinjiang Uygur Autonomous Region, northwest China. The area studied lies in the eastern part of the thrust belt on the southern margin of Junggar Basin, which is piedmont tectonic belt in the Bogda Mountain. Permian strata from the old to young are: the Lower Permian Shirenzigou Formation and Tashikula Formation, the Middle Permian Wulabo Formation, Jingjingzigou Formation, Lucaogou Formation, and Hongyanchi Formation, the Upper Permian Quanzijie Formation, Wutonggou Formation, and Guodikeng Formation. The target strata of the research is Lucaogou Formation. Rock assemblage of the Lucaogou Formation are black, brown and gray thick shale, oil shale with middle - thin dolomite and limestone lenses and a small amount of siltstone layers. According to the differences of lithology, sedimentary structure, fossils, mineral composition and the characteristics of logging curves, the oil shales of the Lucaogou Formation is divided into five lithologic facies which are the black oil shale facies, gray dolomitic facies, mudstone, argillaceous dolomite / limestone facies and micritic limestone / dolomite facies.

Methods

Cores from ZY1 and ZY2 wells were observed on the aspect of lithological character, organic matter abundance, type and maturity. 80 samples from ZK301 and ZK302 bores were used on the aspect of oil content. 192 samples were utilized for organic carbon test, 59 samples were analyzed for Rock-Eval pyrolysis using the standard of GB/T 18602-2012 and for the HI values test. 40 Samples were used for the test of vitrinite reflectivity of oil-immersed while 41 samples were analyzed for mineralogy by X-ray diffraction (XRD) analysis.

Evaluation of hydrocarbon source rocks of Lucaogou Formation shales

Lucaogou formation shales have high content of clay minerals and brittle minerals. In the wells of ZY2 and ZY3, content of brittle minerals (quartz and feldspar) is 28 and 56%, with an average of 54%; content of carbonate minerals (calcite and dolomite) ranges between 3 and 35%, and the average is 12%; the content of clay minerals range between 6 and 54%, with an average of 34%. For the ZY2 well, the Total organic carbon content (TOC) value ranges between 0.59 and 9.76%, with an average of 4.4%. Total organic carbon contents of ZY3 well range between 1.04 and 7.55 %, with an average of 3.65%. The TOC value in a total of 46% samples from the two wells is higher than 4% (Fig.1-A). Therefore, we can conclude that the abundance of organic matter of the source rocks in Lucaogou formation is high. HI/Tmax plot is used for classification of kerogen type. The majority of the samples from ZY2 and ZY3 wells contain Type I and II kerogens (Fig.1-B). Type I kerogen accounted for the total sample of 54%, Type II kerogen accounted for 44%, type III kerogen accounted for only 2%. The

results are basically consistent with the maceral analysis. Therefore, we can conclude that Lucaogou Formation Shales mainly produce oil. The vitrinite reflectance($R_o\%$) samples from ZY2 well varies between 0.64 and 0.9%, and between 0.72 and 0.84% in well ZY3, Their reflectance values are here considered to represent the“true” vitrinite population, and therefore are used as the maturity index. Moreover, thermal maturity as estimated from Rock-Eval T_{max} values ,ranges between a T_{max} values of 439°C to 449°C in ZY2 well and 443.5°C to 451°C in ZY3 well. The results suggest that hydrocarbon source rocks of Lucaogou Formation are in low mature-mature stage from ZY2 well and in mature stage from ZY3 well (Fig.1-C).

Evaluation of oil shale

Oil (tar) yield is an index that demonstrates the ability to generate oil from kerogen contained in oil shales in the retorting process. Oil shales can be divided into three industrial grades: an oil yield $\geq 10\%$ is referred as the high-quality, between 5 and 10% as the medium-quality, and between 5 and 3.5% as the low-quality. Among the 82 samples from ZK301 and ZK302, approximately 19 samples have sapropelitic constituent contents below 5%, with an oil yield basically lower than 3.5%, making the non-oil shale. Sapropelitic shale, accounting for approximately 12.2% of the total samples, is presumed to be high-quality oil shale. The 53 sapropel-containing samples can be further divided into two industrial grades: the low-quality and the medium-quality oil shales, which account for approximately 29.3% and 35.4% of the total samples (Fig.1-D). This test shows that the proportion of medium-quality oil shales is the highest and the Lucaogou Formation shales can be considered as the high quality Hydrocarbon source rock with a good prospect of utilization.

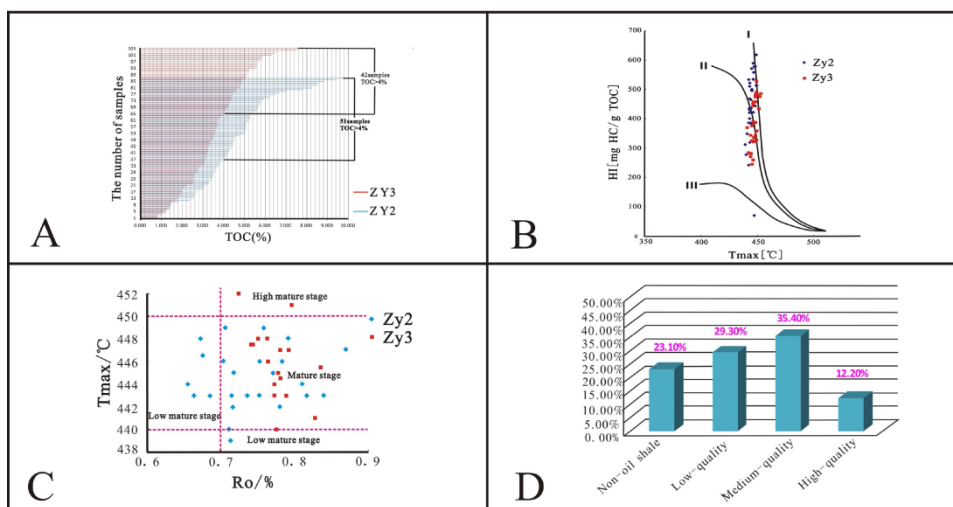


Figure 1 Synthetical evaluation map of Lucaogou Formation Shales

Conclusions

Lucaogou Formation Shales in the eastern part of the thrust belt on the southern margin of the Junggar Basin contain high organic matter abundance, which the TOC average value is higher than 4%; the majority kerogen types are Type I and Type II; hydrocarbon source rocks are in low mature- mature stage, the shales mainly produce oil and a few of the sample can produce gas. Most of the oil shales are medium-quality. Lucaogou Formation Shales not only can be considered as the hydrocarbon source rocks and reservoirs of shale oil, but also can be the oil shale resources for independent mining. The shales could be important goal of non-conventional oil and gas exploration in the future.



References

- He Sheng , Ye Jiaren , Xu Sihuang. (2010).Petroleum and Natural Gas Geology . Wuhan: China University of Geosciences Press.
- Li Peilong , Zhang Zhihuan , Hao Fang. (2010). Sedimentary Structure and Reservoir of Junggar Basin. Beijing: Geological Publishing House.
- Lu Shuangfang , Zhang Min , Zhong Ningning. (2008).Hydrocarbon Geochemistry. Beijing: Petroleum Industry Press.
- Peng Xuefeng,Wang Jinli.(2011). Analysis on the Sedimentary Environment of the Permian Lucaogou Formation in the Southeastern Margin of Junggar Basin .Journal of Xinjiang University.
- Li Jingjing. (2009).Geochemical Characteristics Research on Oil Shale of The Permian Lucaogou Formation in the Northern Bogda Mountain. Beijing: Doctoral Dissertation of China University of Geosciences.
- Alan R.Carroll.(1992).Upper Permian Lacustrine,Oil Shales,Southern Junggar Basin,Northwest,China. The American Association of Petroleum Geologists Bulletin.



Tectonic regime transition from extension to transtension in the Dongying Sag, Bohai Bay Basin, China

Xu, Y., S.G.C
34424508@qq.com

Faculty of Earth Resources, China University of Geosciences, 430074-Wuhan, China

Summary

The Bohai Bay Basin has previously been modelled as either a giant pull-apart or a rift basin without significant strike-slip deformation. Allen et al. (1998) has presented that the Bohai Bay Basin formed as a result of dextral transtension in early Tertiary. In this study, structure styles in different evolution stages and the rules of fault activities were summarized, the stress mechanism and the formation mode of structural transformation were discussed. The thorough analysis about transtensional structure style, the faults activities and its evolution mechanism would provide an important evidence for the study of transtension function mode in Bohai Bay basin.

Geological setting

Dongying Sag is a secondary negative tectonic unit in Jiyang Depression of Bohai Bay Basin. It is abundant of oil and gas resources and one of the highest level of exploration area in China. Dongying Sag is bounded on the north by the Chenjiazhuang Rise, West to Binxian, Qingcheng Rise, and is connected to Luxi Uplift, Guangrao Rise in south, east to Qingtuozi Rise. The distance from the west to the east is 90 km, the north-south width is nearly 65 km. It covers an area of 5400 square kilometers. The sag is a transtensional half graben lacustrine basin which is developed in ancient Paleozoic bedrock terrain background in Cenozoic, the lower part of the basin mainly developed in the Archean and Paleozoic bedrock. In Cenozoic, the basin is overlapping in the south, the north of the basin basement is steep and gentle in the south.

Methods

This study considers basin dynamics, structural geology, and the integration analysis of tectonic-sequence-sedimentary methods. Based on the refined well-seismic calibration and seismic interpretation, using the recent 3D seismic data and abundant of well logging data

Paleogene structure system transformation in Dongying Sag

With the ancient fault and its calculation methods, syn-sedimentary faults activities developed in Paleogene in Dongying sag were analyzed and calculated. The results strongly indicated that these faults were characterized by the features of episodic activities and periodicity activities. Among them, the majority of Binnan fault, Shicun fault and Chennan fault were dominated during Ek-Es4 activity period, represented the extensional structure activities. However, the faults in Gaoqing, Bindong, Lijin, Shengbei, and the central shear zone along with the faults in Chen Guanzhuang-Wang Jiagang were mainly controlled during the Es3-Ed activity period, and many of them were newly coming out faults, characterized by the transtensional structural activities. In addition, from the restoration of the subsidence history about key seismic section and interpretation of the balanced cross section in SN direction and NW-SE direction in basin's central part, it clearly showed that although the central basin subsidence rate in Es3-Es2 sedimentary period was the same or slower than that in Ek-Es4 period, horizontal extension rate was larger than that of Ek or Es4 sedimentary period. All above indicated

that horizontal shift in Es3-Es2 period was greatly strengthened, which was mainly caused by strike-slip activity according to the horizontal shift direction. Thus, the corroboration indicated that the structural evolution during this period in Dongying sag had been strongly influenced by the transtensional structural activities.

Dynamic mechanism of tectonic regime transition

During Ek-Es4 period (65~43.5Ma), it showed retrogressive subduction characteristics of the Pacific plate towards the Eurasian continent for sudden decreasing of the subduction speed, which resulted in the extensional thinning of lithosphere in the direction (NNW-SSE) of subduction and retreat of the Pacific plate, and caused a typical NNW-SSE extension in this period in Bohai Bay Basin. Besides, a series of NE trending basins developed in this period. Therefore, in this period, Dongying sag also had the feature of NNW-SSE trending extension (Fig.1-A). Up to Es3-Es2 period, the subduction direction of the Pacific plate changed from NNW to NWW, which correspondingly caused the dextral strike-slip activity occurred in Tanlu fault zone. Consequently, the stress field of the whole Bohai Bay Basin should be dominated by the dextral strike-slip faults activities. Up until Es1-Dongying Formation period, the subduction acceleration of the Pacific plate led to an obvious enhancement of dextral strike-slip activities in Tanlu fault zone in the east of the basin and Lanliao fault zone in the west. The subduction increase together with the extensional stress field in this period led to the formation of an oblique strike-slip pull-apart basin in Bohai Bay Basin between the two major strike-slip zones, while the nearly SN tensile stress field was formed in the central part of the basin, which was why a series of near EW syn-sedimentary faults developed in this period in Dongying sag (Fig.1-B).

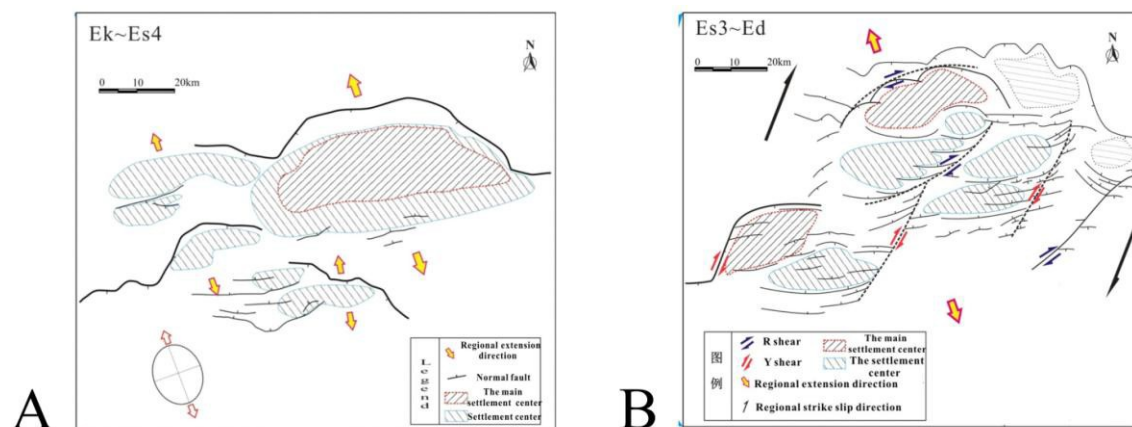


Figure1 The Paleogene in Dongying sag of stress evolution pattern

Conclusions

This study describes the evolution process changed from extensional tectonics to transtensional tectonics on 43.5Ma in Dongying Sag. The dynamic mechanism of transtensional tectonic systems in Paleogene in Dongying sag of Bohai Bay Basin was discussed. During Ek-Es4 period (65~43.5Ma), Dongying sag had the feature of NNW-SSE trending extension. Up to Es3-Es2 period, under the double influences of the dextral strike-slip effect and regional NW-SE extension effect, the basin was in the transtensional tectonic systems.



References

Basile C, Brun J. (1999). Transtensional faulting patterns ranging from pull-apart basins to transform continental margins: an experimental investigation . *Journal of Structural Geology*.

Wu J E, McClay K.(2009) .Whitehouse P, et al. 4D analogue modelling of transtensional pull-apart basins. *Marine and Petroleum Geology*.

Ben-Avraham Z, Zoback Mark.(1992) .Transform-normal extension and asymmetric basins: An alternative to pull-apart models. *Geology*.

Qi J F, Yang Q.(2010) . Cenozoic structural deformation and dynamic processes of the Bohai Bay basin, China. *Marine and Petroleum Geology*.

Northrup C J, Royden L H. (1995).Motion of the Pacific plate relative to Eurasia and its potential relation to Cenozoic extension along the eastern margin of Eurasia. *Geology*.

Rowley D B. (1996).Age of initiation of collision between India and Asia: A review of stratigraphic data . *Earth Planet. Sci. Lett.*



The estimation of reservoir and lithological properties of Productive Series Kirmaky Suite of Pirallahi oil-gas field

Shikhova Leyla¹, Efendiyeva Elza¹

e-mail: shikhovalf@gmail.com

¹Geology and Geophysics Institute of Azerbaijan National Academy of Sciences

Summary

In the paper, the results of the analysis of lithological and petrophysical properties of the new core and geophysical well logging data were summarized, 3D petrophysical and lithofacial models were constructed by kriging interpolation method and perspective areas for further drilling was recommended.

Introduction

The main purpose of this paper is to analyze the lithological and petrophysical parameters on the basis of new geophysical well logging and core data, obtained during the drilling of exploration wells, identification of lithological and petrophysical features of rocks in section and construction of 3D petrophysical and lithofacial models of Productive Series' Kirmaky suite (KS) of Pirallahi oil and gas field.

Theory and Methodology

Pirallahi oil-gas field is characterized by the complex geological structure, as most fields of South Caspian Basin. It is located within the Absheron archipelago, eastward of the Absheron Peninsula. Research covers the northern elevation of field, which is a brachyanticline, whose axis extends in the N-NW direction, complicated by several longitudinal faults, dividing the fold on 3 tectonic blocks. The geological structure of the field is mainly represented by Productive Series (PS) deposits with total thickness of 1380m. The PS deposits of Pirallahi oil-gas field are related to Absheron lithological type. Recent studies have proven that sediments of this lithological type are mainly sourced by a PaleoVolga river from the Russian platform. Spatial distribution of Absheron type sediments is significantly changed in separate stages of Productive Series accumulation and is dependent on Caspian Sea level fluctuations, which have resulted in basinward/landward facial shifts and wide depositional environment changes from fluvial, deltaic to lacustrine setting (Aliyeva, 2004).

The main important object of study is Kirmaky Suite of PS, lithologically represented by frequent alternation of fine-grained sand, gray and brown clays and aleurolite with interstratified layers of gray tight and loose sandstone. There is a clay unit with the thickness up to 65m in the top part of the suite, and the sandiness increases towards the lower horizons (Babayev, 2006). On electrical logging curves the sand packs with apparent electrical resistivity values up to 25-50 ohm and more are easily interpretable in the suite section. The suite is subdivided into two operational objects - Upper and Lower Kirmaky Suite. The thickness does not change rapidly and varies from 240 to 280m. The thickness of Kirmaky Suite increases from the crest of the structure to the flanks, which is due to the fact that the sedimentation occurred while the fold was forming.

In this research work for 3D models construction the deterministic methods of geostatistical modeling were used, in particular the method of universal kriging. The technology of cube calculation by this method includes two stages: a preliminary stage of variogram analysis and calculation of the cubes. Application of variogram model allows to reveal the regularities of petrophysical properties change of reservoir rocks both laterally – on the layers of geological grid, and on vertical section of the geomodel (Zoloeva, 2010).

By applying variogram analysis the structural surface, 3D petrophysical and lithofacial models of Kirmaky suite were constructed, based on 472 well log data (Fig.1). The exponential variogram model was applied, as it more accurately describes the natural processes.

On conducted correlation analysis the linear dependence between the permeability and porosity values, obtained from the core samples, was determined. For determination of the distribution patterns of lithofacies the additional well-to-well log correlation on the data of new drilled wells has been

done. The wells, drilled in the eastern tectonic block of the field, were analyzed and reservoir layers were revealed.

Based on comparative analysis of core and geophysical well logging data (SP) the boundary values between clay, sandy-argillaceous aleurolite and aleurolite sandstone were determined. As a result the clay rocks have VSH (shale volume) value not more than 0,3, sandy-argillaceous aleurolites varies between 0,3-0,75 and aleurolite sandstone and sandstone rocks – 0,75-1.

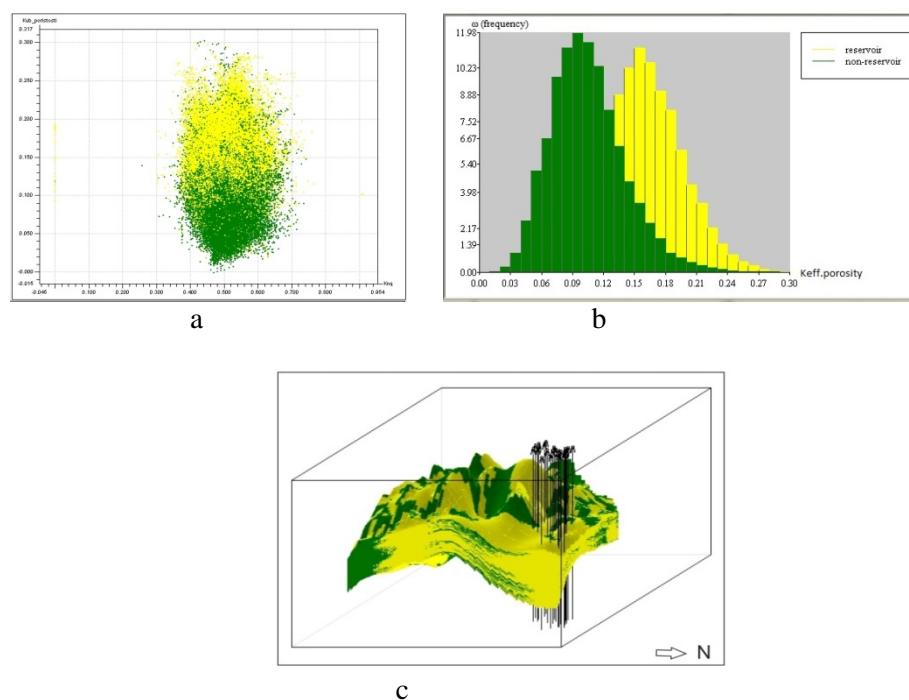


Figure 1. a) cross-plot of distribution of oil-saturation and effective porosity values of Kirmaky suite; b) diagram of porosity distribution in reservoir - non-reservoir formations in the section of KS; c) 3D lithofacial model of KS of Productive Series.

Conclusions

On the basis of conducted analyses the following conclusions have been made:

- the 2D and 3D petrophysical models on oil-saturation, effective porosity, net pay thickness and 3D lithofacial model, as well as the structure map on top values of the suite were constructed by using kriging interpolation method;
- as a result of lithofacial analysis of Kirmaky suite deposits penetrated by new exploration wells in the study area, an increase of sandy aleurolite facies in the lower part of the suite in the direction from south-west to north-east has been revealed and based on new core data the lithological section was compiled;
- the most prospective areas for drilling of exploration and production wells were highlighted in the north-eastern part of the northern fold of the field.

References

1. Aliyeva E.H. and Huseynov D.A. (2004). Lithofacies zonation of Lower Pliocene Productive Series sediments, South-Caspian Basin. AAPG/ASPG International Hedberg Research Conference, Extended Abstracts, Baku, 72-74;
2. Babayev D.H. and Gajiyev A.N. (2006). Deep structure and petroleum potential of the Caspian Sea basin. Baku (in russian);
3. Zoloyeva G.M., et.al. (2010). The practical course of a geological modeling. Moscow “Nedra” (in russian).



An attempt to determine the relationship between acoustic impedance and TOC for Shale Gas exploration in Poland Baltic Basin

Monika Kasperska¹, Kamil Cichostępski¹

email: krol@agh.edu.pl

¹ AGH University of Science and Technology

Summary

Unconventional resources such as shale gas has become an important target in natural gas exploration. The aim of our study is to present a way of identification, characterization and mapping of shale formation riches in TOC by using seismic post-stack inversion. Application shows usefulness of this method to obtain spatial distribution of TOC. Demonstrated results indicates that the increase of the TOC content nonlinearly decrease the acoustic impedance (Løseth H. et all, 2011).

Introduction

In the last years in Poland, shale gas has become an important target in natural gas exploration. Due to the different gas storage condition and accumulation pattern, shale gas needs different approach than conventional hydrocarbons. Usually, in shale formation the reservoir rocks is simultaneously source rocks. To produce gas at economic rates, the most interesting are shale formation which have relatively high total organic carbon (TOC) values. Numerical studies show that the mineral composition, TOC content and the relation between these two components influence the seismic response of the rock formation. The organic matter influences the seismic parameters as compressional velocity (V_p), shear velocity (V_s), bulk density, anisotropy and attenuation. Hence, it should be possible to predict TOC rich shale formation from surface seismic data. One of the most interesting shale formation with high TOC values in Poland are Lower Paleozoic formation of Silurian and Ordovician (Poprawa, 2010). Unfortunately, source rock are often thinner then the tuning thickness. In this paper we propose using seismic post-stack inversion as a procedure which should possible identification, characterization and mapping of shale formation riches in TOC.

Method

During seismic interpretation of Baltic Basin area we have noticed that the increased in TOC is accompanied by nonlinearly decrease of acoustic impedance (AI) (Figure 1). These relationship gave basis to use post- stack seismic inversion for spatial distribution of TOC. Post-stack seismic inversion is a process which provide acoustic impedance assuming zero-offset reflectivity. In seismic inversion the original reflectivity data is converted from an interface property (reflections) to a petrophysical property known as an acoustic impedance (multiplication of velocity and density), which is more suitable for reservoir characterization. There are many algorithms that can be used for estimation of acoustic impedance (AI). We have chosen model based inversion, which we find to be the most robust. In this algorithm, an initial model of earth's geology is designed (through interpolation of well logs measurement – sonic and bulk density - along interpreted seismic horizons) and then perturbed until the derived synthetic section best fits the observed seismic data (Hampson-Russell, 2014). Finally, we tried to map the TOC rich formation across the seismic profile (Figure 2).

Conclusions

Presented results indicate usefulness of post-stack seismic inversion for shale gas imaging, thus there is clear nonlinear correlation between then AI drop with increasing TOC content (Figure 1). The acoustic impedance inverted seismic sections show the decrease of AI values in shale formation. Therefore, it should be possible to follow the source rock and the changes in its thickness across the seismic line (Figure 2). Our studies here were limited to only acoustic parameters of rock formation. Other issues such as the transformation of AI data into TOC profile and application of the simultaneously inversion process to the 3D pre-stack seismic data deserve further investigation.

Acknowledgments

The study was founded by AGH Grants no 15.11.140. 336, 15.11.140. 345 and the research project of NSC nr BG1/GAZGEOLMOD/13: “Construction of the Lower Paleozoic extent’s maps, biostratigraphy and analysis of tectonic evolution of the marginal zone of the Eastern European Platform for estimation of unconventional hydrocarbon deposits distribution” granted to prof. J.Golonka.

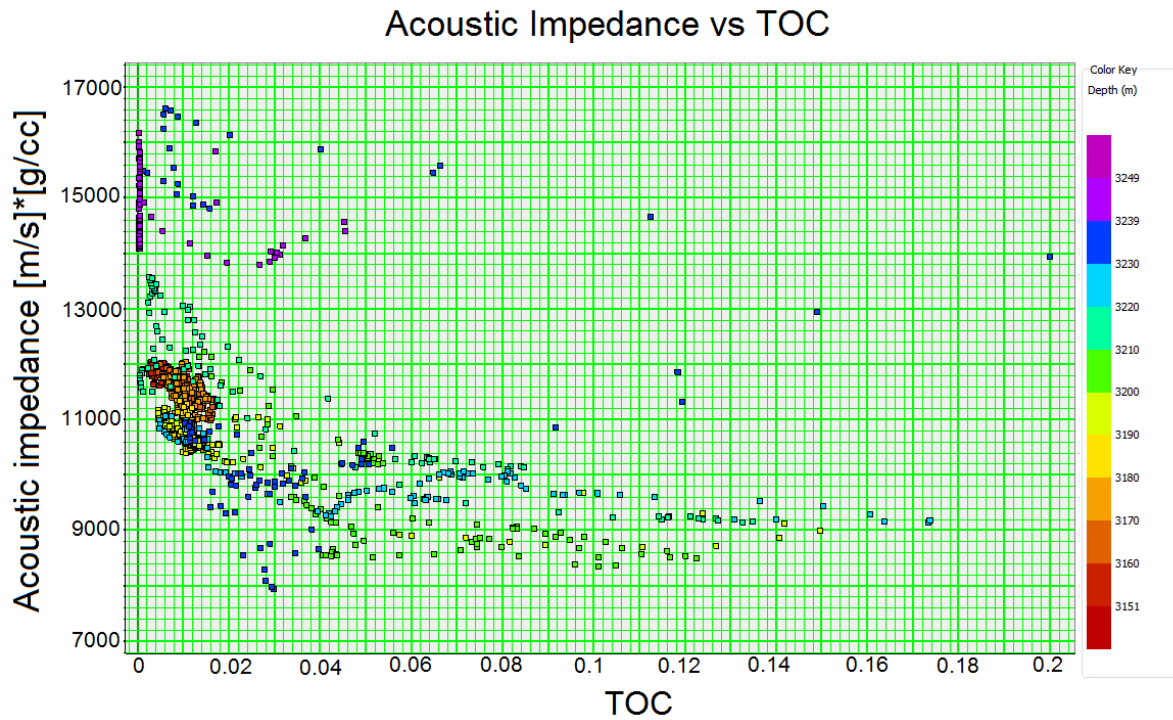


Figure 1 Crossplot: acoustic impedance versus TOC in K-1 well.

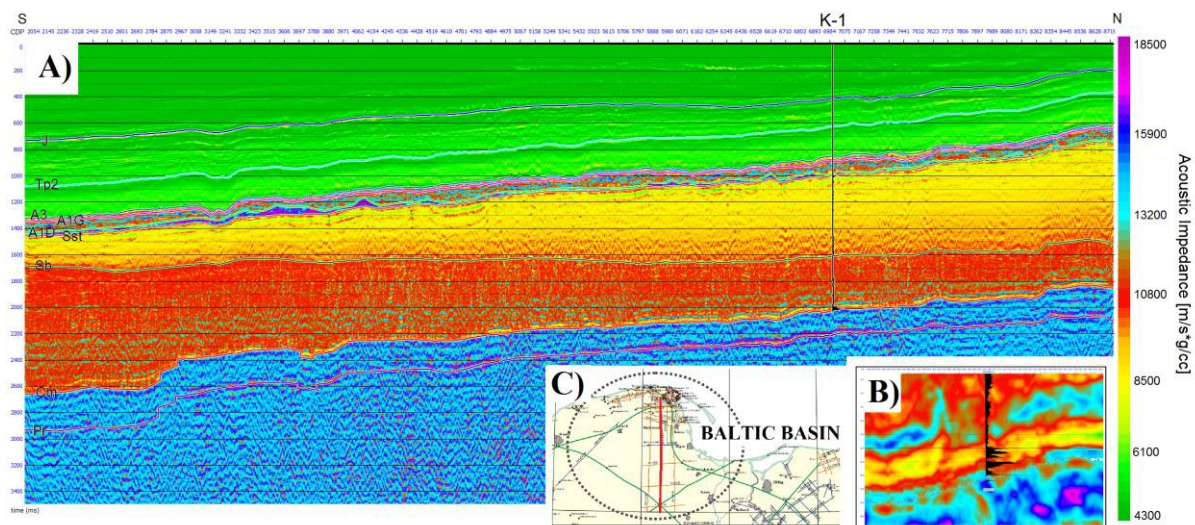


Figure 2 A) Acoustic impedance (AI) of interpreted time seismic profile; B) decrease of AI in vicinity of wellbore; C) localization map of seismic profile.



References

Hampson-Russell (2014). CGG. Calgary

Løseth H., Wensaas L., Gading M., Duffaut. and Spronger M. (2011). Can hydrocarbon source rock be identified on seismic data?. *Geology* 39; 1167-1170.

Poprawa P. (2010). Shale gas potential of the Lower Palaeozoic complex in the Baltic and Lublin-Podlasie basins (Poland). *Przegląd Geologiczny* 58: 226–249.



Similarities between earthquake swarms in West Bohemia, the Czech Republic and those of the Reykjanes peninsula, Iceland

Martin Labuta¹, Josef Horálek, Jana Doubravová, Hana Čermáková
email: labuta.martin@gmail.com

¹Charles University in Prague

Summary

This work presents results of seismic activity from two tectonically different regions and compares them in terms of time-spatial distribution of stress releasing.

Introduction

Earthquake swarms are characterized by series of earthquakes with several dominant shocks of similar strength. The origin of earthquake swarms is mostly a combination of tectonic stress and movement of hydrothermal fluids along the fault plane.

There is a question about any similarities including b-values and the focal mechanism that could explain relations of origin of these swarms occurring in different tectonic settings - in the post-Alpine orogenic area of West Bohemia (Fischer, 2013) and on the active continental margin represented by the South Icelandic rift zone.

Method and/or Theory

For our study we used the Seismon software for picking events in combination with the NLLoc (Lomax, 2000) for locating. The SIL velocity model (Stefánsson, 1993) was used for Icelandic earthquakes. We manually noted the first arrivals of more than 800 events in both areas. From this data set we were able to define b-values using the Gutenberg-Richter law and calculate the moment seismic tensor for the focal mechanism. Additionally, we used the Icelandic Meteorological Office's earthquake catalogue as a control group to verify our research results.

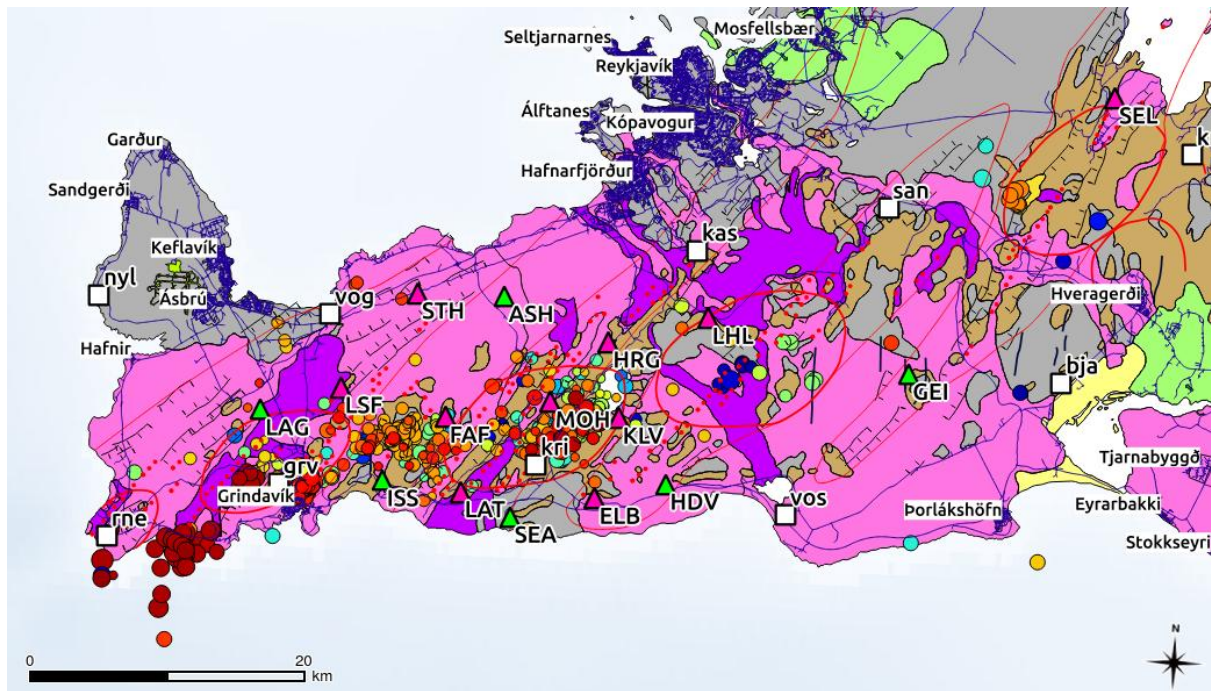


Figure 1 Geologic and tectonic map of the Reykjanes Peninsula with displayed seismic activity from September to October 2013.

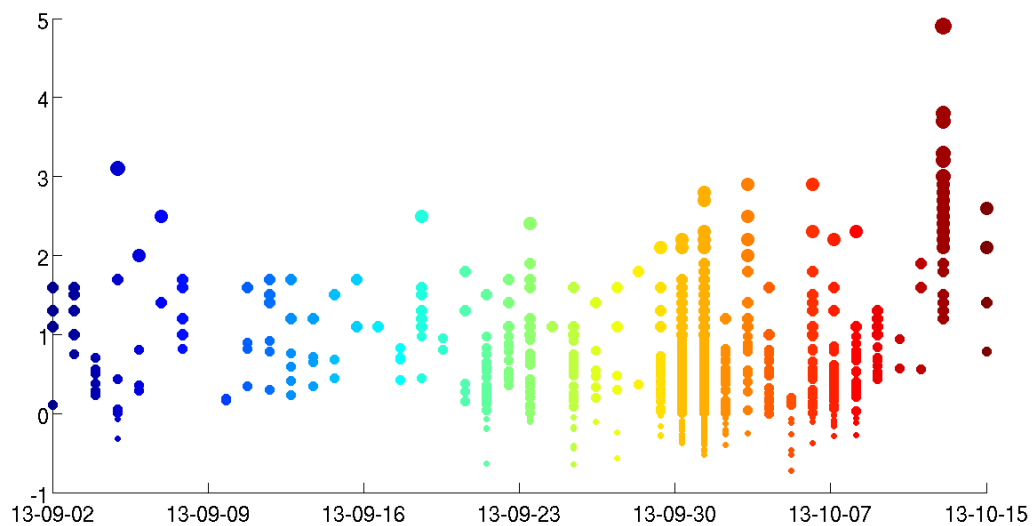


Figure 2 Time distribution of stress released on the Reykjanes Peninsula

Conclusions

We have discovered that the b-value for West Bohemia is higher (1.0) than the Icelandic one (0.8-0.9) and that the focal mechanism changes with depth (WB) rather than with location (I). To conclude, this supports further research to improve our understanding of spatial distribution in those particular areas of releasing accumulated stress.



References

Fischer, T., Horálek, J., Hrubcová, P., Vavryčuk, V., Bräuer, K., Kämpf, H. (2014). Intra-continental earthquake swarms in West-Bohemia and Vogtland: A review. *Tectonophysics*, 611, 1–27.

Lomax, A., J. Virieux, P. Volant and C. Berge, (2000). Probabilistic earthquake location in 3D and layered models: Introduction of a Metropolis-Gibbs method and comparison with linear locations, *Advances in Seismic Event Location* Thurber, C.H., and N. Rabinowitz (eds.), Kluwer, Amsterdam, 101-134.

Stefánsón, R., Bödvarsson, R., Slunga, R., Einarsson, P., Jakobsdóttir, S., Bungum, H., Korhonen, H. (1993). Earthquake prediction research in the South Iceland Seismic Zone and the SIL project. *Seismol. Soc. Am. Bull.*, 83(3), 696–716.



Application of MASW in ground analysis.

Artur Marciniak; Iwona Stan- Kłeczek PhD
email: artmar510@gmail.com
University of Silesia in Katowice

Summary

The application of the MASW technique (Multichannel Analysis of Surface Waves) in the Podleśna limestone quarry allowed the author to estimate the ground parameters such as stiffness and density in specific rock structures and to determine the influence of explosions on the velocity of S waves. It was also a good way to gain experience in doing MASW surveys. Analyses of the data that was gathered showed high velocities of S waves and a clearly visible dispersion, thus it was possible to estimate the dynamic parameters and create a 1D model of the rock formation. The VS 30 parameter, which is one of the main and almost universally adopted parameters for site classification and which characterises the average shear wave velocity in the first 30 m of subsoil, was also specified.

Introduction

For many years ground waves have been recognised as the main disturbances in seismic records, especially Rayleigh waves, which are commonly called *Ground Rolls*. This type of waves carries a great deal of seismic energy that is used during the initiation of the wave. Until 1982 there was no application of *Ground Rolls* to practicality in Geophysics. The development of Spectral Analysis of Surface Waves and rapid technological progress in computing as well as data acquisition systems enabled the development of MASW survey in 1997. The Multichannel Analysis of Surface Waves is one of the latest seismic survey methods in shallow geophysics. The combination of multichannel acquisition devices and modern processing methods allows the dynamic parameters of rock structures to be estimated. By using the characteristic features of a wave based on dispersion, it is possible to specify the S wave velocity. The speed of S waves is connected with the shear modulus and the ground stiffness in inversion modelling can be estimated based on it.

Method

The aim of using the MASW method under the authority of PhD Iwony Stan - Kłeczek in the Podleśna quarry was to specify anisotropy in the propagation of seismic waves in selected directions of every 60°. The individual profiles that were obtained from that survey made it possible to analyse rock structures in order to recognise the depths of ground layers and to determine whether the impact of explosions on the rock formation was noticeable. The MASW data were gathered using a 24-channel PASI 16SG24-N acquisition system with 4.5Hz geophones. The geophone spacing was every three metres with two-metre shoot offset. The hardness of the soil made it impossible to put geophones in the ground. Therefore, they had to be laid on the ground vertically propped up with stones. A hammer was used as the source of initiating the seismic waves. Ground waves were recorded with a visible characteristic dispersion. The data that was obtained was analysed using the WinMASW program. The 1D model of the rock structures was created based on the manual picking mode and inversion modelling of the seismic data with Vp and density optimisation.



Figure 1. (Photo A.Marciniak). The Podlešná limestone quarry - the site of the investigation.

Conclusions

The analysis of data using the WinMASW program allowed the author to specify the depth of the bedrock and to determine the dispersion features of the ground waves. Some of the geoen지니어ing parameters, e.g., VS 30, were estimated and the density of underlying layers was also calculated. The survey that was conducted in the Podlešná limestone quarry and the analyses of the data that was obtained were very educational and useful because they allowed the author to improve the quality of the data processing procedure and the seismic modelling as well as to avoid possible mistakes in his future research projects.



References

1. Sheriff, R. and E. Geldart L. P. (1995). 2nd Edition. Exploration Seismology - Cambridge University Press.
2. Choon B. Park and Richard D. Milner.(1997). Multi Channel Analysis of Surface Waves - Kansas Geological Survey
3. Schultz, P.S. and Claerbout, J.F. (1978). Velocity estimation and downward continuation by wavefront synthesis - Geophysics, vol. 43
4. Sheriff, R. E. (2002). Encyclopedic dictionary of applied geophysics: SEG Geophysical Reference Series No. 13, 4th Ed., - Society of Exploration Geophysicists (SEG), Tulsa, Oklahoma
5. Unal Dikmen. M. and Ozgu Arisoy. and Ismail Akkaya. (2010). Offset and linear spread geometry in the MASW method. Journal of Geophysics and Engineering
6. Shane Donohue. and Dermot Forristal. and Louise A. Donohue. (2013). Detection of soil compaction using seismic surface waves - Soil & Tillage Research



Applicability of VSP to estimate laterally varying fracturing direction in reservoirs

Ivan Karpov¹, Sergey Gorshkalev, Dmitriy Vishnevskiy
email: ivkarpov7@gmail.com
¹ Novosibirsk State University

Summary

This work describes capability to investigate varying fracturing direction in reservoirs along VSP data. Polarization analysis of synthetic data acquired in medium comprising two inhomogeneous azimuthally anisotropic layers is presented.

Introduction

Nowadays petroleum producing companies have an increased interest in carbonate reservoirs. Permeability and porosity of such reservoirs are defined by cavities and fractures. Under tectonic stress, dilatancy occurs and fractures tend to become vertical and aligned with each other. [1]

For petroleum producing companies, it is very important to take fracturing into account in order to correctly exploit a field. In presence of complex geological settings fracturing direction may vary laterally. Vertically fractured strata are traditionally simulated by layers with horizontal transverse isotropy (HTI). Fracturing direction variation can be assigned by variation of isotropy plane direction.

Seismic exploration is the most effective method of fractured reservoirs investigation. When propagating through vertically fractured medium, shear-wave splits into two quasi-shear waves. With traditional to seismics ray configurations, displacement vector of the fast quasi-shear wave is parallel to the jointing. Polarization analysis can yield the displacement vectors directions and, hence, the fracturing direction. Vertical Seismic Profiling (VSP) provides the most precise estimates of the fissuring direction since the wavefields are recorded in the inner points. The purpose of this work is to show the applicability of VSP to assess varying fracturing direction in reservoirs.

Seismic data modelling

To conduct the study, a 3D horizontally layered model was created in the IPGG SB RAS. The wavefield computation was based on Lebedev finite difference scheme on staggered grids [2]. The model contained two HTI-strata, which were located in the topmost part of the section (layer A_1) and in the depth interval 2300-2760 m (layer A_2). This model is inherent to the Yurubchen-Tohomo Zone of Oil and Gas Accumulation. The reservoir in this field is Riphean carbonates (marked in the model as A_2). There are evidences of lateral fracturing direction variation in the stratum.

In both beds A_1 and A_2 , the direction of infinite-fold symmetry axis varied linearly with X-coordinate. A number of vertical impact sources, located at line $X = 0$ m, and three 2850 m deep wells at $Y = 0$ m and $X = 900, 1200, 1500$ m were simulated.

VSP data polarization analysis

Due to HTI anisotropy presence, the PS-wave reflected off the A_2 bed base splits within the layer. The objective of the data processing was to identify the direction of displacement vector of the generated quasi-shear waves, which leads to the prognosis of fracturing direction in the A_2 layer. These waves provide wider A_2 coverage compared to the downgoing waves. In order to avoid the interference of the signal to be analyzed with other waves, parametric wavefield separation was implemented and resulted in obtaining the field of upgoing shear waves on the horizontal components.

The analysis was carried out with two different methods. The first one [3] utilizes 3C-data (one shot VSP). At the beginning, it aligns the components X, Y, Z of the record with the covariance matrix eigenvectors. Resulting components X' and Y' contain the interference signal of the quasi-shear waves, Z' is zero. Then, it finds a rotation angle in the plane of the quasi-shear waves displacement vectors ($X'Y'$) that provides a maximum of the cross-correlation between rotated components. This method yields convenient quasi-shear waves separation and reliable fracturing direction estimation if both quasi-shear waves are intense. However, when azimuth of one of the shot-well lines is close to direction of one of the vertical symmetry planes, one of the quasi-shear waves is characterized by negligible intensity, which results in failure of the method.

In this case pseudo-rotation method [4,5] of polarization analysis is more reliable. It uses $2C \times 2C$ data (horizontal components of VSP data from two shots in orthogonal azimuths) and allows to compute seismograms of synthetic shots lying in arbitrary azimuths. Varying azimuths of the synthetic shot, we find two directions where only one quasi-shear wave exists. These are the directions of the vertical symmetry planes.

On each registration point, we made polarization analysis. The determined azimuths vary regularly both with registration depth and shot-well offset. There is an obvious relationship between the registration depth and the distance from the conversion point to the well: the higher the receiver is located the farther from the well the reflection off the A₂ layer base takes place. Thus, the shear waves cross the anisotropic A₂ stratum at different distances. This results in variation of quasi-shear waves polarization with registration depth. The reflection point coordinate depends on the shot-well offset as well.

The results of both methods of polarization analysis are consistent with modelled fracturing direction. On Figure 1, there is the fracturing direction estimated by the pseudo-rotation approach along VSP data from three wells in comparison with the modelled fracturing direction in the layer A₂.

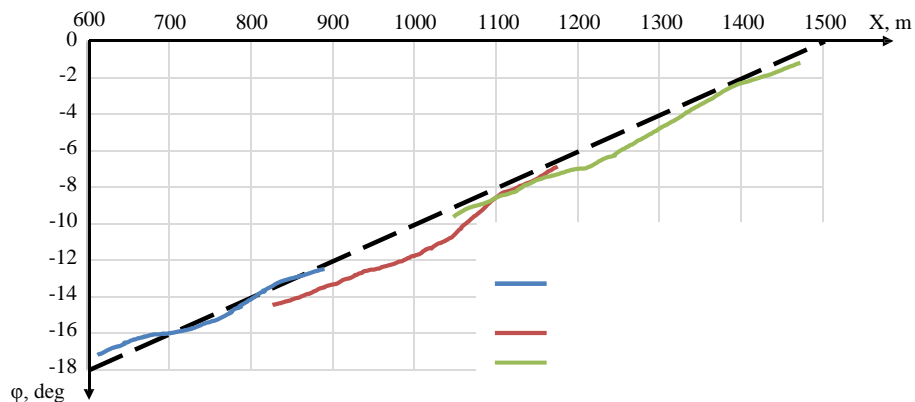


Figure 1 The fracturing direction in the A₂ layer estimated by the pseudo-rotation algorithm in comparison with the fracturing direction in the A₂ layer assigned in the model.

Conclusions

We accomplished the processing of the VSP data simulated in the model comprising two HTI-layers with laterally varying fracturing direction. We used two methods of polarization analysis. Although the cross-correlation function maximum approach is less accurate compared to the pseudo-rotation method, both methods provide convenient estimates of fracturing direction variation. Thus, the work demonstrates a conceptual possibility of analysis of fracturing direction variation in a heterogeneous anisotropic layer using VSP data.



References

1. Crampin S. (1987) Geological and industrial implications of extensive-dilatancy anisotropy. Nature Publishing Group.
2. Lisitsa V.V., Vishnevsky D.M. (2010) Lebedev type scheme for the numerical simulation of wave propagation in 3D anisotropic elasticity. EAGE.
3. Obolentseva, I.R., Gorshkalev S.B. (1986) An algorithm for separating interfering quasi-transverse waves in anisotropic media. USSR Academy of Science.
4. MacBeth C. (1996) Shear wave analysis for azimuthal anisotropy using pseudo rotation of marine VSP. EAGE.
5. Gorshkalev S.B., Karsten W.V., Lebedev K.A., Trigubov A.V., Volkov G.V. (2004) Polarization processing of PS waves for estimation of anisotropy in fractured reservoirs, the Yurubchen-Tokhomo petroleum province: testing new algorithm. Siberian Branch of Russian Academy of Sciences.



Shale Volume Estimation Using Factor Analysis and Neural Network

V.Srivardhan, S. K. Pal

email: vardhan.sri@gmail.com

Department of Applied Geophysics, Indian School of Mines, Dhanbad-826004, India.

Summary

Estimation of volume of shale is a crucial step in reservoir characterization. Shale volume is generally estimated using gamma ray logs, as they directly measure shale radioactivity. But it does not mean that other log signatures do not record the presence of shale, and implies that they are not as easily interpretable as done using only gamma ray logs. In this study a methodology using factor analysis and backpropagation neural network is proposed for the estimation of shale volume using gamma ray logs, density logs, and P-wave velocity. Utilization of several logs gives a better estimation of volume of shale and the accuracy of these techniques is discussed and compared with conventional methods

Factor Analysis

A N by K matrix D is decomposed in factor analysis by the following equation (Szabo et al, 2014)

$$D = FL^T + E \dots \dots \dots (1)$$

Here the factor scores (N by M matrix) are represented F , factor loadings by L (K by M matrix), and E (N by K matrix) is the matrix of residuals. The dimension M determines the number of factors such that $M < K$. The matrix L is determined through the covariance matrix S and obtained by the approximation algorithm of Jöreskog (2007) defined by the below equations.

$$S^* = (\text{diag} S^{-1})^{1/2} S (\text{diag} S^{-1})^{1/2} \dots \dots \dots (2)$$

$$L = (\text{diag} S^{-1})^{-1/2} \Omega_M (\Gamma_M - \theta I)^{1/2} U \dots \dots \dots (3)$$

The eigenvalues and eigenvectors of matrix S^* are represented as λ and ω , the matrix of sorted M eigenvalues and eigenvectors is Γ_M and Ω_M , an arbitrary orthogonal M by M matrix is U , and θ represents the smallest number of factors satisfying the condition given in the below equation.

$$\theta = \frac{\sum_{i=M+1}^K \lambda_i}{K - M} \dots \dots \dots (4)$$

The factor scores are obtained using Bartlett's method (1937) and defined by the below equations.

$$F = (L^T \psi^{-1} L)^{-1} L^T \psi^{-1} D \dots \dots \dots (5)$$

$$\psi = \frac{E^T E}{N} \dots \dots \dots (6)$$

The Kaiser varimax rotation is applied for accounting the variations in the factor loadings with the log responses which ensures that a unique log response is majorly characterized by a unique factor and enhances the interpretability of the results. The volume of shale in this study was estimated using Larionov (1969) relation for Pre-Tertiary and Tertiary rocks and is defined below.

$$V_{sh} = \begin{cases} 0.083(2^{3.7IGR} - 1), & \text{Tertiary or younger rocks} \\ 0.33(2^{2IGR} - 1), & \text{Pre-Tertiary Rocks} \end{cases} \dots \dots \dots (7)$$

Neural Network Backpropagation Technique

Non-linear modelling is carried out using neural networks for input x and weights w . A linear relationship, between the weights and the input is defined in Equation 8 (Luthi and Bryant, 1997).

$$\varphi(x, w) = \sum_{i=1}^p w_i x_i + w_0 \dots \dots \dots (8)$$

Here w_0 is the connection weight bias term which is generally 1. There is a nonlinear relationship between the weighted input and the output $y=f(\varphi(x,w))$ given by Equation 9 and 10. The output varies between 0 and 1 and in this study represents the volume of shale.

$$f(u) = (1 + e^{-\gamma u})^{-1} \dots \dots \dots (9)$$

The first layer of processing is called the input layer, which leads to a layer of processing which finally connects to the output layer. The connections between the layers are facilitated through the

$$y_k = f \left(w_{ok} + \sum_{i \rightarrow k} w_{ik} x_i + \sum_{j \rightarrow k} w_{jk} f \left(w_{oj} + \sum_{i \rightarrow j} w_{ij} x_i \right) \right) \dots \dots \dots (10)$$

definition of the global error function E defined by Equation 11, where d_k is the desired output and y_k is the actual output. In backpropagation technique the local gradient of the error function with respect to the weights is calculated at every iteration and multiplied with a learning factor which calculates the new local error term which may also take into account corrections made in the previous layer.

$$E(n) = \frac{1}{2} \sum_k ||d_k(n) - y_k(n)||^2 \dots \dots \dots (11)$$

The error gets back propagated and new connection weights generated at every step (Haykin 1994).

Case Study

There were two Wells namely F02-1 (depth 544.07-699.98 m) and F03-4 (depth 544.06-699.97 m) which were taken for study from the Netherlands Offshore F3 Block, with surveys undertaken by dGB Earth Sciences. The Well F02-1 has been trained using factor analysis and backpropagation neural network technique to find the volume of shale and has also been applied to Well F03-4. The results of the analysis are presented in Figure 1. The root mean square error (RMSE) for the shale volume estimation which contained calculated results from Equation 7 denoted as C_i and compared

with predicted results P_i is given by Equation 12 for N data points. $RMSE = \sqrt{\frac{\sum_{i=1}^N (C_i - P_i)^2}{N}} \dots (12)$

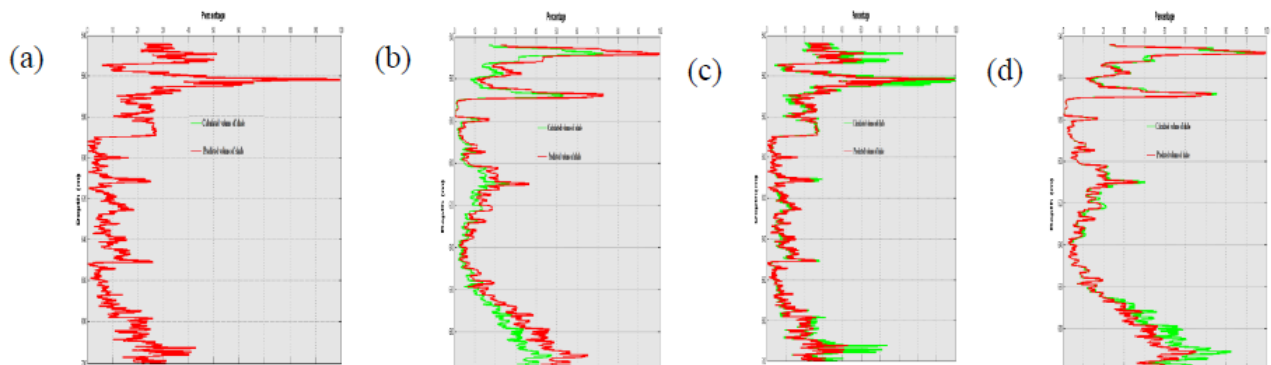


Figure 1(a) Training of Well F02-1 with backpropagation technique.. **1(b)** Volume of shale of Well F03-4 using backpropagation technique. **(c)** Training of Well F02-1 using Factor Analysis. **(d)** Volume of Shale of Well F03-4 with factor analysis. Red and green show P_i and C_i results.

Discussion and Conclusion

The results of training of the neural network are shown in Figure 1(a) with RMSE 1.32×10^{-4} . The same network was applied to well F03-4 and the results are shown in Figure 1(b) with RMSE 0.022. Factor analysis was then applied to Well F02-1 and trained as shown in Figure 1(c) with RMSE 0.06. The training resulted in the empirical equation characterizing the region and given in Equation 13 using multivariate regression analysis. There were two factors which explained the variance in the dataset denoted as f_1 and f_2 . This empirical equation was applied to well F03-4 which had a RMSE of 0.36 and the results presented in Figure 1(d).

$$V_{sh} = e^{(-0.0004f_1 + 0.0473f_2 - 4.0184)} \dots \dots \dots (13)$$

This study reveals that for obtaining good estimates of the volume of shale, the information from a variety of logs can be used and both factor analysis and neural network using backpropagation technique can be applied. In this study neural networks outperform factor analysis with low RMSE.



References

- Bartlett, M. S. (1937). The statistical conception of mental factors. *British Journal of Psychology. General Section*, 28(1), pp. 97-104.
- Haykin, S. (1994). *Neural Network*. MacMillan College Publ. Co., Reading, Massachusetts, 433 p.
- Jöreskog, K. G. (2007). Factor analysis and its extensions. *Factor analysis at, 100*, pp. 47-77.
- Larionov, V. V. (1969). *Borehole radiometry*. Nedra, Moscow.
- Luthi, S. M., and Bryant, I. D. (1997). Well-log correlation using a back-propagation neural network. *Mathematical geology*, 29(3), pp. 413-425.
- Szabó, N. P., Dobróka, M., Turai, E., and Szűcs, P. (2014). Factor analysis of borehole logs for evaluating formation shaliness: a hydrogeophysical application for groundwater studies. *Hydrogeology Journal*, 22(3), pp. 511-526.



Imaging primaries and internal multiples in elastic media

Carlos Alberto da Costa Filho ^{*†}, Matteo Ravasi ^{*}
and Andrew Curtis ^{*}

email: c.costa@ed.ac.uk

^{*} University of Edinburgh, [†] CAPES Foundation

Summary

In this work we present the newly developed elastic Marchenko imaging method which migrates primaries along with internal multiples, instead of removing them from the data prior to imaging. We show imaging results in a synthetic elastic medium and how they compare with a reference migration.

Introduction

The classic approach to image subsurface structures assumes that the seismic reflection data contains no multiples. Thus the data must undergo multiple removal before their use. However, eliminating internal multiples represents a challenge, especially for elastic data (Wu and Weglein, 2014). Nonetheless, a novel method for imaging primaries *and* internal multiples has been devised for acoustic media. The so-called Marchenko imaging method (Broggini et al., 2013; Wapenaar et al., 2013) uses internal multiples in the data during imaging, bypassing any need for internal multiple attenuation. Tests on complex models (Wapenaar et al., 2014; van der Neut et al., 2014) and field data (Ravasi et al., 2015) have shown its effectiveness. The authors have extended these methods to elastic data, establishing a Marchenko theory for elastodynamic waves in solid media, and validated it in isotropic elastic media with horizontal and vertical density variations (da Costa et al., 2014). We apply this theory to image the same elastic synthetic dataset as in da Costa et al. (2014), using pure mode (PP and SS) wavefields.

Elastic Marchenko Imaging

Elastic Marchenko imaging consists of computing elastodynamic up- and down-going wavefields at each subsurface point, and then applying an imaging condition to them. These wavefields may be computed using the following iterative algorithm (da Costa et al., 2014) described below, for $k \geq 0$

$$\mathbf{P}_k^+(\mathbf{x}_F, \mathbf{x}_0, t) = \mathbf{G}_N^{0(\phi)}(\mathbf{x}_F, \mathbf{x}_0, -t) - \theta[t + t_N^0(\mathbf{x}_F, \mathbf{x}_0)] \mathbf{P}_{k-1}^-(\mathbf{x}_F, \mathbf{x}_0, -t)$$

$$\mathbf{P}_k^-(\mathbf{x}_F, \mathbf{x}'_0, t) = \int_{\partial \mathbf{D}_0} \int_{-\infty}^{\infty} \mathbf{G}^-(\mathbf{x}'_0, \mathbf{x}_0, t - t') \mathbf{P}_k^+(\mathbf{x}_F, \mathbf{x}_0, t') dt' d\mathbf{x}_0$$

where $\mathbf{G}_N^{0(\phi)}(\mathbf{x}_F, \mathbf{x}_0, -t)$ is an input vector containing the vertical and horizontal particle velocities (v_z, v_x) and the normal and transverse stresses (τ_{zz}, τ_{zx}) of the (time-reversed) non-converted direct N -wave from point \mathbf{x}_0 to \mathbf{x}_F with traveltime t_N^0 , θ is the Heaviside step function, and \mathbf{P}_k^\pm are auxiliary wavefields arranged as $\mathbf{G}_N^{0(\phi)}$. \mathbf{P}_{-1}^- is initialized as $\mathbf{0}$ and \mathbf{G}^- is the recorded data in a matrix format:

$$\mathbf{G}^- = \begin{bmatrix} G_{(x,xz)}^{-(v,h)} & G_{(x,zz)}^{-(v,h)} & G_{(x,x)}^{-(v,f)} & G_{(x,z)}^{-(v,f)} \\ G_{(z,xz)}^{-(v,h)} & G_{(z,zz)}^{-(v,h)} & G_{(z,x)}^{-(v,f)} & G_{(z,z)}^{-(v,f)} \\ G_{(xz,xz)}^{-(\tau,h)} & G_{(xz,zz)}^{-(\tau,h)} & G_{(xz,x)}^{-(\tau,f)} & G_{(xz,z)}^{-(\tau,f)} \\ G_{(zz,xz)}^{-(\tau,h)} & G_{(zz,zz)}^{-(\tau,h)} & G_{(zz,x)}^{-(\tau,f)} & G_{(zz,z)}^{-(\tau,f)} \end{bmatrix}$$

where each element is an up-going elastic Green's function: superscripts represent the measured quantity and source types respectively, and the subscripts refer to their measured and emitted

directions, respectively. Upon convergence, we construct the up- and down-going wavefields at each image point:

$$\mathbf{G}_N^{\pm(\phi)}(\mathbf{x}_F, \mathbf{x}_0, t) = \mathbf{P}^+(\mathbf{x}_F, \mathbf{x}_0, -t) + \mathbf{P}^-(\mathbf{x}_F, \mathbf{x}_0, t) \pm \mathbf{Q}^+(\mathbf{x}_F, \mathbf{x}_0, -t) \pm \mathbf{Q}^-(\mathbf{x}_F, \mathbf{x}_0, t)$$

where \mathbf{Q}^{\pm} is obtained using a similar algorithm but with $\hat{\boldsymbol{\theta}} = -\boldsymbol{\theta}$. We combine these wavefields using a standard cross-correlational Marchenko imaging (MI) condition:

$$I_{MI}^{NN,ii}(\mathbf{x}_F) = \sum_{\mathbf{x}_0} \int_{-\infty}^{\infty} [\mathbf{G}_N^{+(\phi)}(\mathbf{x}_F, \mathbf{x}_0, t)]_i [\mathbf{G}_N^{-(\phi)}(\mathbf{x}_F, \mathbf{x}_0, t)]_i dt$$

where $[\cdot]_i$ indicates the i th coordinate. By noting also that the first iteration performs dynamically correct elastic reverse time extrapolation (Ravasi and Curtis, 2013), we define the following reference imaging condition (RI) that is equivalent to the standard approach of ignoring internal multiples

$$I_{RI}^{NN,ii}(\mathbf{x}_F) = \sum_{\mathbf{x}_0} \int_{-\infty}^{\infty} [\mathbf{G}_N^{0(\phi)}(\mathbf{x}_F, \mathbf{x}_0, t)]_i [\mathbf{P}_0^{-,+}(\mathbf{x}_F, \mathbf{x}_0, t)]_i dt$$

Numerical results

We compare the two approaches using a synthetic model consisting of several horizontal density layers and a synclinal reflector (da Costa et al., 2014). The P- and S- wave velocities were kept constant at 2.7 m/s and 1.5 m/s. We performed PP and SS imaging using both approaches detailed above (Figure 1). We see that MI exhibits much fewer artefacts than RI, especially for PP imaging.

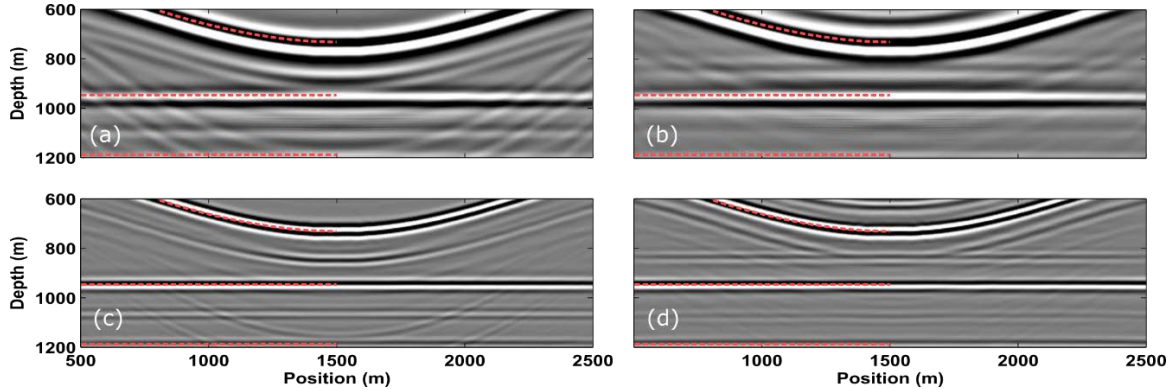


Figure 1 Top row shows PP images using the v_z component in elastic (a) reference imaging and (b) Marchenko imaging. Bottom row SS images using the v_x component in elastic (c) reference imaging and (d) Marchenko imaging. Red dashed lines show left half of the true reflectors.

Conclusions

We have proposed a new technique for imaging primaries and internal multiples in elastic media, and have contrasted it with a reference elastic imaging. Our approach represents a valuable alternative to internal multiple attenuation whose implementation is very challenging for elastic datasets. Our results are encouraging but more tests are required to understand the origin of artefacts.

Acknowledgements

The authors thank the Edinburgh Interferometry EIP sponsors (ConocoPhillips, Schlumberger, Statoil and Total) and the first author thanks the CAPES Foundation.



References

- Broggini, F., Snieder, R., Wapenaar, K. and Thorbecke, J. (2013). Creating the Green's Response to a Virtual Source Inside a Medium Using Reflection Data with Internal Multiples. In *75th EAGE Conference & Exhibition incorporating SPE EUROPEC 2013*. doi:10.3997/2214-4609.20130728
- da Costa Filho, C. A., Ravasi, M., Curtis, A., and Meles, G. A. (2014). Elastodynamic Green's function retrieval through single-sided Marchenko inverse scattering. *Physical Review E*, 90(6), 063201. doi:10.1103/PhysRevE.90.063201
- Ravasi, M., and Curtis, A. (2013). Elastic imaging with exact wavefield extrapolation for application to ocean-bottom 4C seismic data. *Geophysics*, 78(6), S265–S284. doi:10.1190/geo2013-0152.1
- Ravasi, M., I. Vasconcelos, A. Kritski, A. Curtis, C. A. da Costa Filho, and G. Meles (2015). Marchenko imaging of Volve field, North Sea. In *77th EAGE Conference & Exhibition*
- van der Neut, J., Wapenaar, K., Thorbecke, J., and Vasconcelos, I. (2014). Internal multiple suppression by adaptive Marchenko redatuming. In *SEG Technical Program Expanded Abstracts 2014* (pp. 4055–4059). doi: 10.1190/segam2014-0944.1
- Wapenaar, K., Broggini, F., Slob, E., and Snieder, R. (2013). Three-Dimensional Single-Sided Marchenko Inverse Scattering, Data-Driven Focusing, Green's Function Retrieval, and their Mutual Relations. *Physical Review Letters*, 110(8), 084301. doi:10.1103/PhysRevLett.110.084301
- Wapenaar, K., Thorbecke, J., van der Neut, J., Broggini, F., Slob, E., and Snieder, R. (2014). Marchenko imaging. *Geophysics*, 79(3), WA39–WA57. doi:10.1190/geo2013-0302.1
- Wu, J. and Weglein, A. B. (2014). Elastic Green's theorem preprocessing for on-shore internal multiple attenuation: Theory and initial synthetic data tests. In *SEG Technical Program Expanded Abstracts 2014* (pp. 4299–4304). doi:10.1190/segam2014-1513.1



Hydrocarbon Charging History for Reservoir in the Northeastern Baiyun Sag, Pearl River Mouth Basin: Constrained by Fluid Inclusion Data

Jin CHEN¹, Honghan CHEN¹
email: 1195064178@qq.com

¹ Faculty of Earth Resources, China University of Geosciences, Wuhan 430074, China

Summary

A case study was carried out on reservoirs in the northeastern Baiyun Sag, Pearl River Mouth Basin, to determine hydrocarbon charging event and accumulation age. Results showed that Zhujiang and Zhuhai Formation of Well LH29-4-1 is characterized by two oil charging episodes and one natural gas episode. The charging time of hydrocarbon with bluish green fluorescence is around 11.5-0Ma. The homogenization temperature of aqueous inclusions coexist with hydrocarbon fluid inclusion with yellowish green fluorescence is so high, showing characteristic of deep thermal fluid. Through petrographic observation, there is a charging of natural gas.

Introduction

The study area is located on the ocean continental transition with complicated thermal history. The most important source rocks in Baiyun Sag are the type I-II₁ lacustrine sediment of Eocene Wenchang Formation, and the type II-III terrestrial shale and coal-bearing strata of Oligocene Enping Formation (Fu, et al., 2007). The starting time and main periods of oil generation in Wenchang Formation, Baiyun Sag are 35Ma and 17 Ma in the east. The starting time and main periods of oil generation in Enping Formation, Baiyun Sag are: 20Ma and 10Ma in the west; 30Ma and 22Ma in the centre; 22Ma and 8 Ma in the east (Guo and He, 2007).

Method

Fluid inclusion contains significant message of ancient diagenetic condition. Fluorescence excitation and emission readily allows unique luminescence information to be extracted for discrimination of hydrocarbon fluid inclusions with visually identical fluorescence color and emission behavior in the visible region (Kihle, 1995). SD2000 spectrograph and Nikon E400 microscope are used for this study. The fluid inclusion microthermometry is invaluable for discovering the temperatures at which minerals form, the thermal history a rock has experienced, and the compositions of the fluids that traversed a rock in its history (Goldstein and Reynolds, 1994). We used THSMG 600 Cooling-Heating Stage and Nikon E400 microscope for this study.

Basin modeling is a practical method to simulate the burial and thermal history of basin. The homogenization temperature of aqueous inclusions symbiotic with hydrocarbon fluid inclusion could present ancient geothermal in diagenetic process. The hydrocarbon charging time could be determined, casting homogenization temperature of aqueous inclusions in the burial and thermal history chart.

Results

The samples test in this study was selected from 3440.59-3804.98m of LH29-4-1, because it is the reservoir in the study area.

Maximum emission wavelength of hydrocarbon fluid inclusions in samples are mostly round 497nm and 540nm (Fig.1a), indicating bluish green and yellowish green fluorescence. The relative luminescence intensity is varied because of different size of inclusions. The hydrocarbon fluid inclusions can be divided into 2 type: high-mature with bluish green fluorescence and low-mature with yellowish green fluorescence, indicating 2 charging episodes. Cast homogenization temperature of aqueous inclusions to the burial and thermal history chart (Fig.1b). The high-mature hydrocarbon charging time is determined around 11.5-0Ma, while the temperature of low-mature hydrocarbon is

too high. The too high temperature may indicate that low-mature oil comes from deep thermal fluid, not having get thermal balance with country rocks while captured. Through petrography observation, gas inclusions are existed in healed cracks in quartz, indicating that there is a charging of natural gas.

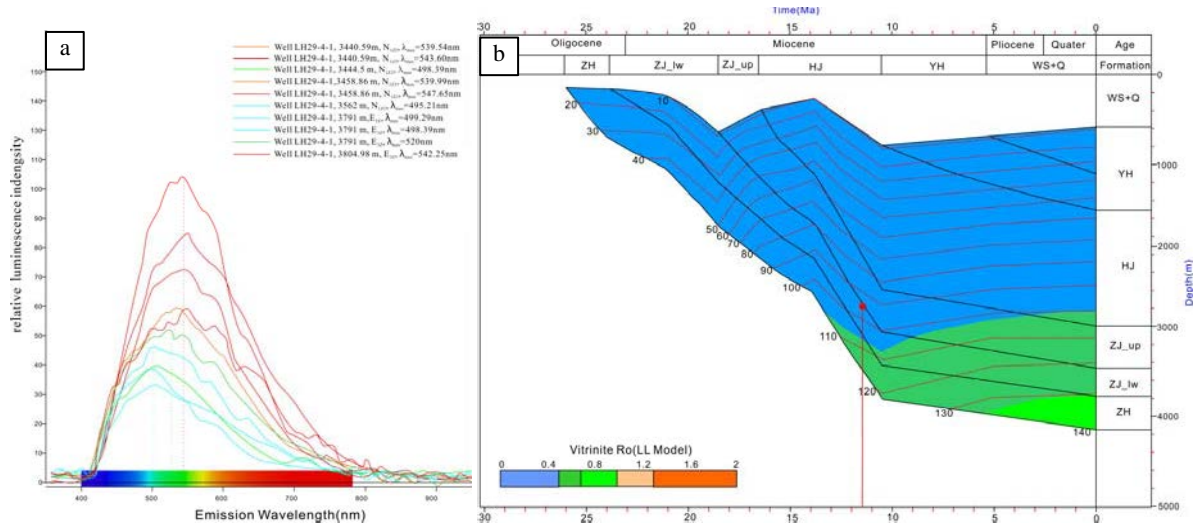


Figure 1 Emission spectra record(a) of hydrocarbon fluid inclusions in samples shows maximum emission wavelength are mostly round 497nm and 540nm, indicating bluish green and yellowish green fluorescence. The relative luminescence intensity is varied. Casting homogenization temperature of aqueous inclusions symbiotic with hydrocarbon fluid inclusion to the burial and thermal history chart(b), the hydrocarbon charging time is determined around 11.5-0Ma.

Conclusions

- 1) Zhujiang and Zhuhai Formation of Well LH29-4-1 is characterized by two oil charging episodes and one natural gas episode.
- 2) The charging time of hydrocarbon with bluish green fluorescence is around 11.5-0Ma. The charging time of hydrocarbon with yellowish green fluorescence can't be determined from homogenization temperature of aqueous inclusions, showing characteristic of deep thermal fluid with high temperature which had not cooled down when it charged in the reservoirs.
- 3) Through petrography observation, gas inclusions are existed in healed cracks in quartz, indicating that there is a charging of natural gas.



References

Fu, N. Mi, L. and Zhang, G. C. (2007). Source rocks and origin of oil and gas in the northern Baiyun Depression of Pearl River Mouth Basin.

Goldstein, R. H. and Reynolds, T. J. (1994). Systematics of fluid inclusions in diagenetic minerals: SEPM Short Course 31, 87 p .

Guo, X. W. and He, S. (2007). Source rock thermal and maturity history modeling in the Baiyun Sag of the Pearl River Mouth Basin.

Kihle, J. (1995). Adaptation of fluorescence excitation-emission micro-spectroscopy for characterization of single hydrocarbon fluid inclusions.



Microseismicity Imaging of Underground Discontinuities around the mining vicinity, Witwatersrand Basin, South Africa

S.B. MNGADI¹, R. J. Durrheim^{2,3} and the SATREPS⁴ Research Group

1. The University of the Witwatersrand, South Africa, siyanda.b.m@gmail.com

2. The University of the Witwatersrand, South Africa, Raymond.Durrheim@wits.ac.za

3. CSIR Centre for Mining Innovation, South Africa, rdurrheim@csir.co.za

4. JST-JICA Science and Technology Research Partnership for Sustainable Development (SATREPS)

Summary

Seismic events and rockbursts are prime worries in deep South African gold mines. Large seismic events often result in infrastructure damage and casualties. This paper investigates stress distribution in the rim pillar and images the evolution and growth of microseismicity induced by structural discontinuities, resulting from mining related activities at Cooke 4 shaft, South Africa. The evolution and growth of several microseismicity clusters is steeply dipping and strike sub-parallel to the mining fronts. The smallest and largest seismic event recorded were -5.3 Mw and 2.4 Mw, respectively. Majority of microseismicity is associated with the mining front, which is consistent with stress modelling.

Introduction

The study area is Cooke 4 shaft, which is situated 40 km south west of Johannesburg, South Africa. The study investigates the stress and seismicity distribution ahead of the mining excavation. Fast Lagrangian Analysis Continua (FLAC) 2D commercial code was used for numerical modelling. Linear elastic constitutive law was used for modelling. Microseismicity in the shaft pillar were monitored by high resolution underground AE sensors and accelerometers. The analysis revealed the mapping outcome of the high-resolution AEs, which were used to delineate the evolution and growth of fractures.

Method

The stress distribution was determined using numerical techniques, finite difference method (Itasca, 1992). The average pillar stress (APS) method was used to estimate the amount of stress levels a pillar of certain width can withstand. High resolution acoustic emission sensors and accelerometers were deployed ~ 1 km underground at level 38, Cooke 4 mine, 28 and 6 sensors, respectively. The average 3D spacing of the sensors is approximately 15 m, and spans a volume of ~ 100 m in diameter (Kgarume, et. al., 2013). Three accelerometers have a flat frequency response of up to 25 kHz and three have flat response of up to 10 kHz. The minimum event magnitude that was detected by these sensors was Mw -5.3 . The objectives were to identify and map seismic sources and monitor localized damage accumulation and evolution (Naoi et. al., 2013).

Results

To prevent rim pillar failure a minimum pillar width of conglomerate and quartzite is 24 m, medium lava, 25 m and soft lava, 54 m. Microseismicity associated with the stope face was of interest in this paper. Multiple planar distributions of AEs, which did not migrate totally as the mining advanced, were observed (observation period: 12 July 2011– 10 October 2011). These planar microseismic clusters strike sub-parallel to the mining front and dip steeply to the south (July 2011). From 1 August 2011 the formation of the new planar cluster appear, which dips to the south. These could be shear

fractures ahead of the stope face (Figure 1). Moriya et al. (in press) suggests that these are Ortlepp shear fractures.

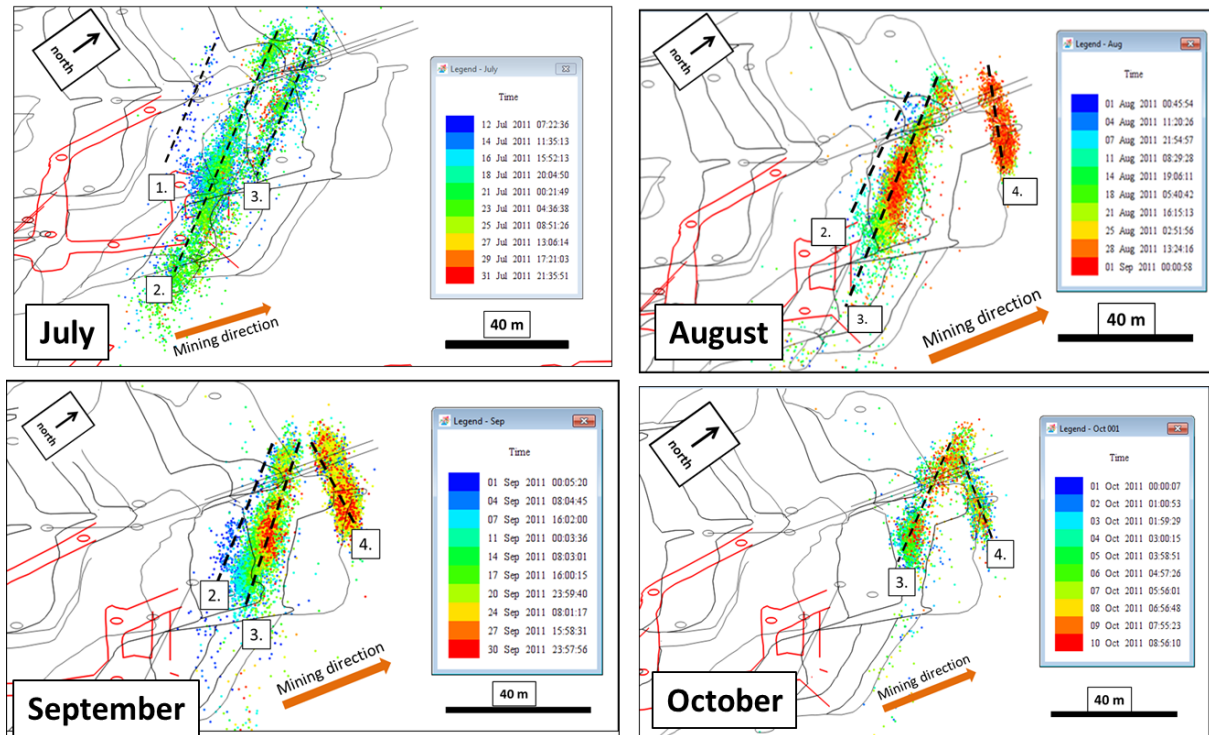


Figure 1: The evolution and growth of microseismicity from 12 July 2011 - 10 October 2011.

Conclusions

The recommended minimum size of the rim pillar for a stable shaft pillar was found to be 24 m, 25 m and 54 m for pillar made of conglomerate and quartzite, medium lava and soft lava, respectively. More than 90% of the microseismic events are associated with the mining front (Naoi et. al., 2013). The evolution and growth of these microseismic events was mapped. These microseismic planes ahead of the stope could be fractures caused by the high stress field ahead of the stope face, which is consistent with the stress modelling.

References

- Itasca consulting group, (1992). Fast Lagrangian Analysis of Continua (FLAC) manual, ver 3.2 volume 1. Minneapolis, Minnesota 55414
- Kgarume, T., Spottiswoode, S., Milev, A., Nakatani, M., Naoi, M., Yabe, Y., Philipp J., Durrheim, R., Ogasawara, H. and Ward, T. (2013). Using acoustic emissions to study rock mass degradation due to stope fracturing. Proceedings of the 13th Biennial Conference of the South African Geophysical Association, South Africa
- Moriya, H., Naoi, M., Nakatani, M., Murakami, O., Kgarume, T., Ward, A. K., Durrheim, R., Philipp, J., Yabe, Y., Kawakata, H. and Ogasawara, H. (in press). Delineation of large localized damage structures forming ahead of an active mining front by using advanced acoustic emission mapping techniques.
- Naoi, M., Nakatani, M., Horiuchi, S., Yabe, Y., Philipp, J., Kgarume, T., Morema, G., Khambule, S., Masakale, T., Ribeiro, L., Miyakawa, K., Watanabe, A., Otsuki, K., Moriya, H., Murakami, O., Kawakata, H., Yoshimitsu, N., Ward, A., Durrheim, R., and Ogasawara, H. (2013). Frequency–magnitude distribution of $-3.7 \geq M_w \geq 1$ mining-induced earthquakes around a mining front and b value invariance with post-blast time. Pure and Applied Geophysics, Springer Basel, DOI 10.1007/s00024-013-0721-7



Challenges for microseismic monitoring acquisition optimization

Georgy Loginov¹
 email: loginovgeorgy@gmail.com
¹Novosibirsk State University

Summary

This paper illustrates challenges of microseismic monitoring acquisition geometry influence on the seismic moment tensor inversion results. I made a number of numerical experiments for homogeneous anisotropic model for geometry types: surface, borehole and combined. Experiments consist of forward kinematic problem solution and amplitudes calculation; inverse problem by the optimization approach; compare solution accuracy and quality for different geometry types. Advantages of combined system are shown, as well.

Introduction

Microseismic monitoring technology that is widely applicable for such tasks as a control of a hydraulic fracturing process or ores mining monitoring [Maxwell S.C., Urbancic T.I., 2001]. Microseismic data interpretation comprises microseismic source locations, origin time and mechanisms restoring as a seismic tensor inversion (SMTI). The quality of microseismic data, in terms of information quantity is highly depends on acquisition system design, geophones orientation and distribution. Such a problem is well studied by [Vavryčuk V., 2007]. Acquisition system, depending on the goal, may be placed on the surface, in a borehole or in a mine. I made a number of numerical experiments for feasibility of different acquisition designs, including combination of borehole and surface. This paper presents my results of acquisition design influence on the source mechanism estimation quality. The advantages of combined acquisition are shown.

Theory

I consider microseismic acquisition geometry influence on the seismic moment tensor inversion (SMTI) result. Let me suppose that the moment tensor \mathbf{M} is a symmetric matrix with 3*3 size [Aki K. and Richards P.G., 2002], which can be described by vector $\mathbf{m} = [M_{11}, M_{22}, M_{33}, M_{23}, M_{13}, M_{12}]$, where M_{ij} are elements of \mathbf{M} . I used an anisotropic VTI model defined with Thomsen parameters ($\nu_{p0}, \nu_{s0}, \epsilon, \delta, \gamma$) and assumed that the medium is homogeneous and no triplications or singularities take place, and the receivers are far from the source as [Vavryčuk V., 2002]. In such a statement wave amplitude \mathbf{A} for a seismic source mechanism, described by moment tensor \mathbf{M} :

$$A_i = M_{kl} G_{ik,l}, G_{ik,l} = \frac{g_i g_k s_l}{4\pi\rho v^3 r}, \quad (1)$$

where: i - the geophone component, \mathbf{G} - is a source Green's function, \mathbf{g} - denotes a polarization vector, \mathbf{s} - the slowness vector, v - the wave velocity, ρ - medium density and r is a distance between the source and the receiver.

The inverse problem is solved as optimization approach and consist of minimization functional $L(\mathbf{m})$, which is minimization between the observed amplitudes \mathbf{A}^{obs} and the synthetic $\mathbf{A}^{syn}(\mathbf{m})$.

$$L(\mathbf{m}) = \sqrt{\sum^{Nr} (A_r^{obs} - A_r^{syn}(\mathbf{m}))^2} \rightarrow \min \quad (2)$$

The inversion can involve amplitudes of P- and S- waves separately and together as well.

Experiments

Let me present results of application of described experiment procedures for a set of survey designs: one, two and three observation boreholes, surface systems and combination of borehole and surface systems. I used a double-couple source mechanism, which is common for microseismic monitoring tasks in case of fracking [Baig A., Urbancic T., 2010] or solid mineral deposits development.

Here I put a one vertically oriented borehole. In such a case the solution is non-unique, because it depends on initial approach, so the moment tensor is cannot be restored. Then I put the surface acquisition geometry. One usually uses more number of geophones that allows covering bigger area of a source radiation. The stable solution gathered in the case of the closeness of geometry centre and source epicentre. However, when the epicentre remotes, the solution is non-unique. In the case of using two or three boreholes, the solution is better in comparison to previous cases. However, for noisy data, (noise level 10% of S-wave amplitude) SMTI result becomes instable.

Let me put a combination of surface and borehole acquisition system (see left panel in the Figure 1) After 100 inversion iterations, 10% S-waves amplitude data noising and random initial guess of the moment tensor I reached a stable solution for both tasks. The SMTI result (right panel in the Figure 1), in terms of P-wave radiation function shows stable solution, which was not reached in other cases.

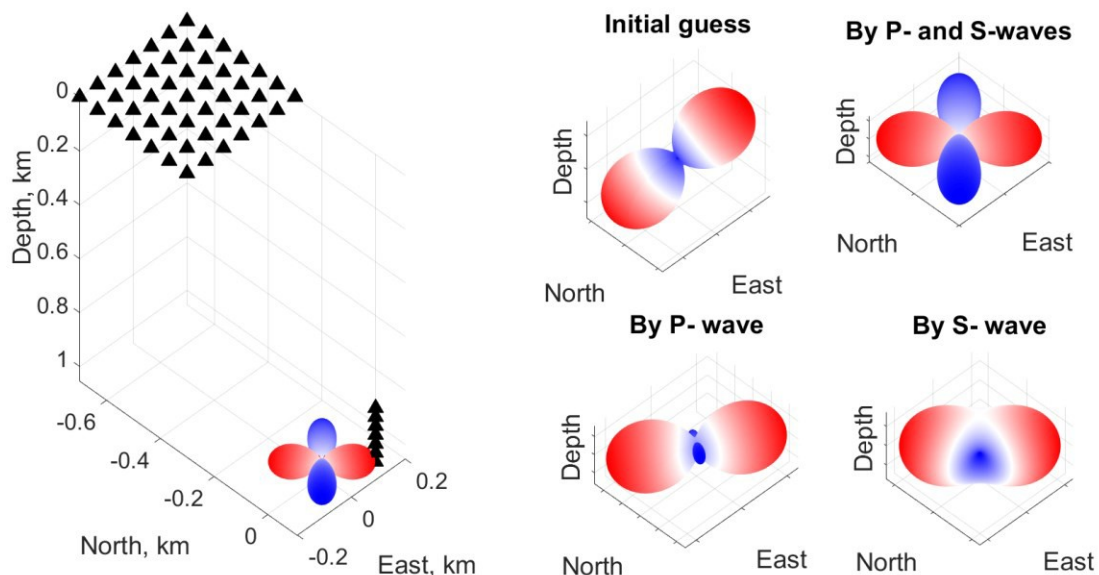


Figure 1 Illustration of the seismic tensor inversion results for combined acquisition design. Left – design, source location and P-wave radiation function diagram (blue – compression, red - depression). Right – seismic moment tensor inversion results, in terms of P-wave radiation function.

Conclusions

The results for SMTI algorithm application presented for different acquisition geometry. The stable inversion results were shown for subsequent acquisitions: *three monitoring wells, surface monitoring system, combined monitoring system (surface and downhole)*. It is also revealed that initial guess influences the solution quality.

Acknowledgments

The author thanks A.A. Duchkov and S.V. Yaskevich for their help in the research. The work was supported by the Russian Ministry of Education and Science (grant RFMEFI60414X0047).



References

Maxwell S.C. and Urbancic T.I. 2001. The role of passive microseismic monitoring in the instrumented oil field. *The Leading Edge* 20, 636–640.

Vavryčuk V. On the retrieval of moment tensors from borehole data // *Geophysical Prospecting*. – 2007. – T. 55. – №. 3. – C. 381-391.

Aki K. and Richards P.G. 2002. *Quantitative Seismology*. University Science Books, Sausalito, California.

Vavryčuk V. 2002. Asymptotic elastodynamic Green function in the kiss singularity in homogeneous anisotropic solids. *Studia Geophysica et Geodetica* 46, 249–266.

Baig A., Urbancic T. Microseismic moment tensors: A path to understanding frac growth // *The Leading Edge*. – 2010. – T. 29. – №. 3. – C. 320-324.

6th IGSC PRAGUE - ABSTRACT BOOK

Proceedings of the 6th International Geosciences Student Conference
„Crossing the Boundaries”, 13 - 16 July 2015, Prague, Czech Republic

Edited by: Petr Taborik, Frantisek Stanek, Jaroslav Jirků

Published by: Charles University in Prague Geophysical Society,
SEG Student Chapter, July 2015, Prague

<http://web.natur.cuni.cz/uhigug/igsc6prague/index.php>